1983

Fenestrations In The Internal Elastic Lamina Of Human Cerebral Arteries And Their Probable Role As A Factor In The Etiology Of Saccular Aneurysms

Gordon John Campbell

CANADIAN THESES ON MICROFICHE

I.S.B.N.

THESES CANADIENNES SUR MICROFICHE

National Library of Canada
Collections Development Branch

Canadian Theses on
Microfiche Service

Ottawa, Canada
K1A 0N4

Bibliothèque nationale du Canada
Direction du développement des collections

Service des thèses canadiennes
sur microfiche

NOTICE

The quality of this microfiche is heavily dependent upon the quality of the original thesis submitted for microfilming. Every effort has been made to ensure the highest quality of reproduction possible.

If pages are missing, contact the university which granted the degree.

Some pages may have indistinct print especially if the original pages were typed with a poor typewriter ribbon or if the university sent us a poor photocopy.

Previously copyrighted materials (journal articles, published tests, etc.) are not filmed.

Reproduction in full or in part of this film is governed by the Canadian Copyright Act, R.S.C. 1970, c. C-30. Please read the authorization forms which accompany this thesis.

THIS DISSERTATION
HAS BEEN MICROFILMED
EXACTLY AS RECEIVED

AVIS

La qualité de cette microfiche dépend grandement de la qualité de la thèse soumise au microfilmage. Nous avons tout fait pour assurer une qualité supérieure de reproduction.

S'il manque des pages, veuillez communiquer avec l'université qui a conféré le grade.

La qualité d'impression de certaines pages peut laisser à désirer, surtout si les pages originales ont été dactylographiées à l'aide d'un ruban usé ou si l'université nous a fait parvenir une photocopie de mauvaise qualité.

Les documents qui font déjà l'objet d'un droit d'auteur (articles de revue, examens publiés, etc.) ne sont pas microfilmés.

La reproduction, même partielle, de ce microfilm est soumise à la Loi canadienne sur le droit d'auteur, SRC 1970, c. C-30. Veuillez prendre connaissance des formules d'autorisation qui accompagnent cette thèse.

LA THÈSE A ÉTÉ
MICROFILMÉE TELLE QUE
NOUS L'AVONS REÇUE

NL-339 (r. 82/08)

Canada

FENESTRATIONS IN THE INTERNAL ELASTIC LAMINA OF HUMAN CEREBRAL ARTERIES AND THEIR PROBABLE ROLE AS A FACTOR IN THE ETIOLOGY OF SACCULAR ANEURYSMS

by

Gordon John Campbell, B.A.Sc., M.A.Sc., P.Eng., C.C.E.

1

Department of Biophysics

Submitted in partial fulfillment
of the requirements for the degree of
Doctor of Philosophy

Faculty of Graduate Studies
The University of Western Ontario
London, Canada
March, 1983

ABSTRACT

Although a number of investigators have implicated a breakdown of the internal elastic lamina in human cerebral arteries with the creation of intracranial saccular aneurysms, a defect or weakness in this tissue layer has not been identified. The main purpose of the research for this thesis was to describe the form and structure of the internal elastic lamina from human cerebral arteries. Since most aneurysms occur in the apical region of bifurcations a second consideration was to compare the form and structure of the straight portions with that of the bifurcations in order to determine whether a difference exists.

Isolation of specimens from the arterial wall for examination by the scanning electron microscope required the development of a specific digestion technique and a new method for assessing the dimensional changes. The net isotropic shrinkage of the internal elastic lamina following freeze drying was 6.9 $\pm$ 0.21 %.

Photomicrographs of the external surface of the internal elastic lamina reveal a continuous sheet penetrated by numerous round fenestrations with smooth borders. Four geometrical characteristics based upon the diameter and number of fenestrations in the field of view for every photomicrograph, were calculated for each specimen:-

i) Diameter: the average diameter of the fenestrations,

ii) Density: the number of fenestrations per square mm,

iii) Percentage Area: percentage of the surface area comprised of fenestrations,

iv) Ligament Efficiency: minimum width of a solid band of material divided by centre-to-centre distance for two or a series of adjacent holes.

Computation of the four geometrical characteristics for cylindrical segments of cerebral arteries revealed that the Diameter decreased linearly with a decrease in arterial diameter (3.6 mm to 0.7 mm) while the Density increased in a non-linear relationship with the most rapid increase evident for the smallest diameter arteries. The combined effect was for the Percentage Area to generally increase with the smallest diameter arteries while the Ligament Efficiency remained essentially constant.

A replication of the fenestrations in a photomicrograph, and a geometrical model (uniform array of holes with the same diameter) with an equivalent ligament efficiency were created in latex sheets for three cylindrical arterial segments with different external diameters. The uniaxial tensile characteristics for the replication and geometrical models were comparable for each specimen although the Diameter, Densities, Percentage Areas and Ligament Efficiencies among these specimens differed. The changes for several spatial geometrical parameters of the fenestrations were also documented during elongation.

A comparison of the four geometrical characteristics in the apical region of bifurcations with the circumjacent region, revealed a significant increase in the Diameter (7.0 $\pm$ 0.34 SEM μm versus 2.1 $\pm$ 0.13 SEM μm), Percentage Area (15.0 $\pm$ 1.1 SEM % versus 1.8 $\pm$

0.2 SEM %) and decrease in Ligament Efficiency (0.65 ± 0.08 SEM versus 0.86 ± 0.006 SEM). A comparison of the stress concentration factors (enlarged and circumjacent regions) revealed the potential for a substantial increase in the stress for the region of enlarged fenestrations.

The uniaxial tensile characteristics (latex sheet) for replications of regions of enlarged in relation to normal fenestrations, revealed an increase in elongation of 47 ± 0.06 SD %. Since this result indicates that a region of enlarged fenestrations should bulge more than the surrounding region of normal fenestrations, the proportional changes in the shape of the bulge were evaluated. A comparison of the spatial geometrical parameters revealed that the area of the enlarged fenestrations increased at an order of magnitude faster than for circumjacent fenestrations. It is proposed that the regions of enlarged fenestrations represent a weakness in the internal elastic lamina which may play a prominent role in the etiology of intracranial saccular aneurysms.

ACKNOWLEDGEMENTS

I would like to express my appreciation to the individuals who have provided me with guidance, encouragement and assistance in this investigation. Dr. Margot Roach stimulated my initial interest in cerebral vascular research and has patiently provided support and advice during the progress of the research and the preparation of the thesis.

Dr. Keith Farrar participated in my Advisory Committee with constructive advice and friendly encouragement. Dr. Bryan Finlay, also a member of my Advisory Committee, extended helpful advice and access to the facilities of Biomedical Engineering at University Hospital. Dr. G. Ferguson maintained an active interest in the research and supplied willing assistance on a number of occasions. Dr. R. Buck provided initial guidance on the techniques associated with the examination of tissues by the scanning electron microscope.

The autopsy material was provided through the assistance of Dr. J. Kaufmann, Director, Department of Neuropathology, University Hospital.

I am very grateful to Miss M. Montoute who patiently typed the original manuscripts which have been incorporated into this thesis. I am also indebted to Wendy Woodiwiss and Robyn Miller for typing the

thesis. The support and constructive discussions with my colleagues from the Department of Biophysics, especially Drs. Tom Macfarlane, Norman Smith and Michael Lee, were of invaluable assistance.

My sincerest expression of gratitude is extended to my wife Karen for her devoted support and encouragement, while I persevered to fulfill the entire requirements of this degree on a part-time basis.

This research was supported by a grant from the Medical Research Council of Canada.

TABLE OF CONTENTS

LIST OF ILLUSTRATIONS

LIST OF TABLES

NOMENCLATURE

A = area of an ellipse (μm^2 or mm^2)

A_i = area of each fenestration (μm^2)

a = major axis of ellipse (μm or mm)

B = percentage of area of fenestrations to the field of view (%)

b = minor axis of ellipse (μm or mm)

C = correction factor

c = centre-to-centre distance of holes (mm)

D = equivalent diameter for a circle (μm)

D_i = diameter of fenestration (μm)

d = hole diameter (mm)

d_f = final displacement of marker from coordinate axis or common point

dh = axial change in hole (mm)

d_i = initial displacement of marker from coordinate axis or common point

dR = change in length (or width) of sample (mm)

e = eccentricity

F = density (number of fenestrations per mm^2)

H = the depth of the bulge

h = longitudinal or transverse dimension of the hole (mm)

K = proportion of one-half the perimeter to length of region of enlarged fenestrations

k_S = proportional increase in strain

k_E = proportional increase in elongation of the regions of enlarged to normal fenstrations

k_1 = proportion of centre-to-centre distances for enlarged to normal

L = one-half the length of the region of enlarged fenestrations

LE = ligament efficiency

m = nearest integer number of holes

N = expansion ratio of hole (mm)

n = number of fenestrations in the field of view

P = perimeter

Q = area of the field of view (mm^2)

q = correction for linear, or areal or volumetric measurement

R = original length (or width) of sample (mm)

r^2 = coefficient of determination

S = radial shrinkage (%)

s = length or width of the sample (mm)

u = number of data points for variable

v = necking

w = number of data points for correction factor

X = raw valve of variable

Y = corrected value of variable

z = proportional change for each marker point

Chapter I

GENERAL INTRODUCTION

1.1 Historical Perspective

Arteries are the tubes within the body which conduct blood from the heart to the periphery of the circulatory system. During the pumping cycle of the heart the arteries expand to accept the volume of blood, but they retract during the filling cycle to maintain pressure within the system. The major structural components of the arterial wall are: elastin which is thought to be highly distensible; smooth muscle which can regulate the diameter of the artery; and collagen which is strong but relatively indistensible (Ham and Cormack, 1974).

The wall of the major cerebral arteries consists of four principal layers. The innermost layer in contact with the blood is a covering of endothelial cells affixed to a basement membrane. The next layer is a single continuous sheet of elastin (internal elastic lamina). The central layer or media is composed of circumferentially oriented smooth muscle with an intercellular substance and some collagen holding them together. The collagen in the outer layer (adventitia) may serve as a sheath to restrain over-expansion of the artery. The single elastin and smooth muscle layers account for the particularly thin wall of the cerebral artery.

The traditional method for studying the form and structure of the wall of cerebral arteries has relied upon the interpretation of transverse and longitudinal serial sections. An alternate method is to examine the surface of a layer of tissue. Dees (1923) was the first to use this alternate method in order to describe the surface of the

internal elastic lamina from the aorta of humans and cows as a fenestrated membrane. Hassler (1962) examined the surface area of the internal elastic lamina from a particular segment of the human cerebral circulation for newborns to 90 years of age. He reported the first data on the size and spatial distribution of fenestrations (windows) in the internal elastic lamina.

There have been a number of studies describing the mechanical properties of the wall of cerebral arteries. Busby and Burton (1964) studied the effect of age on the elasticity of major brain arteries and found that the distensibility decreased with age but the stiffness was not affected even though the content of collagen fibres in the arterial wall increases. The only study which specifically attempted to relate the mechanical characteristics to the structure of the arterial wall was performed by Damude et al (1977). Their method tested the whole arterial wall after treatment by various digestive procedures. The preferred technique of testing the individual components isolated from the arterial wall in order to determine the relative contribution to the mechanical properties has not been conducted because of the technical problems involved.

The segment of the arterial tree which separates a single artery into two branches is termed a bifurcation. The flow stream impinges on the apex or carina of the bifurcation and is similarly divided. The apical region of the bifurcation is of particular interest because it is the predominate site for the formation of saccular aneurysms which are dome-shaped outpouchings of the arterial wall. The predominate consequences of their formation are continuing enlargement, bleeding and possible rupture that may cause death. The rupture of intracranial

saccular aneurysms is one cause of subarachnoid hemorrhage which is a principal cause of stroke. It has been determined from autopsy reports that about five percent of the population may be afflicted by aneurysms, either ruptured or unruptured. Unfortunately, the symptoms of an aneurysm are not evident until significant bleeding or rupture has occurred.

There has been considerable progress in the surgical and medical treatment of aneurysms. However, the understanding of the formation, enlargement and rupture has not progressed as rapidly.

The wall of an intracranial saccular aneurysm is mostly collagen with only fragments of elastin (Hassler, 1961; Nystrom, 1963). Since collagen is the least distensible of the components comprising the arterial wall, it was postulated and confirmed in a study by Scott et al (1972) that intracranial saccular aneurysms are less distensible than cerebral arteries. Scott et al (1972) also reported that the wall thickness of saccular aneurysms was reduced in relation to the cerebral artery. As a result, the factors of increased systemic pressure, increased radius of the aneurysm during enlargement and decreased wall thickness would intensify the stress within the aneurysm wall which increases the likelihood of rupture (Ferguson, 1972). Aneurysms that rupture are usually larger than 4 mm diameter (Crompton, 1966; Crawford, 1959; McCormick and Acosta-Rua, 1970). Since aneurysms of various diameter have been observed, enlargement would appear to be a response to a physical process rather than a congenital abnormality.

Although it has been assumed that the formation of an aneurysm is related to a defect or failure mechanism of the arterial wall, there remains considerable debate about the particular mode of failure.

Forbus (1930) originally identified a defect in the media from cerebral arteries which he contended was a local weakness but he did not show that the defect could compromise the integrity of the arterial wall. Nevertheless, Forbus (1930) did acknowledge that "there are convincing facts which cause us to regard the strength and persistency of the internal elastic lamina as a factor of greatest significance in the development of anatomical aneurysms". Glynn (1940) confirmed that the integrity of the cerebral artery with natural or artificially-induced defects in the media but with the internal elastic lamina intact could be maintained, by demonstrating that the artery was still capable of withstanding 600 mm Hg pressure without rupturing or bulging. Thereafter, it has been acknowledged that degeneration of the internal elastic lamina in the apical region of the bifurcation is a necessary event in the formation of intracranial saccular aneurysms. A number of authors (Cajander and Hassler, 1976; Lang and Kidd, 1965; Nystrom, 1963; Sahs, 1966; Forbus, 1930 and Stehbens, 1963, 1975) have reported "degeneration" or "fragmentation" of the internal elastic lamina in association with aneurysms. The probable cause of this degeneration is thought to be related to mechanical factors.

There have not been any studies which have measured the forces present in the wall of cerebral arteries (straight or bifurcation) or of aneurysms, which could resolve some of the factors affecting the formation, growth and enlargement. However, Macfarlane (1975) in a unique study of the bifurcation, observed changes in the internal apical curvature (i.e., luminal or inner surface) which for some specimens involved flattening of the curvature at or near the apex. His computation (using the Law of Laplace and a number of simplifying

assumptions) of the apical wall tensions in orthogonal directions, revealed that the phenomenon of apical flattening may account for the development of an extremely large wall stress in the direction of the internal apical curvature.

Hassler (1972) has observed enlarged fenestrations in the internal elastic lamina located in the neck region of aneurysms, but did not comment on their size with respect to the results from his previous study (Hassler, 1962). The observation of enlarged fenestrations was particularly interesting since it is an established tenet of engineering practice that holes, especially larger holes or an increased number of holes, weaken a structure.

1.2 Objectives

The principal objective of this investigation is to characterize the form and structure of the internal elastic lamina from human cerebral arteries. A supplementary consideration is to examine the form and structure of the fenestrations in the internal elastic lamina of the apical region of bifurcations in order to determine if a difference could be identified. This difference was then evaluated to determine whether it could contribute to the creation of intracranial saccular aneurysms.

1.3 General Format of the Thesis

The characteristics of any material or tissue may be described by composition, form and structure, and physical properties. After some reflection which included both a review of the existing literature and a series of preliminary studies, it was decided to investigate the form

and structure since the physical properties are influenced by this characteristic. Delineation of physical characteristics remains a more difficult problem, since appropriate test procedures have not been developed for assessing a single layer buried within the multi-laminate wall of the artery. Furthermore, the effects on the physical properties of the various procedures for isolating the tissue layer have not been adequately assessed.

The method chosen for establishing the form and structure involves the use of the scanning electron microscope. In order to prepare suitable specimens and to assess potential artifacts, two digressions were necessary for the purpose of:-

i) developing a procedure for isolating the internal elastic lamina from the arterial walls.

ii) measurement of the shrinkage during preparation of tissue.

The description of the form and structure of the fenestrations in the internal elastic lamina included a series of existing variables but also introduced a single variable (ligament efficiency) which reflected the combined influence, on an equivalent basis, of two single variables.

A data base for the complete group of variables was established for the internal elastic lamina from straight segments in the arterial tree. The straight segments represented a range of diameters of cerebral arteries from the circle of Willis towards the periphery of the arterial tree. The geometrical characteristics for select groups of fenestrations in the apical region of bifurcations were compared,

with the same characteristics of the fenestrations in the circumjacent region. A distinct, statistically significant change indicative of a defect or weakness has been identified.

Since the physical characteristics of the regions demonstrating this anomaly could not be determined with the actual tissue, which is too small and inaccessible, the photomicrographs representing the tissue were replicated in thin sheets of latex rubber. The characteristic physical behaviour and alterations in the spatial geometry for various configurations of the fenestrations were assessed by uniaxially stretching the latex models. The physical behaviour for both the replication and the uniform configuration with an equivalent ligament efficiency were compared in order to validate the effectiveness of ligament efficiency to represent the actual spatial geometry. Another benefit of the models representing the tissue was to suggest relevant trends and stimulate complementary studies with the actual tissue.

It is my philosophy that the process of innovative research begins with the establishment of a firm foundation, by combining an analysis of the present information with the execution of rigorous investigations for the purpose of expanding the existing scientific knowledge. The ultimate aim of this process is to postulate a comprehensive explanation of the matter under investigation. Although the research to be presented in this thesis will not resolve either the factors which dictate the form and structure or the role of the internal elastic lamina in the formation of saccular aneurysms, it is hoped that the results represent a basis for a new perspective that may eventually contribute to the complete understanding of the etiology of intracranial saccular aneurysms.

Chapter 2

EXAMINATION OF TISSUE WITH THE SCANNING ELECTRON MICROSCOPE

2.1 Introduction

The scanning electron microscope has been used successfully for numerous studies in biology and medicine. The major advantages of this instrument are the enhanced resolution capability (less than 50 Å) and the greater depth of field (about 500 times that of light microscopy). Although it is not capable of the high magnifications inherent with the transmission electron microscope, it produces an image of three dimensional quality which depicts a larger region of surface topography. Rapid progress in both the techniques of specimen preparation and instrument design are responsible for the wider application of scanning electron microscopy to biomedical investigations.

The preparation of the tissue is particularly important in the investigations to follow since the tissue of interest (internal elastic lamina) is buried within the arterial wall. This requires isolation of the internal elastic lamina by removing the tissue obstructing the surface to be viewed, without distorting the structure of the tissue of interest. Secondly, quantitative information is to be derived from the photomicrographs which demands consideration of all factors that could significantly influence the accurate measurement of the variables.

This chapter provides a basic description of the function of the scanning electron microscope as well as an assessment of the various specimen preparation techniques for isolation of the internal elastic lamina from the arterial wall. A new method for determining the

dimensional changes associated with the preparation of tissues will be described and used to assess the change in the internal elastic lamina. The correction factor established in this section will be applied to the results in subsequent sections to account for the distortion.

2.2 Basic Technical Description of the Scanning Electron Microscope

A line drawing of the essential components of the scanning electron microscope is presented in figure 1. The scanning electron microscope image is produced by irradiating the specimen with a finely focused beam of electrons. The beam is generated in an electron gun which produces a stream of electrons with energies from one to fifty keV. The electron stream is accelerated past two or more condensing lenses that concentrate the beam. Deflection coils positioned between the last two lenses (or within the final lens) deflect the beam during a series of repeated sweeps (television raster) in a rectangular shape over the sample. The scan generator, which controls the sweep signals of the column deflection coils also synchronizes the deflection coils for the Cathode Ray Tube (CRT) in the display. As a result the position of the electron beam on the specimen corresponds with the spot on the CRT of the display (Black, 1974).

The electron beam creates a small spot of electrons (50 to 500 Å diameter) on the surface of the specimen which penetrates the surface to produce a variety of signals described as secondary electrons, back scatter electrons, characteristic x-rays and several other types of radiation. A detector that is sensitive to the particular output signal from the specimen is connected through a video amplifier to the

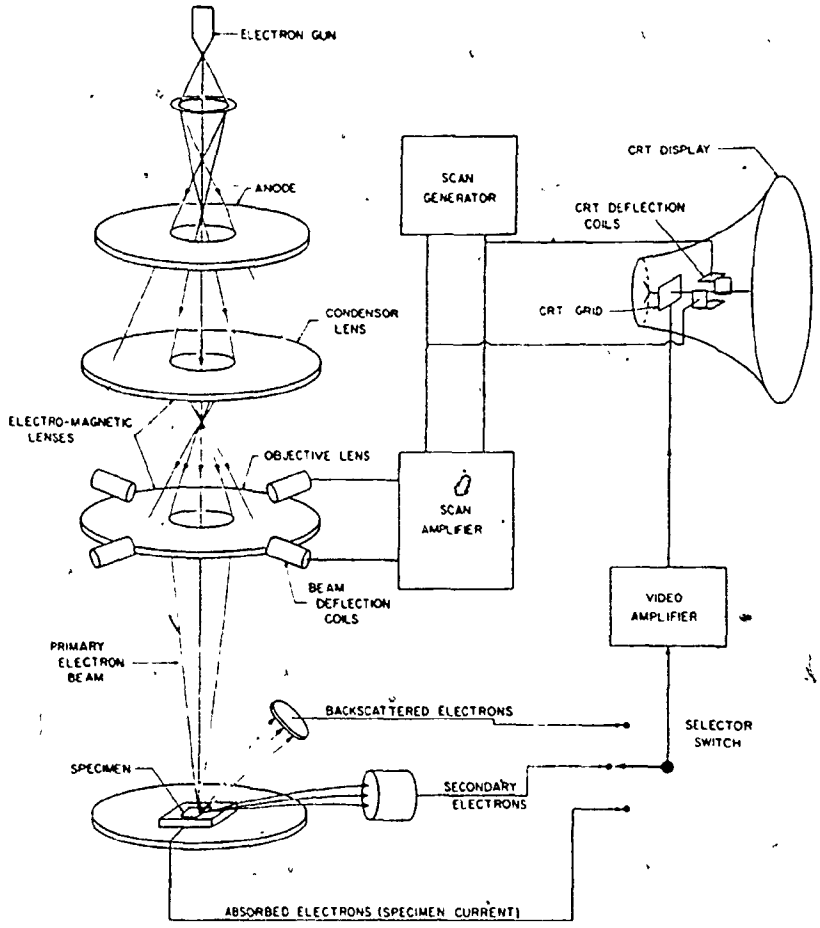

Figure 1 Schematic diagram of the scanning electron microscope.

grid of the display CRT. The intensity of the electron beam in the display CRT is modulated by the strength of the signal transmitted to the CRT grid from the detector. Therefore, as the spot rapidly sweeps across the screen of the display, the brightness is determined by the quantity of electrons liberated from the specimen. A depression on the specimen will appear as a shade of black while a projection will appear white on the screen of the display CRT. The image which is presented on the face of the display CRT is actually constructed on a point-to-point basis as the raster is executed.

The magnification is controlled by varying the size of the area that is scanned on the specimen. Therefore if progressively smaller areas were to be scanned, the magnifications would increase since the image must be enlarged to fill the size of the display CRT. The range of magnifications is generally from 15 to 100,000 times.

The depth of focus for the scanning electron microscope may be 100 or more times the beam diameter which is usually in the range of 2,000 Å to 2 μm. One of the considerations unique to the examination of any biological tissue is that the dried specimen may not be conductive and therefore must be coated with a thin, uniform layer of conducting material in order to prevent bright flashes (charging). In order to prevent contamination of the evacuated column containing the specimen and to ensure an adequate bond between the coating the specimen, tissues are generally dried prior to coating or frozen if a cryogenic stage is available (coating is not necessary).

2.3 Specimen preparation Techniques

Initial attempts to examine the luminal surface of the human

internal elastic lamina with the scanning electron microscope revealed a covering of endothelial cells and basement membrane. It was necessary to remove this layer of tissue and to clean the surface of the internal elastic lamina of extraneous microfibrils and collagen fibres identified by other authors (Sheppard, 1972; Ross and Bornstein, 1971; Stemerman, Baumgartner and Spaet, 1971). A series of treatments were applied to cat carotids in order to evaluate the effectiveness of various treatments. The treatment procedures are presented in Appendix I, section (i).

In order to expose the elastin fibres believed to be contained within the internal elastic lamina it was presumed necessary to remove the ground substance. Cat carotids were again used to evaluate the digestive properties of three procedures. The procedures are presented in Appendix I, section (ii).

As a result of the previous experience with EDTA, formic acid, guanidine hydrochloride and sodium hydroxide applied to cat carotids, it was decided to subject human cerebral arteries to a similar series of treatment. The treatments are presented in Appendix I, section (iii).

The structure of the internal elastic lamina from cat carotids has been shown to be a thin fenestrated sheet interwoven with a jumbled mass of fibres (Figure 2). The human internal elastic lamina also revealed a fenestrated sheet but the treatments applied in this study did not isolate the elastin fibres that had been anticipated.

Imaizumi, et al (1975) have also observed a "hot alkali-insoluble elastin" in the cerebral arteries. The concentration of this insoluble

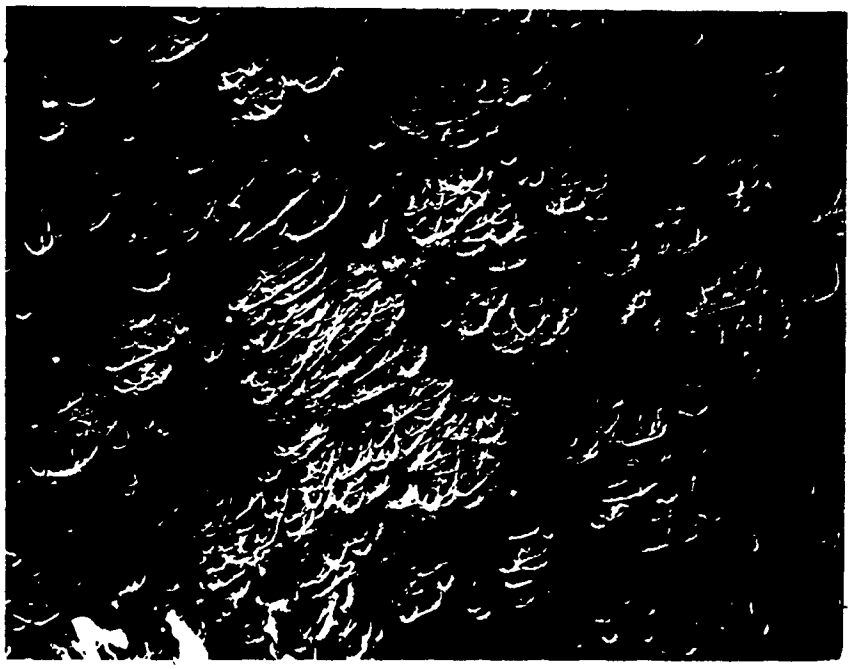

Figure 2 Luminal surface of the internal elastic lamina from cat carotids. Horizontal field of view is 0.325 mm.

elastin was higher than that of the coronary arteries and aorta, and gradually decreased with age.

Fenestrations in the cat carotids varied in shape with a range of diameters from approximately 19.5 μm to 27.6 μm and a density of 400 to 500 per mm^2. The human cerebral vessels also contain an abundance of fenestrations but the size is only 2.0 μm to 2.8 μm and the density is about 4,500 to 6,000 per mm^2. Consequently, the fenestrations of the cat carotid represent about 30 percent of the surface area while the human cerebral artery fenestrations represent only about 2 percent of the surface area.

It is interesting that the internal elastic lamina became detached from the remainder of the arterial wall when treated with formic acid, collagenase and sodium hydroxide. Sheppard and French (1971) noted that the fenestrations of rabbit aorta were filled with collagen fibres. In view of these two factors it is possible that the fenestrations filled with collagen fibres might act as pillars to attach the internal lamina and intima to the underlying tissue. In order to explore the validity of this idea, two techniques were used in an attempt to remove or reflect the internal elastic lamina from human cerebral arteries and examine the interface between the internal elastic lamina and the underlying tissue. The two techniques were 1) to manually scrape or cut and reflect the internal elastic lamina, and 2) to detach the internal elastic lamina with the use of a cannula attached to a vacuum source. These techniques were applied to separate specimens attached to a cork backing. The specimens were then fixed in 2.5 percent phosphate buffered glutaraldehyde and prepared as described

previously for examination with the scanning electron microscope. Strands of tissue between the underlying tissue and the internal elastic lamina were revealed (Figure 3) but neither the type of tissue nor the method of attachment to the internal elastic lamina could be distinguished.

2.4 Conceptualization of a Method for Measuring Dimensional Changes

2.4.1 Introduction

Following the initial use of the scanning electron microscope to examine the morphology of biological tissues, the techniques of tissue-specimen preparation have undergone frequent scrutiny. The elimination or reduction of dimensional changes, usually attributed to fixation or the dehydration and drying process, remains a constant concern. The lack of specific characterization of the dimensional alterations can confuse the identification, description and interpretation of the tissue morphology. Further, some features (e.g. surface striations oriented perpendicular to the longitudinal axis of endothelial cells, Kawamura et al 1974) have been attributed to a specific drying technique without verification that a dimensional change had occurred.

Many investigators acknowledge the existence of dimensional changes in the form of shrinkage. Nevertheless, most investigators have either described the variations in the form and structure according to various drying techniques applied to separate specimens of the same tissue (Lamb and Ingram 1979) or presented vague generalizations such as "little shrinkage occurs" (Bowyer 1977) or "less shrinkage artifact" (Gerrity 1977).

Figure 3 Strands of fibres between the internal elastic lamina (upper surface) and media (lower surface). Horizontal field width is 0.23 mm.

A variety of methods have been developed to acquire quantitative information about shrinkage. Boyd et al (1977) used three techniques to determine the dimensional changes for fresh embryonic and brain tissues during fixation, dehydration and drying: 1) direct linear measurements with an eye-piece graticule in an optical microscope; 2) direct area measurements using a Quantimet 720 image analyzer (QTM 720) with a light microscope input and; 3) indirect linear measurement from photographic negatives. Further studies of liver and brain tissue by Boyd and Boyd (1980), Boyd and Franc (1981) also made use of the Quantimet 720 image and analyzing computer system which converts an areal measurement into linear dimensions.

This technique developed by Boyde et al (1977) converts the before and after areas defined by the outline of the "square" boundary of the specimen into a linear dimensional change. In order to obtain reliable data, a distinct perimeter is required. It is not clear whether the shrinkage is computed as an average of the linear dimensional changes of the specimen boundaries or from the ratio of the areal dimension changes of the complete surface of the specimen. Moreover, only a gross shrinkage is specified and the method has not been adapted for delineating anisotropic (different properties in different directions) or orthotropic (different properties in orthogonal directions) from isotropic (same properties in all directions) dimensional changes.

Consideration of whether the shrinkage of tissue could be orthotropic or anisotropic rather than isotropic has been virtually ignored in the past. The presence of orthotropic or anisotropic shrinkage would distort the morphology of the tissue resulting in an inaccurate interpretation of the structure when viewed by the scanning

electron microscope.

Recently, McGarvey et al (1980) compared the results for measurements taken from photomicrographs obtained by scanning electron microscopy of silver-stained endothelial cells, with casts of the same tissue from different animals obtained in vivo and found anisotropic shrinkage which varied with the drying technique. This technique is applicable specifically to the assessment of endothelial cells.

Schneider (1976) compared the measurements from a differential interference contrast microscope and photomicrographs from the scanning electron microscope, to determine the reduction in the mean diameter of lymphocytes during preparation of the specimens. This technique is also specific for the assessment of the dimensional changes of this cell type. Gusnard and Kirschner (1977) used a similar technique (phase contrast microscopy) to assess the shrinkage of isolated mouse liver nuclei and human erythrocytes.

Since a primary objective of this research was to examine and quantify the structural features of arteries and, in particular, the internal elastic lamina within human cerebral arteries, a technique was required that would provide information, pertaining to: the gross shrinkage; a comparison of shrinkage between the longitudinal and circumferential orientations; and regional disparities in the shrinkage. It was also desirable that the technique withstand freeze-drying and/or critical point drying with graded acetone dehydration. A new method which accommodates most of the above requirements has been developed and will be described. It is anticipated that this method could also be used on other tissues with a reasonably flat surface region.

2.4.2 Description of the New Method

The conceptual basis for the procedure to be described below is that all points on the surface of a material which undergoes a dimensional change (expansion or contraction) will adjust their spatial location by moving either closer or further from every other point, by an amount proportional to the initial distance between the points. Therefore, if a single point is arbitrarily selected from a random or systematic array of points on the surface of a material, then any dimensional change can be computed as a proportion between the single point, and the initial and final distances for each of the remaining marker points. The proportional distances can be expressed with respect to a rectangular coordinate axis, with its origin at the single point, or as the direct path between the single point and each marker. The proportional change along the direct path between the points represents the actual shrinkage or expansion. The proportional changes with respect to a preferred axis would isolate whether the changes are isotropic or anisotropic. Localized variations in either of the above proportional changes would indicate possible distortion of the material.

Fresh specimens of the desired tissue are mounted, and then affixed to a firm backing such as cork (stiff specimens may not require this step). A random array of marker points is next applied to the surface of the wet specimen. For the purpose of the ensuing discussion, the term "wet specimen" will refer to either the fresh or fixed specimen; the term "processed specimen" will be used for subsequent observations obtained from the same specimen after the various stages of fixation, dehydration and/or drying.

A suitable marker system has been devised which consists of a mixture of fluorescent polystyrene microspheres [+] with a range of diameters from 9 to 12 μm and a cyanoacrylate adhesive [*]. A very watery mixture is produced by adding approximately 0.5 mm^3 of fluorescent microspheres to 2 or 3 drops of cyanoacrylate adhesive. The proportion of microspheres to cyanocrylate adhesive should be adjusted until only a few discrete microspheres are evident in each dab of the marker system applied to the surface of the specimen. The low viscosity (1-40 cP) cyanoacrylates were found to be preferable since the microspheres did not represent distinct points with the use of higher viscosity cyanoacrylates. This may have been due to attenuation of the ultraviolet light by the filler substance added to increase the viscosity or a thicker coating covered the surface of the microspheres.

Dabs of the marker systems are applied to the surface of the tissue by a fine glass fibre with an approximate diameter of 5 μm which has been drawn to a long tapered tip of about 10 to 20 μm. The procedure for applying the dabs consists of cleaning the glass tip in acetone, dipping the tip in the marker mixture and briefly touching the tip to the specimen, once or twice. This procedure, which is best performed with the aid of an operating microscope, is repeated until the surface is dotted with an adequate array of marker points. Care must be exercised during the application of the dabs to

+ Fluorescent Polystyrene Microspheres, Particle Information Services Inc., 2957 Woodland Park Road, P.O. Box 702; Grants Pass, Oregon 97526

* Ethyl-oc-cyanoacrylate (product designations 414, 495) Loctite Canada Inc., 515 Timberlea Blvd., Mississauga, Ontario, CANADA L4S 2S3

avoid air-drying of the specimen. In this case, adequate wetness was assured by occasionally applying a drop of distilled water to the surface of the cork adjacent to the specimen. The water permeates into the cork and flows under the specimen.

Under ultraviolet illumination the microspheres encased in cyanoacrylate cement appear as dots on the surface of the specimen, even when the specimen is very wet. The cyanoacrylate adhesive is an excellent adhesive for bonding the microspheres to the wet surface of the tissue, since: the adhesive is reasonably non-stringing (i.e. does not tend to form strings); polymerization is initiated by the presence of moisture; contraction of the adhesive during curing is negligible; it transmits ultraviolet light; and it does not appear to adversely affect the surface of the tissue.

Following the application of the marker points, the wet specimen complete with backing is placed on the adjustable stage of a light microscope with the preferred axis of the specimen aligned with the long or short axis of the camera back. The requirement for the orientation of the specimen with respect to a preferred axis is optional if an assessment for the presence of anisotropic dimensional changes is not to be considered. The surface of the specimen must be aligned perpendicular to the optical axis of the microscope.

The light microscope is equipped with an ultraviolet light source and appropriate filter arranged to provide EPI-illumination (preferred) or incident-light illumination for fluorscence microscopy. The selection of objective and eye piece lenses is dependent upon the size of field to be viewed. An objective lens with a large working distance is recommended, otherwise condensation from the wet specimen will form

MARKER	DIMENSIONAL CHANGE		
	Y-CHANGE (%)	X-CHANGE (%)	RADIAL CHANGE (%)
2	-3.4	-3.2	-3.3
3	-1.8	-3.0	-2.0
4	-5.4	-5.1	-5.3
5	-5.2	-6.8	-5.5
6	-4.1	-6.7	-5.8
7	-6.3	-6.0	-6.1
8	-6.0	-5.4	-5.5
9	-4.8	-5.6	-5.3
10	-4.7	-5.9	-5.4
11	-5.0	-5.3	-5.2
12	-2.1	-5.6	-5.1
13	-2.9	-6.4	-5.7
14	-4.4	-5.5	-5.1
15	-3.7	-5.7	-4.8
16	-3.7	-5.9	-5.0
17	-4.0	-8.4	-6.1
18	-1.9	-8.1	-5.5
19	-6.5	+3.0	-5.5
20	-2.7	-1.0	-2.2
21	-2.7	-1.3	-2.2
22	-3.4	-4.3	-3.9
23	-2.6	-4.3	-3.6
24	+1.6	-3.6	-3.4
Mean (%)	-3.7	-4.8	-4.7
S.D. (%)	1.8	2.5	1.3
S.E.M. (%)	0.4	0.5	0.3

Table 1 Linear freeze drying shrinkage of glutaraldehyde - fixed internal elastic lamina from one specimen of human cerebral artery. Dimensional changes correspond with the numbered markers shown in Figure 6.

An example of the photomicrographs for the wet and processed tissue is illustrated in Figures 4 and 5 respectively. The tissue in this case is the internal elastic lamina from human cerebral arteries which has been isolated by the technique described in Section 2.6.2. The preparation procedure for examination by the scanning electron microscope is fixation in 2.5% glutaraldehyde followed by freeze-drying. The horizontal or long dimension of the photomicrograph represents the longitudinal axis of the artery and coincides with the X-coordinate axis. The vertical direction represents the Y-coordinate axis or circumferential direction of the artery. The honeycomb pattern, partly visible in the background of Figure 4, is the cork backing.

The negative for each region of the wet specimen is mounted in an enlarger and the image projected on tracing paper. Two points corresponding to the bottom corners of the projected image which indicate the orientation of the preferred axis are marked on the tracing. These are represented on the tracing illustrated on Figure 6 by the "+" marks at the bottom. The outline of each dab of cyanoacrylate adhesive for the wet tissue is traced and the position of each microsphere or particle is marked. The continuous lines and solid circles in Figure 6 represent the markers on the wet specimen illustrated in Figure 4.

The negatives for the corresponding regions of the processed tissue are next mounted in an enlarger. A marker point (usually a fluorescent microsphere) common to both negatives is selected as the single point (marker 1 in Figure 6) to be superimposed. The preferable location of the single point (designated common point) is near the

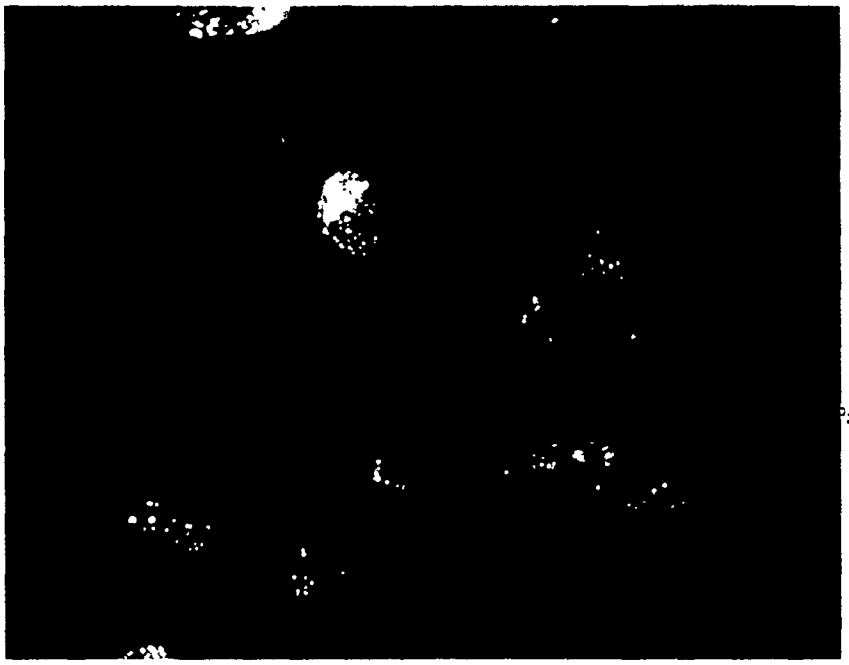

Figure 4: A photomicrograph illustrating a region of markers on the surface of a wet specimen of the internal elastic lamina from a human cerebral artery. (Horizontal field width: 2.2 mm)

Figure 5 The corresponding photomicrograph of the same region as shown in Figure 4 after freeze-drying. (Horizontal field width = 2.2 mm)

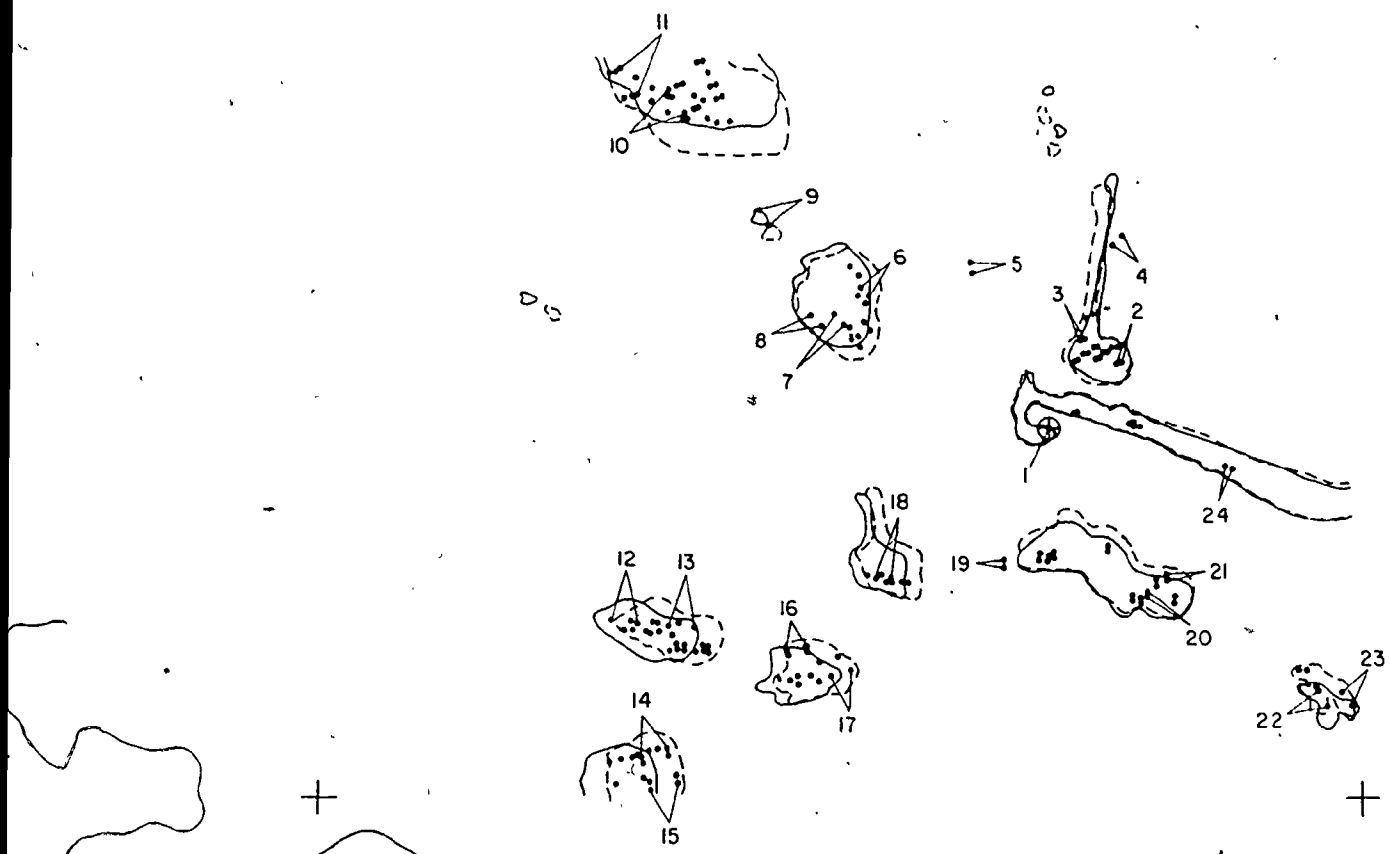

FIGURE 6 The composite tracing for the locations of the markers illustrated in Figures 4 and 5 (Horizontal separation of "+" marks = 2.2 mm)

centre of the region to be analyzed to ensure a balance of marker points about the common point, but markers nearer the periphery are also acceptable.

The tracing of the location of the markers on the wet specimen is aligned such that the common points coincide, and the wet specimen tracing rotated until the markers on the processed tissue are approximately located between (for the case of shrinkage) or beyond (for the case of expansion) the corresponding markers on the wet tissue and the common point. Exact positioning is unnecessary since a computer programme has been developed which optimizes the location of the set of markers on the processed tissue tracing with respect to the wet tissue tracing. The process of tracing the outline of the dabs of cyanoacrylate adhesive and marking the position of each microsphere is repeated. A sequence of photomicrographs representing the adjustment of the focus to accommodate undulations in one region on the surface, are superimposed, one at a time; and the distinct portion of the photomicrograph is reproduced on the tracing. The results for the processed tissue illustrated in Figure 5 are represented by the broken lines and open circles in Figure 6. The combined tracing for the wet and processed tissue has been termed the "composite".

The range of 9 to 12 μm for the diamter of the microspheres was purposely selected in order that the projected image of the photomicrographs, which represented a final magnification of 144X, would result in a mean diameter of 1.5 mm for the micropheres. Discrimination of microspheres and outline of the cyanoacrylate dabs is greatly enhanced by viewing the projected image rather than examining the prints illustrated in Figures 4 and 5, since the fine detail is lost.

The coordinates for each pair (wet and processed tissue) of markers selected from available markers must be determined in order to compute the relative dimensional changes. Each field of view (photomicrograph) was adequately represented by about 20 to 25 pairs of markers. Usually only one or two microspheres are selected as markers from each dab of cyanoacrylate, since additional markers from the same dab represent unnecessary duplication, unless the dab is very long in shape. Examination of the marker points by scanning electron microscopy (Figure 7) revealed that the cyanoacrylate dabs were shrivelled in appearance or resembled caps and did not create any significant distortion of the tissue which in this case was very delicate. Furthermore, the dabs demonstrated some pliability since the radial dimensional change (Table 1) of marker 24 was comparable to the mean radial dimensional change, even though it is encased in the same dab as the common point. The tissue beneath some of the dabs appeared to form a slight hump which could have been produced, probably during drying, as a result of the presence of the dab. The humps were more prevalent for either thick dabs or the higher viscosity cyanoacrylate.

Individual microspheres without an apparent encapsulation by the cyanoacrylate are selected with caution since the microspheres could have been erratically displaced from their position by the drying process or handling. The measurement of isolated microspheres sprinkled on the surface (i.e. without adhesive) provided a more discrete marker and similar results for the shrinkage, but the dispersion of the data (standard deviation) was increased considerably. A case in point is illustrated by isolated markers 4,5 and 19 in Figure 6. The proportional displacements in the X and Y directions for

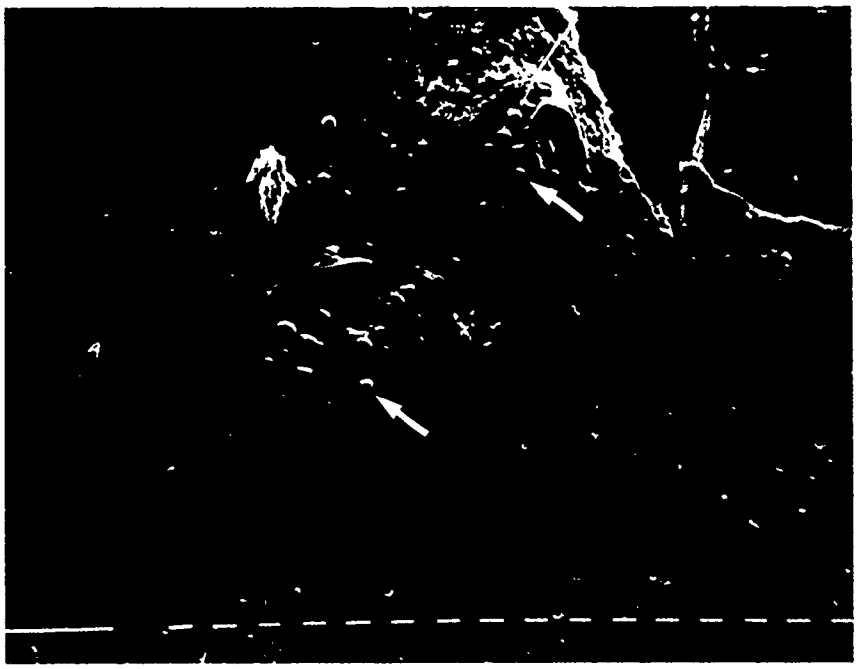

Figure 7 An example of a dab of cyanoacrylate adhesive on the surface of a tissue specimen. The arrows identify microspheres encapsulated within the cyanoacrylate adhesive. (Short white bars represent 10 μm)

markers 4 and 5 are comparable to the mean values. However, there is a distinct discrepancy between the proportional displacement in the X-direction of marker 19 and the mean value. This discrepancy could be attributed to the erratic displacement of the marker point in the X-direction.

A computer programme has been developed for the purpose of facilitating measurement and storage of the coordinates, and computation of the dimensional changes. A further advantage of the computer programme was the incorporation of an optimization procedure to improve the visual alignment of the wet and processed markers, without requiring a locating mechanism or device. The structure of the computer programme will be presented in section 2.5.

The composite tracing is affixed to the platen of a digitizer (Hewlett Packard Model 9864A) connected to a computer (Hewlett Packard 9830A). Each pair of selected coordinates, designated numbers 2 to 24 in Figure 6, is digitized with respect to a coordinate axis whose origin is located at the common point (marker 1) and oriented according to the preferred axis of the specimen (X-axis represents left-right orientation). Markers located within 2 mm (1.3% of the field width) of the axes through the common point denoted on the composite were excluded since the digitized points within this band resulted in noticeable differences in the values for the dimensional changes. This variation is attributable to the error of the measurement which significantly influences the result when the proportional changes are computed.

A total of three dimensional characteristics representing the proportional dimensional changes parallel to the X-axis and Y-axis, as well as along the direct path (radial direction) between the common point and the marker point for each pair of markers are computed according to the relationship that:

$$z = \left[\frac{|d_f| - |d_i|}{|d_i|} \right]^n_2 \qquad (1)$$

where: z = proportional change for each marker point from 2 to n.

d_f = final displacement of marker from coordinate axis or common point.

d_i = initial displacement of marker from coordinate axis or common point.

Subsequently, either a negative sign representing shrinkage (i.e. d_f is less than d_i) or a positive sign in the case of expansion (i.e. d_f is greater than d_i) is assigned to the result. The dimensional change in the radial direction represents the actual expansion or contraction of the tissue. A comparison of the dimensional changes parallel to the X and Y axes determines whether the dimensional changes are uniform (isotropic) or non-uniform (anisotropic) in mutually-perpendicular directions. Furthermore, a comparison of the radial dimensional changes among the individual markers or groups of markers will isolate regional disparities.

The group of coordinates depicting the processed tissue markers are then translated along the positive and negative coordinate axes

and/or rotated about the common point in uniform increments by the computer. After each incremental displacement the dimensional characteristics, means and standard deviations are updated and compared with previous results. The final location represents the lowest standard deviation for the proportional displacement of the markers with respect to the X and Y axes. Subsequently, the three dimensional characteristics listed above for each pair of coordinate points along with the average dimensional change, standard deviation (S.D.) and standard error of the mean (S.E.M.) for the final position of markers are recorded. The final results for the specimen illustrated previously are listed in Table 1, (positive value represents expansion, negative value represents contraction or shrinkage). The positions of all the markers on the processed tissue have been uniformly adjusted by the computer in order to optimize the alignment of the wet and processed markers. This adjustment is reflected in the final results presented in Table 1.

2.4.3 Verification

In order to assess the effectiveness of the technique, a set of six points were randomly marked on a sheet of graph paper. A second series of points with coordinates decreased by 10% towards both the X and Y axes (representing isotropic shrinkage) of the coordinate system with origin at the centre of the graph paper and axes oriented parallel to the ruled lines, were marked on a separate sheet of graph paper. A third set of points with coordinates decreased by 20% towards the X axis and 10% towards the Y axis (representing anisotropic shrinkage)

MARKER	DIMENSIONAL CHANGE		
	Y-CHANGE (%)	X-CHANGE (%)	RADIAL CHANGE (%)
2	-3.4	-3.2	-3.3
3	-1.8	-3.0	-2.0
4	-5.4	-5.1	-5.3
5	-5.2	-6.8	-5.5
6	-4.1	-6.7	-5.8
7	-6.3	-6.0	-6.1
8	-6.0	-5.4	-5.5
9	-4.8	-5.6	-5.3
10	-4.7	-5.9	-5.4
11	-5.0	-5.3	-5.2
12	-2.1	-5.6	-5.1
13	-2.9	-6.4	-5.7
14	-4.4	-5.5	-5.1
15	-3.7	-5.7	-4.8
16	-3.7	-5.9	-5.0
17	-4.0	-8.4	-6.1
18	-1.9	-8.1	-5.5
19	-6.5	+3.0	-5.5
20	-2.7	-1.0	-2.2
21	-2.7	-1.3	-2.2
22	-3.4	-4.3	-3.9
23	-2.6	-4.3	-3.6
24	+1.6	-3.6	-3.4
Mean (%)	-3.7	-4.8	-4.7
S.D. (%)	1.8	2.5	1.3
S.E.M. (%)	0.4	0.5	0.3

Table 1 Linear freeze drying shrinkage of glutaraldehyde - fixed internal elastic lamina from one specimen of human cerebral artery. Dimensional changes correspond with the numbered markers shown in Figure 6.

according to the same coordinate system were marked on a separate sheet of graph paper. Both sets of points for anisotropic and isotropic shrinkage have been designated "shifted points".

Each point was selected in succession to represent the common point. The location of the remaining points for both the hypothetical isotropic and anisotropic shrinkage conditions were adjusted according to four configurations:

i) The common points were aligned to coincide and the remaining shifted points were aligned visually between the common point and the original points. The process was repeated for each point defined as the common point and a separate composite created in each case for both sets of shifted points.

ii) The group of shifted points were purposely translated a short but unknown distance from i) above along the positive and negative directions of the X and Y co-ordinate axes. Again, separate composites were created for each translation, each point defined as common, and both sets of shifted points.

iii) The group of shifted points were purposely rotated a small but unknown displacement from i) above, both clockwise and anti-clockwise. Separate composites for each rotation, each point defined as common and both sets of shifted points were created.

iv) The set of shifted points were purposely translated along one of the coordinate axes a short distance as well as rotated clockwise or counter-clockwise a small

displacement from i) above. Composites for only one point defined as common were created.

For the group of six points this represented eighty-one possible configurations.

In each case the computer programme correctly identified the mean shrinkage with respect to the X and Y axes (i.e. 10% and 10% or 20% and 10% respectively), usually within 1% deviation and a standard deviation of less than 1% (the original shift of the points on the graph paper contributed to the standard deviation). Consequently, the verification scheme confirmed:

i) The validity of the hypothesis that dimensional changes of a material can be determined by computation of the proportional displacement of a random set of points, with respect to any point defined as common between the original and final conditions of the material.

ii) That the technique is capable of identifying both isotropic and as well as anisotropic dimensional changes in the plane of the field of view.

iii) That the optimization scheme incorporated into the computer programme effectively accommodates misalignment between the original and final location of the marker points.

iv) That the technique will accurately characterize the dimensional changes along both an X and Y axis, as well as the radial dimensional change.

2.4.4 Discussion

Although it is generally recognized that the scanning electron microscope is a beneficial instrument for studying the form and structure of tissue, its use has been relegated principally to providing pictures for illustrative purposes. Tissue preparation techniques as well as alterations in tissue form and structure during the preparation process (especially drying artifacts) remain contentious issues. Furthermore, it is disappointing that more researchers have not employed this excellent research instrument to generate quantitative information about tissue form and structure. One solution for alleviating some of the scepticism associated with the creation of artifacts would be the inclusion of a shrinkage assessment along with the pertinent data or information. This requirement assumes that recognized standard techniques are available which can be readily adapted to various tissues and preparation procedures.

Although the technique described in this section has only been tested on one tissue, it could be readily applied to any wet tissue with a reasonably flat surface area. The technique has been found suitable for analyzing dimensional changes after processing by fixation followed by air-drying, freeze-drying, and critical point drying (ethanol/amyl acetate dehydration). Adaptation for use with acetone dehydration (critical point drying) and propylene oxide/benzene dehydration (camphene drying) requires a suitable adhesive since cyanoacrylates are soluble in acetone and prophylene oxide. A comprehensive survey to determine whether appropriate adhesives exist has not been conducted. Moreover, this technique is not suitable for

assessing dimensional changes during coating, since the fluorescence is obscured by the coating.

The capability of the technique to detect dimensional changes according to a set of mutually-perpendicular axes oriented in a preferred direction, as well as radial dimensional changes, permit the identification and analysis of non-uniform dimensional changes, identification and analysis of distortion in a localized region within the perimeter of the tissue, and the gross shrinkage of the specimen. It is conceivable that the technique could be applied directly to specimens which form part of a study (rather than producing duplicates for the shrinkage assessment) since the markers are unobtrusive except at low magnifications. Partitioning of the field of view would permit a comparison of the dimensional changes for each segment (provided sufficient markers are distributed within the regions of interest). If regional discrepancies are observed, then the local dimensional changes can be determined by selecting a common point within the region of interest and creating a composite for analysis.

It is hoped that the other researchers who appreciate the need for a quantitative description of the form and structure of tissue and of dimensional alterations during the preparation of tissues will include specific information pertaining to the dimensional changes along with the results of their study. The technique presented here could provide this information in certain cases which should alleviate some of the concerns associated wtih the interpretation of the photomicrographs obtained with the use of the scanning electron microscope.

2.4.5 Summary

A new method is presented for determining the dimensional changes which can occur during the fixation, dehydration and drying of tissue specimens prepared for examination by the scanning electron microscope. Photomicrographs of a random array of markers (fluorescent microspheres 9-12 μm dimater, encapsulated in dabs of cyanoacrylate adhesive) on the surface of specimens are obtained with the aid of an optical microscope equipped for fluorescent microscopy. One marker, which is common to each pair of photomicrographs representing the wet and processed conditions of the specimen, is selected from the array of markers. The tracings which depict the outline of the dabs and the location of the microspheres, for the wet and processed specimens are combined into a single composite with the one superimposed marker representing the origin of a set of mutually-perpendicular axes. A newly developed computer programme acquires the coordinates of the marker points, optimizes the alignment of the marker points and computes the proportional dimensional changes in two mutually-perpendicular directions, as well as along the direct path between the common marker and the remaining markers.

2.5 Optimization of the Alignment of the Marker Points

2.5.1 Introduction

The computer programme to be described in this section acquires the coordinate pairs of the marker points, optimizes the alignment between the two sets of marker points and computes the proportional dimensional changes in two mutually-perpendicular directions, as well as along the direct path between the common marker and the set of

remaining markers, for each composite. The group of composites is then combined to represent the shrinkage for the exposed surface area of the specimen.

2.5.2 Principle of the Optimization Procedure

The orientation of the X coordinate axes in Figure 6 is parallel to an imaginary line joining the "+" marks at the bottom of the figure. The orientation of the X axis may be random or defined according to a preferred direction which may be selected on the basis of a particular anatomical feature (e.g., longitudinal axis of an artery).

The initial alignment between the wet and dry markers was performed visually, with the original location of the markers on the wet tissue, providing a reference. In order to refine this initial alignment, the markers are adjusted until their final location minimizes the dispersion of the mean dimensional changes. With the origin located at the common point, the coordinate pairs for the location of the markers on the wet tissue (designated wet markers) and the markers on the dried specimens (designated dry markers) are measured and recorded. Coordinate pairs for the wet markers are considered to be firm and therefore do not change. The coordinate pairs for the dry markers are considered soft and may be adjusted by shifting and/or rotating them as a unit with respect to the common point.

Conceptually, the arrangement of the wet and dry markers can be considered analogous to fixed and floating rims, respectively, of a wheel. Only the fixed rim (wet markers) is connected to the hub (common point). Consequently, the floating rim can be translated

(shifted) and/or rotated with respect to the hub. The dry markers remain fixed with respect to each other but their collective location with respect to the hub or common point can be modified within specified limits.

The proportional dimensional changes between the wet and dry conditions for each marker point is computed with respect to the X and Y axis. The mean and standard deviation for the proportional dimensional changes are then computed for the original location of the entire group of marker points, as well as after each subsequent adjustment of the dry marker points.

A single optimization criterion utilizing two variables (i.e., the X standard deviation and the Y standard deviation) is used to establish the best location of the dry marker points. The present sum of the X standard deviation plus the Y standard deviation is compared with the previous best sum of the X standard deviation plus the Y standard deviation. If the individual values for both of the standard deviations is less, or their combined sum is less, then the present location of the markers is considered an improvement (i.e., the dispersion has been reduced). The present coordinate pairs are retained for comparison with future results and the search continues. Conversely, if both values are greater, or their combined sum is greater, then the cycle is repeated after computing a new location for the dry markers. The iteration procedure may be halted when a minimum has been identified for the combined sum of the X and Y standard deviations or a specified limit has been encountered. The results may be reviewed before proceeding with further iterations or terminating the procedure.

The search procedure continues to test various single or multiple adjustments to the entire group of dry markers. Ultimately, the procedure selects the location of the dry marker points with the combined sum of the standard deviations at the minimum value. A description of software is presented in Appendix II.

2.5.3 Example of Programme Execution

The data manipulation for the set of markers illustrated in Figure 6 (identified as composite 7 from specimen 28-19) will be presented to demonstrate the results of the optimization procedure. The coded response, standard deviation and mean, along with the results for each of the four optimization levels are presented in Figure 8. The coding scheme is listed below:-

PS = provisional array, shift

OS = optimal array, shift

PR = provisional array, rotation

OR = optimal array, rotation

PS + PR = provisional array, shift plus rotation

OS + OR = optimal array, shift plus rotation

Each time the programme selects an amended location of the dry marker points (viz., the sum of the X and Y standard deviations is less) it outputs the code along with the standard deviations and means.

It is apparent from the second coded "PS" in Figure 8 that a shift along the X axis improved the location of the dry marker points with respect to the original location. Figure 9 illustrates that the first incremental shift along the +X axis resulted in a lower value for the combined sum of the standard deviations. The second shift along the +X

axis increased the combined sum of the standard deviations which terminates subsequent +X shifts. Since the first -X incremental shift also increases the combined sum for the standard deviations, further -X shifts are terminated and the programme proceeds to +Y shifts. The expanded series of results presented in Figure 9 are for illustrative purposes only and normally would not be computed past the three shifts mentioned above.

The first incremental shifts along both the +Y and -Y axis, as illustrated in Figure 10, do not decrease the combined standard deviation. Consequently, no responses are presented in Figure 8. Again, the expanded series of results presented in Figure 10 are for illustrative purposes and normally would not be computed after the first shifts. The coded response "OS" in Figure 8 indicates that the amended dry markers are assigned to the optimal array.

The coded "PR" responses in Figure 8 indicate that a series of rotations have steadily improved the location of the marker points. The results presented in Figure 11 illustrate that the first two incremental rotations in the negative (clockwise) direction improved the combined sum of the X and Y standard deviations. However, the third incremental rotation increased the combined sum which terminates any further anti-clockwise rotations. Since the first positive (anti-clockwise) rotation also increases the combined sum, the process is terminated. The expanded series of results presented in Figure 11 are presented for illustrative purposes only. The comparison between the provisional parameters for the best shift and best rotation results in selection of the rotation (indicated by "OR) for assignment to the optimal array, standard deviations and means.

28-19(8) Complete Optimization
Data loaded from file 195
Maximum Rotation is 5 degrees
Maximum shift is 5 mm

CODE	Y - CHANGE		X - CHANGE	
	S.D.	MEAN	S.D.	MEAN
PS	0.0313	0.0419	0.0337	0.0503
PS	0.0313	0.0419	0.0297	0.0502
OS	0.0313	0.0419	0.0297	0.0502
PR	0.0313	0.0419	0.0337	0.0503
PR	0.0258	0.0407	0.0311	0.0497
PR	0.0213	0.0396	0.0292	0.0491
PR	0.0183	0.0384	0.0282	0.0486
PR	0.0178	0.0372	0.0283	0.0480
OR	0.0178	0.0372	0.0283	0.0480

Level 1
Best Y-change: SD=0.0177 and Mean=0.03724
Best X-change: SD=0.0283 and Mean=0.0480
Cont Optimize? (1-Yes, Ø-No) for best X & Y + rotation

PR	0.0313	0.0419	0.0297	0.0502
PR	0.0259	0.0407	0.0270	0.0496
PR	0.0214	0.0395	0.0252	0.0490
PR	0.0185	0.0384	0.0245	0.0484
PR	0.0179	0.0372	0.0249	0.0479
OR	0.0179	0.0372	0.0249	0.0479

Level 2
Best Y-change: SD=0.0179 and Mean=0.0372
Best X-change: SD=0.0249 and Mean=0.0478
Cont Optimize? (1-Yes, Ø-No) for rotation + X-Y single shift

Level 3
Best Y-change: SD=0.0179 and Mean=0.0372
Best X-change: SD=0.0249 and Mean=0.4787
Cont Optimize? (1-Yes, Ø-No) for rotation + X-Y multiple shift

Level 4
Best Y-change: SD=0.0179 and Mean=0.0372
Best X-change: SD=0.0249 and Mean=0.0478
Optimization Complete

Figure 8 The coded responses as well as the standard deviations and means for the four optimization levels associated with the analysis of the marker points illustrated in Figure 6.

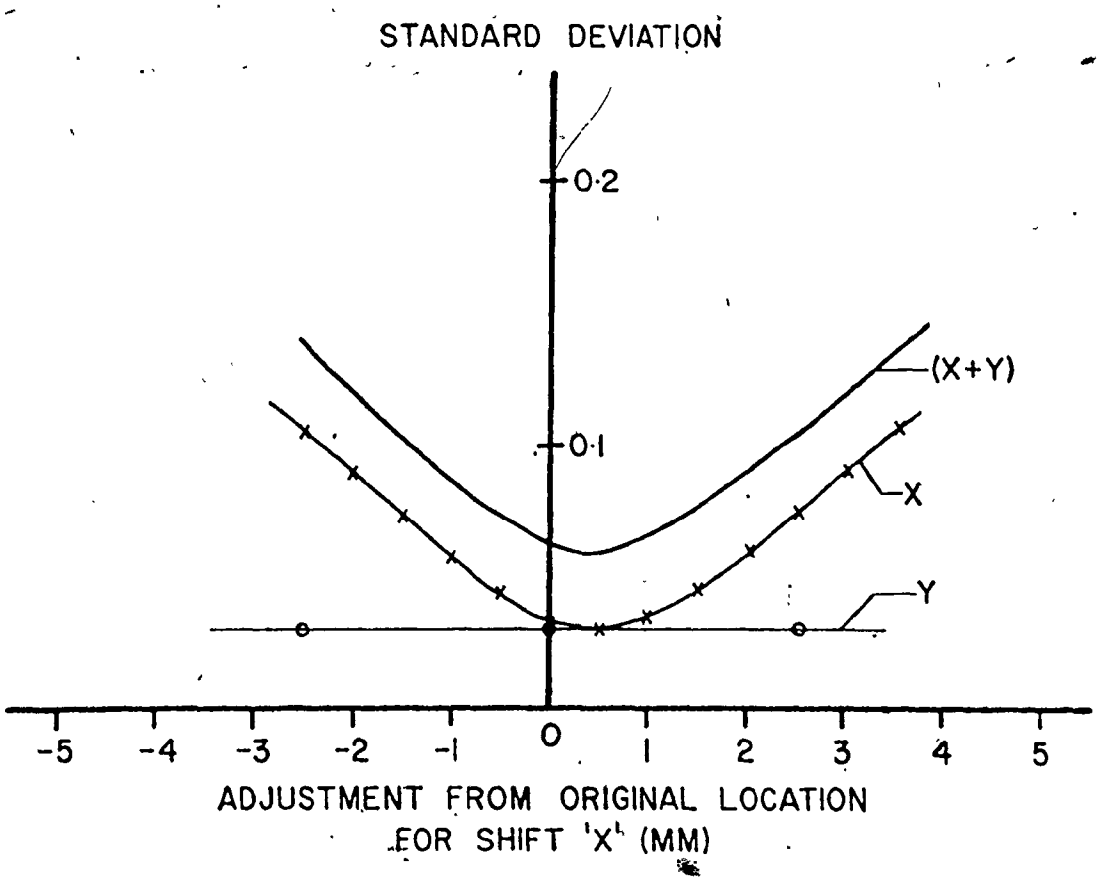

Figure 9 The graph showing the change in the standard deviation for the mean X-dimensional change with incremental shifts along the X-axis from the initial location (origin).

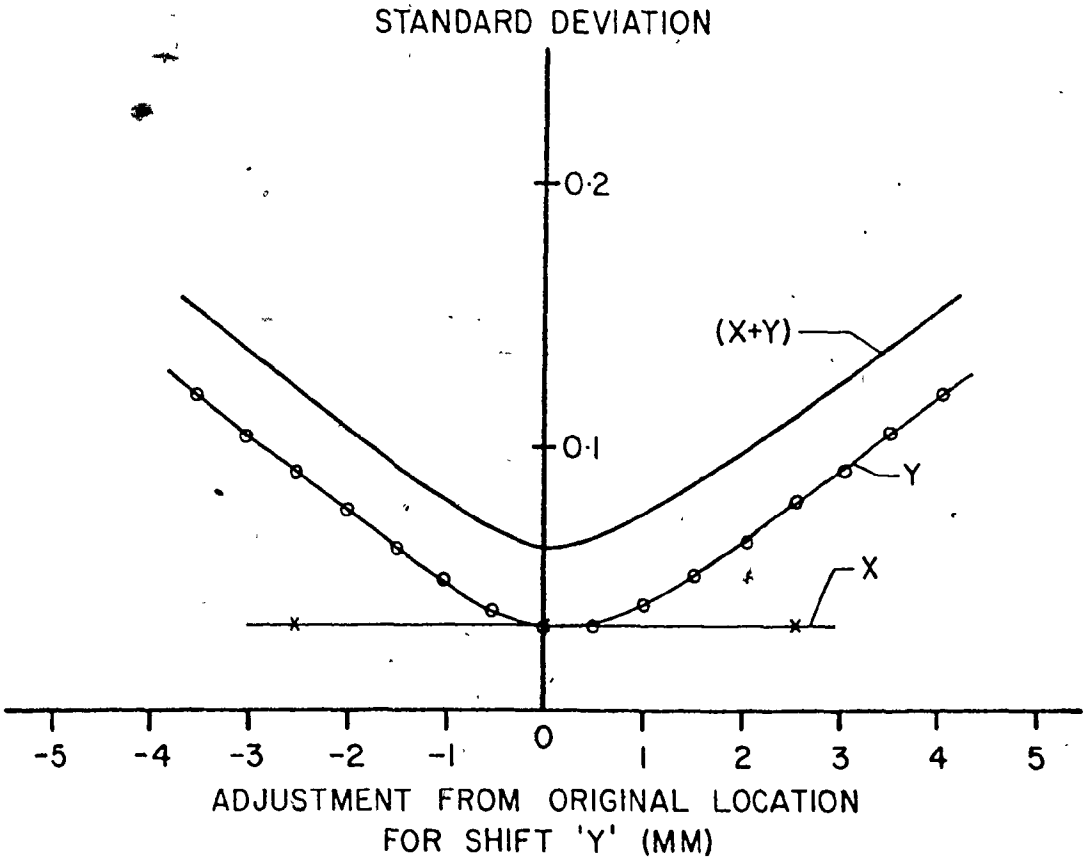

Figure 10 The graph depicting the change in the standard deviation of the mean Y-dimensional change with incremental shifts along the Y axis from the initial location (origin).

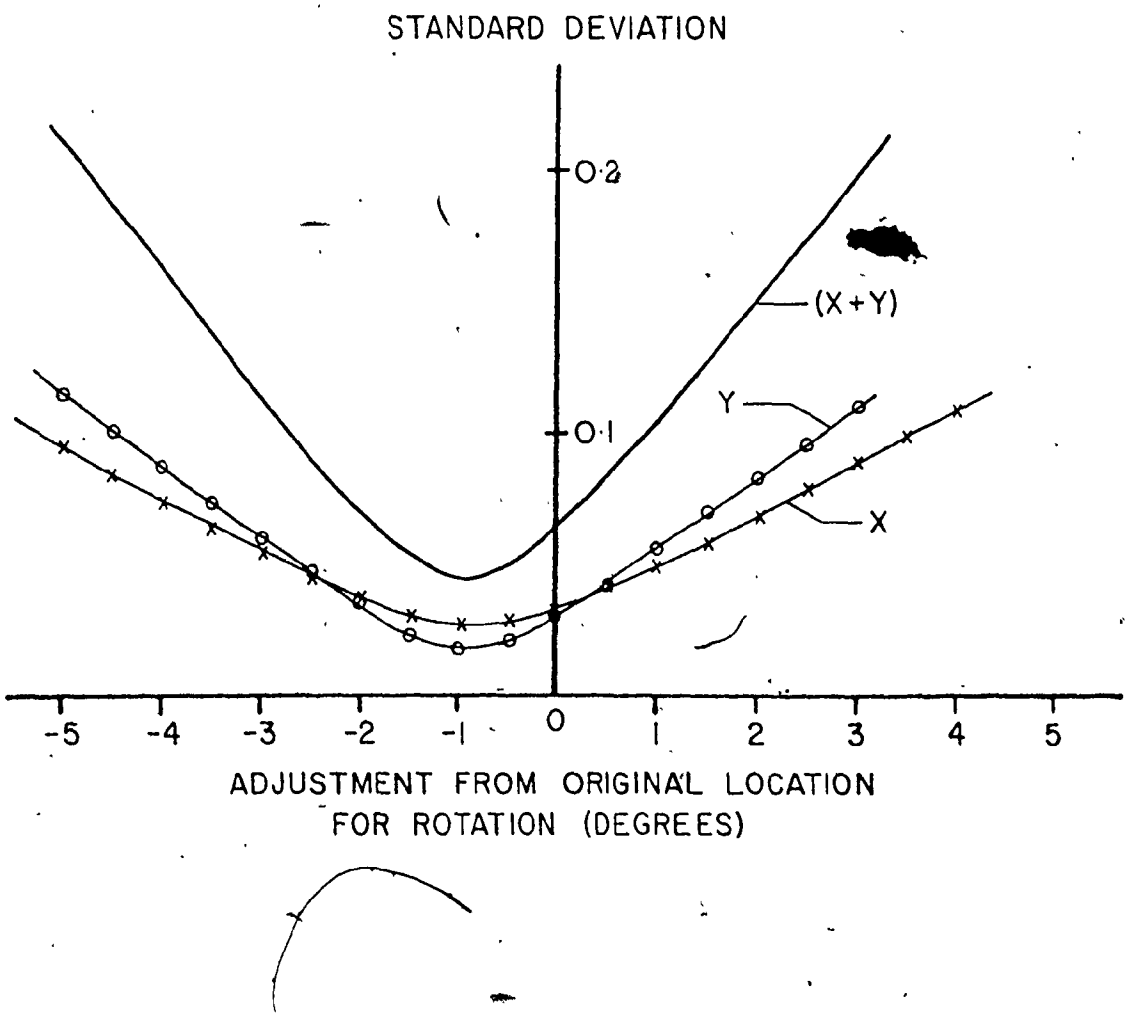

Figure 11 The graph illustrating the change in the standard deviations for the X and Y dimensional changes with incremental rotations about the origin (common point). The positive values represent anti-clockwise rotation from the initial location (origin).

Following output of the standard deviations and means for level 1, the best location in level 2 is determined as indicated by the second series of "PR" responses in Figure 8. The results for the level 2 optimization (Figure 12) are similar to the results for the rotations shown in Figure 11, except that the values for the X standard deviation are decreased slightly. A comparison with the previous best parameters resulted in selection of the provisional array generated in level 2 (as indicated by the second "OR" response) which is then assigned to the optimal array, standard deviations and means. The results for the existing means and stardard deviations are again printed.

The absence of any coded reponses for levels 3 and 4, indicates that the procedure did not identify any further improvements. Although the facility is provided to proceed through four levels of optimization, the analyses of the composites to date have not required progression past level 2.

The coordinates representing the firm location of the wet markers along with the original and amended coordinates for the dry markers are presented previously (subsection 2.4.2) in Table 2. The final results of the Y, X and radial dimensional changes for the optimal location of the numbered markers illustrated in Figure 6 are presented in Table 1. The coordinates for the markers are presented in Table 2.

The values corresponding to the Y, X and radial dimensional changes listed in Table 1 for the original location of the markers, were -4.9% (± 3.13% standard deviation), -5.03% (± 3.37% standard deviation) and -4.61% (± 0.87% standard deviation), respectively. Although the standard deviations for both the X and Y dimensional changes were substantially reduced (0.73 and 0.57 of the original

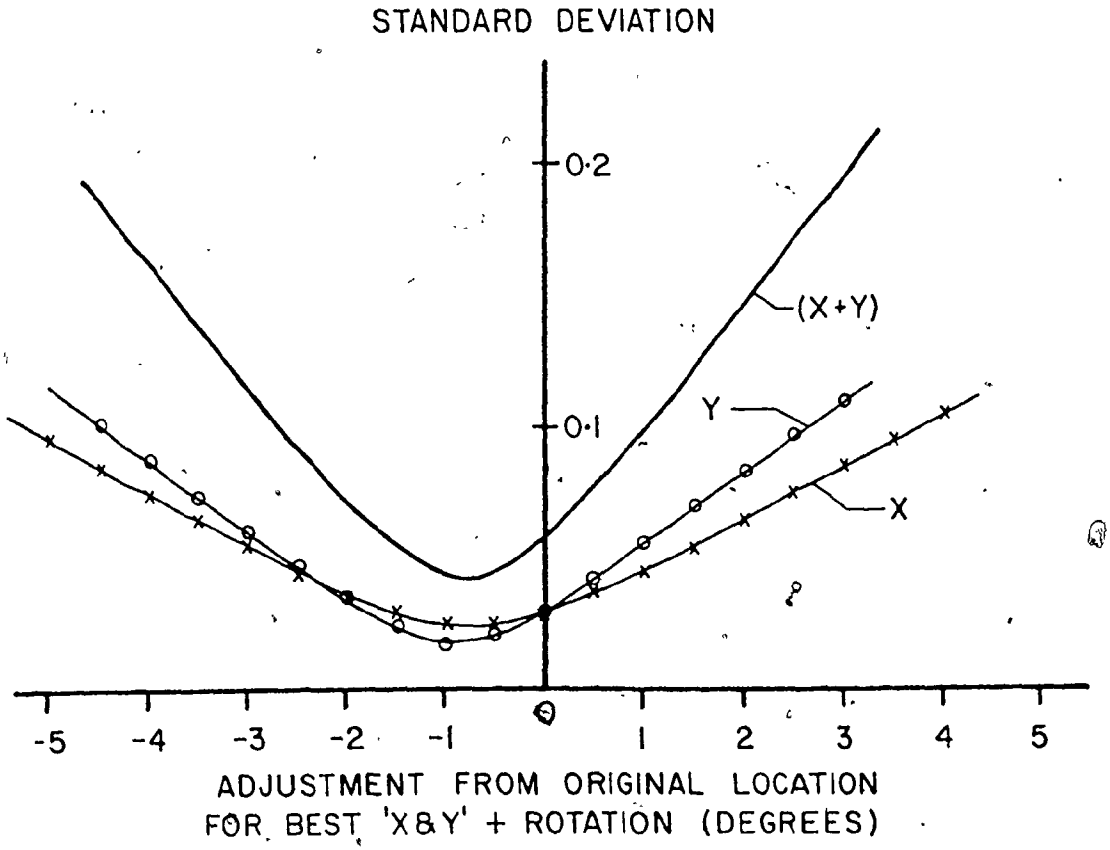

Figure 12 The change in the standard deviations for the X and Y mean dimensional changes for the best X and Y location combined with incremental rotations about the origin (common point). The positive values represent anti-clockwise rotation from the initial location (origin).

N	WET		DRY			
	X	Y	X	AX	Y	AY
1	214.63	102.64	214.63	214.63	102.64	102.64
2	21.80	18.60	20.27	21.10	18.34	17.97
3	11.11	25.17	9.84	10.79	24.92	24.73
4	21.96	54.16	19.43	20.84	41.61	51.25
5	-22.72	46.43	-22.46	-21.19	43.63	44.01
6	-55.47	39.23	-59.92	-51.77	36.70	37.61
7	-63.58	31.59	-60.78	-59.76	28.55	29.60
8	-70.18	31.32	-67.38	-66.37	28.28	29.44
9	-86.26	60.24	-82.94	-81.45	55.93	57.36
10	-112.25	94.46	-107.66	-105.60	88.13	89.98
11	-126.23	100.53	-121.64	-119.49	93.43	95.52
12	-128.90	-53.91	-121.28	-121.71	-54.91	-52.79
13	-111.88	-55.65	-104.26	-104.71	-55.88	-54.06
14	-120.17	-91.74	-112.55	-113.59	-89.69	-87.72
15	-117.10	-101.13	-109.23	-110.44	-99.33	-97.42
16	-76.30	-62.16	-71.22	-71.77	-61.14	-59.89
17	-63.34	-69.50	-58.25	-58.92	-67.71	-66.69
18	-50.44	-42.03	-46.12	-46.34	-42.02	-41.22
19	-13.11	-38.89	-13.37	-13.50	-36.61	-36.38
20	29.33	-46.92	29.32	29.04	-45.14	-45.65
21	35.41	-42.33	35.15	34.95	-40.55	-41.17
22	83.00	-77.26	80.19	79.41	-73.21	-74.60
23	90.36	-76.99	87.30	86.52	-73.44	-74.96
24	55.15	-11.04	52.86	53.18	-10.28	-11.21

Table 2 Listing of the coordinates (millimeters) for the wet markers (original location) and dry markers (original and amended locations), with respect to Marker 1. Marker 1 is the common point whose coordinates represent an arbitrary location.

values respectively), the standard deviation associated with the radial dimensional change did not change. The means associated with each of the standard deviations have not changed appreciably. In most cases, the standard deviation for the optimal location associated with the mean of the radial dimensional changes was less than either of the standard deviations for the mean Y or X dimensional changes.

The final results for 8 of the 9 composites which comprise the complete set for this particular specimen were comparable to the single example described above. The single exception demonstrated a significant amount of asymmetrical shrinkage in the Y direction which probably resulted from local distortion of the tissue.

2.5.4 Discussion

The computer programme has been structured to achieve effectively its tasks of collecting the coordinate points and manipulating the location of the coordinates for the dry specimens in order to determine the optimal position which minimizes the combined sum of the dispersions for the proportional dimensional changes with respect to the X and Y coordinate axes. The program was validated by computing the dimensional changes for the hypothetical wet and dry locations of a set of six points marked on a sheet of graph paper. The locations of the "dry" points represented a known planar-isotropic or planar-orthotropic anisotropic shrinkage. Furthermore, the location of the "dry" markers was purposely shifted and/or rotated an unknown amount in order to portray misalignment between the "wet" and "dry" markers. The computer programme correctly identified the mean dimensional change with respect to the X and Y axes, usually within 1%

deviation and a standard deviation of less than 1%, for all configurations analyzed.

An examination of the graphs (Figures 9, 10, 11 and 12) relating the standard deviation to the incremental change in the location of the dry points reveals that the shape of the curve is parabolic with the vertex (minimum) oriented towards the standard deviation of zero. The curves exhibit four prevalent characteristics:

i) the parabolic shape varies from very broad to moderately narrow.

ii) the axis of symmetry for either or both curves may be offset from the zero point (original location) of the incremental axis.

iii) the axes of symmetry for the curves representing the standard deviations of the X and Y dimensional changes may be displaced from each other.

iv) the magnitude of the vertices (minima) representing the X and Y standard deviations may be substantially different.

The effect of incrementally shifting the location of the dry markers along the X and Y axes (level 1) identifies separate magnitudes and positions of the minima for the standard deviations pertaining to the X or Y dimensional changes. Incremental rotations (level 1) concurrently identify the magnitude and position of the standard deviation minima for the X and Y dimensional changes. Selection of the best location for the X and Y single shift combined with the incremental rotation (level 2) usually tends to reduce the deviation between the axes of symmetry and/or reduce the magnitude of the

vertices which, in effect, reduces the combined sum of the standard deviations for the X and Y dimensional change. This effect is observed with the particular composite presented in Figure 6. Although the deviation between the axes of symmetry (X and Y standard deviations) may be reduced, the offset from the zero point of the incremental axis may remain.

A comparison of the ratio of the Y and X means for the markers in a composite (i.e., the Y dimensional change divided by the X dimensional change), between the original and amended locations for specimens exhibiting both isotropic and anisotropic shrinkage, revealed essentially equal numbers of unaffected, an increase and a decrease. This indicates that the optimization procedure functions independently of the means and does not demonstrate a preference to force the results toward a particular shrinkage pattern.

The capability of identifying planar-orthotropy or planar-anisotropy could yield valuable information about the structure of the tissue which may not be readily apparent. Assessment of tissue for evidence of planar-orthotropy or planar-anisotropy could be accomplished with this computer programme by rotating the X-Y coordinate axis about the common point (the locations of the wet and dry markers remain stationary), and computing the mean and standard deviations for X or Y dimensional changes, as well as the radial dimensional changes at each increment. If the results for both X and Y dimensional changes are reported at each position, then a rotation of 90° from the original location is required. Alternatively, if the results for only the X or Y dimensional changes are reported at each position, then a rotation of 180° is required.

The mean X or Y dimensional changes for planar-isotropic shrinkage would not be expected to change significantly. A series of rotations from the original location to a rotation of 180° in 1° increments executed on the group of six points marked on graph paper with the dry markers adjusted to represent isotropic shrinkage, confirmed that the mean X and Y dimensional changes remained essentially constant.

The mean X or Y dimensional changes for planar-orthotropic or planar-anisotropic shrinkage would be expected to cycle between the extreme values. Concurrently, it would be anticipated that the standard deviation associated with the X or Y extrema would pass through a minimum. Planar-orthotropy would be indicated by a phase difference of 90° between the extrema. A phase difference other than 90° for the extrema would suggest that the shrinkage was anisotropic. Furthermore, the standard deviation for the X or Y dimensional change at the extrema should be less than the standard deviation for the radial dimensional change which represents a diversity of orientations depending upon the polar location of the markers. A similar series of rotations (original to 180° in 1° increments) for a set of six points marked on graph paper, with the dry markers adjusted to represent 20% shrinkage along the X axis and 10% shrinkage along the Y axis, corroborated both the phase difference of 90° for the extrema of the X or Y mean and standard deviation, as well as the lower value for the X or Y standard deviation as compared to the radial standard deviation. Moreover, it was evident that the minima for the X or Y standard deviation is an important indicator of the extrema since transients were evident at the intermediate positions beween the extrema during the transposition of the X or Y mean dimensional changes. These

transients appear to be related to marker points which are being approached by the coordinate axis but are not sufficiently close to be excluded from the computation of the dimensional changes.

In order to evaluate the effectiveness of the program if the initial orientation of the X and/or Y axes did not align with the extrema of unequal shrinkage, the composite representing the 6 points referred to in the preceeding example was rotated 30° and digitization of the markers repeated. The optimization procedure (levels 1 and 2 only) successfully selected a best location. Evaluation of the results for a series of rotational increments (0° to 180° at 1° increments) identified two extrema with magnitudes within 1% of the anticipated values but with a phase difference of about 60° rather than the actual value of 90°. Users should be aware of this anomaly and if anisotropy is suspected along an axis which deviates substantially from the X or Y coordinate axes, then the composite may be rotated to achieve alignment and the analysis repeated, or the points may be adjusted to a new X-Y axes with the use of Special Function Key f_8 and the analysis repeated.

2.5.5 Summary

The process of dehydration and drying associated with the preparation of tissue specimens for examination by the scanning electron microscope usually results in dimensional changes in the form of shrinkage. A new method has been devised which requires specification of the new location of marker points which have been affixed in a random pattern to the surface of the specimen. A new computer programme has been developed which acquires the coordinate

pairs of the marker points, optimizes the alignment between the location of the marker points for the wet (fresh or fixed) and processed (dehydration with an intermediate fluid, and/or drying) conditions of the specimens, and computes the proportional dimensional changes in two mutually-perpendicular directions, as well as along the direct path between the origin and each of the marker points. Techniques for using the programme to assess whether the shrinkage may be planar-orthotropic or planar-anisotropic are suggested.

2.6 Dimensional Changes of the Internal Elastic Lamina During Drying

2.6.1 Introduction

The dehydration (substitution of the water with an intermediate fluid) and drying procedures associated with the preparation of tissue for examination by scanning electron microscopy, usually result in dimensional changes in the form of shrinkage. These changes have been shown to vary with the type of tissue (Boyde et al, 1977) as well as the drying technique (Boyde et al, 1977; McGarvey et al, 1980). Consequently, the dimensional changes, if severe, may result in misleading or invalid interpretation of tissue form and structure. Similarly, the quantitative description of the form and structure will be inaccurate.

There are numerous studies which have used the scanning electron microscope to examine the surface of arteries. However, only two studies (McGarvey et al, 1980 and Grut et al, 1977) have investigated the dimensional changes associated with the shrinkage of components comprising the arterial wall. The study by Grut et al (1977) used a micrometer to assess the change in dimensions of purified aortic

elastin and found that the cross-sectional shrinkage of the freeze-dried specimens was zero whereas the shrinkage for air-drying was 60%. Grut et al (1977) did not present any data to verify the reliability or precision of the technique.

McGarvey et al (1980), compared the dimensions, of individual endothelial cells from plastic casts with measurements made from photomicrographs obtained with the scanning electron microscope. Shrinkage was found to occur with all of the drying methods. They also observed substantial differences in shrinkage for some of the drying methods between the longitudinal and circumferential directions in both the abdominal and thoracic regions of the aorta. The authors assumed that the shrinkage of the Batson's casting material was essentially negligble, based upon the previous study by Reidy and Levesque (1977). However, Legg and Gow (1981) have reported a volumetric shrinkage of 16 % for the Batson's resin. This would represent a linear shrinkage of about 5.6 % (assuming isotropic shrinkage) which does not account for the variation in shrinkage between the longitudinal and cirumferential directions reported by McGarvey et al (1980). Nevertheless, a consistent differential shrinkage between the longitudinal and circumferential directions of the cast could explain this variation but would not explain the absence of variation for the remaining drying methods.

Since it is of interest to measure the form and structure of fenestrations in the internal elastic lamina from human intracranial arteries with the use of the scanning electron microscope, it was decided to determine the tissue shrinkage in the plane of observation. Freeze-drying was selected for the tissue since Boyde et al (1977)

recommended it as the method of choice, and Grut et al (1977) reported negligible shrinkage for purified porcine elastin after freeze-drying. The primary objectives of the study to be presented were:-

i) to assess whether the net shrinkage is related to the outside diameter of the artery;

ii) to determine a net linear shrinkage associated with the internal elastic lamina from cerebral arteries of various outside diameters;

iii) to assess whether the circumferential and/or longitudinal shrinkage(s) is(are) related to the outside diameter of the artery;

iv) to compare the relative circumferential and longitudinal shrinkages (planar-orthotropic shrinkage).

v) to compare the shrinkage of the cork backing with the tissue shrinkage.

vi) to evaluate whether the tissue exhibits planar-anisotropic shrinkage (i.e., whether any directional difference in shrinkage are non-orthogonal).

vii) to compare the effect of freeze-drying with critical point drying.

viii) to compare the shrinkage (freeze-drying) at bifurcations with the cylindrical portion of the artery.

2.6.2 Methods

Cerebral arteries (designated series I) were obtained at autopsy in situ from a 64-year old male. Subsequently, the complete circle of Willis and larger peripheral branches were carefully removed in toto

and stored at 4°C in isotonic saline for not more than 17 days.

Straight cylindrical segments were isolated from the arterial tree. The external diameter of the non-pressurized artery was determined with the aid of two transverse measurements, approximately perpendicular to each other, while the artery was immersed in saline. The specimen was next sectioned longitudinally along one side. Finally, each specimen was floated on to a cork backing, spread and pinned along the longitudinal edges, as illustrated in Figure 13, in an unstretched condition with the adventitial surface exposed. Specimens less than 0.6 mm in diameter could not be obtained since suitable micro-surgical instruments for performing the longitudinal sectioning were not available.

The specimens were next treated to remove the adventitia and smooth muscle coats by a method similar to that of Steven et al (1974). The pinned specimens were placed in a solution of NaOH maintained at a concentration of 0.1 N by periodically replenishing the evaporated water, for 70 minutes, at a temperature of 75°C. This temperature was selected after several previous trials demonstrated that treatment at 100°C as recommended in other publications, resulted in an apparent temporary contraction (until removal of the media and adventitia was complete) of the specimen followed by detachment from the pins. Moreover, treatment below a temperature of 65° did not satisfactorily remove the covering tissue. Seventy minutes of sodium hydroxide treatment was found adequate to ensure removal of the smooth muscle and collagen. These specimens were then neutralized by processing through five minutes 0.1 N NaOH (room temperature), five minutes distilled water, two minutes 0.1 N HCl and five minutes isotonic saline. The

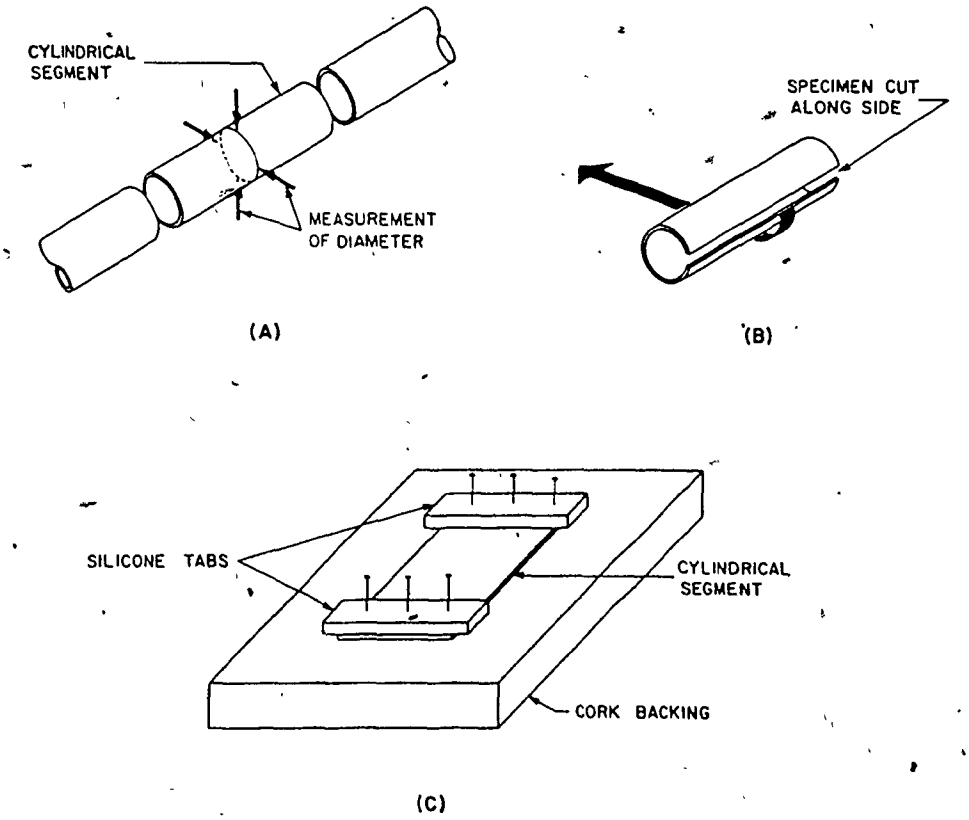

Figure 13 Preparation and mounting of the specimens on on the cork backing.

A - Specimen is isolated from the arterial tree and the diameter measured.

B - Sectioning of the specimen along the lateral border.

C - The specimen pinned in place with the adventitial surface exposed.

specimens were fixed in phosphate buffered 2.5% glutaraldehyde for a minimum of 48 hours.

The process of freeze-drying consisted of first immersing the specimen in distilled water for one hour. Upon removal, excess water was eliminated and the specimens were stored overnight in a freezer maintained at -15°C. Subsequently, the tissue was placed in a Virtis, Model # 10-030 Freeze Drier at -50°C and 0.1 torr for three hours.

The method for assessing the dimensional changes has been detailed previously in sections 2.4 and 2.5 (Campbell and Roach 1981b, Campbell 1982). Typically, about nine composites were created for each specimen; except for the very small diameter specimens, in which case, only three composites or less were possible due to the small size of the specimen. An average shrinkage for each specimen was determined from the set of composites by calculating a weighted mean based upon the number of markers for each composite. In total, 138 composites were compiled and analyzed from 19 specimens (series I) of various outside diameters (0.6 mm to 4.5 mm).

In order to assess the comparative shrinkage of the cork backing, two specimens of the cork backing were processed according to the same procedure described previously for the tissue, freeze-dried and the shrinkage measured. Planar-anisotropy (different properties in different directions for the plane of observation) was evaluated for only two specimens from series I by computing the results for the proportional dimensional changes along the X axis in increments of 1° from the initial orientation of the mutually perpendicular axes to a rotation of 180°. The terms planar-isotropy, planar-orthotropy and planar-anisotropy will be used throughout, since the shrinkage is

determined only for the plane of observation (i.e., shrinkage of the thickness is not measured).

This technique could not be used to determine the dimensional changes following critical point drying because the cyanoacrylate adhesive was dissolved by the acetone. Nevertheless, the presence of round fenestrations in the internal elastic lamina allowed the measurements of their diameter and density with a subsequent comparison of the results. Adjacent segments from two sets of specimens, prepared according to the preceding procedure for freeze-drying, were freeze-dried and critical point dried. The fenestrations depicted in the photomicrographs obtained with the scanning electron microscope were measured for each of the six specimens. The mean values for the diameters and densities were compared.

Two specimens at the bifurcation from human cerebral arteries were isolated, sectioned along the longitudinal borders and treated according to the process described above. The procedure for assessing the shrinkage (freeze-drying) was again applied. The orientation of "longitudinal" followed the external curvature of the apex while the "circumferential" direction was across the saddle of the apex.

2.6.3 Results

i) Regression of net linear shrinkage with outside diameter of the artery.

The results for the radial shrinkage of series I specimens are presented as a scattergram in Figure 14. The coefficient of determination (r^2) for a least squares linear regression was 0.0016, which indicates that only 0.16% of the variation in shrinkage

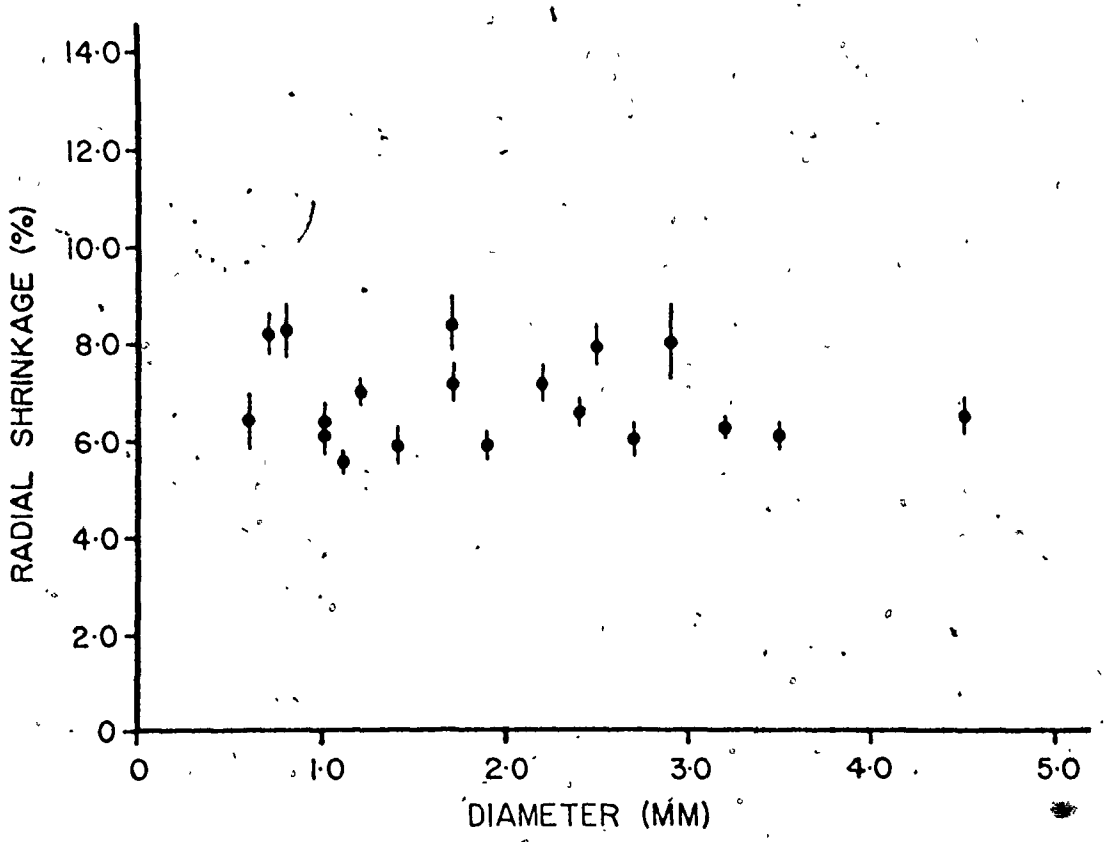

Figure 14 Scattergram of linear radial shrinkage for the range of arterial diameters in Series I (freeze-dried). Error bars represent ± 1 SEM.

is accounted for by the fitted regression. Similarly, testing (Zar, 1974 pg. 239) at the 95% confidence level failed to confirm that the value of 0.04 for the correlation coefficient (r) was significant. Moreover, particular non-linear relations were not evident. Accordingly, it has been concluded that the radial shrinkage does not depend upon the diameter of the artery.

ii) Net linear shrinkage

It has been shown in i) above that the radial shrinkage is independent of the external diameter of the artery. Consequently, a mean value of 6.9% $\pm$ 0.21% SEM has been computed from the specimens to represent the net linear shrinkage of the internal elastic lamina.

iii) Regression of circumferential and longitudinal shrinkage with external diameter of the artery

The scattergrams representing the shrinkage in the circumferential and longitudinal directions for the specimens from series I are presented in Figures 15 and 16, respectively. The coefficients of determination (linear regression) between the shrinkage and outside diameter was 0.13 for the circumferential shrinkage and 0.05 for the longitudinal shrinkage. Testing of the correlation coefficients (0.36 for circumferential and 0.22 for longitudinal) at the 5% level of significance failed to confirm the significance of a linear relationship for either shrinkage. As well, particular non-linear relationships were not evident. The results indicate that the shrinkages are essentially constant regardless of the external diameter of the artery.

iv) Relative circumferential and longitudinal shrinkage (planar-orthotropy)

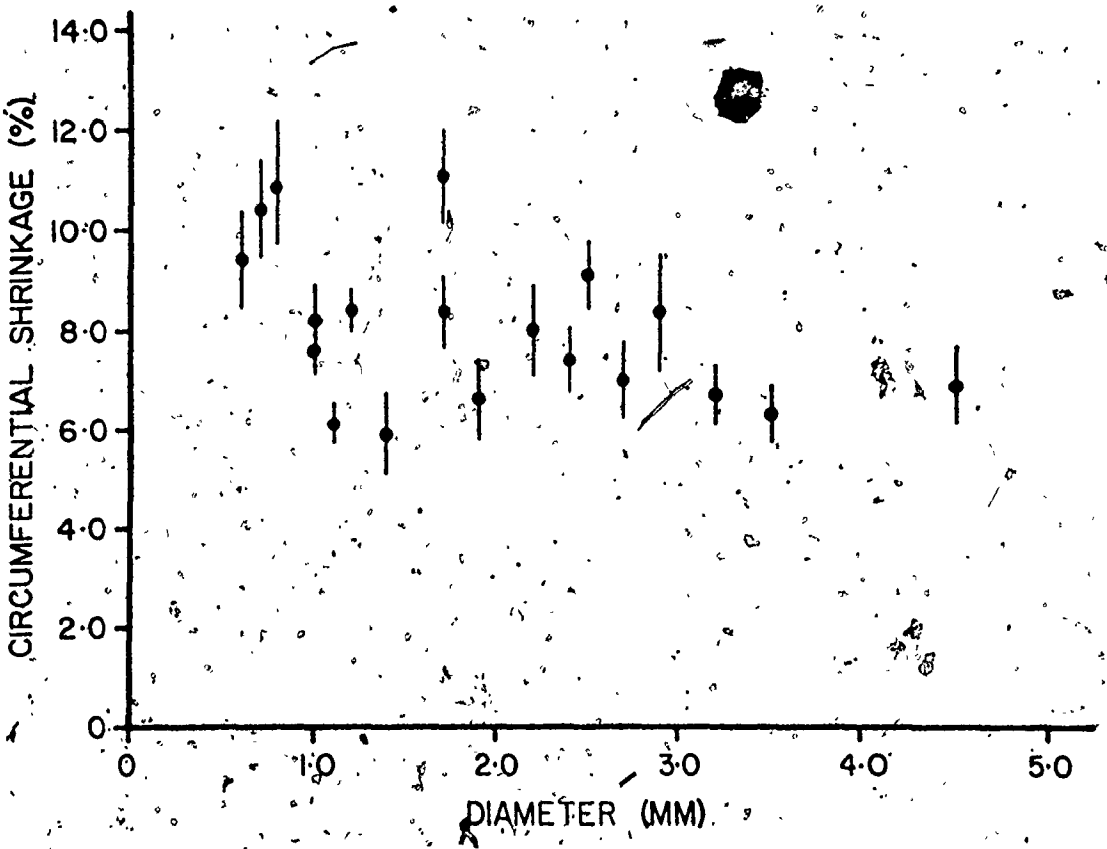

Figure 15 Scattergram of the linear circumferential shrinkage for the range of arterial diameters presented in Figure 14. Error bars represent ± 1 SEM.

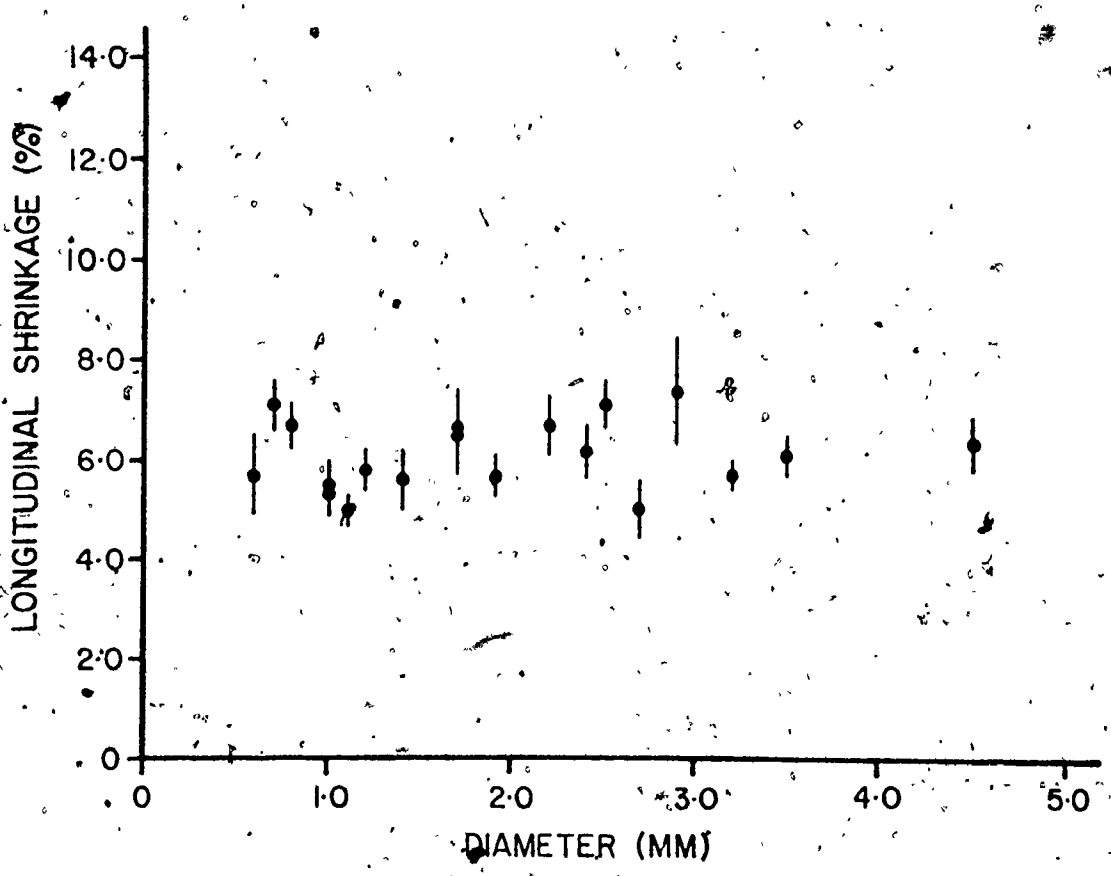

Figure 16 Scattergram of the linear longitudinal shrinkage for the range of arterial diameters presented in Figure 14. Error bars represent ± 1 SEM.

A comparison of the relative circumferential and longitudinal shrinkages (series I) revealed that the circumferential shrinkage exceeded the longitudinal shrinkage for each of the 19 specimens. Moreover, the mean value for the circumferential shrinkage (8.0% ± 0.36% SEM) was slightly greater than the mean for the longitudinal shrinkage (6.1% ± 0.16% SEM). Since the circumferential and longitudinal shrinkages were determined for each specimen (i.e., a paired condition) a paired-sample "t" test was computed for each individual specimen, as well as the separately pooled circumferential and longitudinal shrinkages for the group of 19 specimens. The results for both the individual specimens and the pooled values failed to confirm that the differences were significant at the 95% level of confidence. Consequently, it has been concluded that the shrinkage of the tissue does not demonstrate planar-orthotropy.

v) Shrinkage of the cork backing

The mean radial shrinkage for the cork was computed to be 3.3% ±0.67% SEM. The comparison for orthogonal directions revealed that the shrinkage was planar-isotropic. A two-sample "t" test between the radial shrinkage for the freeze-dried specimens from series I and the cork revealed a significant difference ($p < 0.001$) which verifies that the shrinkage of the cork would not influence the measurement of the shrinkage of the tissue.

vi) Planar-anisotropy

Assessment of the composites for two tissue specimens revealed that the standard deviation for the shrinkage passed through two minima that corresponded closely with the circumferential and longitudinal directions of the arteries. The mean shrinkage and standard deviations

demonstrated variable results at the intermediate positions between the longitudinal and circumferential orientations. This variability appears to be affected by the proximity of marker points to the rotating axis as well as local irregularity of the shrinkage. Nevertheless, in almost every instance the standard deviation of the radial shrinkage was typically less than the standard deviation for either the longitudinal or circumferential shrinkage. This result is consistent with a tissue or material that exhibits planar-isotropic shrinkage.

vii) Bifurcation specimens

The mean radial, circumferential and longitudinal shrinkages for the bifurcation specimens were 5.2% $\pm$0.25% SEM, 5.4% $\pm$ 0.39% SEM, and 4.6% $\pm$ 0.21% SEM respectively. A comparison (t-test) between the cylindrical and bifurcation specimens for radial shrinkage did not reveal a significant difference. ($p > 0.05$).

viii) Critical point drying

The statistical comparison (two sample t-test) of the results for the two sets of adjacent specimens did not reveal a significant difference ($p > 0.1$) for either of the two sets of specimens.

2.6.4 Discussion

This study has demonstrated that there is limited shrinkage associated with the freeze-drying of isolated internal elastic lamina from human cerebral arteries. The value of 6.9% that has been computed for the linear shrinkage compares favourably with the net linear shrinkage of 4.5% (Boyde and Franc, 1981) for freeze-dried mouse livers. Furthermore, this study has confirmed that the radial

shrinkage of the internal elastic lamina is independent of the diameter of the artery.

Although the consistent difference (19 of 19) between the circumferential and longtudinal shrinkages has not been shown to be statistically significant, it was considered a matter of interest to investigate whether pinning along the circumferential borders rather than the longitudinal borders of the specimen could influence the shrinkage. A second series of four specimens (designated series II) from the circle of Willis of a 38-year old male was prepared and analyzed according to the procedure presented previously, except that the circumferential borders were pinned.

Each of the four specimens demonstrated less circumferential shrinkage (mean 4.4% $\pm$ 0.3% SEM) than longitudinal shrinkage (mean of 5.8% $\pm$ 0.08% SEM) which is the converse of the results for series I. The paired-sample "t" test computed for the shrinkages of the four specimens indicated that the difference was not significant at the 95% confidence level.

The difference between series I and II for the circumferential shrinkage of the specimens with similar external diameters was confirmed statistically by the two-sample "t" test ($p < 0.001$). A similar comparison between the longitudinal shrinkages for series I and II did not substantiate a difference ($p > 0.2$). As a consequence of the distinct reduction for the circumferential shrinkage between series I and II, the difference for the mean radial shrinkage between series I (6.9% $\pm$ 0.21% SEM) and series II (5.3% $\pm$ 0.12% SEM) was also verified by the two-sample "t" test ($p < 0.02$). Therefore, the results for series I and II could not be pooled. The apparent reversal in the

pattern of the relative circumferential and longitudinal shrinkages when the circumferential rather than the longitudinal borders were pinned, implies that the pinning technique may have an effect on the shrinkage, although this study did not attempt to determine whether the age difference between the donors could also influence the results.

The lack of statistical confirmation that the planar shrinkage varies with direction indicates that the tissue has behaved, macroscopically, as a homogeneous planar-isotropic material. This statement does not imply that the other properties (e.g., tensile) of the internal elastic lamina will also behave accordingly.

Since the tissue has been characterized as planar-isotropic, a single correction factor,

$$C = \frac{100}{100-S}$$

where: C = correction factor

S = radial shrinkage (%)

can be applied to distinct features in order to account for the shrinkage. The relationship for instituting this correction factor may be expressed as:

$$Y = XC^q \qquad (3)$$

where: Y = corrected variable

X = raw value of variable

q = 1 for correction of a linear measurement

2 for correction of an area measurement

If the three-dimensional shrinkage is verified to be isotropic, then a value of 3 may be substituted for "q" in both the preceding and

succeeding equations. The precision associated with any variable modified by the correction factor must be computed by the relationship (Barford 1967):-

$$D_y = Y \left[\frac{u D_x^2}{(u-1) X^2} + \frac{q^2 w D_s^2}{(w-1) S^2} \right]^{1/2}$$

where: D_y = standard deviation of corrected variable

u = number of data points for variable

D_x = standard deviation of variable

w = number of data points for correction factor

D_s = standard deviation of correction factor

The absence of a statistically significant difference between the freeze-dried and critical point dried specimens indicates that the shrinkage for both methods is essentially equivalent for this tissue.

The comparison of the shrinkage in the cylindrical segments with respect to the apex of the bifurcations did not reveal any difference. Moreover, the results for the circumferential and longitudinal directions at the apex were comparable which indicates isotropic shrinkage.

2.6.5 Summary

The shrinkage associated with the freeze-drying of the internal elastic lamina isolated from the human cerebral arteries of various outside diameters has been assessed with the use of the new technique. The net linear shrinkage for freeze-drying remains essentially constant

at 6.9% ± 0.21% SEM regardless of the outside diameter of the artery. A comparison of the shrinkage between the circumferential and the longitudinal orientations of the tissue did not reveal a statistically significant difference which means that the shrinkage is planar-isotropic. The shrinkage attributable to critical point drying was indistinguishable from the shrinkage for freeze-drying. There was no difference in shrinkage between the cylindrical and bifurcation specimens.

Chapter 3

FENESTRATIONS IN THE INTERNAL ELASTIC LAMINA OF HUMAN CEREBRAL ARTERIES

3.1 Introduction

The basic organization of the wall of all arteries is similar in that three concentric layers (or tunica) can be distinguished: i) an inner layer (tunica intima) on the luminal side; ii) the intermediate layer (tunica media); and iii) the outer coat (tunica adventitia). The boundary between the tunica intima and tunica media is demarked by the internal elastic lamina. A thinner external elastic lamina between the tunica media and adventia can also be found in many arteries.

The formation of an artery starts with the mesenchymal cells in the periphery of the developing endothelial tube becoming arranged to loosely ring the tube. The mesenchymal cells differentiate into a cell with characteristics resembling a smooth muscle cell. It is this type of cell that produces the elastin and probably the other intercellular substances in the intima and media of a developing artery. Electron microscopic studies have shown elastin in a developing aorta is recognized as bands of homogeneous material that are located close to developing smooth muscle cells. Microfibrils (110 Å in diameter) projecting from the developing smooth muscle cells are arranged in swathes. The presumed role for the microfibrils is to serve as guides or molds for the elastin deposits. The mechanisms which determine the shape and structure of the arterial wall are not well understood.

The chapter which follows will present a brief review of the existing information on the various components of the arterial wall with specific reference to cerebral arteries as well as an examination

with the scanning electron microscope of the layers which constitute the arterial wall. A method which incorporates the concept of ligament efficiency for modelling the spatial geometry of the fenestrations in the internal elastic lamina will also be introduced and evaluated. The final section of the chapter examines a group of parameters which characterize the fenestrations in the internal elastic lamina from cylindrical segments of the arterial tree with a range of external diameters.

3.2 Structure of the Arterial Wall

3.2.1 Intima

The innermost (luminal) layer of the artery consists of a tube of endothelial cells with their long axes generally aligned longitudinally. The endothelial cells are attached to a subendothelial layer of delicate fibroelastic connective tissue. It has been shown that the orientation of the longitudinal axes of the endothelial cell border and nuclei correspond with the direction of flow (Flaherty et al 1972). This observation has been used to determine the flow pattern in the bifurcation region (Langille and Adamson, 1981).

3.2.2 Elastin and Elastic Lamellae

It is widely recognized that most elastic and muscular arteries contain multiple layers of elastic tissue. The innermost layer (internal elastic lamina) is a continuous sheet of elastin, perforated by an array of small round holes or fenestrations. The fenestrations are assumed to function as ports through which all substances can diffuse to nourish cells deep within the media. However, it has been

postulated by Ham and Cormack (1974, pg 570) that the fenestrations would also permit the growth of the lamina by depositing elastin on the inner surface of the holes as they are stretched during growth.

Previous studies using the scanning electron microscope have examined the luminal surface of the human aorta (Albert and Nayak, 1976) as well as the medial laminae after digestion (Carnes et al 1977). Berry (1973) has examined the elastic structure at arterial branches and bifurcations and discovered two patterns: i) insertion of the elastic lamellae into an irregular raphe where the lamellae of the branch originate; and ii) individual lamellar units are reduced by fusing with each other. Cook et al (1975) examined the elasticity of the internal elastic lamina from the external iliac artery by measuring the changes in the shape of fenestrations in the intact artery.

Biochemical and histochemical studies to determine the composition of elastin are reported in the review articles by Sandberg (1976) and Ayer (1964). Steven et al (1974) also investigated the biochemical structure of elastin along with the stress-strain characteristics. Carton et al (1962) measured the elastic properties of single elastic fibres. The dynamic mechanical properties of water-swollen elastin under physiological conditions have been investigated by Gosline and French (1979).

Most of the studies mentioned above were conducted on either whole or digested segments of the fibrous bovine ligamentum nuchae or the elastic lamellae of the aorta isolated by chemical digestion. Very little research has been specifically directed towards determining

the form and structure, and mechanical characteristics of the internal elastic lamina.

3.2.3 Media

The smooth muscle cells which constitute a major portion of the media are arranged in a helical pattern (Walmsley and Canham, 1979). The muscle cells are embedded in a moderately thick layer of glycoprotein substructure. Buried within this matrix are small bundles of collagen fibrils corresponding to a network of delicate reticular fibres. The smooth muscle cells can exist in a state of partial contraction but this tone may be modulated to produce a constriction or dilatation in order to influence the flow of blood as well as blood pressure (Ham and Cormack 1974, pg 549) probably at the arteriolar level.

3.2.4 Adventitia

Fibroblasts, strands of elastin and bundles of collagen fibres are found in the adventitia. The loose consistency of this layer along with the predominant longitudinal orientation of the components do not inhibit the pulsatile fluctuations in the diameter of the artery but restrict the retraction when the artery is cut (Bloom and Fawcett, 1975). Smith et al (1981) have shown that the principal orientation for the collagen in the deep layers of the adventia is circumferential.

3.3 Scanning Electron Microscope Examination of the Cerebral Artery

3.3.1 Introduction

Cerebral arteries are classified as either muscular or

distributing arteries since their tunica media consists primarily of smooth muscle which can actively alter the diameter of the vessel. The unique feature of cerebral arteries is the singular elastic lamina and a thin wall. Occasionally, the internal elastic lamina is duplicated (i.e. layered) which is usually described as a split internal elastic lamina. The only evidence of an external elastic lamina is a fibrous mesh (Merei et al, 1980b).

An analysis of the microstructural components by Moritake et al, (1981) demonstrated a lower porportion of elastin content in cerebral arteries than extracranial arteries. Furthermore, the relative proportion of collagen to elastin was substantially greater for cerebral than extracerebral arteries. The relative proportion of collagen to elastin for the age group over 50 was significantly greater than the under 50 age group which is consistent with the findings for other arteries.

Klassen et al (1968) observed thickening of the intima, internal elastic lamina, and "branching side pads" for cerebral arteries with increasing age. Thickening of the internal elastic lamina with increasing age was also reported by Hassler (1962). Velican (1970) and Imaizumi et al (1975) have reported on the histochemical changes in the constituents of cerebral arteries. Enzymatic treatments applied to cerebral arteries (Damude et al, 1977) which were shown to have removed either the microfibrils or all the elastin of the cerebral wall, progressively affected the elastance (i.e. slope of the tension-strain curve at the origin, indicative of the behaviour of elastin) with successively longer periods of perfusion.

The mechanical properties of intact cerebral arteries have been assessed by Nagasawa et al (1979), and Hayashi et al (1980a, 1980b). The consensus of the authors was that intracranial arteries were stiffer than extracranial arteries while the stiffness generally increased with age but the trends of the elastic properties were not uniform with age.

Examination of the structural components of the arterial wall has been confined mainly to the endothelial surface of cerebral arteries since techniques for the selective isolation of the desired tissue within the wall had not been adequately developed. Succeeding sections will present photomicrographs of the various layers, with particular emphasis directed towards the internal elastic lamina.

3.3.2 Description of Form and Structure

During the process of preparing and examining a large number of specimens for the assessment of the treatment procedures discussed previously in section 2.3, some specimens presented a unique opportunity to describe the various components of the wall of human cerebral arteries. The luminal surface of the wall is shown in Figure 17. The oval humps are believed to be the endothelial nuclei with their long axes oriented in the direction of the blood flow. No tissue treatments were applied to the specimen prior to fixation.

Following the treatment of tissue with sodium hydroxide, three layers of tissue remain; viz. the subendoethelial area or basement membrane, internal elastic lamina, and fibrous mesh. These layers are illustrated in Figure 18. The basement membrane is a continuous sheet

2

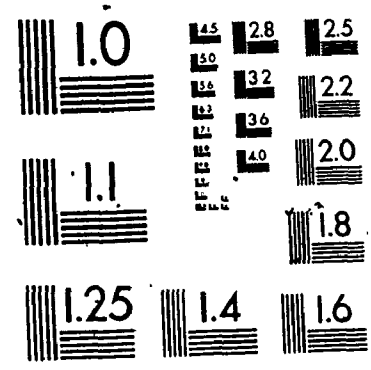

Figure 17 Endothelium of cerebral arteries. Horizontal field of view represents 0.45 mm.

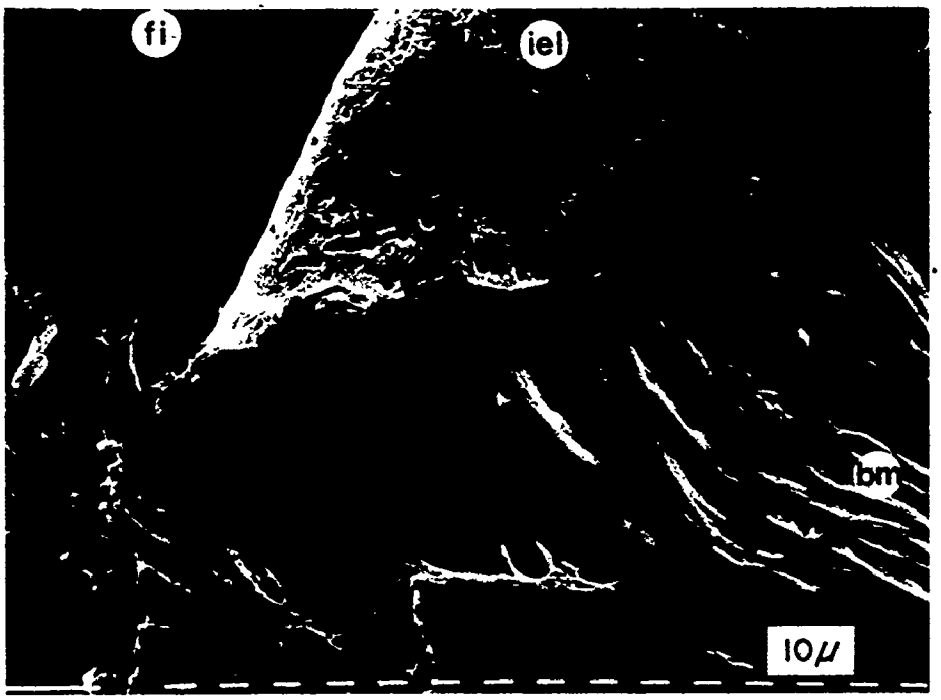

Figure 18 The tissues isolated after treatment of the cerebral artery with sodium hydroxide. Luminal surface is right portion of photomicrograph. fi = fibrous tissue, iel = internal elastic lamina, bm = basement membrane. Short white bars represent 10 μm.

penetrated by very small fenestrations (Figure 19). This tissue layer obscures the larger fenestrations evident in the internal elastic lamina, although the outlines of the fenestrations are indicated by the slight depressions evident in Figure 19. The luminal surface of the internal elastic lamina shown in Figure 20 has a stippled appearance with distinct fenestrations. The same fenestrations in the luminal surface are also evident in the external surface (Figure 21), although the texture of the tissue is much smoother on the external side. It is particularly interesting that the predominant structure of the internal elastic lamina is a continuous sheet of tissue with only a minor indication of a fibrous component.

The external surface was covered in some regions by a fine fibrous debris (Figure 22) which has been identified as elastin buried within the media and adventitia.

The internal elastic lamina shown on the left of Figure 23 has been reflected to reveal the underlying media. The smooth muscle cells appear to be arranged in parallel rows. Figure 24 provides a higher magnification of the smooth muscle cells surrounded by the ground substance. Both specimens were treated with guanidine hydrochloride prior to fixation.

The adventitia (Figure 25) is characterized as an array of fibres whose orientation was not analyzed.

3.3.3 Discussion

Collectively, the various components form the wall of the artery and determine the mechanical characteristics. The functions of the

Figure 19 Luminal surface of the basement membrane from cerebral arteries. Horizontal field of view represents 0.055 mm.

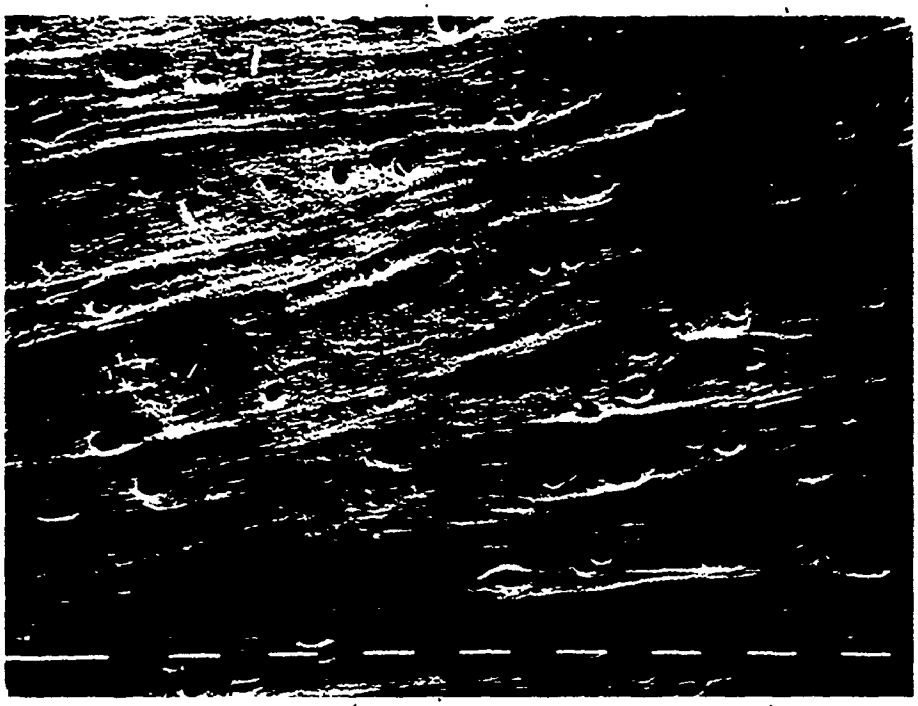

Figure 20 Luminal surface of the internal elastic lamina from cerebral arteries. Short white bars represent 10 μm.

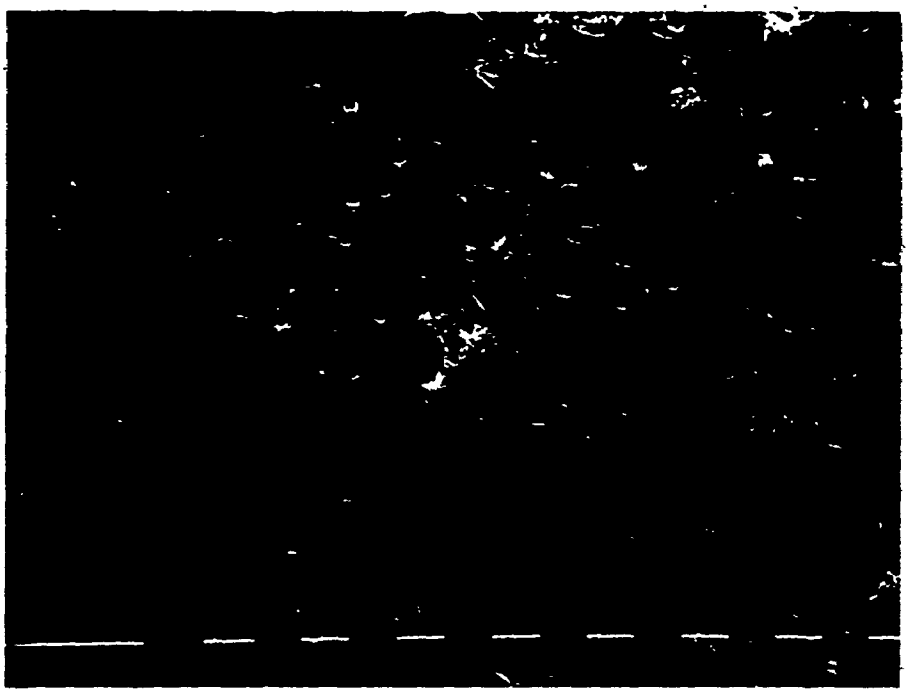

Figure 21 External surface of the internal elastic lamina from cerebral arteries. Short white bars represent 10 μm.

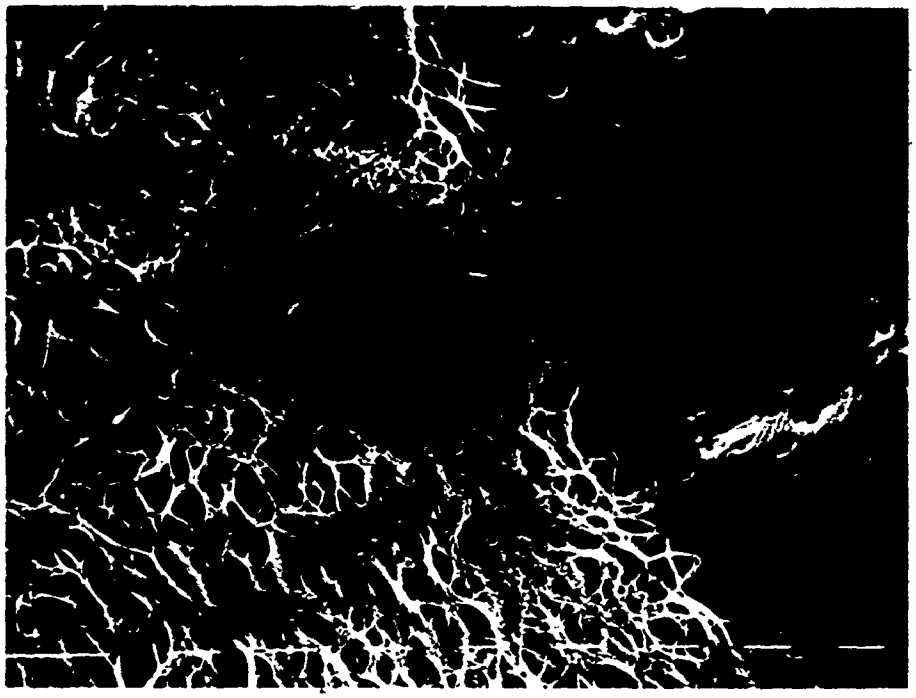

Figure 22 The fibrous layer which obscured the surface of many specimens is illustrated on the left portion of the photomicrograph. (Short white marks represent 10 μm).

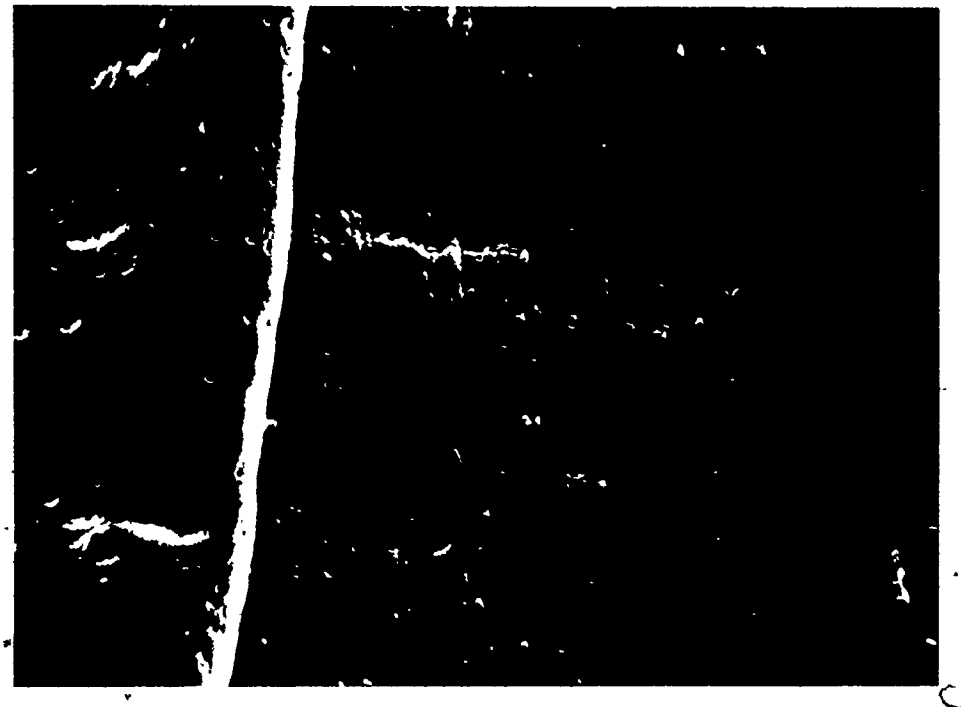

Figure 23 Luminal surface of the media (right portion) from cerebral arteries. Horizontal field width represents 0.293 mm.

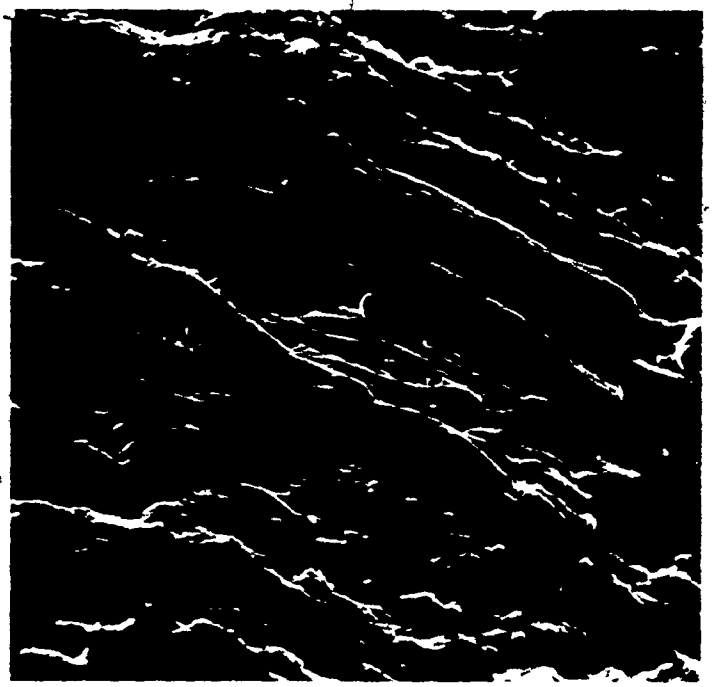

Figure 24 Smooth muscle cells in the media of human cerebral arteries. Horizontal field width represents 0.202 mm.

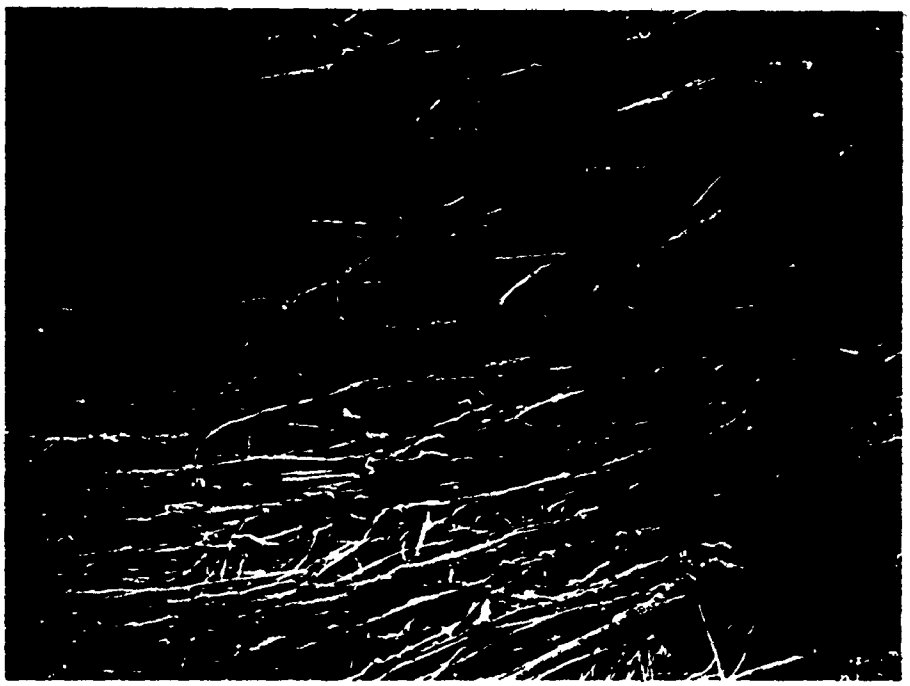

Figure 25. Adventitia from cerebral arteries. Horizontal field width represents 2.26 mm.

endothelial and smooth muscle cells as well as the collagen in the adventitia and the internal elastic lamina have not be resolved.

The endothelial layer provides a smooth surface in contact with the flowing blood but it is not considered to contribute to the mechanical strength of the wall. The media represents the thickest layer of the arterial wall, composed of long thin smooth muscle cells which modify the diameter of the artery. However, the strength of this tissue layer is dubious since smooth muscle cells have a low elastance and breaking strength (Roach, 1970), and they are embedded in ground substance which must provide an adequate bond among the cells. The adventitia is generally considered to prevent overdistension of the artery.

Elastin is generally considered to be highly extensible but posesses a low breaking strength. However, most testing has been conducted on the fibrous bovine ligamentum nuchae which is considerably different in form and structure, than the internal elastic lamina of arteries. None of the components have been tested after isolation from the arterial wall without the use of a harsh treatment procedure. The possible effect of these treatment procedures on the mechanical characteristics has not been assessed.

Only the internal elastic lamina is a continuous sheet of tissue (with fenestrations) that is not dependent upon the strength and bonding characteristics of a matrix substance to maintain the integrity of the tissue layer. A major concern with any multi-phase material containing fibres buried in a matrix is the adhesion between the constituents and the characteristics of the matrix. Therefore, it could be reasonably concluded that the internal elastic lamina will

play a significant role in determining the mechanical characteristics of the arterial wall. The internal elastic lamina could maintain the functional integrity of the wall (as demonstrated by Glynn 1940), following degeneration or failure of the other components within the wall. However, disruption of the internal elastic lamina could compromise the functional integrity of the wall perhaps leading to any of the pathological states related to subarachnoid hemorrhage.

3.3.4 Summary

The various layers of the cerebral arterial wall (endothelium, internal elastic lamina, media, adventitia) have been examined with the scanning electron microscope. To date the mechanical characteristics of the arterial wall have not been assessed by testing the various layers in isolation. Both the media and adventitia possess both a fibrous and matrix components which are dependent upon their mutual adhesion to maintain the structure of the tissue. Since the internal elastic lamina is a continuous sheet it is not dependent upon adhesion characteristics for maintaining the functional integrity of the tissue layer. Therefore, it would be anticipated that the structure of the internal elastic lamina would resist degradation better than the other tissue layers. However, degradation of the internal elastic lamina could compromise the structural integrity of the arterial wall perhaps leading to subarachnoid hemorrhage.

3.4 The Use of Ligament Efficiency to Represent the Spatial Geometry of Fenestrations in the Internal Elastic Lamina

3.4.1 Introduction

Examination of the internal elastic lamina isolated from human cerebral arteries, with the scanning electron microscope (subsection 3.3.2) has shown that the tissue is a continuous sheet permeated by an apparently random distribution of round or oblong fenestrations or windows (Campbell & Roach, 1981a). The size and density (number of fenestrations per mm^2) of the fenestrations vary with the external diameter of the artery (section 3.6). Furthermore, clusters and bands of enlarged fenestrations (Campbell & Roach, 1981a) were observed in the apical region of the bifurcations from cerebral arteries.

Although single-value characteristics such as diameter and density provide relevant information, it is difficult to describe the complete spatial geometery of the fenestrations with a single variable which incorporates both the diameter and the density. Percentage area of fenestrations in the field of view is a possible variable, but changes in the diameter alone would have a more significant influence than density alone on the result, because of the squared term (i.e., radius squared) in the equation.

The term "ligament efficiency" (Peterson, 1974, page 109) has been used to describe the spatial geometry of holes in flat plates. This term is defined as the minimum width of the solid band of material divided by the centre-to-centre distance for two, or more adjacent holes. Therefore, a high value for ligament efficiency (values are always between 0 and 1) implies a combination of small holes with substantial centre-to-centre distances, whereas, a lower value

represents larger holes and/or closer spacing.

A review of the literature has not revealed any studies that have used the concept of ligament efficiencies to model a random pattern of holes. Traditionally, a ligament efficiency has been used to describe the spatial geometry of holes in a sheet for the analysis of stress concentration in a material (Peterson, 1974, pages 108-244).

The intention, in this section is to:-

i) present a method for computing the ligament efficiency for a non-uniform (random) array of holes.

ii) create a simplified arrangements of holes, based upon the same ligament efficiency as the actual spatial geometry of the fenestrations.

iii) compare the elastic (stress-strain) properties of a uniform array of perforations with an identical ligament efficiency to a replication of the fenestrations in the form of models that have been prepared by cutting circular perforations or fenestrations in a thin sheet of latex rubber.

3.4.2 Method

Three photomicrographs (scanning electron microscopy) depicting the internal elastic lamina from digested human cerebral arteries (not pressurized) with external diameters of 3.4 mm (designated "a"), 1.1 mm (designated "b") and 0.7 mm (designated "c") in Figure 26, were selected for analysis. These straight segments of cerebral arteries represent the range of external diameters studied. The procedure for isolating the internal elastic lamina from a segment of the arterial wall has been described in subection 2.6.2.

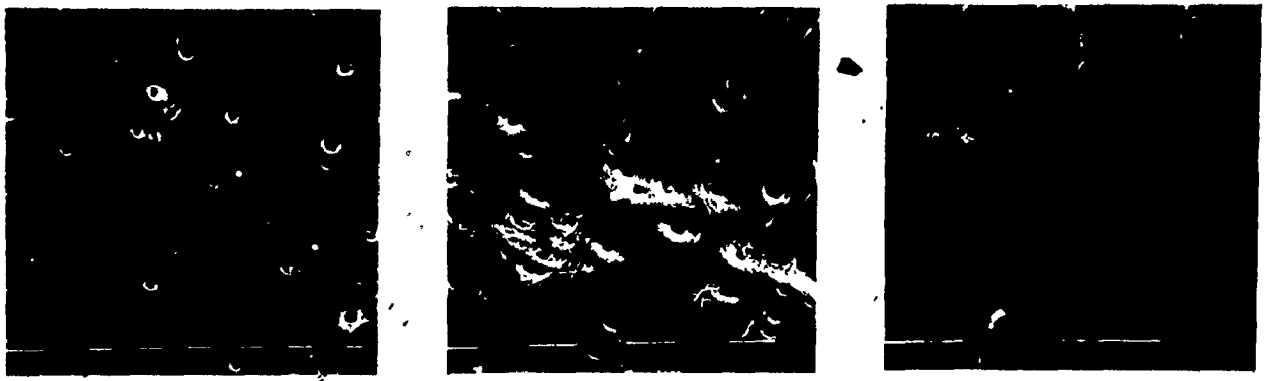

Figure 26 Photomicrographs of the surface of the internal elastic lamina (human cerebral) for the three arteries of different external diameters - (a - 3.4 mm; b - 1.1 mm; c - 0.7 mm) used to assess the ligament efficiency. The short white bars represent 10 μm.

The negative for each photomicrograph was mounted in an enlarger and the image projected on the platen of a Hewlett Packard Digitizer (model 9864A) interfaced with a Hewlett Packard 9830A microcomputer. The images represented a final magnification of 1150 for the 3.4 mm diameter, 2250 for the 1.1 mm diameter, and 4500 for the 0.7 mm diameter. These magnifications were selected in order that a reasonable number of fenestrations (about 40) were depicted on the photomicrograph.

Since the fenestrations are generally round or oblong in shape, two sets of two points representing the dimensions of the major and minor axes for the inside border of each fenestrations were digitized and entered into the microcomputer for further processing and storage. Only fenestrations which appeared to pass completely through the internal elastic lamina were measured. The area (A) for each fenestration was computed with the use of the equation for an ellipse:-

$$A = \frac{\pi ab}{4} \qquad (5)$$

where: a = major axis

b = minor axis

Four geometrical characteristics pertaining to the fenestrations were then computed from each photomicrograph:-

i) Diameter (D)

The diameter of a circle (D) with an equivalent area to the ellipse was determined by the relationship:-

$$D = (ab)^{1/2} \qquad (6)$$

An average diameter for all the fenestrations depicted in each photomicrograph was also computed.

ii) Density (F)

The number of fenestrations per mm^2 was calculated from the total number of fenestrations contained in the field of view by the equation:-

$$F = \frac{n}{Q} \qquad (7)$$

where: n = number of fenestrations

Q = area of field of view (mm^2)

Only one density could be computed for each photomicrograph.

iii) Percentage Area (B)

Fenestrations comprised the percentage of the surface area (computed by the summation of the area for each fenestration, A_i) with respect to the total area depicted in the field of view is computed with the equation:-

$$B = \frac{\sum_{i=1}^{n} A_i}{Q} \times 100 \qquad (8)$$

iv) Ligament Efficiency (LE)

The basic equation to calculate a ligament efficiency, based on a constant diameter (d) and uniform centre-to-centre spacing (c), for either a pair of holes, or a uniform distribution of holes with an equivalent number of rows and columns is:-

$$LE = \frac{c - d}{c} = 1 - \frac{d}{c} \qquad (9)$$

where d = hole diameter

c = centre-to-centre spacing

However, the diameters of the fenestrations in the internal elastic lamina are not constant, nor are the fenestrations equally spaced. Nevertheless, these constraints were imposed upon the spatial geometry of the fenestrations by modelling the spatial geometry of the fenestrations as a uniform pattern (equal numbers of rows and columns) of holes with a constant diameter (d), as illustrated in Figure 27. The diameter (d) is computed as the average diameter for the n fenestrations shown in the photomicrograph and converted from the micrometres to millimetres:

$$d = \frac{\sum_{i=1}^{n} D_i}{1000n} \qquad (10)$$

Calculation of the centre-to-centre distance is based on the assumption that the n fenestrations within the field of view may be divided into an equal number of rows and columns ($n^{1/2}$). The linear dimension for the field of view is the square root of the area or $Q^{1/2}$. The centre-to-centre distance may therefore be represented by:

$$c = \left[\frac{Q}{n}\right]^{1/2} \qquad (11)$$

Substitution of the preceding two expressions into the initial equation for the ligament efficiency produces the relationship:-

$$LE = 1 - \left[\frac{\sum_{i=1}^{n} D_i}{1000n} \Big/ \left[\frac{Q}{n}\right]^{1/2}\right] \qquad (12)$$

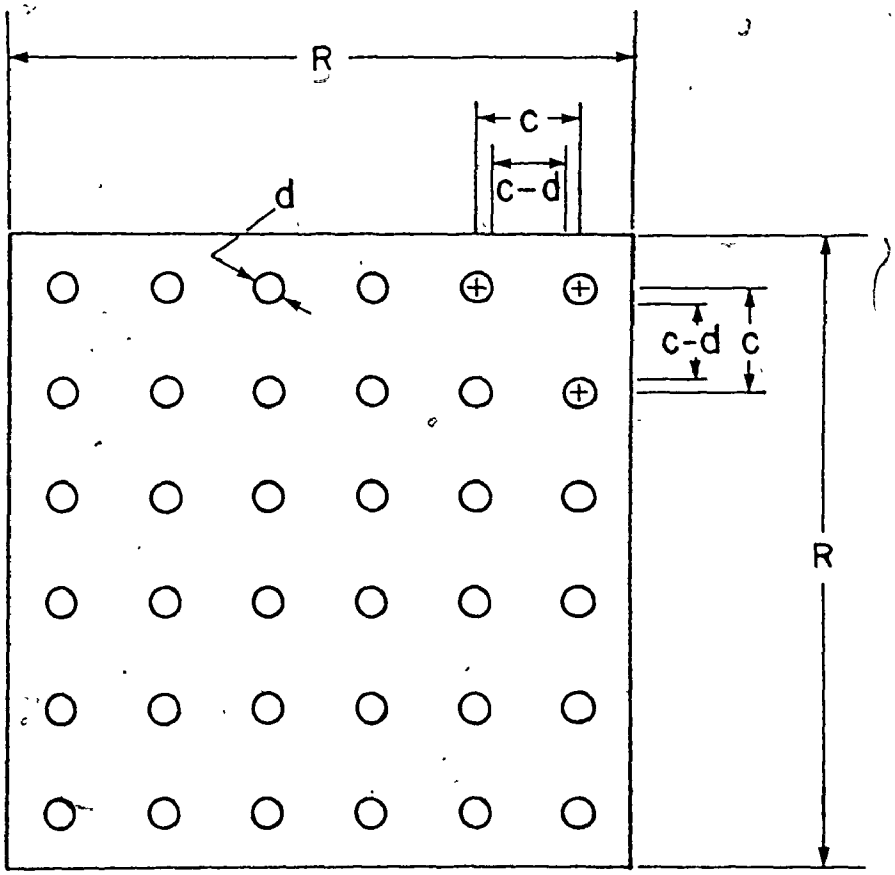

Figure 27 Uniform array of circles representing the outline of the perforations for a 6 x 6 model of the fenestrations in the 0.7 mm artery.

This expression may then be re-arranged to yield:

$$LE = 1 - \left[\frac{\sum_{i=1}^{n} D_i}{1000\ (Qn)^{1/2}} \right] \qquad (13)\ **$$

A replication of the fenestrations in the internal elastic lamina for each of the three photomicrographs was produced by tracing the outline of the inside border of each fenestration on tracing paper which had been laid over an enlargement (50.8 mm x 50.8 mm glossy print) of the photomicrograph. The 50.8 mm enlargements represent final magnifications of 736, 770 and 1451 for the 3.4 mm, 1.1 mm and 0.7 mm diameter arteries, respectively. Each replication was next transferred to the surface of a sheet of latex rubber * by overlaying the latex rubber on the tracing paper mounted on a light table and tracing the outline of each fenestration on the latex rubber.

Latex rubber was selected since it was a readily available elastomer with similar mechanical characteristics (high resilience, high extensbilty, and low modulus of elasticity) to elastin (Ross and Bornstein, 1971). Furthermore, Gosline (1976) has compared the mechanical characterists of elastin to polymeric rubbers.

Models of the spatial geometry were created by computing the average diameter of the fenestrations from the photomicrographs, as well as the average centre-to-centre distance for the same numerical

* Dental Dam Material, The Hygiene Corp, Akron, Ohio 44310, USA

** See Appendix VII for alternate expression

ligament efficiency calculated from the photomicrograph. Since the number of rows/columns for the model ($n^{1/2}$, where n is the number of fenestrations in the photomicrograph) was not an integer, two models for each replication were created, one with the integer above "n", and the other with the integer below "n". For example, if the number of fenestrations in the photomicrograph was 46, which would require 6.78 holes per row or column, then the first model would consist of 36 holes (i.e., six rows x six columns) and the second model, 49 holes (i.e., seven rows x seven columns). Since the total number of holes in each model varies from the number of fenestrations in the photomicrographs, the edges of the models must be scaled accordingly. Therefore, the linear dimension of the edge of the model with a lesser number of holes will be shorter and the edge of the model with a greater number of holes will be longer than the length of 50.8 mm for the replication. The linear dimension of the edge (R) in Figure 27 is calculated according to the relationship (with "m" the nearest integer value):-

$$R = c \times m \qquad (14)$$

The outline of the holes within the external edge of the model were drawn on tracing paper and transferred to latex sheets by the procedure described previously.

Two opposing sides of every latex sheet were trimmed along the edge while the remaining ends were sandwiched between two strips of 1.3 mm aluminium sheet which were aligned along the edge of the model. Double-sided masking tape between the latex sheet and the aluminium strips ensured a secure attachment. Since the latex sheet has been

described as orthotropic (Burton, 1970), the orientation of each model with respect to the aluminium strips was the same in order to ensure consistency during testing.

The aluminium strips were then mounted in the grips of a constant-rate-of-crosshead movement testing machine.* Every solid latex sheet was stretched in uniaxial tension at a crosshead speed of 100 mm/min. to a maximum elongation of 30%. Although the initial length of the sample varied, which would result in a different strain rate for each sample, testing of a single sample of the latex sheet at various crosshead speeds (10 mm/min to 500 mm/min) gave overlapping results. Therefore, the variation in the strain rate does not influence significantly the load/deformation properties of the latex sheet.

Each sample (unperforated) was cycled through three sequences of loading and unloading, since the performance of the sample did not change appreciably after the second cycle (during loading). The load/deformation record for each specimen was subsequently converted to a stress-strain curve. The stress is computed as "engineering stress" (i.e., the load was divided by the original cross-sectional area).

Perforations were cut in each of the samples to represent the shape of the fenestrations and circles, in the replication and model samples respectively. The samples were remounted in the testing machine and the tensile test repeated. The stress-strain curves for the perforated samples were again computed.

The conditions of the latex rubber models with either holes marked, but not perforated, or with the perforations cut out, will henceforth be referred to as "solid" and "perforated" respectively.

* Model 1125, Instron Corporation, Canton, Massachusetts, USA

3.4.3 Results

Table 3 presents the geometrical characteristics for the photomicrographs in Figure 26, which represent the three arterial specimens with different external diameters used as typical of the range to be studied. An analysis of the shrinkage during preparation of the specimens (section 2.6), revealed a linear shrinkage of only 6.9% (Campbell & Roach, in press). The geometrical characteristics reported in Table 3 for diameter and density (remainder are not affected) have not been corrected for shrinkage. Note in Table 3, that while the external diameter of the artery decreases, the average diameter of the fenestrations also decreases, but the density increases substantially. The combined effect is to increase the percentage area comprised of the fenestrations while decreasing the ligament efficiency.

The characteristics of the perforations in the latex, which model the fenestrations in the three specimens mentioned above, are presented in Table 4. The absence of a difference among the diameters for the fenestrations (replication) as well as the perforations (model) consistent with Table 3, is attributable to the differences in magnification.

Figure 28 illustrates the stress-strain curves for the solid and perforated latex replication of the fenestrations in the 0.7 mm diameter artery (Figure 26). The stress-strain curves for the 6 x 6 model (solid and perforated) representing the 0.7 mm diameter artery are also shown in Figure 26. Both sets of results demonstrate similar (but not identical) curved shapes. Note the similar relative differences between the solid and perforated conditions. The stress-

External Diameter (mm)	N	Diameter (μm)	Density (#/sq mm)	Percentage Area (%)	Ligament Efficiency
3.4	35	3.2	1920	1.8	0.86
1.1	41	1.9	9412	2.5	0.82
0.7	46	1.5	37551	7.0	0.71

TABLE 3 - Geometrical Characteristics of Fenestrations (not corrected for shrinkage)

External Diameter (mm)	Models	Diameter (mm)	Centre-to-Centre Distance (mm)	Ligament Efficiency
3.4	5 x 5, 6 x 6	1.2	8.6	0.86
1.1	6 x 6, 7 x 7	1.4	8.0	0.82
0.7	6 x 6, 7 x 7	2.2	7.5	0.71

TABLE 4 - Geometrical Characteristics of Perforations (based upon Table 3)

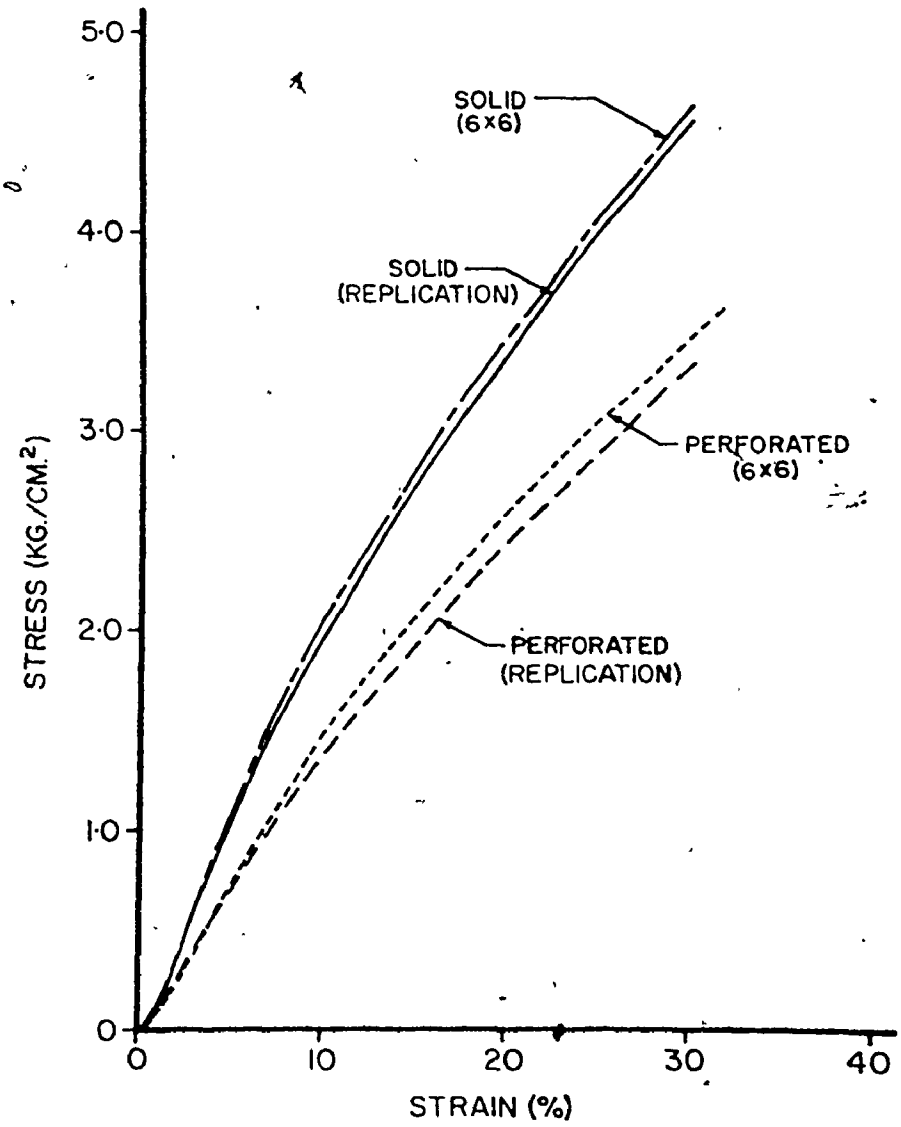

Figure 28 Sets of stress-strain curves for the solid latex sheet and perforated conditions of the replication and 6 x 6 model configurations (0.7 mm external diameter artery). Note that the perforated condition exhibits greater distension.

strain curves for the remaining models are comparable.

Since the primary interest is to assess the change in stress-strain properties from the solid to the perforated condition, the stress values for the perforated condition were standardized by dividing by the stress for the solid condition at the same strain.

The results illustrated in Figure 29a for the 3.4 mm diameter artery, show no real difference between the replicated configuration and both the 5 x 5 and 6 x 6 models, throughout the range of elongation. The computed stress for all three configurations in the perforated condition has been reduced to about 92% of the stress for the solid material. The deviations evident within the initial 6% of elongation are attributable to a combination of hand tremor during the digitization, limited difference between the values in this portion of the curve which accentuates the measurement errors, and stabilization of the moving crosshead and recording pen following actuation of the testing machine.

A similar assessment of the results depicted in Figure 29b for the 1.1 mm artery also demonstrate good agreement between the replicated and model configurations (6 x 6 and 7 x 7) to the maximum of 30% elongation. Again, a noticeable difference between the two modelled configurations is not evident. The computed stress in the perforated condition is reduced to about 91% of the stress in the solid material. The close agreement in the standardized stress values between the samples representing the 3.4 mm diameter of the 1.1 mm diameter arteries is considered to be a coincidence, since the magnifications are different.

The standardized stresses for the replicated and modelled

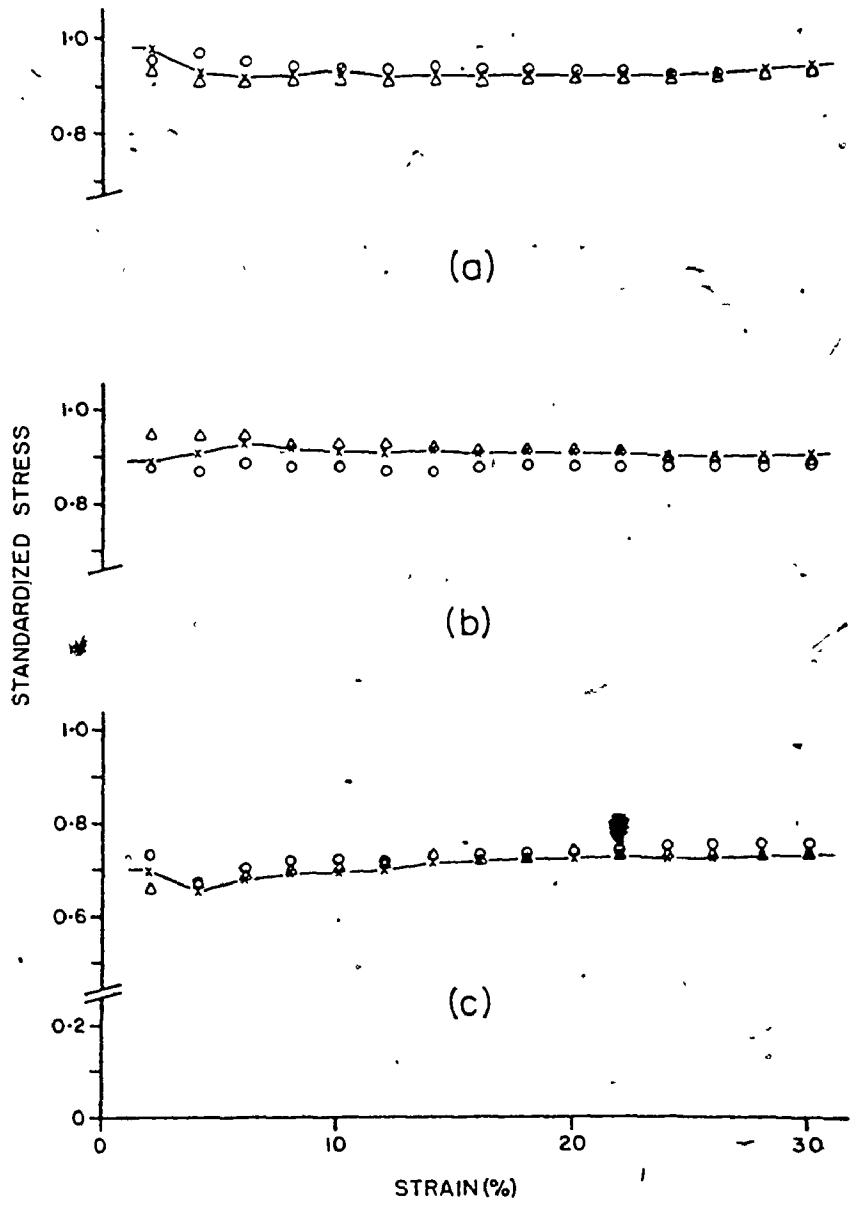

Figure 29 Standardized stress-strain curves (the lines join the values for the replication).
(a) 3.4 mm artery
x - Replication
Δ - 5 x 5 Model
o - 6 x 6 Model
(b) 1.1 mm artery
x - Replication
Δ - 6 x 6 Model
o - 7 x 7 Model
(c) 0.7 mm artery
x - Replication
Δ - 6 x 6 Model
o - 7 x 7 Model

configurations (6 x 6 and 7 x 7) of the 0.7 mm diameter artery (Figure 29c) also agree over the range of elongation. The results for the two models are not different. In this instance, the computed stress in the perforated material is reduced to about 70% of the solid material.

3.4.4 Discussion

The shift of the stress-strain curve confirms that the perforated condition of the material demonstrates greater elongation at equivalent stress values to the solid condition. It would be anticipated that as the number and/or diameter of the holes increase, then the stress-strain curve would shift further away from the curve for the solid material (i.e., demonstrate greater strain). The relationship between enlargement of the holes or an increase in their number, and the changes in the stress-strain curve have not been assessed in this study.

Standardization of the perforated condition, with respect to the original solid condition of the latex sample, provides an appropriate method for comparing any change in the replicated and modelled configurations. The good agreement between the modelled and replicated configurations validates the use of the ligament efficiency to model the spatial geometry of the fenestrations in the internal elastic lamina. Consequently, the apparent random pattern of fenstrations may be represented by a uniform array of holes with a constant diameter. The absence of a distinction between the standardized stress values for the two models representing each replication, indicates that it is not

necessary to interpolate between the number of holes for the true number of fenestrations.

There are also many other possible configurations for the models, such as staggering alternate rows, but the computation of the spacing for an equivalent ligament efficiency becomes more complicated. Since the uniform configuration provides such good agreement with the replicated configuration, other configurations were not investigated.

The close agreement also confirms that the variations in magnification does not affect the agreement, provided a reasonable number of fenestrations or perforations are present. If the intermediate magnification of 770X for the 1.1 mm diameter artery had been imposed upon the other two specimens, then the number of fenestrations evident from the photomicrograph for the 3.4 mm diameter artery would have been reduced to only 8 or 9, but the diameter would be doubled for the same size of sample. By comparison, the number of fenestrations present in the photomicrograph of the 0.7 mm diameter artery would increase to an unwieldy 184 with the diameter reduced to one-half the present value.

Although the selection of three different magnifications has precluded a comparison of the relative reduction of the stress values at the same strain values, it was evident that there is a substantial decrease in the stress for the 0.7 mm diameter artery with the larger diameter and shorter centre-to-centre distance (50.8 mm square replication), than for the 1.1 mm diameter artery. The absence of the same substantial difference for the 3.4 diameter artery with a smaller diameter of perforations but larger centre-to-centre distance (50.8 mm square replication) in comparison to the 1.1 mm diameter artery has not been resolved.

The major significance of this study has been to validate that the tensile characteristics of a uniform array of constant diameter perforations in a latex model, closely duplicate the random arrangements of fenestrations with varying diameters but with an identical ligament efficiency. This simplication facilitates the analysis of the spatial geometry during tensile elongation. A further discusion of the spatial geometry for these specimens will be presented in section 3.5.

3.4.5 Summary

The spatial geometry of fenestrations (windows) in the internal elastic lamina from human cerebral arteries is characterized by a single parameter termed "ligament efficiency", which is a ratio of the solid band of material to the centre-to-centre spacing between two or more holes. As a result, the apparent random distribution of fenestrations with variable diameters may be represented as a uniform array of holes each with the same diameter.

The actual arrangements of fenestrations from three separate tissue specimens were replicated in thin latex sheets by transposing the image of the fenestrations from photomicrographs obtained with the scanning electron microscope. In a similar manner, the uniform array of holes with an equivalent ligament efficiency are modelled in latex sheets. The tensile (stress-strain) properties of the latex sheets representing the replication and model configurations were comparable for all three specimens, even though their individual ligament efficencies were different. The close similarity between the elastic characteristics for the two configurations, verifies the application of

ligament efficiency to represent the spatial geometry of a perforated material such as the fenestrated internal elastic lamina.

3.5 The Use of Ligament Efficiency to Analyze Changes In the Spatial Geometry of Fenestrations During Tensile Elongation

3.5.1 Introduction

The preceding section demonstrated that the tensile properties of an elastomeric sheet with a random array of perforations (replication of fenestrations) is closely modelled by a uniform array of perforations with a constant diameter and the same ligament efficiency. This model of the spatial geometry facilitates the analysis of the changes in the spatial geometry of non-uniform perforations during stretching. Although the model cannot be directly compared with the fenestrations in the internal elastic lamina, it can provide an indication of their behaviour.

Several studies (Hayashi et al, 1980a, 1980b; Busby & Burton, 1965; Chalupnik et al, 1971; Moritake et al, 1974 and Nagasawa et al, 1979) have investigated the mechanical characteristics of the intact cerebral artery. However, to date the mechanical characteristics of the internal elastic lamina have not been established.

The internal elastic lamina of intracranial cerebral arteries is a single layer of elastin forming a fenestrated sheet in the wall of the artery, near the lumen. For this reason, the internal elastic lamina must be isolated from the wall in a suitable condition, before the tensile characteristics can be determined. Moreover, the extreme thinness and delicate nature of the tissue present considerable problems in handling, since the tissue is very susceptible to tearing

or folding into a blob. These factors, along with the lack of a specimen of sufficient size, have precluded the determination of the tensile properties of the internal elastic lamina for the present.

The tensile characteristics of elastin fibres, most notably bovine ligamentum nuchae, have been assessed by others (Hass, 1942; Carton et al, 1962; Steven et al, 1974). Most of these studies have isolated or purified the elastin tissue by such methods as autoclaving, hot alkaline, hot formic acid, or enzymatic agents. The major concern is the effect of these techniques, particularly where heat is applied, on the biochemical structure and possibly the mechanical characteristics of the tissue. Since the effects of these treatments on the tissue have not been investigated, the results using purified or isolated elastin must be interpreted with caution when referring the results to the in vivo condition.

At present, there are no direct methods for examining the behaviour of the fenestrations in the internal elastic lamina of cerebral arteries during stretching. As a consequence, I directed my attention to the modelling of fenestrations in the internal elastic lamina in the form of a latex rubber sheet with perforations. This portion of the study seeks to examine the behavior of the perforations (models only) within the latex sheet during uniaxial extension of the sheet to thirty percent strain.

3.5.2 Methods

Following the uniaxial tensile test described in subsection 3.4, photographs were taken of each sample in the solid (holes marked on the sample) and perforated condition, while the sample was still mounted in

the constant-rate-of-crosshead testing machine (Instron model 1125). Photographs were taken while the sample was in an unstretched condition as well as at 10, 20, and 30 percent elongation. Figure 30 illustrates the perforated replication and 6 x 6 model for the 1.1 mm external diameter artery illustrated in Figure 26 of section 3.4, in both the unstretched and stretched conditions.

The image for the negative of each photograph was projected on the platen of the Hewlett Packard digitizer. Since the shape of the circular holes form an ellipse when the latex rubber is stretched, both the longitudinal (major axis) and transverse dimensions (minor axis) of a single row of holes (the number is represented by "m" below) closest to the centre of the sample were recorded and averaged, along with the width of the sample, at each elongation.

The measurements were then converted into the following set of geometrical parameters:

i) Area (A)

The area is computed from the measurement of the major axis (a) and minor axis (b) with the use of the equation for an ellipse (5).

ii) Ligament Efficiency (LE)

The ligament efficiencies for both the longitudinal and transverse directions are calculated at each discrete elongation of the sample (s represents length or width of sample and h represents the corresponding dimension of the hole) by the equation:

$$LE = 1 - \left[\frac{\sum_{i=1}^{m} h}{s} \right] \qquad (14)$$

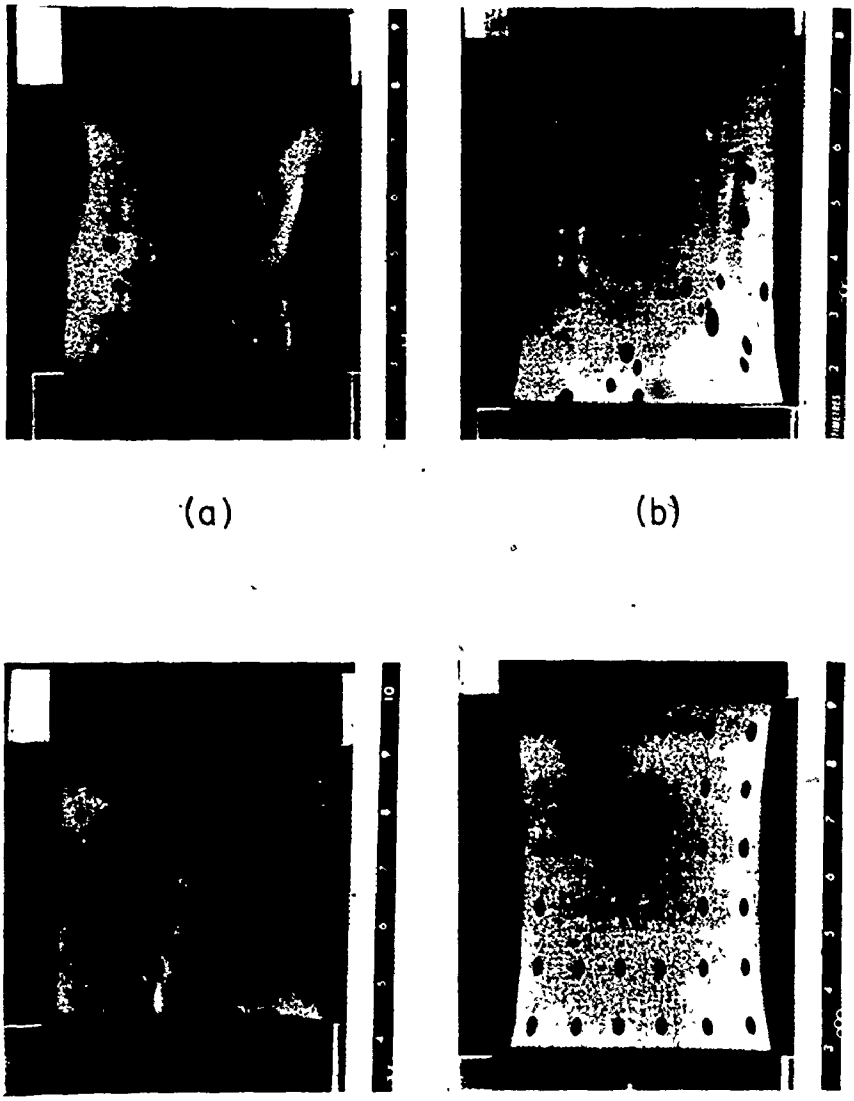

Figure 38 Photographs depicting the replication and 6 x 6 model of the 1.1 mm external diameter artery mounted in the grips of the uniaxial tensile testing machine.

a) Replication (perforated) in the unstretched condition.
b) Replication (perforated) at 30% elongation.
c) 6 x 6 model (perforated) in the unstretched condition.
d) 6 x 6 model (perforated) at 30% elongation.

This relation has been derived from equation (9) in subsection 3.4.2 by substituting s/m for c and $\left[\sum_{i=1}^{m} b\right]/m$ for d, and re-arranging the terms.

iii) Eccentricity (e)

The eccentricity of an ellipse is defined by the equation (Selby, 1972, page 356):

$$e = \frac{(a^2 - b^2)^{1/2}}{a} \qquad (15)$$

In this case, the eccentricity will be used to represent the shape factor since the eccentricity has the value of 0 for a circle and 1 for a slit.

iv) Necking (v)

The ratio of transverse unit strain to longitudinal unit strain is expressed by:

$$v = \frac{dW/W}{dL/L} \qquad (16)$$

where:

W = width of sample

dW = change in width

L = length of sample

dL = change in length

The values for necking were computed only for the models with an odd number of rows/columns since the centre row would coincide with the narrowest width of the sample.

v) Expansion Ratio (N)

Linear expansion (dh/h) of the hole (diameter h) in the longitudinal direction in relation to the linear expansion (dR/R) of the solid sheet (length R) is expressed by Burton (1970) as:

$$N = \frac{dh/h}{dR/R} \qquad (17)$$

For the case of a solid material with circles marked on it, the value would be equal to 1 for any elongation greater than zero.

The preceding set of parameters was calculated for each of the three samples listed in subsection 3.4.

3.5.3 Results

As illustrated in Figure 30, progressive elongation of the latex sheet transformed the holes into elliptical slits while reducing the width at the centre of the specimen. The value for necking of the three samples was computed to be 0.36 $\pm$0.013 SEM for the solid condition and 0.39 $\pm$0.013 SEM for the perforated condition. The t-test showed no significant difference (i.e., $p > 0.05$). The expansion ratios for the perforated models of the 3.4, 1.1 and 0.7 mm external diameter arteries were 3.4 $\pm$0.12 SEM, 3.5 $\pm$0.08 SEM and 2.3 $\pm$ 0.06 SEM respectively.

Linear regressions (least squares) were computed for the combined results of the two models (i.e., 5 x 5 and 6 x 6) pertaining to each of the three samples, for the diameter, area and ligament efficiency. The r^2 values (coefficient of determination) for the linear regressions were usually 0.92 or greater, except for slopes approaching the horizontal which generated correlation coefficients that were not significant even though a linear relationship appeared obvious. Since the slope in this latter condition is approaching zero, the r^2 computation is not a reliable indicator of the fit for linear relationships that approach a constant.

The results for the perforated condition of each sample will be reported and discussed separately from the other two, since the

influence (if any) of different relative magnifications on the results has not been assessed in this study. The solid condition has been considered a mutual condition for the three samples permitting inter-sample comparison. The ratio of the values for the perforated condition in relation to the solid condition also provides an indicator for inter-sample comparison.

i) Transverse and Axial Diameters

The change in the transverse and axial diameters (nearest row of holes to the centre) during stretching of the three samples are illustrated in Figure 31. The results for the transverse diameter of 3.4 mm are presented alone (Figure 31a), since the three sets of results did not differ appreciably, or there was a slight deviation which was most noticeable at the thirty percent elongation.

The axial diameters for the three samples increased with elongation, for both solid and perforated conditions. The axial diameter for the perforated condition increased at a faster rate than the solid condition, in each case. Agreement between both models of each sample for changes in geometry was excellent. This observation concurs with the results for the standardized stress-strain curves shown in section 3.4, where the tensile properties for both models were also very similar.

The slopes representing the relationship between the axial diameter and elongation for the three samples are presented in Table 5. A ratio of the slopes corresponding to the solid (holes marked on sample) and perforated conditions is also listed in Table 5. The individual slopes for the axial elongation of the holes in all three

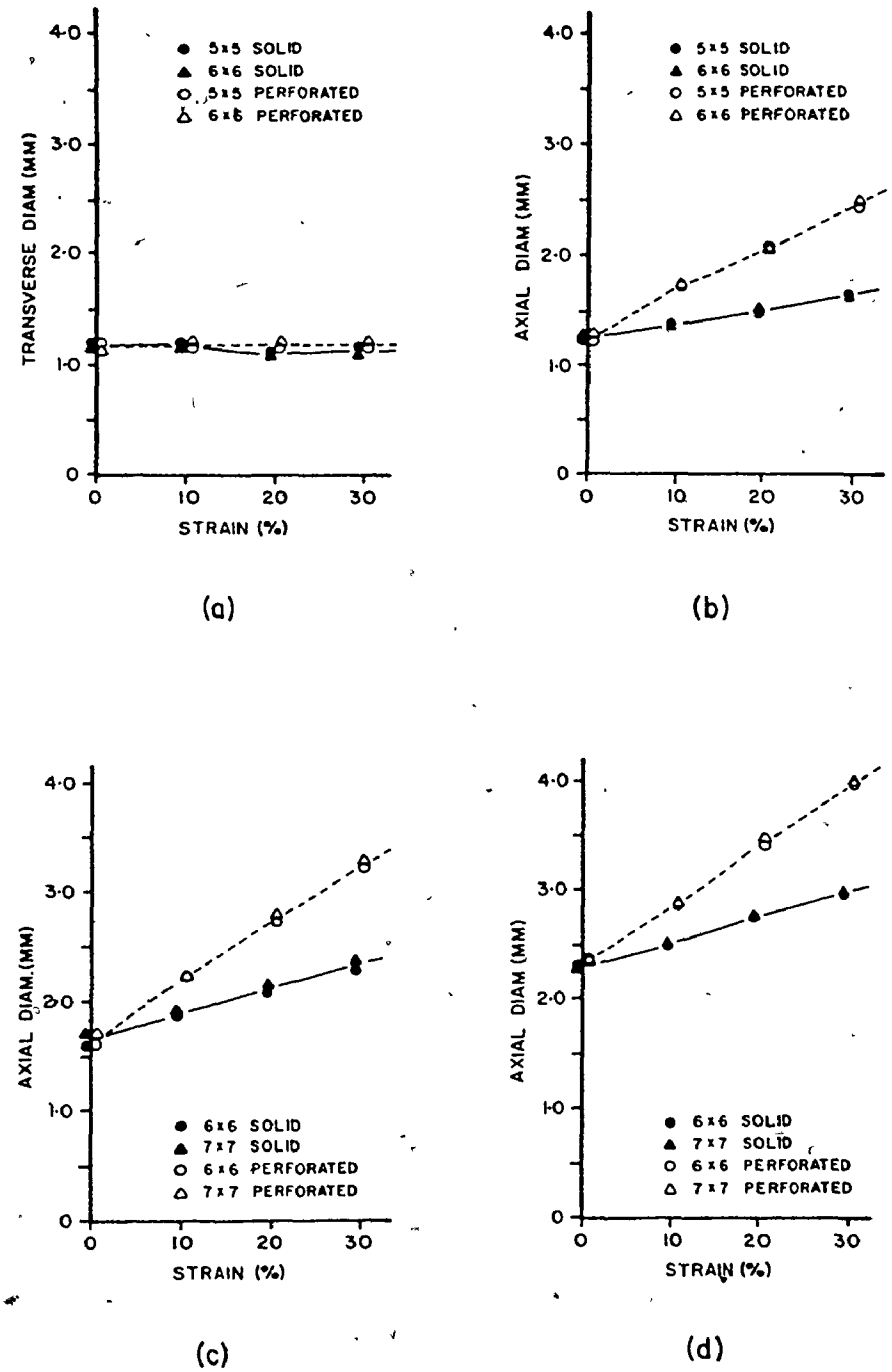

Figure 31 Curves depicting the change in transverse (a) or axial (b to d) diameter with increasing strain.
a) and b) 3.4 mm external diameter
c) 1.1 mm external diameter
d) 0.7 mm external diameter

	AXIAL DIAMETER	AREA	AXIAL LE
3.4 mm Diameter			
Solid	0.014(1)	0.01 (1)	-0.00018(3)
Perforated	0.041(1)	0.038(1)	-0.0025 (1)
Perforated/Solid	2.9	3.8	N.R.
1.1 mm Diameter			
Solid	0.019(1)	0.026(1)	-0.00045(2)
Perforated	0.054(1)	0.068(1)	-0.0037 (1)
Perforated/Solid	2.8	2.6	8.2
0.7 mm Diameter			
Solid	0.024(1)	0.037(1)	-0.0002(3)
Perforated	0.056(1)	0.11 (1)	-0.0034(1)
Perforated/Solid	2.3	3.0	N.R.

Notes: (1) $p \ll 0.001$
(2) $p < 0.01$
(3) $p > 0.01$
N.R. not relevant

TABLE 5 - SLOPES FOR LINEAR REGRESSION

samples varied among the samples, but was consistently greater for the perforated than for the solid condition. There were also differences in the slopes ($p << 0.001$) among the three samples for the solid condition. The relative slopes for the perforated , with respect to the solid condition were similar for the 3.4 and 1.1 mm diameter arteries, but different for the 0.7 mm diameter artery.

ii) Area

The increase during the elongation for the area of the solid and perforated conditions of each sample are presented in Figure 32 and Table 5. It is evident from the curves that the area for the perforated condition increased at a faster rate than the solid condition in each case. The slopes for both the solid and perforated condition were again unique to each sample. The slopes of the areas for the solid and perforated conditions of the sample representing the 3.4 mm external diameter artery are both marginally less than the respective slopes for the axial diameter (Table 5). A similar comparison (perforated and solid) of the slopes for the samples representing the 1.1 and 0.7 mm external diameter arteries showed the converse, i.e., the slopes were greater for the area than the axial diameter. The relative rate of increase in the area for the perforated condition with respect to the solid condition, was more pronounced for the samples representing the 3.4 and 0.7 mm external diameter arteries, than the 1.1 mm diameter artery.

iii) Ligament Efficiency

The results for a typical transverse ligament efficiency, as well as the axial ligament efficiencies for the three samples are presented in Figure 33. Since the values of the transverse ligament efficiency

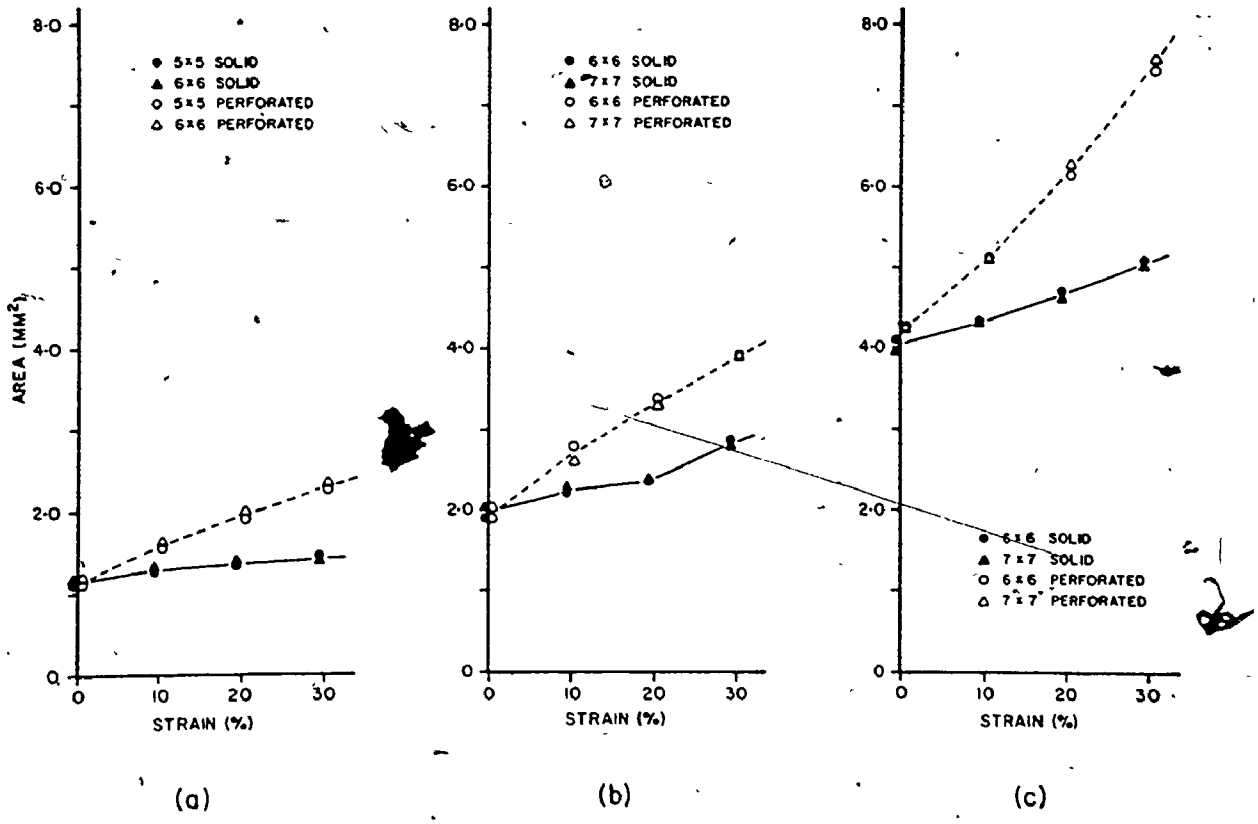

Figure 32 Change in the area of the marked and perforated holes with increasing strain.
a) 3.4 mm external diameter
b) 1.1 mm external diameter
c) 0.7 mm external diameter

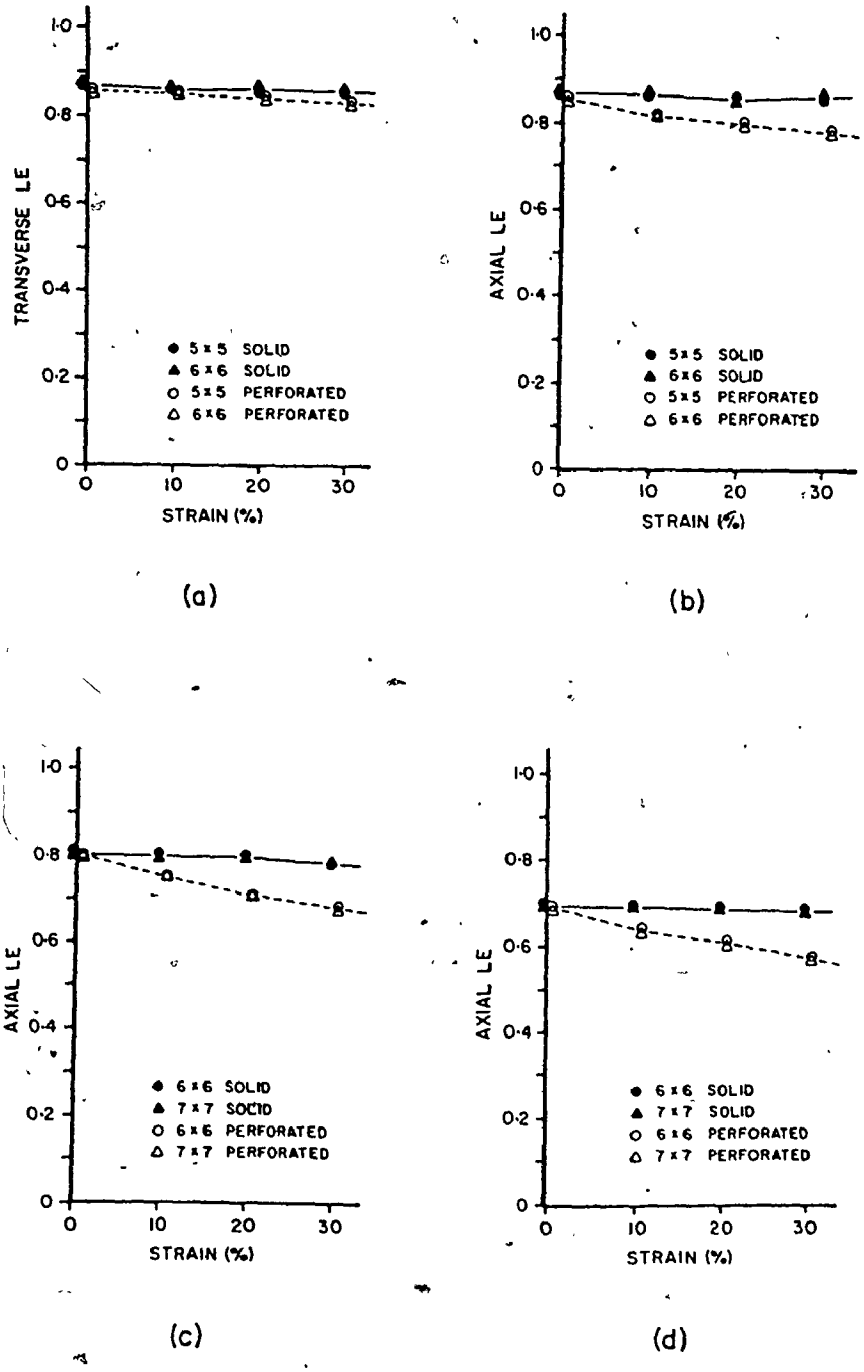

Figure 33 Graphs of transverse (a) and axial (b to d) ligament efficiency with increasing strain.
a) and b) 3.4 mm external diameter
c) 1.1 mm external diameter
d) 0.7 mm external diameter

for all three specimens were essentially the same during elongation, only the results for the 3.4 mm external diameter specimen have been illustrated. The axial ligament efficiency for the solid specimens did not change with elongation. Nevertheless, a distinct decrease with increasing elongation was observed following perforation of the solid specimens. The results for the solid conditions of the samples representing arterial diameters of 3.4 and 0.7 mm are constant (slope of zero), whereas the slope for the 1.1 mm diameter artery attained statistical significance (Table 5). As a result, the computation of the ratio of "perforated/solid" is not relevant.

iv) Eccentricity

The eccentricities for the three samples for both the solid and perforated conditions demonstrated a non-linear increase with elongation (Figure 34) which is most marked at low strains. In each sample the ellipse was narrower in the perforated than in the solid condition.

3.5.4 Discussion

The main purpose of the second portion of this study has been to examine the changes in the geometry of the uniform pattern of perforations during stretching of the sheet of latex rubber. The results for uniaxial elongation of the three samples confirm the observation by Burton (1970) that the axial diameter of the perforation expands more rapidly than the surrounding solid material. The rate of change of the axial diameter, area and axial ligament efficiency varied among the three specimens, but each set of results was unique to the particular model of the associated tissue.

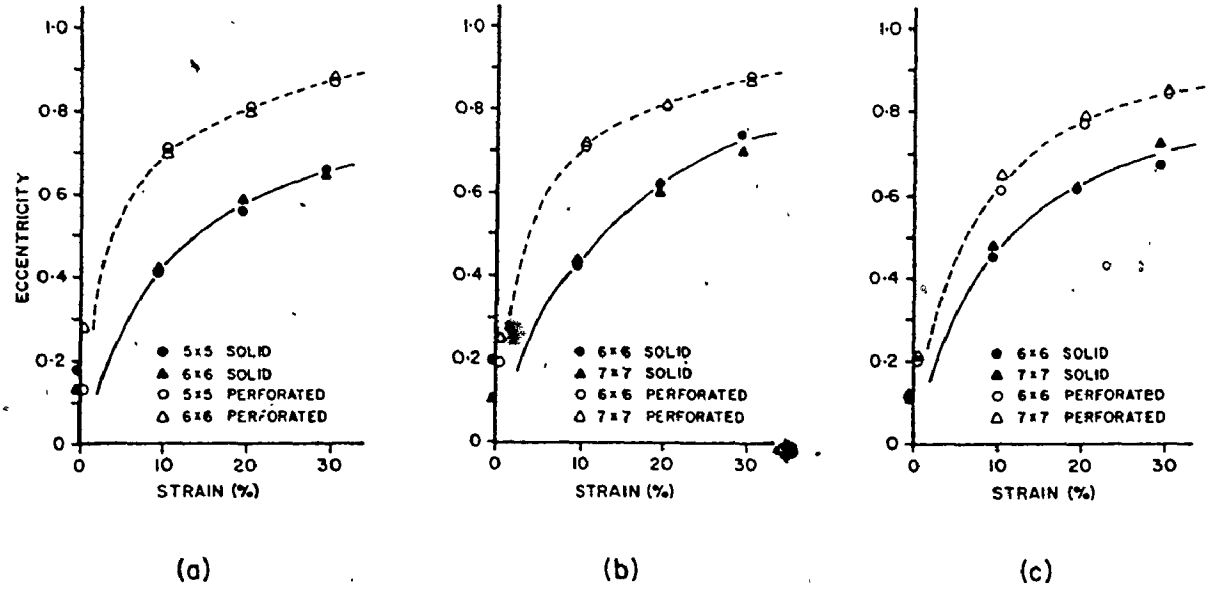

Figure 34 Plots of shape factor (eccentricity) with increasing strain.

a) 3.4 mm external diameter
b) 1.1 mm external diameter
c) 0.7 mm external diameter

A pattern for the distortion of the perforations has emerged from this study. In each case the transverse diameter, and transverse ligament efficiency did not change appreciably with elongation regardless of whether the sample was solid or perforated. If the pattern was only marked on the latex sheet, then the axial diameter (as demonstrated by the expansion ratio) as well as the area, increased in the same proportion as the elongation of the sheet, while the ligament efficiencies remained essentially constant. The rate of change (slope) of the axial diameter and area with elongation of the solid condition was not constant for the three samples (all differences significant at $p < 0.01$).

The axial diameter and area for the perforated condition of the samples expanded in excess of the proportional elongation of the material. Consequently, the ligament efficiency continuously decreased during elongation. The eccentricity increased more rapidly for the perforated than the solid condition, but did not approach an asymptotic condition within the thirty percent elongation. The rate of change for any of the parameters was a unique function of the geometry of the perforations in the sample.

The expansion ratios for the models of the arteries with external diameters of 3.4 and 1.1 mm were in close agreement, in contrast to the expansion ratio for the model of the 0.7 mm diameter. Burton (1970) verified that the expansion ratio should initially be three and then "decrease to unity where the ellipse has been stretched very greatly.." however, Burton has presented two expressions (equation "10" in his paper) coupled by equal signs for computing the expansion ratio. The first of the expressions has been used here (equation "17" in

subsection 3.5.2) in order to obtain the single value for the three samples reported in the results. The initial value was very close to three and tended to decrease with progressive elongation.

It is particularly interesting that the relative results for the expansion ratios (i.e., the results for the 3.4 mm and 1.1 mm arteries concur while the 0.7 mm artery is distinctly less) resemble the relative results for the standardized stress results. This observation suggests that the decrease in the stress values (standardized stress) for the material with perforations could be related to the expansion ratio. However, further studies would be required to verify whether a relationship exits.

3.5.5 Summary

During uniaxial extension of the latex model, the holes (both marked on the sheet and perforated) demonstrated a distinctive change in their shape, from circular to elliptical. Measurements of the axial and transverse diameters of a consistent row of holes, along with the width of the sample at distinct elongations were converted into an area, ligament efficiency (transverse and axial) and shape factor (eccentricity). Values for the expansion ratio of the holes and necking of the latex sheet were also computed. The perforations expanded more rapidly than with the holes only marked on the solid material, which translated into a more rapid increase for the axial diameter, area and eccentricity, while the axial ligament efficiency decreased more rapidly. The transverse diameter and transverse ligament efficiency remained essentially constant. Necking of the latex sheet was consistent for all of the specimens (both solid and

perforated). The relative expansion ratios appear to parallel the relative changes for the standarized stresses presented in section 3.4

3.6 The Geometrical Characteristics of Fenestrations in the Internal Elastic Lamina of Human Cerebral Arteries

3.6.1 Introduction

Although it had been observed in the late 19th century that the elastic lamella in arteries contained fenestrations (windows), Dees (1923) was the first to investigate them. More recently, Hassler (1962) presented the results for the diameter, density (number per square millimeter) and percentage area of fenestations for consistent segments of the internal carotid and anterior cerebral arteries (human), over a life span of 90 years. Other authors (Lang and Kidd, 1965; Hassler, 1972; Cajander and Hassler, 1976) have mentioned fenestrations, but at best presented only scattered data on their geometric characteristics.

The form and structure of fenestrations in relation to the external diameter of the artery have not been investigated to my knowledge. The purpose of this study was to determine the relationship of various relevant characteristics with respect to the external diameter of the artery, for the internal elastic lamina from human cerebral arteries.

3.6.2 Methods

Cerebral arteries (designated series A, B, C and D) which did not exhibit any atherosclerotic disease were obtained at autopsy. Series

A, C and D were from females, aged 62, 48 and 50 respectively; series B was from a male aged 65. The cerebral arteries for all subjects were obtained *in situ*. The complete circle of Willis and peripheral branches were carefully removed *in toto*, photographed *in vitro*, and stored in isotonic saline at 4° C. Each series consisted of straight segments (totalling 9 or 10), about 1 cm in length, isolated from the various parts of the cerebral circulation.

The external diameter of the non-pressurized artery was determined with the aid of a travelling microscope by computing the average of two transverse measurements, approximately mutually perpendicular, while the artery was immersed in saline. The specimen was then sectioned longitudinally along one side. Next, each specimen was floated on to a cork backing, spread and pinned along the longitudinal edges, as illustrated previously in Figure 13, in an unstretched condition with the adventitial surface exposed. Specimens less than 0.7 mm in diameter could not be obtained, since suitable micro-surgical instruments for performing the longitudinal section were not available.

The specimens were next treated to remove the adventitia and smooth muscle coats by the method described previously in subsection 2.6.2. All specimens were treated and fixed within 18 days of death, since, during preliminary studies, no discernible degradation of the external surface was observed over a period of 31 days.

The process of freeze-drying the specimens has been presented in subsection 2.6.2. All specimens were sputter coated with gold in a Technics, Hummer I Sputter Coater and the external surface of the internal elastic lamina was examined with a Phillips (model SEM 500) scanning electron microscope.

At least 10 photomicrographs for each specimen at a single magnification of either 640, 1250, or 2500 were obtained of areas free of debris, and containing at least 30 fenestrations. All photomicrographs were obtained without tilting the specimen and a constant focal plane was maintained by adjusting the stage rather than the focus adjustment, in order to correct the focus. The purpose of this technique was to minimize both distortions and measurement error.

The films for all four series were mounted in an enlarger and each image was projected on the platen of a Hewlett Packard digitizer (model 9864A). The images represent a final magnification of 1150, 2250 or 4490. At least six photomicrographs for each specimen were selected for measurement.

Since the fenestrations were generally round or elliptical in shape, two sets of two points representing the length of the major and minor axes for the inside border of each fenestration were digitized and entered into a Hewlett Packard 9830A microcomputer for further processing and storage. Only fenestrations which appeared to pass completely through the internal elastic lamina were measured. The area for each fenestration was calculated with the use of equation (5)for an ellipse. Four geometrical characteristics were next computed:-

i) Diameter

The diameter of a circle (D) with an area equivalent to the ellipse was determined by relationship (6). An average diameter for all the fenestrations in the photomicrographs (minimum of six photomicrographs) was also computed.

ii) Density

The number of fenestrations per square millimeter (density) was

calculated from the number of fenestrations contained in a single field of view by equation (7). Only one density could be computed for each photomicrograph.

iii) Percentage Area

The percentage of the surface area comprised of fenestrations (summation of the area for each fenestration) with respect to the total area depicted in the field of view is computed with relationship (8). Only one percentage area could be calculated for each photomicrograph.

iv) Ligament Efficiency

Equation (13) for calculating the ligament efficiency has been derived in subsection 3.4.2. A single ligament efficiency was calculated for each photomicrograph.

It has been demonstrated with the use of latex rubber sheets, that the uniform pattern of perforations with a constant diameter and the same ligament efficiency as the replication of the fenestrations in the internal elastic lamina are equivalent in their uniaxial tensile behaviour. Therefore, although the ligament efficiency is an idealization of the actual spatial geometry, it provides a single-value parameter which effectively characterizes the combined change in the diameter and/or density of the fenestrations.

In section 2.6 it was reported that the linear shrinkage of the internal elastic lamina during freeze drying was 6.9% $\pm$ 0.92 SD. The influence of shrinkage on the absolute values of the diameter and density (percentage area and ligament efficiency are not affected) has been accommodated by applying an appropriate correction factor (equation (2) from subsection 2.6.4). The effect of applying the correction factor would be to increase the value for the diameter, but

decrease the value for density. Similarly, the value for the dispersion of the data has also been corrected to account for the combined dispersion of the data obtained in the present study, as well as the data associated with determining the correction factor.

Each plot of diameter, density, percentage area and ligament efficiency, against the external diameter of the artery was analyzed by successively adding higher order terms to obtain a polynomial regression (least squares) with the best fit. Following each step, the "F" statistic was computed in order to determine whether the coefficient associated with the largest power in the model is significant (i.e. $p < 0.05$).

3.6.3 Results

A total of 38 specimens represented by 242 fields of view were analyzed in this study. Many more specimens were prepared but were excluded, either because they were not flat, or more commonly, because a layer of fibrous tissue obscured the surface even after extending the sodium hydroxide treatment to four hours. A previous study by Merei et al (1980b) has shown that these are elastic fibres buried in the media and adventitia. The measurements from a typical total of 330 fenestrations were converted into the single average diameter for each specimen. A minimum of six values were computed for the remaining characteristics of density, percentage area and ligament efficiency of each specimen.

i) Diameter

The average diameter of the fenestrations decreased (right to left in Figure 35) as the artery decreases in diameter distally from the circle

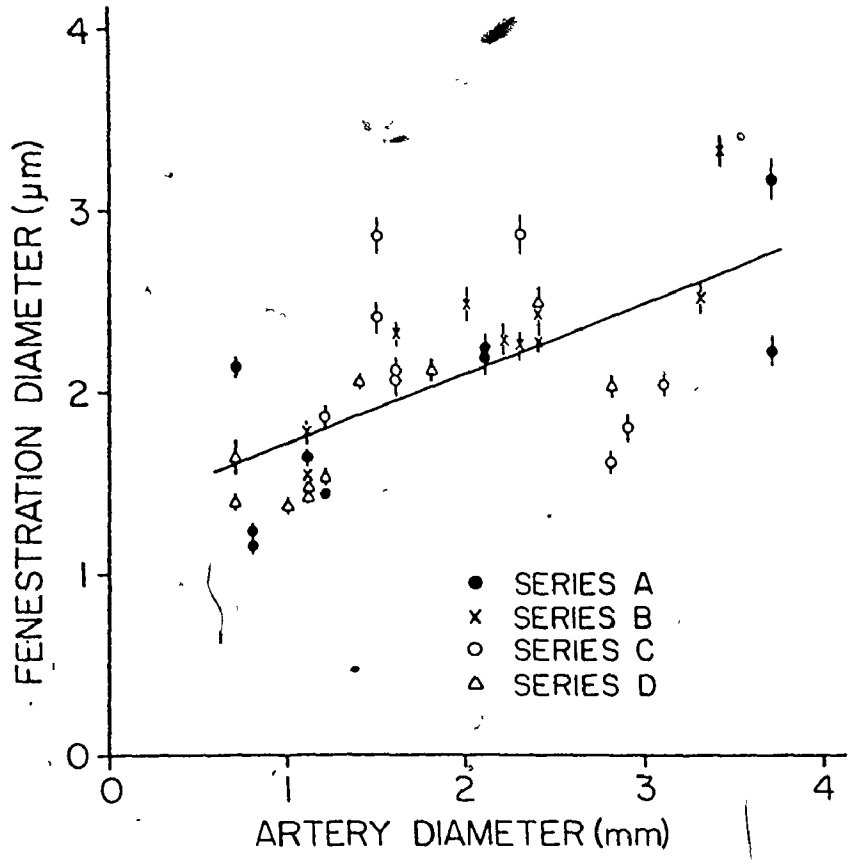

Figure 35 The relation between the diameter of the fenestrations (mean ± SEM) and the external diameter of the artery. The solid line represents the equation for the best fit, presented in the text.

of Willis. There were no prominent differences in the diameters among the four series taken from different subjects. The least squares curve which best fit the data was the linear regression line $Y = 1.33 + 0.39X$ ($p < 0.01$) with a correlation coefficient of 0.66. The best fit line is illustrated in Figure 35.

ii) Density

Figure 36 illustrates a plot of density with the external diameter of the artery. There is a moderate increase in the density (right to left in Figure 36) from the largest arteries in the circle of Willis to arteries with an external diameter greater than 1 mm. At 1 mm external diameter and less, the increase in the density appears to increase rapidly, although I was not able to obtain data for arteries less than 0.7 mm. The agreement in the data among the four subjects is again very good. The least squares polynomial which best describes the data was the third order polynomial $Y = 56161 - 64170X + 25737X^2 - 3330X^3$ with a correlation coefficient of 0.92. This polynomial was significant at $p << 0.001$ and all coefficients were significant at $p << 0.001$. The best fit line is illustrated in Figure 36. A logarithmic regression provided a less satisfactory fit.

iii) Percentage Area

The combined effect of diameter and density on the computation of the percentage area is shown in Figure 37. The general trend for a decrease in the arterial diameter (i.e. right to left) is for the percentage area to increase. There is again good general agreement in the results among the four subjects. The increase in percentage area for the small diameter arteries is attributable to the rapid increase in the density. The least squares polynomial which best represents the

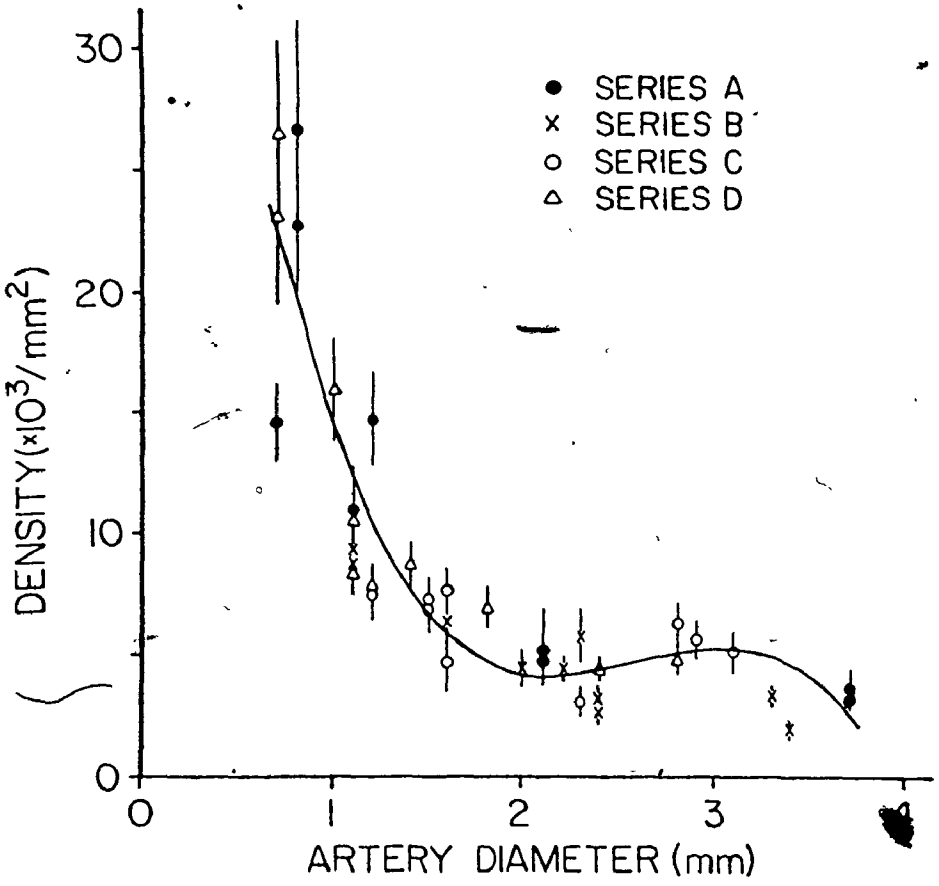

Figure 36 The change in density of the fenestrations (mean ± SEM) in relation to the external diameter for the artery. The solid curve represents the equation for the best fit, presented in the text.

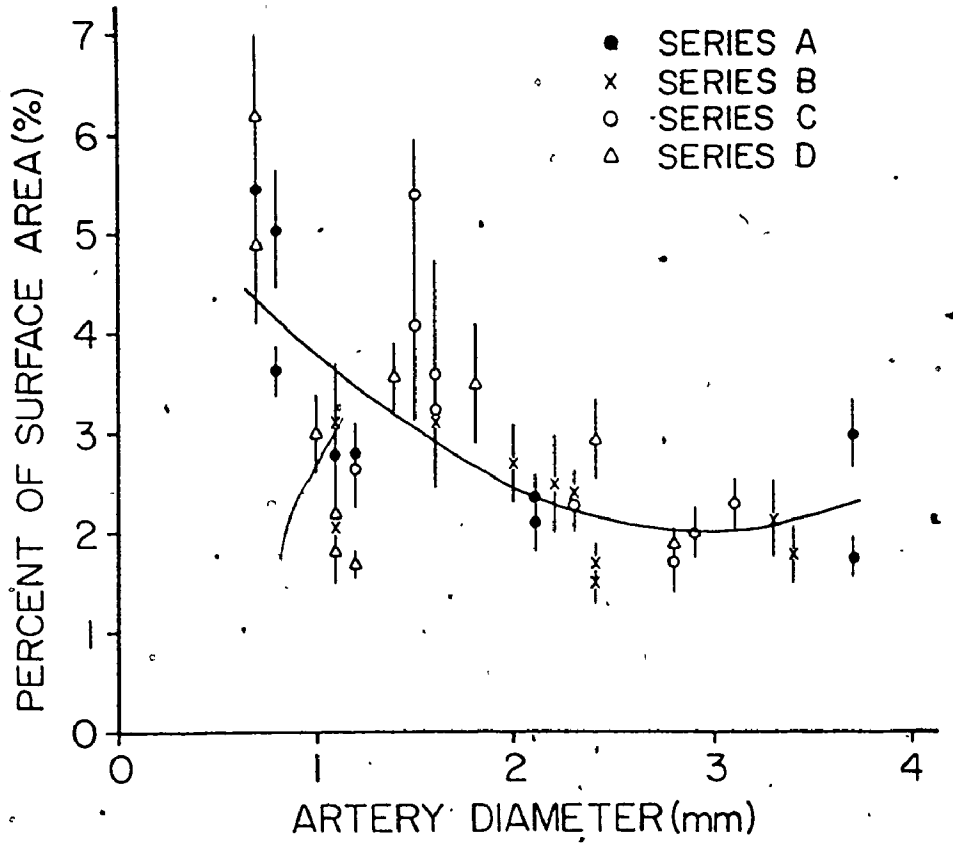

Figure 37 The representation of the percentage area for the fenestrations (mean ± SEM) with respect to the external diameter of the artery. The solid curve represents the equation for the best fit presented in the text.

data was the second order polynomial $Y = 5.95 - 2.65X + 0.45X^2$ with a correlation coefficient of 0.64. This polynomial was significant at $p << 0.001$. The linear term was significant at $p < 0.001$ and the quadratic term was significant at $p < 0.01$. The best fit curve is illustrated on Figure 37.

iv) Ligament Efficiency

The results for the ligament efficiency with arterial diameter, depicted in Figure 38, visually appear to represent a horizontal line. If the data points corresponding to $X = 0.7$ are excluded, then this impression is confirmed ($r^2 = 0.098$ is not significant, therefore the data is fitted best by the constant $Y = 0.838$). If the data points at $X = 0.7$ were included then the data is best described by the second order polynomial $Y = 0.74 - 0.084X - 0.016X^2$ which has a significance level of $p < 0.005$. The linear term is significant at $p < 0.005$ and the quadratic term is significant at $p < 0.05$. The best fit curve with the values at $X = 0.7$ excluded has been depicted on Figure 38.

3.6.4 Discussion

The characteristics of diameter, density, percentage area and ligament efficiency showed remarkable similarity among the four subjects.

A comparison of the fenestration diameters for the arterial segments (anterior circulation) closest to the anterior communicating artery revealed an average value of 2.1 μm for the present study which is considerably less than the value of 6.8 μm reported in the study by Hassler (1962) for a comparable age group. However, the diameter from

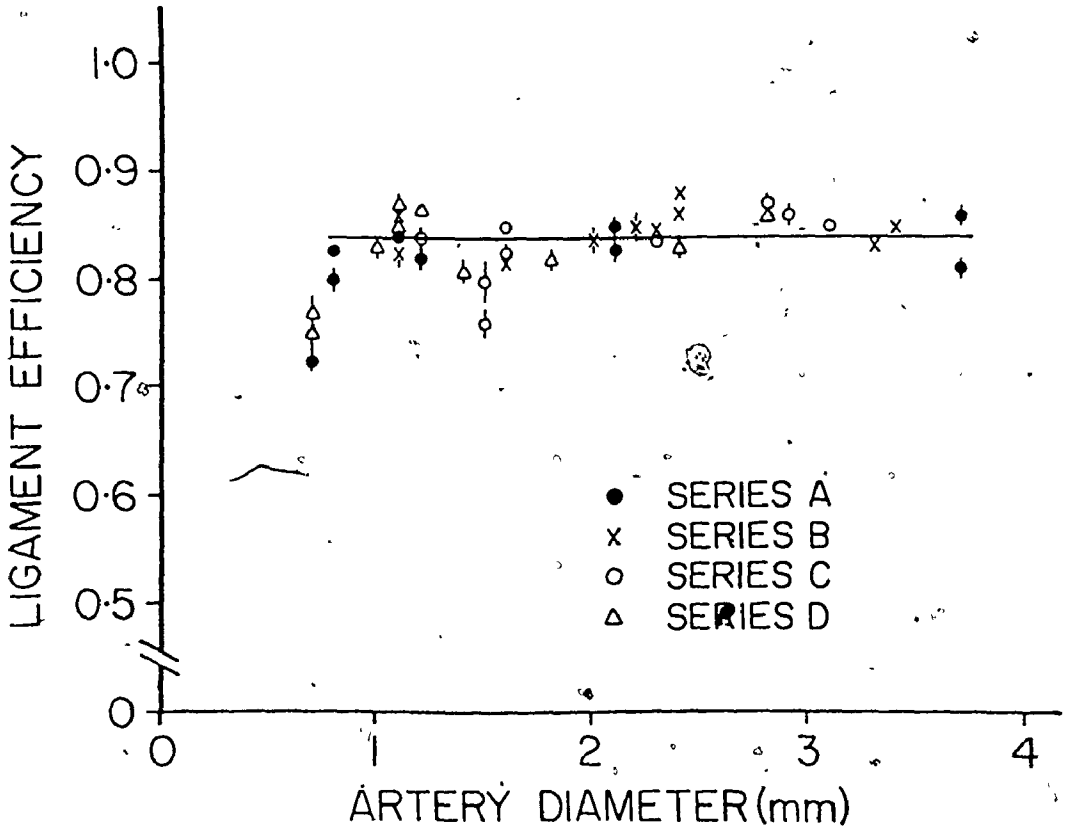

Figure 38 The values for ligament efficiency (mean ± SEM) are plotted with respect to external diameter of the artery. The solid line (excluding the values for the diameters less than 0.8 mm) represents a constant.

this study is comparable to the diameters of "1 to 2 μm" quoted by Lang and Kidd (1965). The difference between the values in this study and that of Hassler (1962) could possibly be attributable to a difference in the measurement scheme, since Hassler (1962) measured the "maximum diameter of the windows" whereas, in our study, the internal or minimum diameter was measured. Furthermore, the enhanced resolution capabilities of the scanning electron microscope may have resulted in the measurement of many small fenestrations, not discernible with the light microscope. There is also a difference for the percentage areas between the two studies, which again could be accounted for by the difference in diameter.

There is reasonable agreement for the same age groups between an average fenestration density of 4670 per square mm for the present study and 3800 per square mm in the study by Hassler (1962) for specimens from the anterior circulation. Since Hassler does not mention the shrinkage associated with his technique, correction for shrinkage would further reduce his value for density which would further increase the difference with respect to my results. The variation between the results again could be attributable to the technique employed by Hassler (1962) which may not have removed the debris embedded in the fenestrations, perhaps obscuring some fenestrations. The enhanced resolution of the scanning electron microscope could also account for the variation.

There is recent preliminary evidence (Potter & Roach, 1983) that the diameter of the fenestrations increased in the region of sustained distension resulting from a postenotic dilatation. The decrease in the fenestration diameter with the decrease in arterial diameter shown in

the present study, resembles the decrease in the circumferential wall stress that would be anticipated as the external diameter of the artery decreases. This would suggest that the diameter of the fenestrations is influenced by the local wall stress. However, this relationship cannot be confirmed until the relative thicknesses of the arterial wall and internal elastic lamina have been established for the range of external diameters examined in this investigation.

Rodgers et al (1967) observed that no elastin was found in human renal arteries less than 0.1 mm in diameter. Rodgers et al (1967) also reported that Oppenheim (1918) described the internal elastic lamina of small arteries in cross section as consisting of small dots (presumably, the intervening ligaments between fenestrations) which become more closely spaced as the size of the artery increased and finally merged into a continuous membrane. Therefore, the dramatic change in the density for the arteries with the smallest diameter may represent the characteristics of this transition to an absence of the internal elastic lamina.

The percentage area is a single-value function incorporating both the average diameter and density of the fenestrations. Changes in the diameter alone would have a more significant influence than density alone on the results, because of the squared term (i.e., radius square) in the equation. This may account for the noticeable scatter in the results for percentage area, compared with the ligament efficiencies.

The apparent consistency in the ligament efficiency with decreasing arterial diameter suggests that the general spatial geometry of the fenestrations in the internal elastic lamina may be dictated by a relationship which is uniquely described by ligament efficiency. The

substantial increase in density and concomitant decrease in the ligament efficiency for the smallest arteries (less than 1 mm) indicates a possible transformation in the characteristics as mentioned previously.

The purpose for the presence of fenestrations in the internal elastic lamina has not been resolved. Hassler (1962) suggested that the fenestrations are ". . . narrow gateways facilitating the important passage of nutrients to the media . . ." Bjorkerud (1969) observed that smooth muscle cells appeared in the "pores" of the internal elastic lamina, 24 hours after the inner surface of the rabbit aorta was damaged. The subsequent formation of a subendothelial network or parallel ribbons of smooth muscle cells which constitute the first stage of the developing intimal thickening suggest that the smooth muscle cells migrate from the media to the subendothelium. Therefore, the presence of the "pores" or fenestrations may be to provide an opening for the smooth muscle cells in the process of repair.

Although it is generally recognized that the smooth muscle cells produce elastic units which aggregate and fuse to form larger units (Haust, 1965) the method of formation of the elastic lamina has not been resolved. Consequently, the process for determining the shape and size of fenestrations has also not been investigated. The apparent consistency of the value for the ligament efficiency for the range of arteries in this investigation suggests a mechanism which dictates a consistent spatial geometry.

3.6.5 Summary

Four geometrical characteristics which represent the fenestrations

in the internal elastic lamina have been calculated for human cerebral arteries of varying external diameter. Specimens from the circle of Willis and peripheral cerebral arteries of four subjects were isolated from the arterial tree, photographed with the scanning electron microscope, and measurements taken from the photomicrographs before the geometrical measurements were computed. Correction factors determined from the previous study were applied to the data in order to account for the shrinkage of the tissue during preparation. The decrease for the diameter of the fenestrations with the decrease in the external diameter of the artery was represented by a linear relationship. The pronounced increase in the number of fenestrations per square millimeter (density) for the arteries of small external diameter was modelled by a third order polynomial. The general increase for the percentage area of the surface comprised of fenestrations in relation to the decrease in the external diameter of the arteries was modelled by a second order polynomial. The ligament efficiency (ratio of the minimum width of the solid band of material to the centre-to-centre distance for two or more adjacent holes) was virtually constant for the arteries with external diameters greater than 0.7 mm. Although, neither the purpose for the presence of fenestrations in the internal elastic lamina, nor the process for forming the internal elastic lamina (and hence the fenestrations) have been resolved, the constant value for the ligament efficiency suggests a mechanism that dictates a consistent spatial geometry based upon ligament efficiency.

Chapter 4

THE PROBABLE ROLE OF FENESTRATIONS AS A FACTOR IN THE ETIOLOGY OF INTRACRANIAL SACCULAR ANEURYSMS

4.1 Introduction

Blood is supplied to the brain by the two carotid and two vertebral arteries which feed a loop of arteries referred to as the circle of Willis. Emanating from the circle of Willis are several major branches (anterior cerebrals, middle cerebrals, posterior cerebrals) which form a distribution system to supply blood to all parts of the brain. The typical anatomical terms associated with the circle of Willis are depicted in Figure 39.

An arterial lesion associated with the circle of Willis and the larger peripheral cerebral arteries are aneurysms which are classified as a "localized and persistent dilatation that results from the yielding of the components of the wall of the heart or blood vessels" (Stehbens 1972, page 351). Although there are several classifications of aneurysms, the particular type of interest for the ensuing discussion is the saccular arterial aneurysm or intracranial saccular aneurysm which forms a dome-shaped outpouching, usually at the apex or carina of a bifurcation. Figure 40 illustrates a saccular aneurysm at the apex of a bifurcation. The terms associated with a saccular aneurysm at a bifurcation are illustrated in Figure 41.

About 85 % of the aneurysms are found in the anterior circulation (includes both anterior and middle cerebral arteries) while 15 % are observed in the posterior circulation (includes posterior, basilar and vertebral arteries). The most common sites on the anterior circulation are at the origins of the anterior or posterior communicating arteries

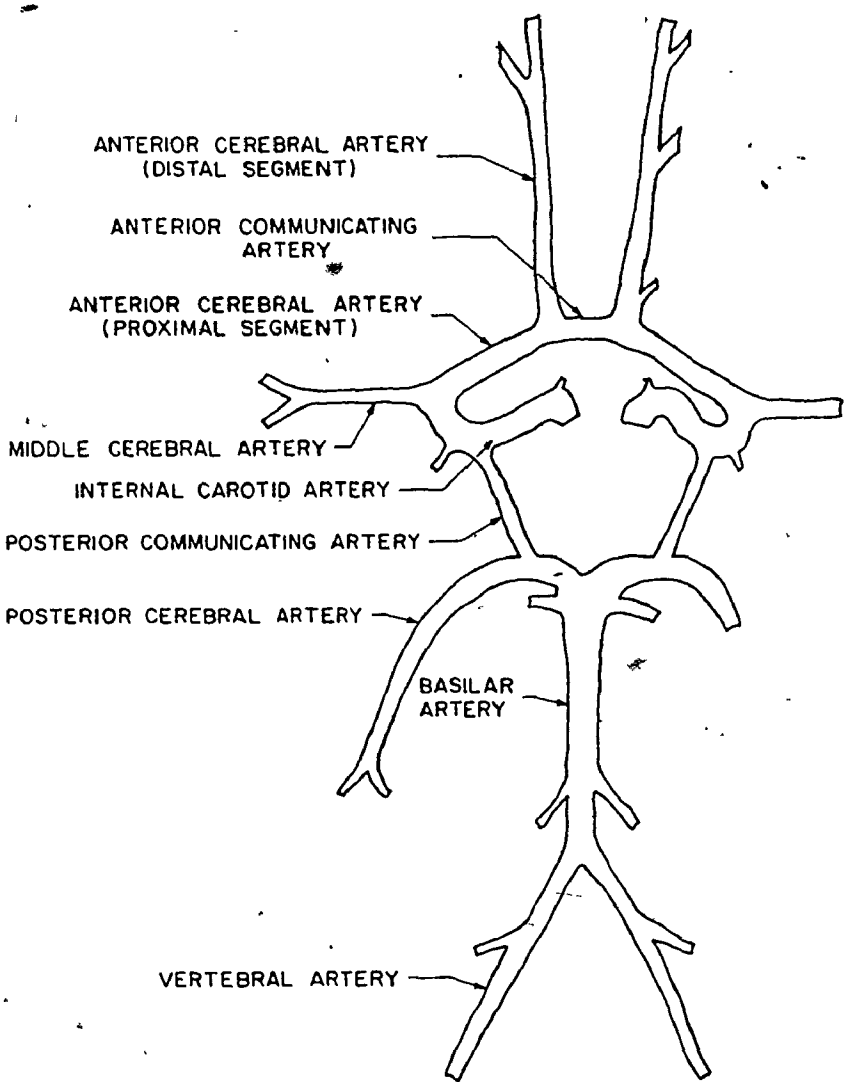

Figure 39 The anatomical terms associated with the circle of Willis (human cerebral arteries).

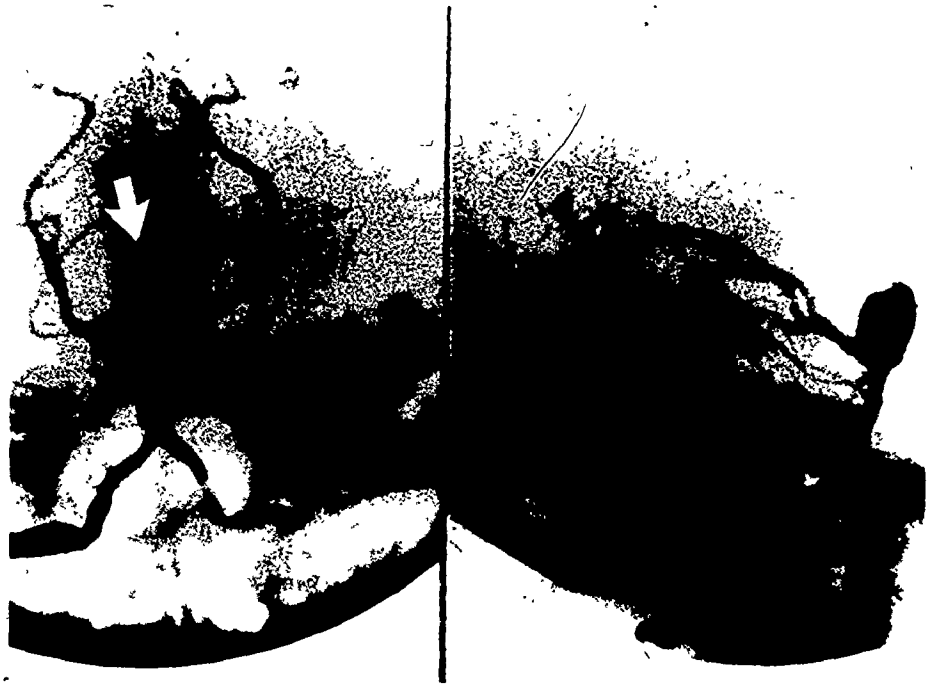

Figure 40 An angiogram illustrating a saccular aneurysm (arrow) at the bifurcation (reproduced with permission of Dr. G. G. Ferguson).

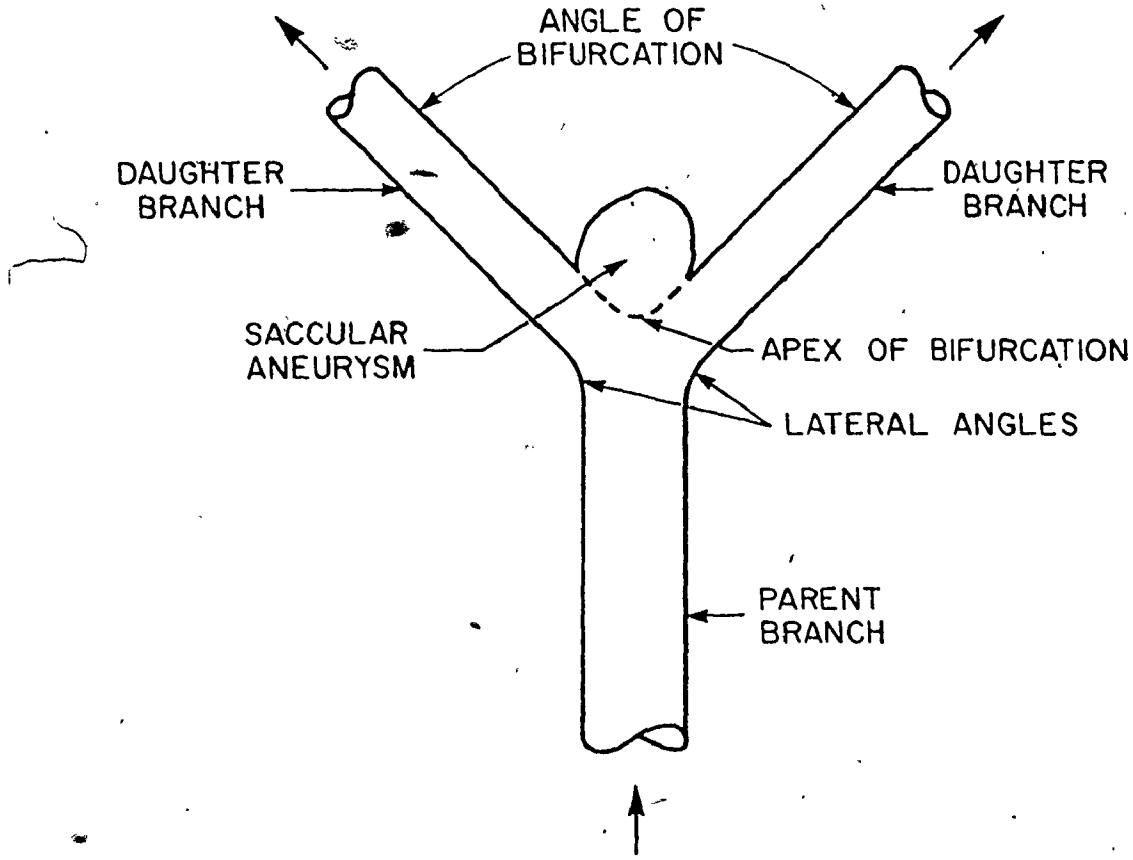

Figure 41 The terminology associated with an intracranial saccular aneurysm.

as well as the bifurcation of the middle cerebral arteries. The basilar bifurcation is the most common site on the posterior circulation (Stehbens, 1954).

The usual consequence of the formation of an aneurysm is the continued enlargement with the probability of eventual bleeding and even rupture that may cause death. The rupture of an intracranial saccular aneurysm is one cause of subarachnoid hemorrage which is a principal cause of "stroke". The incidence of an aneurysm is greatest during the fourth to sixth decades of life and women appear to be more susceptible than men.

Although there has been considerable progress in the operative and medical treatment of saccular aneurysms, the understanding of the formation, enlargement and rupture has not advanced as rapidly. The analysis of several autopsy reports has indicated that about 5 % of the population may be afflicted by aneurysms (ruptured and unruptured).

The ensuing review of the literature pertaining to the initiation, growth and rupture of intracranial saccular aneurysms is intended to familiarize the reader with the relevant investigations but it is not intended to represent a comprehensive survey of the literature on the subject. The sections following the review will present complementary studies to the previous investigations of i) the form and structure of fenestrations in the internal elastic lamina from cerebral arteries; ii) the tensile characteristics and change in spatial geometry of models of the form and structure of fenestrations in the internal elastic lamina from cerebral arteries in the apical region of bifurcations.

4.2 Pathogenesis of Intracranial Saccular Aneurysms

4.2.1 Etiology

The wall of the aneurysm is devoid of media, which usually terminates in the neck region of the aneurysm. The internal elastic lamina also ends abruptly in the neck region of the aneurysm with only remnants observed in the aneurysm wall. The walls of large aneurysms are usually thicker consisting mainly of thickened hyaline connective tissue.

There is a general consensus that both the internal elastic lamina and media must be absent or considerably weakened for an aneurysm to form. It has not been resolved which layer is more important in the evolution of an aneurysm and whether congenital or degenerative factors play a major role.

Forbus (1930) reported medial defects in the cerebral arterial wall of about three quarters of the subjects he studied. He postulated that these defects were a focal weakness in the vessel wall which caused degeneration of the elastic membrane due to continued overstretching of the membrane caused by stresses induced by the hemodynamics of the blood flow at the apex. Glynn (1940) found medial defects in about 90% of the arteries from subjects both with and without aneurysms. Furthermore he observed the medial defects along the lateral borders of the bifurcations where aneurysms do not form. He also evaluated the structural integrity of the arterial wall by inflating segments with natural medial defects and other segments with an artificial defect produced by scraping away the media and adventitia

proposed that degeneration of the internal elastic lamina was the most significant factor, caused by atherosclerosis or other factors.

Carmichael (1945) studied two hundred patches of atheroma in cerebral vessels over 1 mm. in diameter. He postulated that defects in the media and internal elastic lamina must be present for the formation of an aneurysm. However, even if both defects were present, the development of aneurysms could be delayed by fibrosis of the intima.

Hassler (1961) presented the first comprehensive study on the peculiarities of the cerebral arteries and their association with saccular aneurysms. He was one of the first to recognize that degeneration of the internal elastic lamina was a consequence of "exhaustion and overstretching."

Stehbens (1972, 1975b) has rejected the medial defect theory. Instead Stehbens (1975b) has described three types of lesions. The first was "funnel-shaped dilatation" which is an area of attenuation or loss of media, degenerate or absent internal elastic lamina and attenuated adventitia. The distinction between these areas and the medial defects described by Forbus (1930) was that the medial discontinuity in these dilatations was not abrupt and the adventitia was not thickened. The second type of lesion was "areas of thinning" which was basically a thin wall with possible attenuation of the adventitia, along with absence of the media and internal elastic lamina. These areas demonstrate a bulge with a pressure of only 30 cm. of water. The third type of lesion was "small evaginations" which are visible microscopically as a bulge of the intima through a part of the medial defect or at the junction of the defect with normal tissue. Usually there was degeneration of the elastin, but the internal elastic

lamina was found intact in some cases.

Cajander and Hassler (1976) found lysosomal granules in extracellular space of cerebral aneurysms. They have suggested that these granules originate from leukocytes located on the luminal side of the vessel creating autolysis of the elastica thereby influencing the development of aneurysms.

4.2.3 Enlargement and Prognosis

The growth and rupture of a saccular aneurysm is dependent upon the mechanical and pathological considerations of the wall structure as well as intraluminal hemodynamics and extramural constraints. Scott et al (1972) obtained static pressure/volume curves of human saccular aneurysms and cerebral arteries. They found that the elastance (tension/strain) of the walls of aneurysms was noticeably greater than for the arteries, which led them to theorize that the increase was attributable to the absence of elastin in the aneurysm wall whereas the arterial wall contains a combination of collagen and elastin. The thinner wall of the aneurysm would also create a higher stress.

The influence of hypertension on the origin, growth and rupture remains unresolved. Chason and Hindman (1958) reported hypertension, diagnosed clinically or at autopsy in about 80% of patients with aneurysms (ruptured and unruptured). Stehbens (1962) also observed that hypertension was more prevalent in patients with aneurysms (54%) than a control group. In the Cooperative Study of Intracranial Aneurysms (Locksley, 1966) the incidence of hypertension was higher in patients with larger aneurysms which would imply that hypertension contributed to the enlargement. Andrews and Spiegel (1979) found that

hypertension was not more prevalent for the aneurysm population in relation to the age matched general population, except for females aged 18 to 54 years. The incidence was twice as great for both male and female hypertensive patients under 55 years of age. Increasing age, increasing systolic pressure and increasing diastolic pressure all corresponded with an increased number of aneurysms for females but not males. Conversely, McCormick and Schmalstieg (1977) reported no notable difference between age and sex matched autopsy population for patients with ruptured and unruptured aneurysms. Neither was there evidence of an association between hypertension and multiplicity of aneurysms, the age when aneurysms become evident nor rupture. Saccular aneurysms can arise and even rupture in the absence of hypertension.

Turbulence is also considered a major factor in the growth and rupture of aneurysms. The normal velocity of flow in cerebral vessels is sufficient to produce turbulence in the sac of human intracranial saccular aneurysms (Ferguson 1970). However, Ferguson (1970) discounted turbulence as a causative factor in the initiation of aneurysms because calculation of the Reynolds number based on the blood flow velocity and diameter of the internal carotid artery suggested that turbulence was unlikely to occur at major intracranial bifurcations without aneurysms.

Previously, Roach (1963) had shown that the post-stenotic dilatation that occurs in peripheral arteries was the result of turbulence that weakened both the elastin and to a lesser extent the inter-collagen links of the vessel wall. Foreman and Hutchison (1970) found that normal blood flow through stenotic vessels induced peaks of vibrations that coincided with natural resonant frequencies of the

vessel wall. These studies appear to support the concept that turbulence at arterial bifurcations can weaken the aneurysmal walls, causing the growth of an aneurysm and that the weakening may precede noticeable histological changes in the vessel wall. Musical high-pitched bruits recorded by Ulinger and Wasserman (1977) from aneurysms were represented as a flexible Helmholtz resonator. This self-excitation, rather than turbulence, was thought to produce resonant vibrations of the arterial wall and concomitant structural fatigue.

Two further factors mentioned by Sekhar and Heros (1981) as possible contributing factors for the initiation of aneurysms are axial stream impingement on the apex of bifurcations and the effect of pulsatile flow. The dissipation of the kinetic energy at the apex of bifurcations has also been implicated as a cause of structural fatigue.

Factors such as mechanical fatigue, occlusion of the vasa vasorum or enzymatic digestion have also been mentioned as factors leading to a focal weakening which may result in rupture or further deposition of collagen and restrengthening (growth). The process of microrupture, reorganization of fibres and growth is believed to be cyclical.

Different autopsy studies have revealed that the size of aneurysms that ruptured were 4 mm. (Crompton 1966), 6-15 mm. (Crawford 1959) and 5 mm. (McCormick and Acosta-Rua, 1970). The study by Crawford (1959) showed that a substantial proportion ruptured at the fundus of the aneurysm. Aneurysms that remain intact due to the strength of their wall may then enlarge to gigantic proportions or remain static in size and even thrombose.

4.3 Fenestrations in the Internal Elastic Lamina at Bifurcations of Human Cerebral Arteries

4.3.1 Introduction

The structure of the internal elastic lamina of cerebral arteries has never been clearly delineated. In addition, the role of the internal elastic lamina in the formation of intracranial saccular aneurysms, known to form predominantly at bifurcations, remains an enigma.

Dees (1923) first described the internal elastic lamina of human and bovine aortas and renal arteries as a continuous sheath penetrated by small windows. However, Nystrom (1963) described the elastic lamina of human arteries as a fibrous structure. Lang and Kidd (1965) stated that the elastic lamina of human cerebral arteries is split into layers with the luminal surface a meshwork of fibres which transforms into a sponge-like layer, and finally forms a solid mass in the layer adjacent to the media.

Hassler (1962) examined the fenestrations, which he described as windows, contained within the elastic lamina of cerebral arteries of humans, from newborns to the age of ninety years. He presented data to describe relevant characteristics of fenestrations in the internal elastic lamina of straight cylindrical segments isolated from the intracranial portion of the internal cartoid and anterior cerebral arteries. Cook, Salmo and Yates (1975) examined the "length" and "number of gaps" in the internal elastic lamina of the external iliac artery from humans of age twenty to seventy years. Other authors (Lang and Kidd (1965), Hassler (1972), Cajander and Hassler (1976) have made reference to fenestrations, but did not provide data concerning their

characteristics. A subsequent paper by Hassler (1972) showed large fenestrations at the neck of a saccular aneurysm obtained at autopsy. Nevertheless, specific information on the size of these fenestrations was not presented.

The present study was undertaken in order to: (i) establish numerical values for the fenestrations in the apical region of bifurcations; (ii) resolve whether the enlarged fenestrations observed by Hassler (1972) existed prior to the development of the aneurysm, or whether they had evolved as a consequence of distention of the internal elastic lamina during enlargement of the aneurysm.

4.3.2 Methods

Cerebral arteries (designated series I, II, III and IV) which did not exhibit any visible atherogenic disease were obtained at autopsy and stored at 4°C for 4 to 17 days in isotonic saline. Series I, was a circle of Willis obtained from a 62 year old male. The other cerebral arteries were obtained in situ: series II, from a 62 year old female; series III, from a 65 year old male; and series IV, from a female aged 58. Subsequently, the complete circle of Willis and larger peripheral branches were carefully removed in toto. The complete arterial tree from series III and IV was photographed in vitro and stored in isotonic saline at 4°C.

Every bifurcation from the four series was isolated from the arterial tree and then sectioned along the lateral borders from the daughter branch to the parent artery (in order to minimize damage to the apex). The specimen was then floated on to a cork or balsa wood backing, spread and pinned (as illustrated in Figure 42) in an

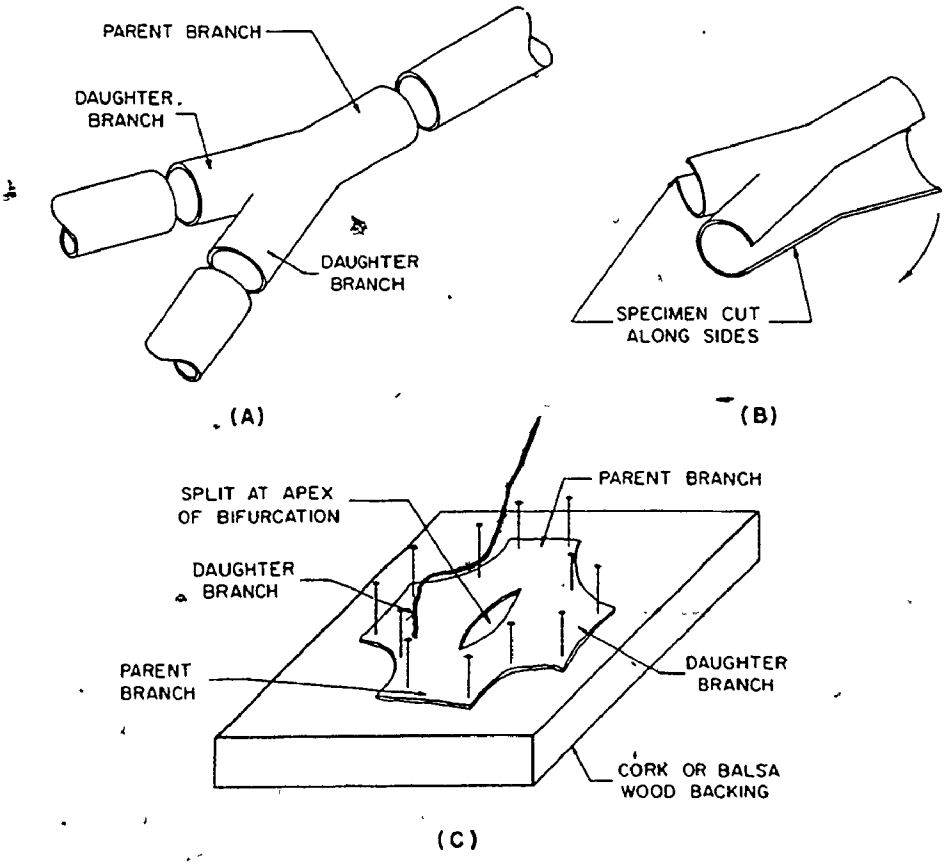

Figure 42 Preparation and mounting of the bifurcation specimens. A - Specimen is cut from the arterial tree. B - Sectioning of the specimen along the lateral borders. C - The final pinned position of the specimen on the cork or balsa wood backing with the adventitial surface exposed.

unstretched condition with the adventitial surface exposed. The specimens were next treated to remove the adventitia and smooth muscle coats by the method described in subsection 2.6.2. All specimens were treated and fixed within 18 days of death. No degradation of the elastin was observed for a period of 31 days.

Series I and II specimens were processed through graded acetones (30%, 50%, 70%, 90%, 95%, 100% and 100%) followed by critical point drying in a Polaron Model E 3000 Critical Point Drying Apparatus. Series III and IV specimens were freeze-dried (subsection 2.6.2). A difference in shrinkage between the two methods was not established in section 2.6.

Subsequently, all specimens were sputter coated with gold in a Technics, Hummer II Sputter Coater and the external surface of the internal elastic lamina was examined with a Philips Scanning Electron Microscope model SEM 500.

The surface of each specimen was scanned initially at magnifications of 40 and 160 to provide a general impression of the surface topography and as well to delineate areas of interest. Ten photomicrographs at magnifications of 640 or 1250 were obtained of areas with fenestrations of "normal" size when judged in relation to adjacent straight segments. Only areas free of debris and containing a minimum of at least 30 fenestrations with distinct borders were selected. Photomicrographs containing at least 30 fenestrations from the same bifurcation, in regions with "enlarged" fenestrations were also obtained. In this manner each bifurcation acted as its own control for a later comparison of regions of normal and enlarged fenestrations. All photomicrographs were obtained without tilting the

specimen and a constant focal plane was maintained by adjusting the stage rather than the focus adjustment in order to maintain the focus. The purpose of this method was to minimize both distortions and measurement error.

The films from all four series were mounted in a Simmon Omega B-22 enlarger and the image projected on the platten of a Hewlett Packard Digitizer (Model 9864A). Six of the photomicrographs were selected from the "normal" group for measurement. All photomicrographs of reasonable quality from the region of enlarged fenestrations were selected for measurement since there were fewer fenestrations.

Since the fenestrations were generally round or elliptical in shape, two points representative of the borders of the major axis and of the minor axis for the internal diameter of each fenestrations were digitized and the values entered directly into a Hewlett Packard 9830A microcomputer for further processing and storage. Only fenestrations which appeared to pass completely through the internal elastic lamina were measured.

The area for each fenestration was computed with the use of the equation for an ellipse (equation (5)).

Three geometric characteristics (Diameter, Density, and Percentage Area) were computed.

4.3.3 Results

Althought 54 bifurcation specimens were prepared, only 28 were deemed acceptable for analysis (Table 6) either because they were not flat, or more commonly, because a layer of fibrous tissue obscured the surface even after four hours of treatment with NaOH.

Specimens	Series Numbers I	II	III	IV	TOTAL
BIFURCATION					
Number prepared	2	24	17	11	54
Number analyzed	2	6	10	10	28
Number with enlarged fenestrations	1	2	6	4	13
Number with gaps	-	17 of 20	9 of 12	9 of 10	35 of 42
CYLINDRICAL					
Number prepared	3	20	22	13	58
Number analyzed	0	9	16	9	34
Number with enlarged fenestrations	0	0	0	2	2
Number with gaps	0 of 0	0 of 9	0 of 16	2 of 9	2 of 34

TABLE 6 - Specimen Series Listing

Figure 43 illustrates a typical example of the topography of the internal elastic lamina as viewed in the scanning electron microscope. The fenestrations penetrating the internal elastic lamina are generally round or slightly oblong, with smooth contours. There are remnants of fibrils on the surface and, in addition, there appear to be fibres buried in the matrix.

Thirteen of the twenty-eight bifurcation specimens analyzed (Table 6) had regions in the vicinity of the apex where the fenestrations were noticeably enlarged as shown in Figure 44. The shape of these enlarged fenestrations was again either round or oblong with smooth contours. Although two of the six analyzed specimens from series II demonstrated possible regions of enlarged fenestrations, the quality of these regions was inadequate for analysis. Nevertheless, they have been included in the group of bifurcations with enlarged fenestrations.

The remaining 15 specimens did not demonstrate enlarged fenestrations in the regions analyzed. Nevertheless, enlarged fenestrations may have been present but were obscured by the partial covering of fibrous material. The fenestrations from these 15 specimens were either round or oblong, similar to the group of normal fenestrations surrounding the regions of enlarged fenestrations.

A group of straight arterial segments prepared concurrently, revealed enlarged fenestrations in only two of the thirty-four specimens analyzed (Table 6). The scarcity of regions of enlarged fenestrations in the straight segments suggests that the enlarged fenestrations are almost exclusively located in the apical region of the bifurcation. This factor, together with the absence of distention of the specimen, virtually eliminates drying artifacts as the cause of

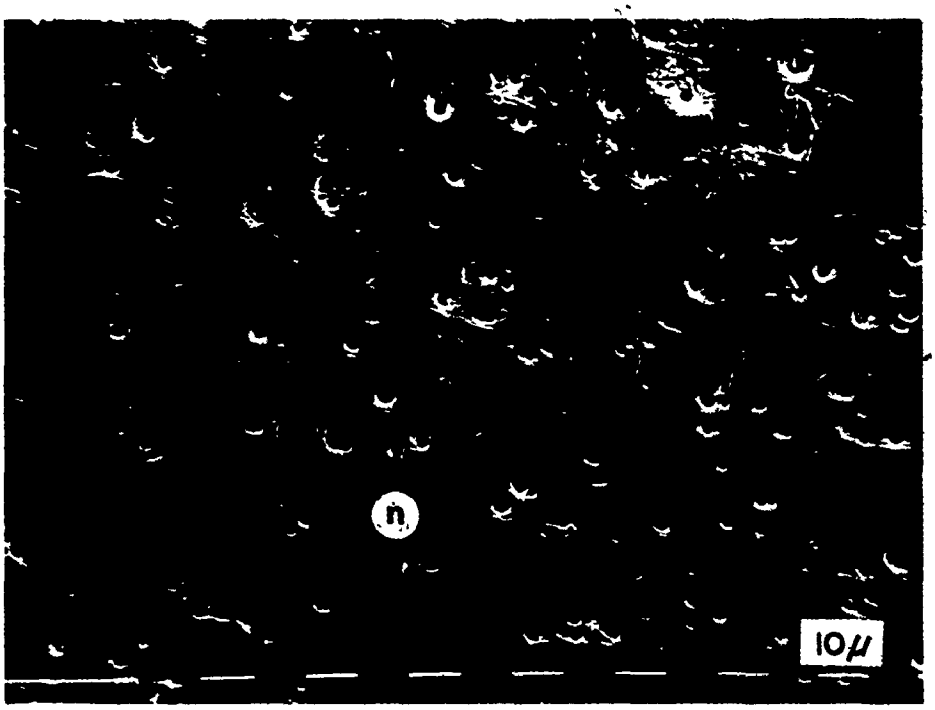

Figure 43 A typical illustration of the external surface of the internal elastic lamina from the human cerebral arteries. n = normal fenestrations. (Short white marks represent 10 μm).

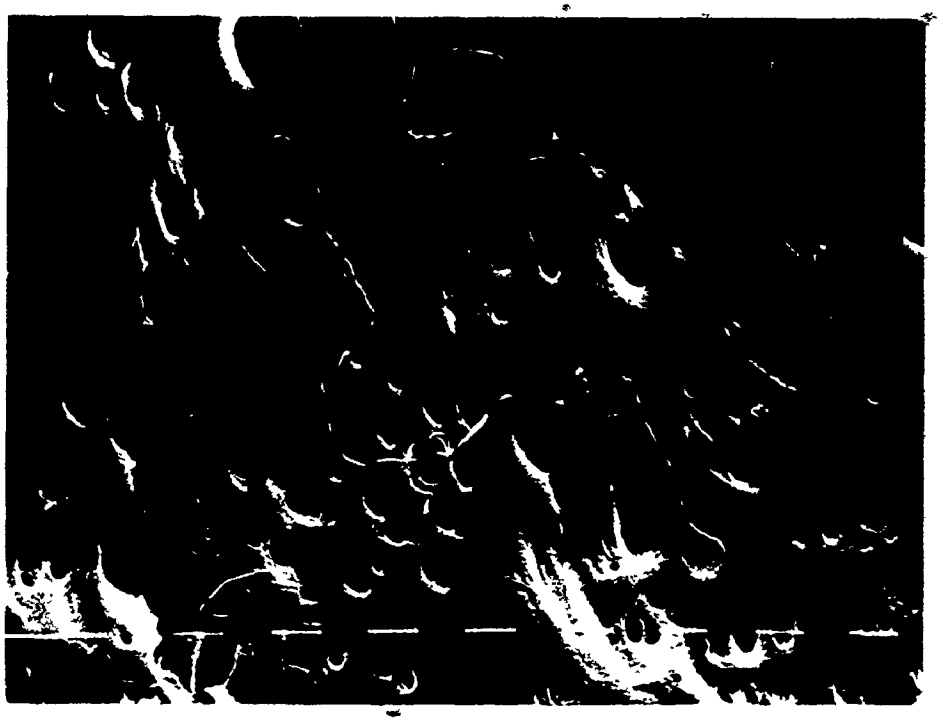

Figure 44 Illustration of enlarged fenestrations near the apex of the bifurcation. (Short white marks represent 10 μm).

the enlarged fenestrations. The pliable nature of the arterial wall facilitated the process of unfolding the specimen from the bifurcation shape, in order to conform to the flat cork backing. Folds were observed in the internal elastic lamina following isolation, which permitted flattening without stretching. The regions of enlarged fenestrations generally formed clusters (Figure 45) or circumferential bands (Figure 46) in the region of the apex of the bifurcation and on the medial aspect of the daughter branches.

During examination of series II with the scanning electron microscope, large elliptical gaps were observed at the centre of most of the specimens (85%) corresponding to the apical region of the bifurcation (Figure 47). Visual examination of a few untreated specimens from series III and IV did not usually reveal the gaps until a slight tension was applied between the daughter branches. A split oriented across the saddle of the bifurcation became enlarged to form an elliptical gap. The presence of these gaps was confirmed during subsequent examination with the scanning electron microscope in about 80% of the specimens from series III and IV (Table 6). The regions of enlarged fenestrations were usually adjacent ot the gaps and the circumferential bands mentioned previously were oriented in the same direction as the long axis of the gap. In most cases, the lip of the gap could not be examined since it had been reflected under the specimen. However, in at least three cases the split in the internal elastic lamina had propagated through a region of enlarged fenestrations (Figure 48). The internal elastic lamina in the apical region of some specimens appeared disrupted with a fibrous matrix forming the major structural element.

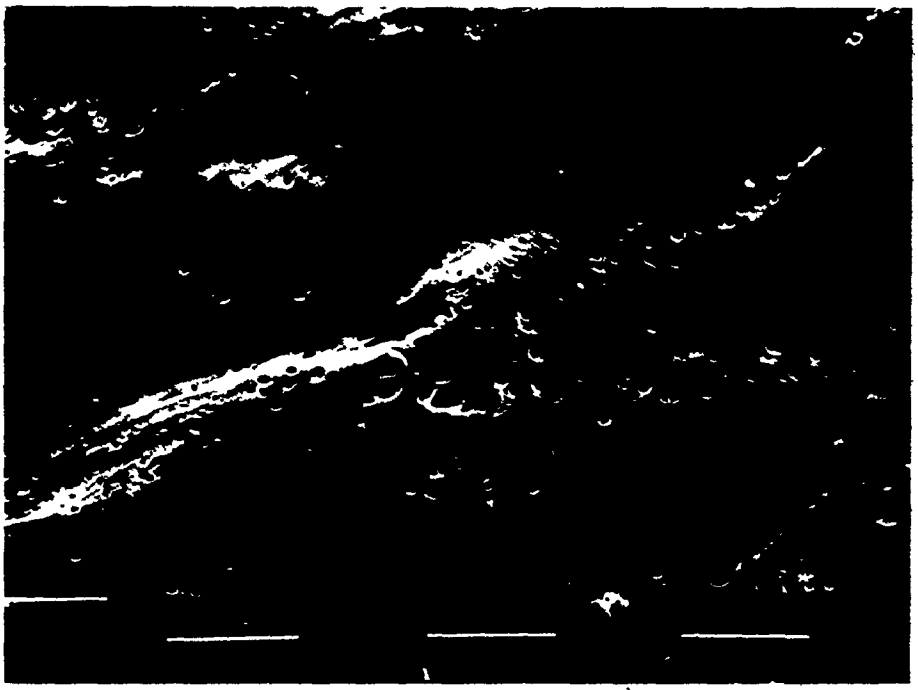

Figure 45 A cluster of enlarged fenestrations is shown in the centre of the photomicrograph. Short white bars represent 100 μm.

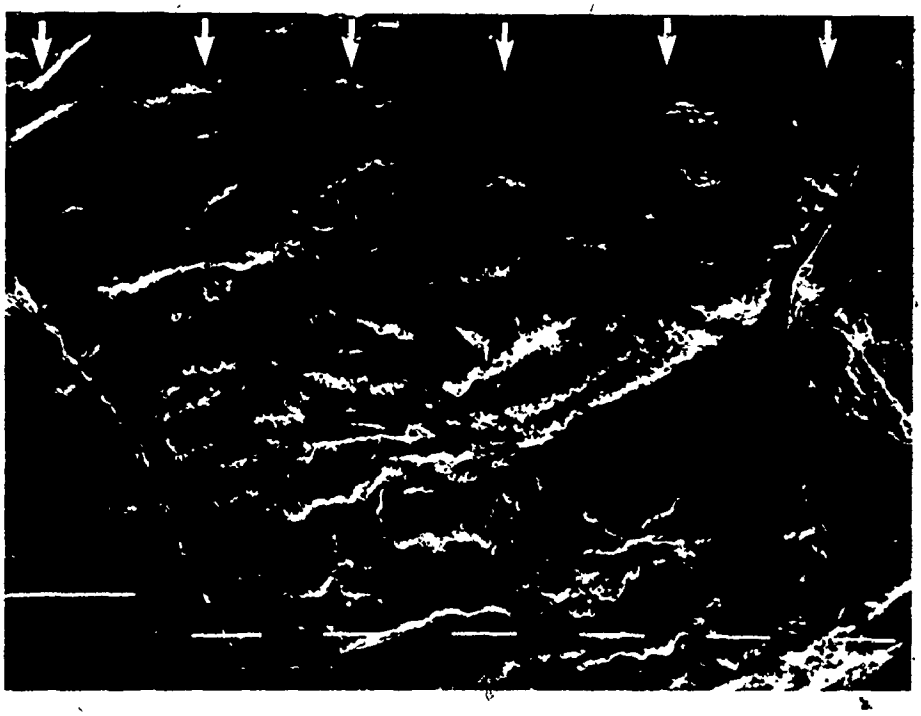

Figure 46 Regions of enlarged fenestrations in the form of circumferentially-oriented bands (indicated by arrows). The bands are located in the daughter branch, downstream from the apex of the bifurcation (at right of photomicrograph). Short white bars represent 10 μm.

Figure 47 Splits observed at the apex of the bifurcation, became gaps when observed by the SEM. g = gap. (Short white marks represent 100 µm).

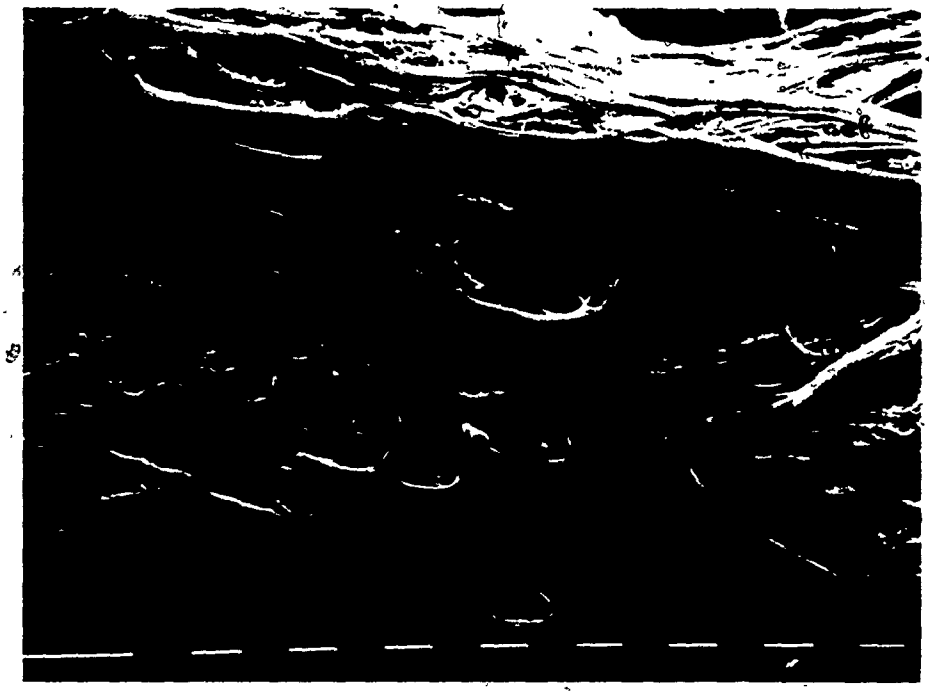

Figure 48 A region of substantially enlarged fenestrations at the edge of a gap. (Short white marks represent 10 μm).

Table 7 lists the specimens and mean values for diameter, density, percentage area (not corrected for shrinkage). The definitions and methods for computation of these characteristics have been outlined previously.

Figure 49 shows a typical histogram of fenestration diameters for a bifurcation with regions of both enlarged and normal fenestrations. A least squares polynomial has been computed and the curve overlaid to demonstrate each distribution. The distribution curve of the diameters for the normal fenestrations was very peaked, with few fenestrations less than 0.3 μm or larger than about 7 μm. The distribution curve for the diameter of the enlarged fenestration was less peaked (due to the great dispersion) and distinctly skewed to the right. The peak for the enlarged fenestrations was shifted to a larger value and there are many fenestrations that are greater than 10 μm, with some as large as 30 μm.

Figure 50 illustrates a typical graph of density versus diameter. Two distinct groups are evident. A greater variation of density was apparent for the normal fenestrations, whereas the enlarged fenestrations demonstrated more variability of the average diameter. The graph of percentage area and diameter illustrated in Figure 51, again demonstrates two groups. The increase in percentage area with an increase in diameter has been attributed to the influence of the product of the diameters for the computation of the percentage area. A similar graphical representation of percentage area and density (Figure 52) did not reveal a similar increase in area with increased density, even in the case where the largest density was a factor of four greater than the smallest density.

Fenestration Group	Circulation (Branch)	No. of Fenestrations Measured (± SEM)	Mean Diameter µm (± SEM)	Mean Density (mm^{-2}) (± SEM)	Mean Percentage Area (± SEM)
ENLARGED					
I-1	Circle	67	6.6 (±0.4)	1042 (±88)	18.5 (±4.5)
II-1	-	-	- -	- -	- -
II-2	-	-	- -	- -	- -
III-1	Basilar	274	7.4 (0.3)	1475 (70)	8.7 (1.5)
III-2	Post. Cerebral (1)	213	7.7 (0.5)	2411 (546)	13.8 (2.7)
III-3	Middle Cerebral (2)	282	7.2 (0.4)	2196 (264)	13.0 (1.7)
III-4	Middle Cerebral (2)	149	5.4 (0.3)	3794 (308)	11.5 (1.3)
III-5	Ant. Cerebral (1)	198	9.2 (0.5)	1991 (400)	15.6 (1.6)
III-6	Ant. Cerebral (2)	119	7.3 (0.5)	3335 (909)	19.1 (2.0)
IV-1	Post. Cerebral - Post. Communicating	206	7.2 (0.6)	2136 (270)	21.0 (8.0)
IV-2	Post. Cerebral (1)	558	5.5 (0.2)	3274 (465)	11.8 (0.8)
IV-3	Int. Carotid	145	7.5 (0.4)	3077 (209)	18.5 (2.6)
IV-4	Ant. Cerebral (2)	309	5.7 (0.2)	3934 (204)	14.0 (0.8)
		229 (±40)	7.0 (±0.34)	2606 (±284)	15.0 (±1.1)

TABLE 7 – Synopsis of Specimens (not corrected for shrinkage)

Fenestration Group	Circulation (Branch)	No. of Fenestrations Measured (± SEM)	Mean Diameter μm (± SEM)	Mean Density (mm^{-2}) (± SEM)	Mean Percentage Area (± SEM)
NORMAL					
I-1	Circle	211	1.6 (±0.06)	4478 (±355)	1.1 (±0.2)
II-1	-	340	2.3 (0.09)	4178 (425)	2.7 (0.6)
II-2	-	254	2.0 (0.1)	2634 (355)	1.4 (0.2)
III-1	Basilar	384	2.0 (0.06)	6016 (1455)	1.7 (0.3)
III-2	Post. Cerebral (1)	214	2.2 (0.07)	4510 (482)	2.1 (0.2)
III-3	Middle Cerebral (2)	369	3.3 (0.08)	1913 (74)	2.0 (0.3)
III-4	Middle Cerebral (2)	238	1.5 (0.05)	7236 (674)	1.8 (0.4)
III-5	Ant. Cerebral (1)	317	2.5 (0.08)	4987 (964)	2.4 (0.3)
III-6	Ant. Cerebral (2)	385	1.9 (0.05)	3993 (321)	1.5 (0.3)
IV-1	Post. Cerebral - Post. Communicating	296	2.3 (0.07)	4946 (616)	2.4 (0.3)
IV-2	Post. Cerebral (1)	292	1.8 (0.04)	3029 (336)	0.9 (0.1)
IV-3	Int. Carotid	253	2.2 (0.07)	5369 (418)	2.5 (0.4)
IV-4	Ant. Cerebral (2)	255	1.6 (0.05)	5410 (499)	1.4 (0.3)
		293 (±17)	2.1 (±0.13)	4518 (±397)	1.8 (±0.16)

TABLE 7 — Synopsis of Specimens (Continued)

Fenestration Group	Circulation (Branch)	No. of Fenestrations Measured (± SEM)	Mean Diameter μm (± SEM)		Mean Density mm^{-2} (± SEM)		Mean Percentage Area (± SEM)	
WITHOUT ENLARGED								
I-2	Circle	244	1.8	(±0.06)	5178	(±400)	1.7	(±0.3)
II-3	"	292	1.6	(0.05)	3583	(268)	0.9	(0.1)
II-4	"	286	1.3	(0.05)	2966	(153)	0.6	(0.1)
II-5	"	307	1.6	(0.05)	3183	(418)	0.8	(0.2)
II-6	"	279	2.3	(0.09)	2893	(287)	1.8	(0.6)
III-7	Vert. Basilar	477	2.4	(0.05)	2473	(219)	1.3	(0.2)
III-8	Middle Cerebral (1)	387	1.9	(0.08)	4014	(870)	2.0	(0.6)
III-9	Carotid	268	2.7	(0.08)	5216	(1453)	2.5	(0.2)
III-10	Ant. Cerebral (2)	281	2.4	(0.08)	5374	(1228)	2.3	(0.6)
IV-5	Post. Cerebral - Post. Communicating	234	2.4	(0.09)	7809	(780)	4.8	(1.5)
IV-6	Carotid	265	2.5	(0.10)	4237	(824)	2.3	(0.4)
IV-7	Post. Cerebral (2)	275	1.3	(0.04)	9824	(1629)	1.5	(0.3)
IV-8	Middle Cerebral - Ant. Communicating	235	1.6	(0.05)	7724	(1457)	1.7	(0.1)
IV-9	Ant. Cerebral (1)	267	1.6	(0.05)	4471	(495)	1.1	(0.1)
IV-10	Ant. Cerebral (2)	302	1.6	(0.05)	6408	(376)	1.6	(0.2)
		294 (±16)	1.9	(±0.12)	5024	(±548)	1.7	(±0.27)

TABLE 7 - Synopsis of Specimens (Continued)

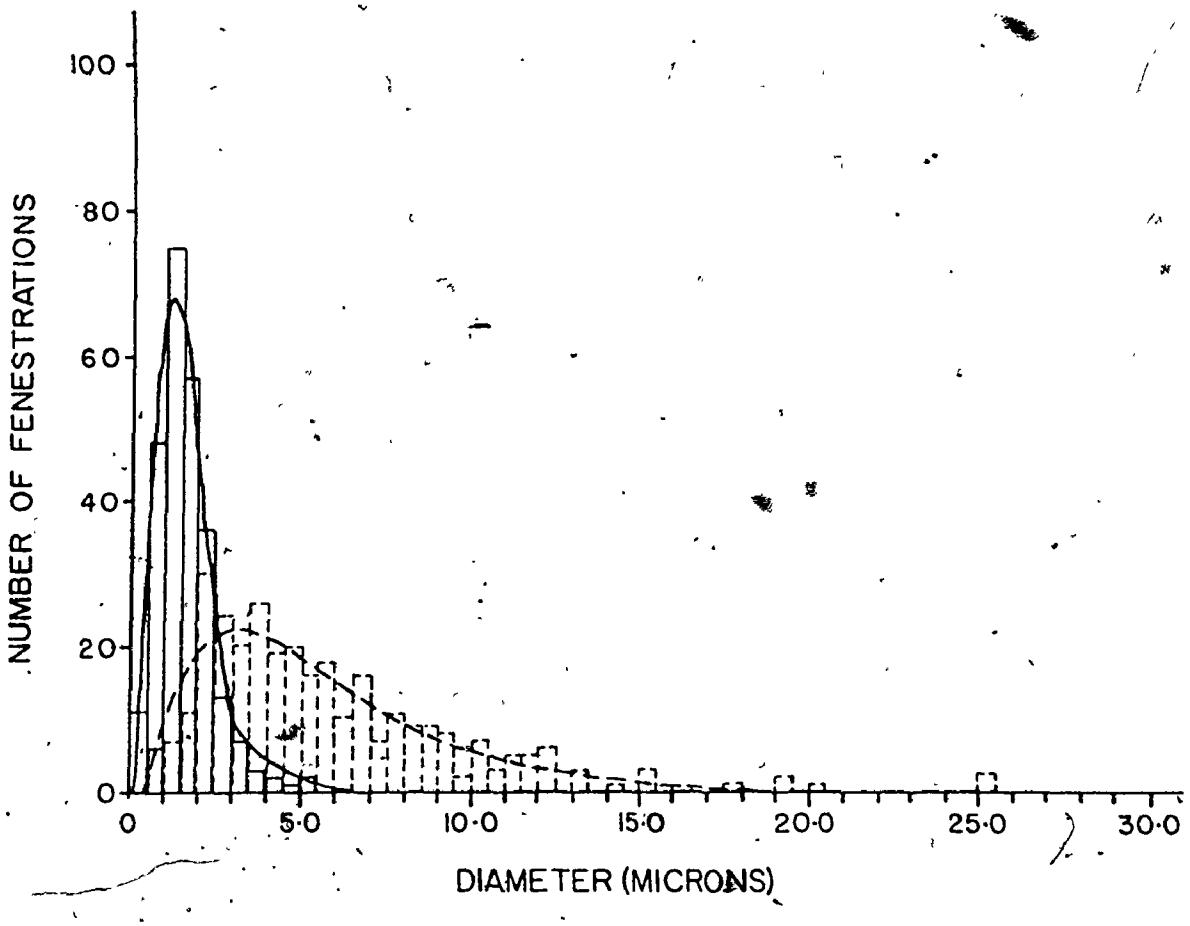

Figure 49 The distribution curve and histogram for the diameter of the normal (solid lines) and enlarged fenestrations (broken lines) for a particular specimen.

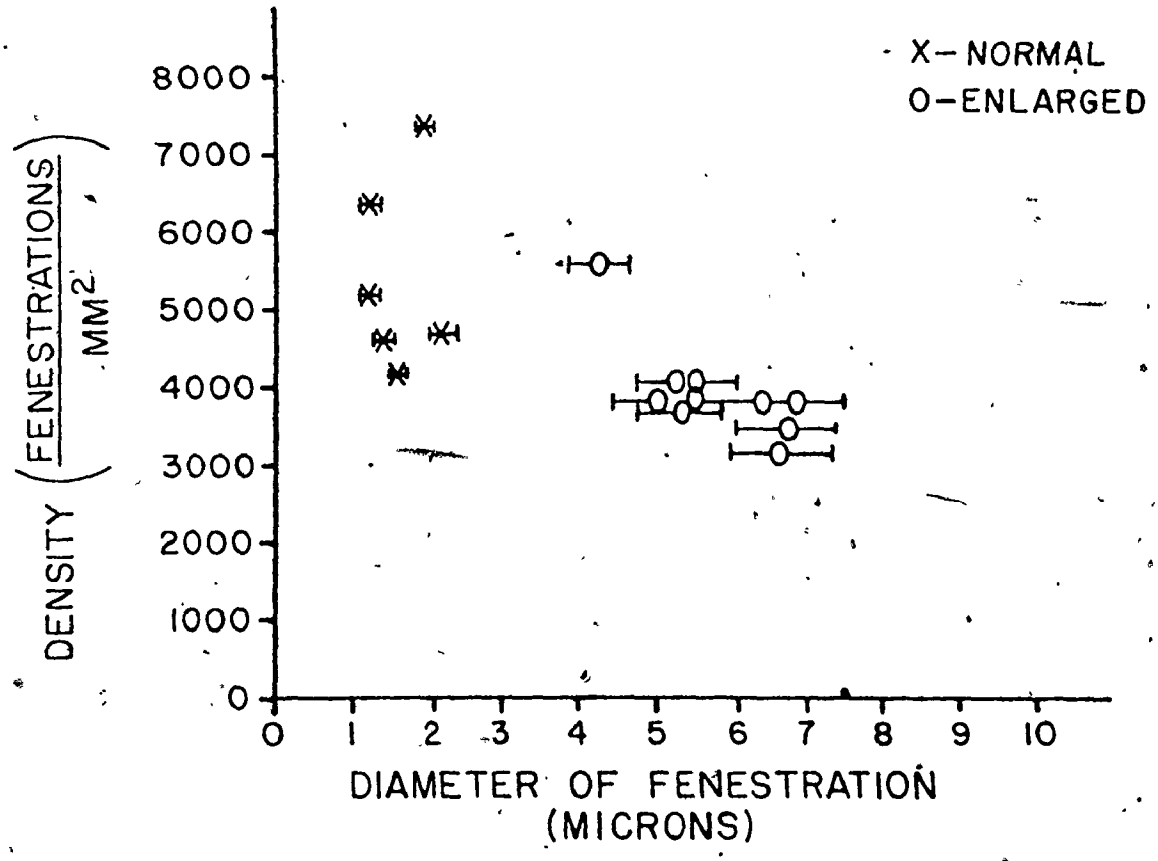

Figure 50 A typical graph of fenestration diameter with respect to fenestration density for normal and enlarged fenestrations. (Error bars represent ± 1 SEM).

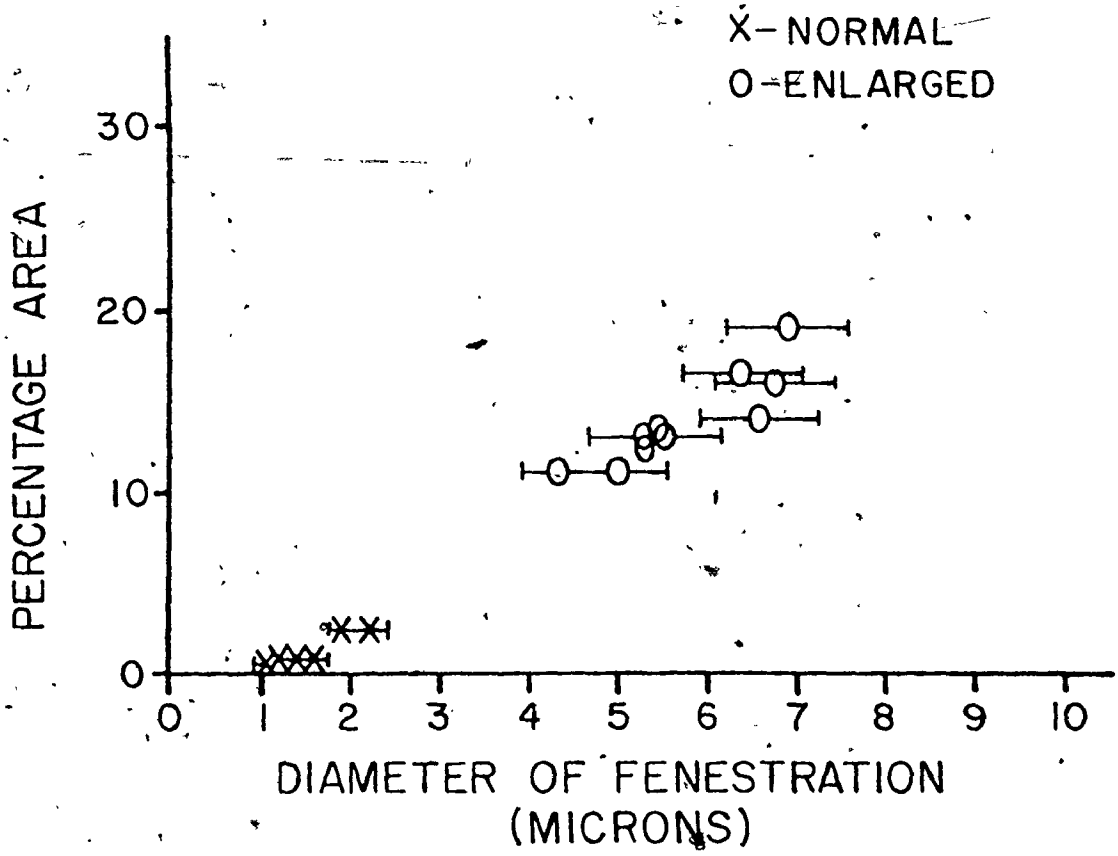

Figure 51 A typical graph of fenestration diameter with respect to percentage are for normal and enlarged fenestrations. (Error bars represent ± 1 SEM).

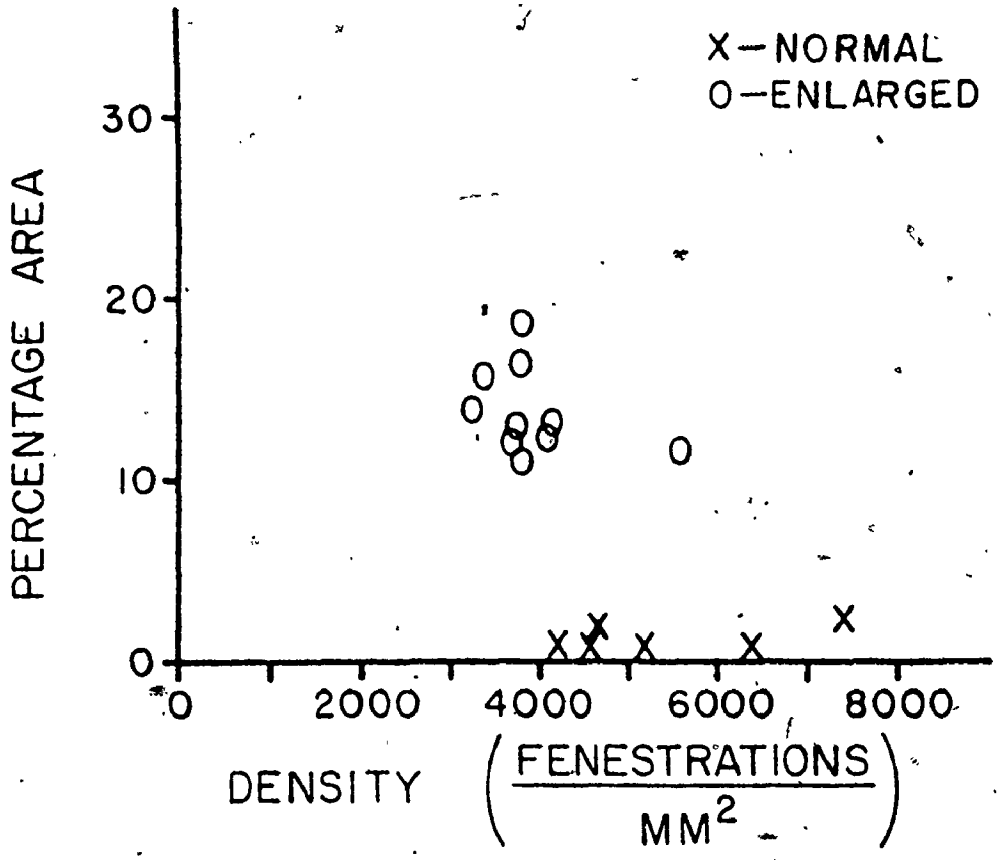

Figure 52 A typical graph of fenestration density with respect to percentage area for normal and enlarged fenestrations.

In order to assess the validity of the assumption that there are two distinct classifications (enlarged and normal fenestrations), a single factor analysis of variance was performed on the data and the Neuman-Keuls multiple range test (Zar, 1974, page 151), at the 0.01 level of significance, was utilized to isolate any specimens which did not conform to an assigned classification. The results in Table 8 are presented as the proportion of specified specimens that did not agree with the mean value of other specimens for a particular group. The mean values for the diameter, density and percentage area for both the normal and enlarged fenestrations are essentially the same within each group, except for a limited number of specimen comparisons made between extreme values.

It is evident from the data presented in Table 7 that the mean diameter for the enlarged fenestrations (7.0 $\pm$ 0.34 SEM μm) is greater than that for the normal fenestrations (2.1 $\pm$ 0.13 SEM μm). The density for the enlarged fenestrations (2606 $\pm$ 284 per sq mm.) is lower than that for the normal fenestrations (4518 $\pm$ 397 SEM per sq mm.). In addition, the percentage area has increased from 1.8 $\pm$ 1.1 SEM percent for the normal fenestrations to 15.0 $\pm$ 1.1 SEM percent for the enlarged fenestrations.

Since the characteristics for both the enlarged and normal fenestrations have been computed for each bifurcation, a paired sample t-test was employed to establish whether the differences in the characteristics were significant. The t-test showed that the enlarged and normal fenestrations were significantly different in diameter ($p < 0.0005$) and area ($p < 0.005$) but not different in density ($p > 0.20$).

Fenestration Group	Number of Comparisons for each Characteristic	Summation of Comparisons Among Mean Values of the Characteristics for Specimens Within a Specified Group		
		Diameter ($p = .01$)	Density ($p = .01$)	Percentage Area ($p = .01$)
Normal (13 Specimens)	78	III-3 ≠ 7 of 12	III-4 ≠ 3 of 12 III-3 ≠ 2 of 12	ALL EQUAL
Enlarged (11 Specimens)	55	III-5 ≠ 3 of 10	IV-4 ≠ 5 of 10	ALL EQUAL
Without Enlarged (15 Specimens)	105	ALL EQUAL	IV-7 ≠ 11 of 14 III-7 ≠ 3 of 14	IV-5 = 14 of 14
Combined Normal and Without Enlarged (28 Specimens)	378	III-3 ≠ 10 of 27	IV-7 ≠ 23 of 27 IV-5 ≠ 7 of 27 IV-8 ≠ 7 of 27 III-4 ≠ 4 of 27	IV-5 = 27 of 27

TABLE 8 - Analyses of Variance

A comparison (analysis of variance) among the mean values of the characteristics for the fenestrations from bifurcations without enlarged fenestrations revealed one specimen (IV-5) whose mean value of area was different from the remaining ten specimens. One photomicrograph which exhibited an unusually large percentage area has been isolated as the source of the discrepancy for this specimen. A second specimen (IV-7) demonstrated a higher mean density in comparison to a majority of the other specimens.

An analysis of variance comparison (diameter, density, and percentage area) among the combined group of bifurcations without enlarged fenestrations and normal fenestrations from bifurcations with enlarged fenestrations, revealed that the characteristics for several of the specimens deviated from some of the remaining specimens. Since there was no clear majority of deviations for either group it has been concluded that the characteristics for the two groups are equivalent.

4.3.4 Discussion

The characteristics of diameter, density and percentage area measured in this study showed a remarkable similarity between the four subjects. The average fenestration diameter of the normal fenestrations in this study was about 2.1 μm which is considerably less than the values of 6.8 and 3.5 μm, for the cylindrical segments of the anterior cerebral artery and internal carotid artery respectively, reported in the study by Hassler (1962) for this age group. However, the range of the diameters for the normal fenestrations in this study is in close agreement with the 1 to 2 μm quoted by Lang and Kidd (1965). The reasons for the discrepancies between the values in this

study and that of Hassler (1962) were outlined in subsection 3.6.4.

It has not yet been established whether the gap observed at the apex of many of the bifurcations existed *in vivo* or was accidentally produced during removal of the arterial tree from the brain. In either case, the existence of the gaps suggests that there is a distinct weakness in the internal elastic lamina at the apex of the bifurcation. Furthermore, Macfarlane (1975) observed a similar apical defect which he described as "... a narrow band extending around the apex of the bifurcation." The presence of enlarged fenestrations in this region and their absence in the trunk specimens suggest that they may contribute to this weakness.

Distension of the fenestrated internal elastic lamina by transmural pressure is analogous to a system of holes in a flat plate under stress. It is an established fact, from the analysis of stress in flat plates, that holes introduce localized areas of stress in the vicinity of the holes, that may be many times higher than the stress in the adjacent solid material. This phenomenon is termed stress concentration and is represented by the Stress Concentration Factor. The significance of stress concentration is dependent upon the number, shape, size and distribution of the holes, as well as the type of stress (uniaxial or biaxial) and orthogonal proportion of the stress.

The parameter "ligament efficiency" which has been defined previously, is used to describe the spatial geometry of holes in flat plates. Lower ligament efficiencies imply that the solid material between the fenestrations must bear an increased load resulting in an increased stress. It is evident from Figure 44 that the ligament

The examination of a series of specimens, subsequent to the completion of this study, revealed one particularly fortuitous specimen. Visual examination of the intact artery showed a slight outward bulge in the apical region of the bifurcation. Microscopic examination (Figure 53) revealed an extensive region of the enlarged fenestrations, greater than any previous region of enlarged fenestrations. The results for the diameter (8.1 ± 0.3 SEM μm), density (2432 ± 388 SEM per mm^2), percentage area (18.5 ± 1.4 SEM %) and ligament efficiency (0.61 ± 0.02 SEM) for the region of enlarged fenestrations in this specimen are comparable to the previous results for the larger group of enlarged fenestrations. These observations suggest that a region of enlarged fenestrations may be associated with the formation of a bulge.

The presence of enlarged fenestrations in the internal elastic lamina of normal intracranial arteries, without evidence of an intracranial aneurysm, has been verified in this study. Since these regions of enlarged fenestrations may represent areas of weakened tissue and since they have been found almost exclusively in the apical region of the bifurcation, they could be considered a defect in the internal elastic lamina. Whether or not the regions of enlarged fenestrations could influence the development of an intracranial aneurysm has not been conclusively verified.

4.3.5 Summary

Measurements of fenestrations (or windows) in the internal elastic lamina at the bifurcation of human cerebral arteries, were obtained from photomicrographs (Scanning Electron Microscope). Thirteen of

efficiencies in regions with elliptical fenestrations could be less in the direction of the major axis than in the direction of the minor axis.

An average ligament efficiency was computed (equation (13)) for each specimen in the three groups. The computed mean value for the ligament efficiency of the enlarged fenestrations was 0.65 $\pm$ 0.008 SEM which is distinctly less than that for the normal fenestrations (0.86 $\pm$ 0.006 SEM). A paired sample t-test between the ligament efficiencies of the enlarged fenestrations and the normal fenestrations revealed a significant difference ($p < 0.005$). A review of the Stress Concentration Factors from the available literature (Peterson, 1974, Faupel, 1964) for a number of different hole sizes and configurations, and as well variations of stress, revealed an increase for the regions of enlarged fenestrations. However, none of the configurations reviewed were completely representative of the apparent random distribution of enlarged and normal fenestrations observed in cerebral arteries.

In several regions of enlarged fenestrations depicted in the photomicrographs, the computed ligament efficiency was less than 0.55, which could create an average stress concentration of about 1.3 to 2.2 times the stress in an adjacent cylindrical branch. An additional factor which would be expected to increase the stress concentration in the internal elastic lamina is the corner formed at the apex of the bifurcation. The Stress Concentration Factor derived analytically (Faupel, 1964, page 764) at the edge between a side branch and the main cylinder (analogous to the apex of the bifurcation) of a closed system

under internal pressure is 3.94 times the stress in an adjacent cylindrical segment. As a consequence of the combined effects of the enlarged fenestrations and apical geometry, the stress sustained by the internal elastic lamina in the apical region could be as much as an order of magnitude greater than the stress in an adjacent straight segment. A further decrease in the ligament efficiency or degradation of the tissue could result in an excessive stress concentration causing rupture of the internal elastic lamina.

It has been stated by several authors (Nystrom 1963, Lang and Kidd 1965, Cajander and Hassler 1976, Stehbens 1963, Stehbens 1975b) that degradation, fragmentation, and splitting of the internal elastic lamina are associated with the initiation of aneurysms. Since the 2.1 μm diameter of the normal and without enlarged fenestrations is substantially less than the standard 7 μm sections prepared for light microscopy, then the fenestrations would not be visible and the internal elastic lamina would appear to resemble a solid sheet. However, if serial sections were prepared through the regions of the enlarged fenestrations where many diameters are greater than 7 μm, then the intervening ligaments would appear as fragments of the internal elastic lamina.

It is therefore proposed that the micro-aneurysms formed by evagination of the internal elastic lamina into the smooth muscle observed by other authors (Stehbens 1963, Stehbens 1975b, Forbus 1930, Sahs 1966) are actually regions of enlarged fenestrations with low ligament efficiencies. This would result in an excessive distension of the internal elastic lamina in this region which would be observed as a bulging of the internal elastic lamina and underlying tissue.

The examination of a series of specimens, subsequent to the completion of this study, revealed one particularly fortuitous specimen. Visual examination of the intact artery showed a slight outward bulge in the apical region of the bifurcation. Microscopic examination (Figure 53) revealed an extensive region of the enlarged fenestrations, greater than any previous region of enlarged fenestrations. The results for the diameter (8.1 $\pm$ 0.3 SEM μm), density (2432 $\pm$ 388 SEM per mm^2), percentage area (18.5 $\pm$ 1.4 SEM %) and ligament efficiency (0.61 $\pm$ 0.02 SEM) for the region of enlarged fenestrations in this specimen are comparable to the previous results for the larger group of enlarged fenestrations. These observations suggest that a region of enlarged fenestrations may be associated with the formation of a bulge.

The presence of enlarged fenestrations in the internal elastic lamina of normal intracranial arteries, without evidence of an intracranial aneurysm, has been verified in this study. Since these regions of enlarged fenestrations may represent areas of weakened tissue and since they have been found almost exclusively in the apical region of the bifurcation, they could be considered a defect in the internal elastic lamina. Whether or not the regions of enlarged fenestrations could influence the development of an intracranial aneurysm has not been conclusively verified.

4.3.5 Summary

Measurements of fenestrations (or windows) in the internal elastic lamina at the bifurcation of human cerebral arteries, were obtained from photomicrographs (Scanning Electron Microscope). Thirteen of

Figure 53 Photomicrograph of an extensive region of enlarged fenestrations. (Short white bars represent 100 μm).

twenty-eight bifurcations revealed regions of enlarged fenestrations among the normal fenestrations in the vicinity of the apex. The mean diameter for the enlarged fenestrations (7.0 ± 0.34 SEM μm) was significantly greater than the mean diameter (2.1 ± 0.13 SEM μm) for the normal fenestrations. The number of fenestrations per sq mm. was less (2606 ± 284 SEM per sq mm.) for the enlarged fenestrations than for the normal fenestrations (4518 ± 397 SEM per sq mm.). The proportion of the area of internal elastic lamina comprised of fenestrations increased to 15.0 ± 1.1 SEM percent for the enlarged fenestrations from a mean of 1.8 ± 0.16 SEM percent for the normal fenestrations. Fenestrations from bifurcations without enlarged fenestrations, demonstrated similar characteristics to the normal fenestrations. More than 80% of the specimens exhibited a gap in the internal elastic lamina in the apical region of the bifurcation. Based on a comparison of stress concentration factors, it is proposed that the presence of enlarged fenestrations represents a weakness in the internal elastic lamina at the bifurcation apex which may contribute to the initiation of microaneurysms.

4.4 A Physical Model for the Formation of Evaginations

4.4.1 Introduction

Despite considerable research on the etiology of intracranial saccular aneurysms, the mechanism for their creation remains unresolved. At present, there are two main theories about their etiology, *viz.*, congenital defects and developmental defects. Consideration of the factors which invalidate the congenital theory are extensively discussed by Stehbens (1972, 1975b). The current evidence

(Stehbens, 1981) strongly supports the degenerative theory of development.

Stehbens (1981) identified three early changes related to the development of saccular aneurysms: i) areas of thinning; ii) funnel-shaped dilatations; and iii) microscopic evaginations. The micro-evaginations are essentially small bulges of the luminal surface into the wall of the media. Stehbens (1981) commented that one micro-evagination". . . exhibited a fragmented elastic lamina, with a small mural thrombus and fibrin and red-cell infiltration of the wall." Sahs (1966) attached considerable importance to the evagination, commenting ". . . they (small outpouchings) may be the precursor of saccular aneurysms." A further observation was that the elastic layer had undergone conspicuous fragmentation and that further fragmentation would result in widening, which may progress to a recognized saccular aneurysm. The significance of fragmentation of the internal elastic lamina during the formation of saccular aneurysms has also been mentioned by other investigators (Nystrom 1963, Merei and Gallyas 1980a).

The internal elastic lamina of human cerebral arteries has been described as a fenestrated sheet (Hassler 1962, Campbell and Roach 1981a, Stehbens 1981). Regions of enlarged fenestrations in the apical region of cerebral arterial bifurcations have been reported in subsection 4.3 (Campbell and Roach 1981a), as well as by Merei and Gallyas (1980a). It was deduced that serial sections (typically 4-7 μm thick), which are cut through areas of enlarged fenestrations with an average diameter of 7 μm, would make the elastin appear fragmented since the enlarged fenestrations would appear as gaps with intervening

bands in the internal elastic lamina, while the adjacent areas of normal fenestrations (diameter 2.1 μm) would resemble a solid sheet. It is significant that enlarged fenestrations have been reported at the mouth of saccular aneurysms (Hassler 1972, Merei and Gallyas 1980a).

Since it could be logically concluded that regions of enlarged fenestrations may stretch more readily than the adjacent areas of normal fenestrations, the regions of enlarged fenestrations could transform into a micro-evagination. In this subsection the tensile properties, as well as the spatial geometry, for regions of normal and enlarged fenestrations will be investigated with the use of perforated latex models.

4.4.2 Methods

Since the internal elastic lamina is buried within the arterial wall, isolation of the desired region of the internal elastic lamina, in a form suitable for mechanical testing is at present impractical. Most existing methods require the application of excessive heat (50°C or greater) which might cause irreversible protein damage that could influence the mechanical characteristics of the tissue, but this has not been confirmed to our knowledge. The technical difficulties in handling such a thin, fragile tissue along with the lack of an appropriate testing procedure have necessitated consideration of an alternate technique. The technique entails replicating the image of the actual fenestrations (both normal and enlarged) from a photomicrograph in a latex rubber sheet, followed by a comparison of the relative tensile characteristics.

Part A - Geometrical Parameters

Photomicrographs obtained with the scanning electron microscope for regions of normal and enlarged fenestrations from the same specimen, are illustrated in Figure 54. The specimen is a bifurcation from the anterior circulation of a 50-year-old female, obtained at autopsy. The procedure for isolating the internal elastic lamina from the arterial wall has been described previously (Subsection 3.6) and will not be repeated here. An analysis of the shrinkage during preparation of cylindrical specimens and of bifurcations (Subsection 2.6) has revealed a linear shrinkage of only 6.9%. Since the intent of this study was to compare the relative tensile properties, the geometric characteristics reported subsequently for both the normal and enlarged fenestrations have not been corrected for shrinkage.

The negative for each photomicrograph was mounted in an enlarger and the image projected on the platen of a Hewlett Packard digitizer (model 9864A) interfaced with a Hewlett Packard 9830A microcomputer. Both images in Figure 54 are shown at the same final magnification.

Two sets of two points each, which represented the lengths of the major and minor axes for the inside border of each fenestration, were digitized and entered into the microcomputer for further processing and storage. Only fenestrations which appeared to pass completely through the internal elastic lamina were measured. The area for each fenestration was computed with the use of the equation for an ellipse. The four geometric characteristics of Diameter, Density, Percentage Area and Ligament Efficiency were computed. The equations for computing the characteristics, including the derivation of the expression for computing a ligament efficiency for the case of a random

(a) (b)

Figure 54 Photomicrographs of the surface of the internal elastic lamina (human cerebral) illustrating:
(a) a region of normal fenestrations
(b) a region of enlarged fenestrations
The short white bars represent 10 μm.

pattern of holes with unequal diameters, have been presented in section 3.4.

Part B - Mechanical Testing

A replication of the fenestrations in the internal elastic lamina for both photomicrographs was produced by tracing the inside border of each fenestration shown on a 50.8 x 50.8 mm glossy print (magnification of 770) onto the surface of a sheet of latex rubber.

Models of the spatial geometry (termed "geometrical models") of the fenestrations were created with a single (average) diameter, a uniform array of rows and columns, and the same ligament efficiency. Since the number of rows/columns for the actual geometry was not an integer (i.e., 6.6 for the normal and 4.6 for the enlarged) it was necessary to create two geometrical models for each replication. One geometrical model consisted of the number of rows/columns with the closest integer value less than the actual number, while the other geometrical model consisted of the closest integer value greater than the actual number. The square border of the model must also be scaled accordingly. The outline of the holes and external border were again traced on the latex sheet.

Two opposing ends of each latex sheet were trimmed along the edge while the remaining edges were sandwiched between two strips of 1.3 mm thick aluminum sheet that were aligned along the transverse border of the model. The aluminum strips were attached to the latex rubber with double-sided masking tape. The aluminum strips were then mounted in the grips of a constant-rate-of-crosshead-movement testing machine (Instron model 1125). The latex samples (unperforated) were stretched in uniaxial tension at a crosshead speed of 100 mm/minute to a maximum

elongation (strain) of 30%, through three sequences of loading and unloading. The load/deformation record for each specimen was subsequently converted into a stress/strain curve. The stress computed was "engineering stress".

The perforations were cut in both the replication and geometrical model samples. The samples were again mounted in the testing machine and the tensile test repeated, except the samples for the enlarged fenestrations were elongated to 60%. The stress/strain curves for the perforated samples were subsequently computed.

The condition of the latex rubber models with the holes marked but not perforated will subequently be termed "solid". Models with the perforations cut out will henceforth be referred to as "perforated".

Part C - Spatial Geometry

Following each uniaxial tensile test (described previously in Part B), photographs were taken of each sample mounted in the testing machine. The photographs for the normal fenestrations were obtained in the unstretched condition, as well as at 10, 20 and 30% elongation (strain). A similar series was obtained for the enlarged fenestrations, except that the series was extended to the 40, 50 and 60% elongation, for the perforated condition only. Since it was found during preliminary studies that stretching to 60% was not followed by immediate return to the initial length, an extended series was not obtained for the solid condition. This procedure was selected since I believe that the material properties of the latex itself should not change between the tests on the solid and the perforated conditions.

Figure 55 illustrates the perforated replication and 7 x 7 geometrical model for the normal fenestrations in both the unstretched

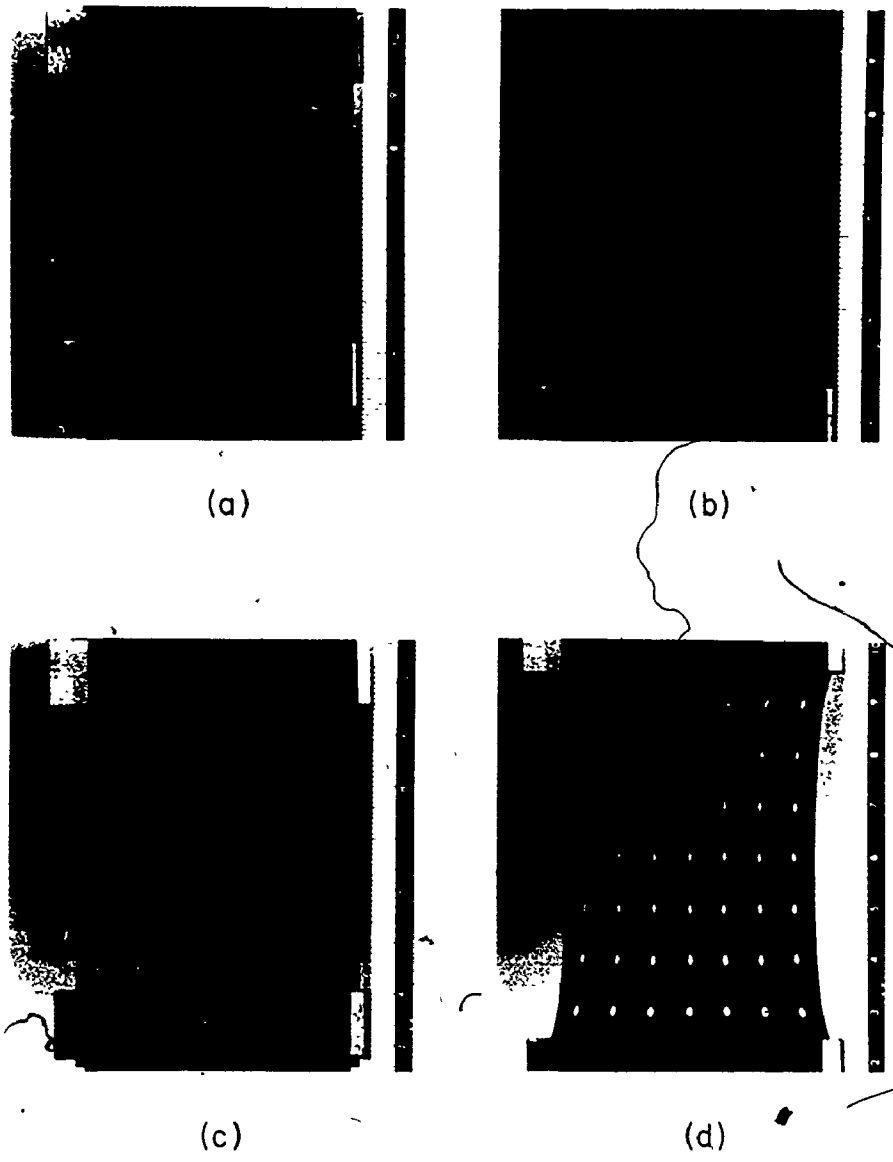

Figure 55 Photographs depicting the replication and 7 x 7 model of the normal fenestrations, mounted in the grips of the uniaxial tensile testing machine.
(a) replication (perforated) in the unstretched condition
(b) replication (perforated) at 30% elongation
(c) 7 x 7 model (perforated) in the unstretched condition
(d) 7 x 7 model (perforated) at 30% elongation

and 30% elongated conditions. A similar arrangement for the replication and 5 x 5 geometrical model of the enlarged fenestrations is presented in Figure 56.

The image from the negative for each photograph depicting the stretched condition of the sample, was projected on the platen of the Hewlitt Packard Digitizer. Since the circular holes transform into an ellipse when the rubber is stretched, the longitudinal and transverse dimensions of a single row of holes (solid or perforated) closest to the centre of the sample were recorded and averaged along with the width of the sample coincident with the hole.

The series of measurements were converted into the set of spatial parameters: Area, Ligament Efficiency, Eccentricity and Expansion Ratio. The equations associated with these parameters have been presented in subsection 3.5.2.

4.4.3 Results

A) Geometrical Parameters

Table 9 presents the characteristics of the normal and enlarged specimens, computed from the photomicrographs illustrated in Figure 54. The values for both the normal and enlarged fenestrations compare favourably with the mean values for the larger group of specimens, presented in section 4.3.

B) Mechanical Testing

The corresponding characteristics for the perforations in the latex, which model the spatial geometry of the fenestrations, are presented in Table 10. The stress/strain curves for the solid condition were essentially identical and have been combined on Figure

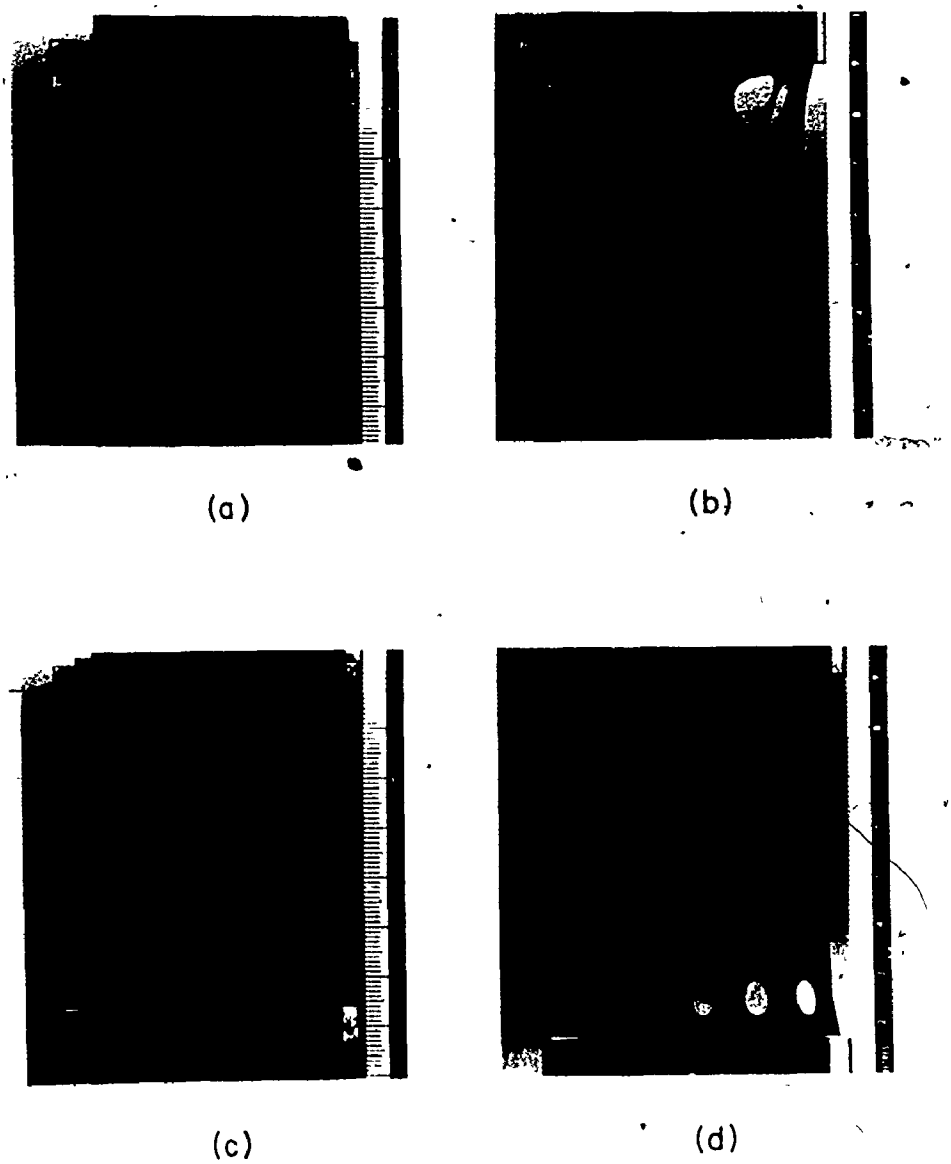

Figure 56 Photographs showing the replication and 5 x 5 model of the enlarged fenestrations, mounted in the grips of the uniaxial tensile testing machine.
(a) replication (perforated) in the unstretched condition
(b) replication (perforated) at 30% elongation
(c) 5 x 5 model (perforated) in the unstretched condition
(d) 5 x 5 model (perforated) at 30% elongation

	N	DIAMETER (μm)	DENSITY (#/sq. mm)	PERCENTAGE AREA (%)	LIGAMENT EFFICIENCY
Normal	43	1.5	9861	2.2	0.85
Enlarged	21	5.9	4821	17.4	0.59

TABLE 9 - Geometrical Characteristics of Fenestrations in the artery (not adjusted for shrinkage)

	MODELS	DIAMETER (mm)	CENTRE-TO-CENTRE DISTANCE (mm)	LIGAMENT EFFICIENCY
Normal	6 x 6, 7 x 7	1.2	7.7	0.85
Enlarged	4 x 4, 5 x 5	4.6	11.1	0.59

TABLE 10 - Geometrical Characteristics of Perforations in the latex model (based upon Table 9)

57. The stress/strain curves (Figure 57) for the perforated replication of the normal fenestrations demonstrated a slight but distinct shift towards increased strain (elongation) at the same stress values as the solid sheet. That is to say, the replication tended to stretch slightly more under the same stress conditions. The stress/strain curves for the perforated replication of the enlarged fenestrations exhibited a pronounced shift to increased strain (elongation) at the same stress values as the solid sheet. The mean increase in the elongation of the replication of the enlarged in relation to the normal fenestrations (based upon 16 increments of stress from 0.2 to 3.2 kg/cm^2) was 47% $\pm$ 0.06% SD.

In order to compare the relevant change in the stress/strain characteristics for the solid condition to the perforated condition for both the replication and geometrical models, the stress/strain characteristics for the perforated condition were standardized with respect to the solid condition. The results (in terms of standardized stress) for the sample containing normal fenestrations, presented in Figure 58, exhibited a reduction to about 0.92 of the original value (solid condition). There is close agreement between the geometrical model and replicate configurations.

The standardized stress values for the enlarged fenestrations decreased to about 0.66 of the value for the solid condition (Figure 58). The agreement between the geometrical model and replicate configurations for the enlarged fenestrations is reasonable but not as close as the normal fenestrations. In both cases (normal and enlarged) both geometrical model configurations (6 x 6 and 7 x 7, 4 x 4 and 5 x 5 respectively) were in agreement, which eliminated the necessity to

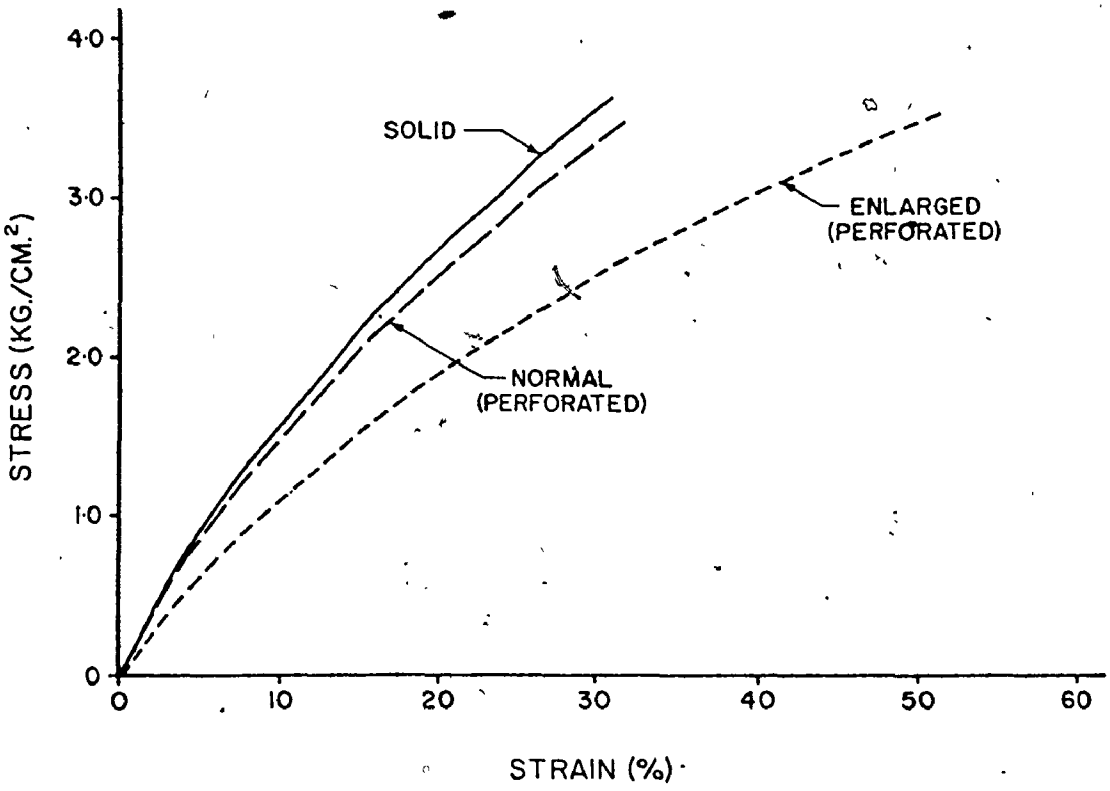

Figure 57 The stress-strain curves for the solid latex as well as the replications of the normal and enlarged fenestrations.

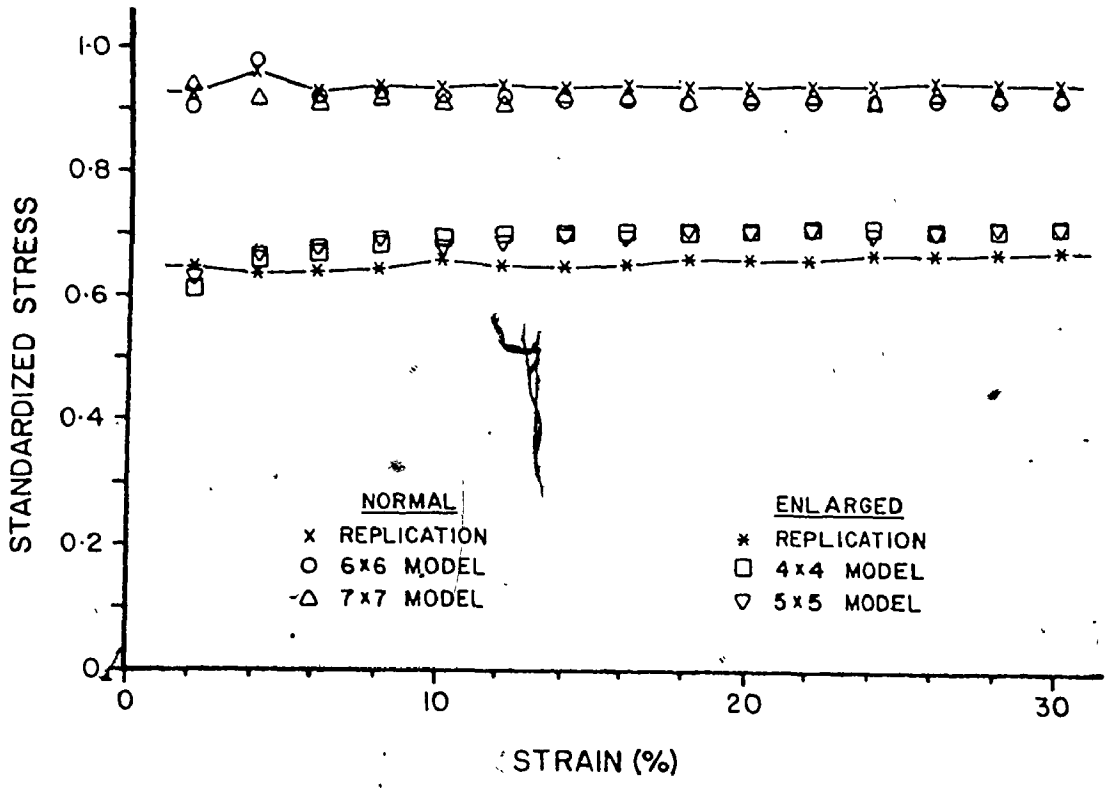

Figure 58 Standardized stress-strain curves for the replications and models of the normal and enlarged fenestrations.

interpolate between the geometrical models to account for the difference between the actual numbers of rows/columns and the nearest integers.

C) Spatial Geometry

The satisfactory agreement between the geometrical models and replication for the regions of normal and enlarged fenestrations, demonstrated in the preceding section, has facilitated the analysis of the Spatial Geometry, since the regular shape of the uniform pattern of perforations in the geometrical models may be measured rather than the irregular shape and pattern of fenestrations in the replications.

It is evident from Figures 55 and 56 that progressive elongation of the latex sheet transformed the circular holes into elliptical slits. The width of the sheet was also reduced. The results for the two geometrical models representing each specimen have been combined and a linear regression (least squares) fit has been applied to the data for diameter, area, and ligament efficiency. The r^2 (coefficient of determination) values for the slopes were 0.92 or greater ($p < 0.001$) except for slopes near the horizontal which were considerably less. Since the slope is approaching zero for this latter situation, the r^2 computation is not a reliable indicator of the fit.

The results for the tensile properties as well as the spatial geometry of the two models created for both the normal and the enlarged regions appeared equivalent. Consequently, the results have been reported in this section for only one of the two models of each specimen.

The results for the transverse diameter (solid and perforated) associated with the models of both normal and enlarged fenestrations are presented in Figure 59. None of the curves appear to deviate substantially from the initial diameters. This observation is further confirmed by the low value of the slopes which are presented in Table 11. The slopes for the perforated condition of the axial diameters for both the normal and enlarged fenestrations are greater than the solid condition as shown in Figure 60 and confirmed in Table 11. It is also interesting that the rate of increase of the axial diameter for the perforated condition of the enlarged fenestrations exceeds the rate of increase of the normal fenestrations by the factor of 2.7.

The expansion ratios computed for the normal and enlarged specimens were 3.02 $\pm$ 0.6 SEM and 2.26 $\pm$ 0.01 SEM respectively. Therefore, although the rate of increase of the axial diameter for the enlarged fenestrations greatly exceeded the rate for the normal fenestrations, the expansion ratio for the larger diameter holes was actually less.

When the transverse and axial diameters are combined for the calculation of the relevant areas, the perforated conditions again increased more rapidly than the solid condition (Figure 61, Table 11). However, the more startling observation is that the rate of increase for the enlarged fenestrations is an order of magnitude greater than that for the normal fenestrations.

The results for the transverse ligament efficiency shown in Figure 62 and confirmed in Table 11, exhibit a horizontal slope. The slope for axial ligament efficiency for the solid condition is also horizontal (Figure 63, Table 11). However, the axial ligament

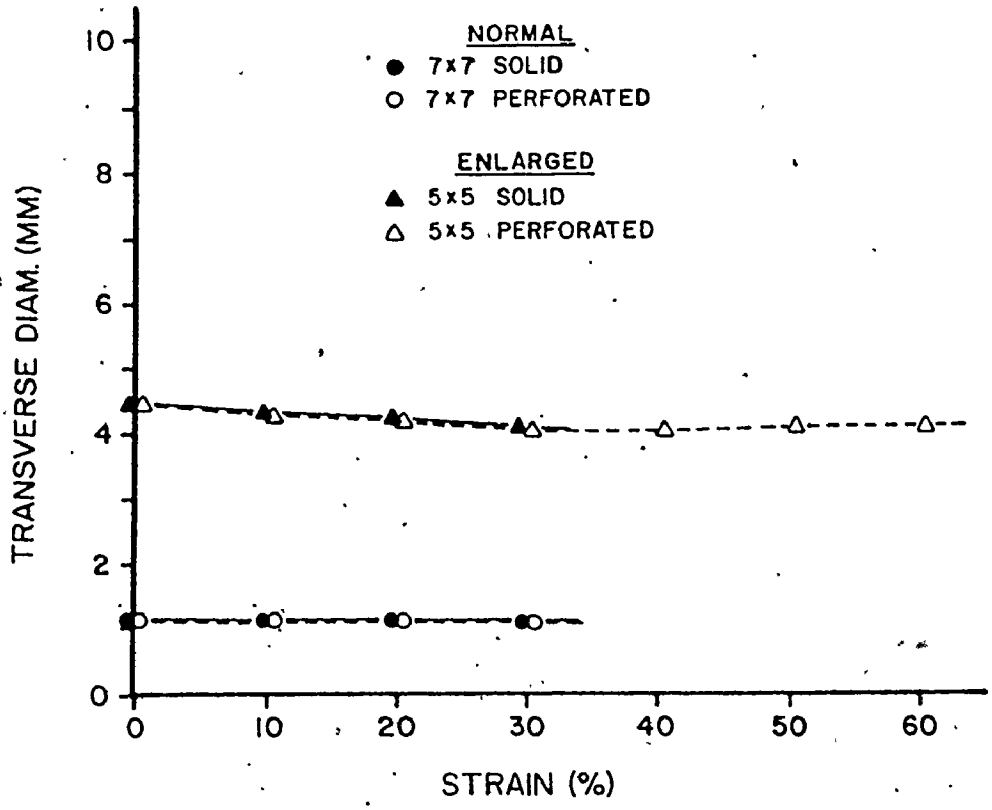

Figure 59 Graph demonstrating the change in transverse diameter of the fenestrations with increasing strain.

	TRANSVERSE DIAMETER	AXIAL DIAMETER	AREA	TRANSVERSE LE	AXIAL LE
Normal					
Solid	-0.002	0.011	0.0073	-0.002	0
Perforated	-0.013	0.036	0.03	-0.00035	-0.0025
Perforated/Marked	(1)	3.2	4.0	(1)	(2)
Enlarged					
Solid	-0.015	0.044	0.086	-0.00035	0
Perforated	-0.006	0.099	0.3	-0.00063	-0.003
Perforated/Marked	(1)	2.23	3.5	(1)	(2)
Enlarged/Normal					
Solid	(1)	3.9	11.8	(1)	(2)
Perforated	(1)	2.7	10.2	(1)	1.2

NOTES:

(1) Not Relevant
(2) Not Defined

TABLE 11 - Slopes of Linear Regression

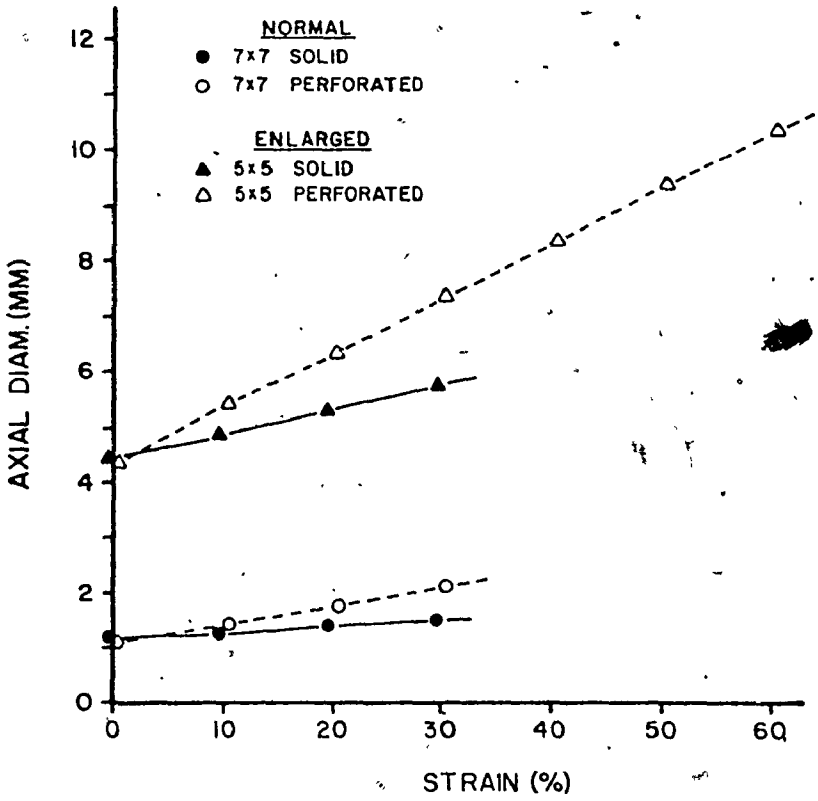

Figure 60 Change in axial diameter of the fenestrations with increasing strain.

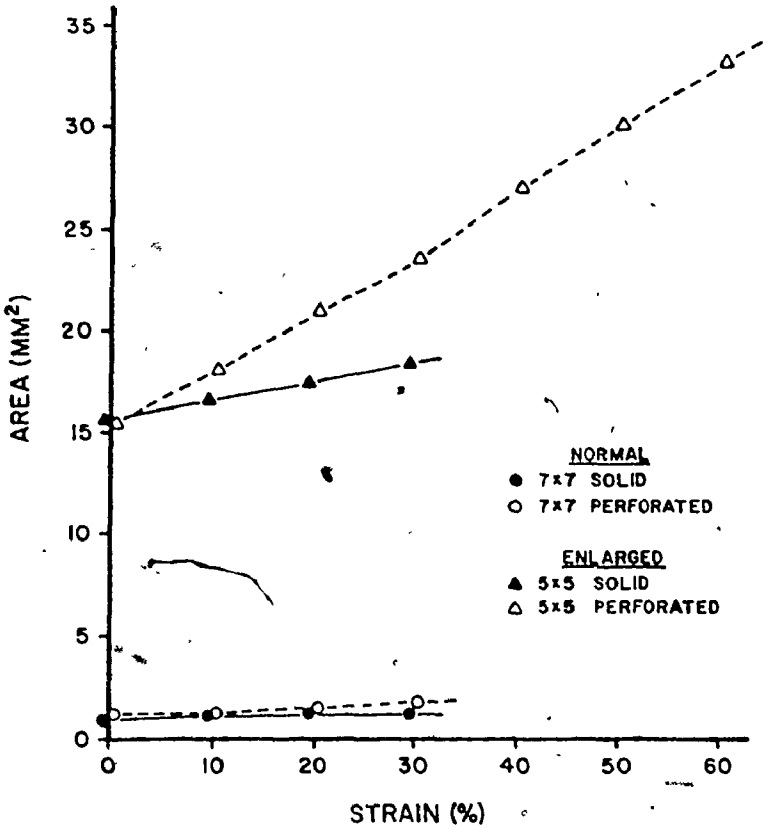

Figure 61 Curves depicting the change in the area of the fenestrations with increasing strain.

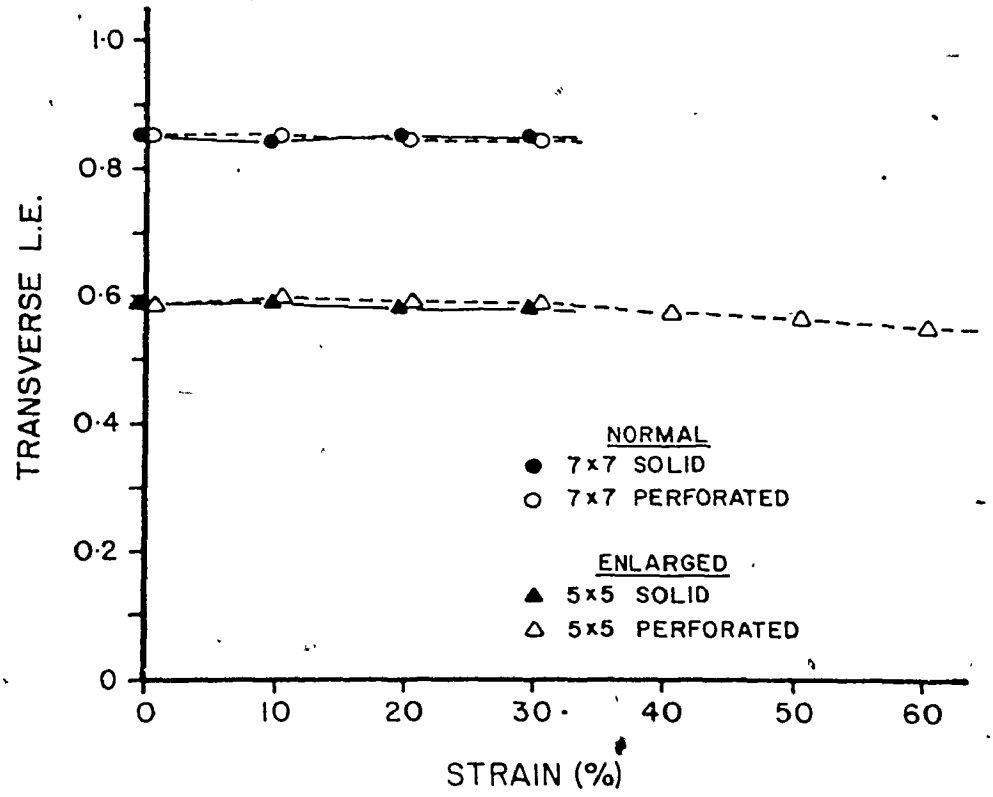

Figure 62 Plots of transverse ligament efficiency (fenestrations) with increasing strain.

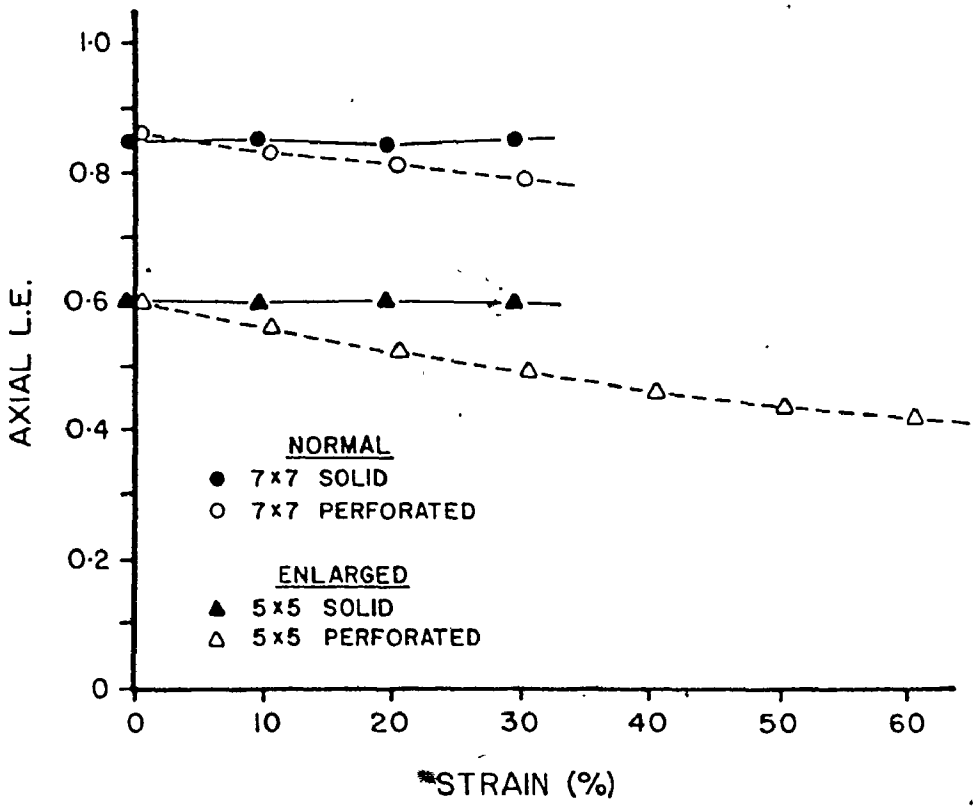

Figure 63 Change in axial ligament efficiency (fenestrations) with increasing strain.

efficiency for the perforated condition decreases with increasing strain as depicted in Figure 63. The relative rate of this decrease listed in Table 11 is 1.2 for the enlarged with respect to the normal, which indicates that the rates are comparable.

The eccentricity for both the solid and perforated conditions of both specimens increased rapidly with initial strain, with progressive moderation of the rate at higher strains (Figure 64). The perforated condition of both samples increased more rapidly and maintained a greater magnitude throughout the elongation. It is intriguing that the results for both the solid (normal and enlarged) and perforated (normal and enlarged) conditions were remarkably similar.

4.4.4 Discussion

The characteristics of the fenestrations for both the normal and enlarged fenestrations listed in Table 11 are in good agreement with the previous results for the larger population of specimens (section 4.3). Replication in latex rubber of the actual geometry for both the normal and enlarged fenestrations at the same magnification, has provided a means for comparing the tensile properties of the same material with two distinct perforated configurations. The obvious increase at comparable stress levels with elongation of the specimen with enlarged fenestrations illustrated in Figure 57, indicates that a region of enlarged fenestrations in the internal lamina should bulge more than the surrounding region of normal fenestrations.

If the shape of the bulge in the internal elastic lamina is depicted to be elliptical in cross-section, (as shown in Figure 65), then the depth of the bulge (H) can be related to a known proportional increase in the length (K) of a localized region of the internal

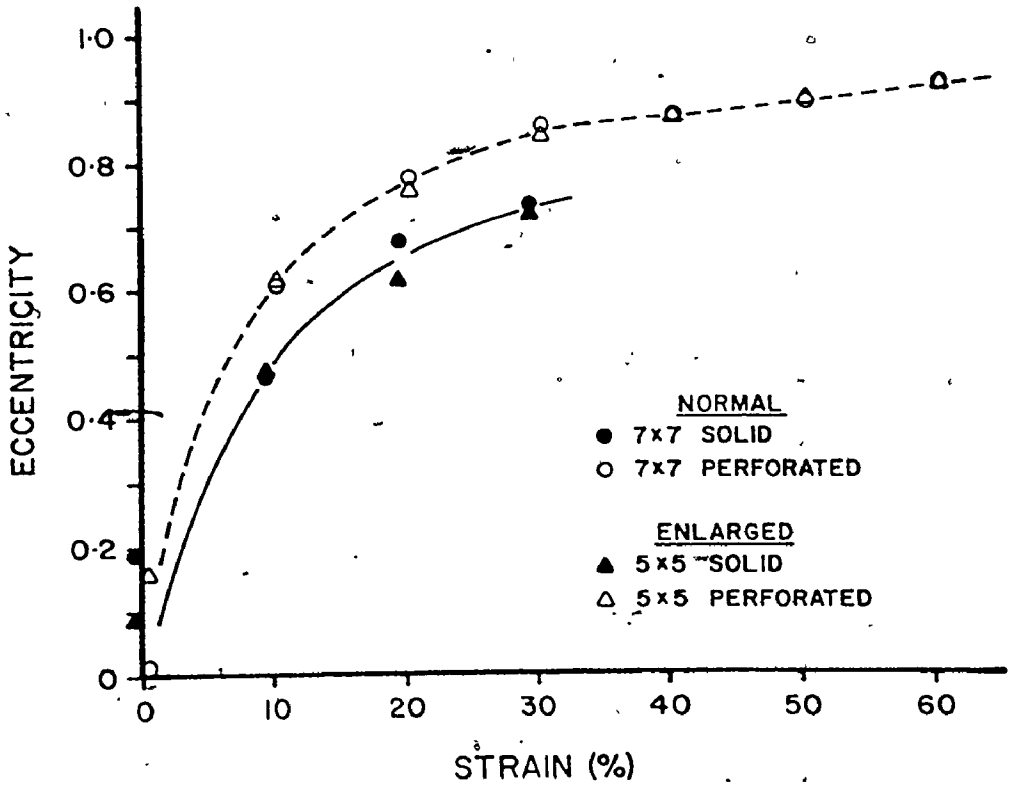

Figure 64 Plots of eccentricity (ellipse) with increasing strain.

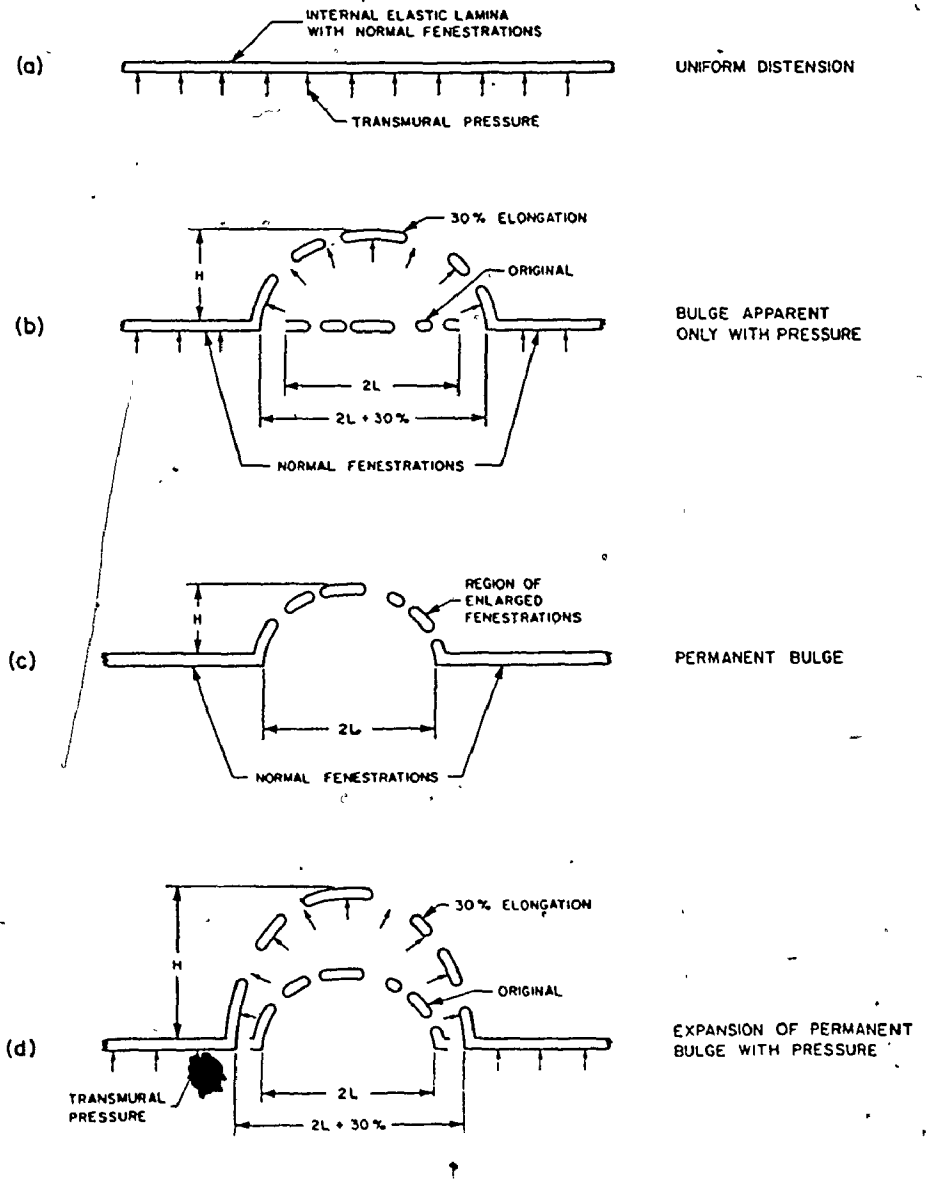

Figure 65 Schematic representation of the effect of transmural pressure on normal and enlarged fenestrations.
(a) normal fenestrations only
(b) formation of bulge (30% strain) in a region of enlarged fenestrations, created by transmural pressure (relative dimensions of bulge are drawn to scale).
(c) formation of a permanent bulge by the enlargement of a region of fenestrations (relative dimensions of a bulge are drawn to scale).
(d) expansion (30% strain) of a permanent bulge by transmural pressure (relative dimensions of bulge are drawn to scale).

elastic lamina. The standard solution (approximate) for computing the perimeter of an ellipse is (Selby 1972, page 13):

$$P = 2\pi \left[\frac{L^2 + H^2}{2} \right]^{1/2} \qquad (18)$$

where: P = perimeter

L = semi-major axis (i.e., one-half of the length of the region of enlarged fenestrations)

H = semi-minor axis (i.e., the depth of the bulge)

This expression may be re-arranged:

$$H = \left[\frac{P^2}{2\pi^2} - L^2 \right]^{1/2} \qquad (18)$$

For a proportional increase in one-half of the perimeter, the applicable expression is:

$$K = \frac{P/2}{2L} \qquad (19)$$

Substitution of equation (19) into equation (18) and re-arranging, yields the result:

$$H = L(0.81K^2 - 1)^{1/2} \qquad (20)$$

In the case of a continuous internal elastic lamina with normal fenestrations, the transmural pressure would cause a uniform distension of the internal elastic lamina (Figure 65a). In order to assess the factors affecting the creation of a bulge in regions of enlarged fenestrations, three conditions are considered.

i) Bulge Apparent Only With Pressure

The regions of normal and enlarged fenestrations when examined with the scanning electron microscope, usually appear as a continuous flat surface without any discernible evidence of a permanent bulge in the region of enlarged fenestrations. Nevertheless, the technique of mounting the specimen on a flat surface along with the small size of the regions of enlarged fenestrations could account for the flat appearance. Under the influence of transmural pressure, a stress would be induced in the arterial wall. If the pressure is sufficient or the wall weakened to permit the stretching of the internal elastic lamina, then the results depicted in Figure 65 would predict that the region of enlarged fenestrations would stretch more than the circumjacent region with normal fenestrations. The increased elongation of 47% presented earlier for the regions of enlarged fenestrations in relation to the normal fenestrations, may be converted to an appropriate K value by the expression:

$$K = 1 + (k_S \times k_E) \qquad (21)$$

where k_S = proportional increase in strain

k_E = proportional increase in elongation of the regions of enlarged to normal fenestrations

Solution of equation (20) with the substitution for K of 1.47, 1.294 and 1.441 for 10%, 20% and 30% strains respectively, results in corresponding bulge depths (H) of 0.13, 0.30 and 0.41 per unit length (2L). That is, the depth of the bulge for the 30% strain, would represent 0.41 or 41% of the length of the region of enlarged fenestrations. The dimensions of the bulge representing 30% strain, shown in Figure 65b, have been drawn to scale, in order to demonstrate this relationship.

ii) Permanent Bulge

Another possibility is that the enlargement of the fenestrations has created a permanent bulge. In this instance, the increase in the linear dimension in the region of the enlarged fenestrations is attributable to an increase in the centre-to-centre distance, since it is assumed that the average width of the ligament remains constant, while the fenestration diameter increases. Therefore, the original normal fenestrations increase in size, but do not coalesce. Computation of the average ligament width for the model configurations representing the two samples presented in Figure 54 was 8.54 μm for the normal fenestrations and 8.52 μm for the enlarged fenestrations. Similarly, the ligament width computed from the preceding section on enlarged fenestrations revealed average values of 12.8 μm for the normal fenestrations and 13.0 μm for the enlarged fenestrations. The exceptional agreement for each of the two groups, suggests that the fenestrations have enlarged without consuming the internal elastic lamina. This finding also suggests that the conversion from normal to enlarged fenestrations, perhaps as a consequence of accommodation to increased stress, could create a permanent bulge. A further discussion about enlargement of the fenestrations will be presented later. A proportional increase in the length of the region of enlarged fenestrations (K) is calculated as the ratio of the average centre-to-centre distance for enlarged in relation to the normal fenestrations. For the regions of enlarged and normal fenestrations presented here, the result for "K" is 1.44. Substitution of this value into equation (20) yields a depth for the bulge of 0.41 per unit length. This result is depicted in Figure 65c with the dimensions

of the bulge drawn to scale.

iii) Effect of Transmural Pressure on Permanent Bulge

Under the influence of transmural pressure, the permanent bulge described in the preceding section (ii) would increase in size. The increase represents a summation of the proportional increases for the length of the regions presented in sections i) and ii):

$$K = k_1 + (k_S \times k_E) \qquad (22)$$

where: k_1 = ratio of centre-to-centre distances for enlarged to normal (section ii)

Substitution into equation (20) for K values of 1.587, 1.734 and 1.881 for strains of 10, 20 and 30% respectively, resulted in corresponding bulges of 0.51, 0.60 and 0.68 per unit length (2L). An illustration of the results has been presented in Figure 65d with the dimensions of the bulges representing the original condition, as well as 30% strain, drawn to scale.

It is acknowledged that this analysis has ignored the influence of other components of the wall on the formation of the bulge. Also, the shape of the bulge is two-dimensional, whereas, the relative elastic characteristics were determined from uniaxial tensile measurements.

The preceding analysis suggests that the formation of evaginations in the elastic lamina may be attributable to regions of enlarged fenestrations. Consideration of whether enlargement of the fenestrations is a primary effect which directly results in an evagination or whether there is another effect such as a medial defect or thinning, is beyond the scope of this investigation.

The close agreement for the standardized stress between the

replication and the model configurations (geometrical) of the normal fenestrations as well as a reasonable agreement for the comparable configurations of the enlarged fenestrations (Figure 58), substantiates the rationale for the use of the geometrical model configurations based upon equivalent ligament efficiencies to represent the average spatial geometry of fenestrations during progressive stretching. In the complementary investigation (sections 3.4 and 3.5) the same modelling technique for straight segments of cerebral arteries of various external diameter with variation in the characteristics of the fenestrations and photomicrographs at different magnifications, also provided similar excellent agreement between the stress/strain characteristics of the replication and geometrical model configurations.

It was evident from Figures 59 and 62 that progressive elongation did not diminish the transverse diameter nor affect the transverse ligament efficiency. Nevertheless, the axial diameter for the enlarged fenestrations increased at a faster rate than the normal fenestrations. This effect resulted in a progressive decrease in the ligament efficiency as well as a substantial increase in the average area of the enlarged fenestrations in relation to the normal fenestrations. It is interesting that the eccentricities which represent the shape factor for both the enlarged and normal fenestrations are equivalent, even though the increase in their axial diameters and areas are considerably different.

Infiltration by fibrin and red blood cells into the arterial wall between the internal elastic lamina and the media has been reported by a number of authors (Stehbens 1981, Stehbens 1963, Nystrom 1963). The

pronounced increase in the average area for the enlarged fenestrations with respect to the normal fenestrations may play a role in this infiltration.

Stehbens (1975a) has also studied the degenerative changes in the intimal cushions or pads present at bifurcations. He cited their susceptibility to lipid accumulation to substantiate his hypothesis that the cushions are sites of mild but persistent injury, indicative of an early stage of atherosclerosis. One of the degenerative changes identified (Stehbens 1960) for the formation of cushions was elastin fragmentation which suggests that perhaps enlarged fenestrations may play a role in the development of atherosclerosis.

Klynstra and Bottcher (1969) have shown that the preferred sites of fatty streaks and spots in pig thoracic aorta demonstrate enhanced permeability. Oka (1979) and Niimi et al (1979) have stated that the permeability of the endothelium is enhanced by wall shear stress, stretch, vibration, circumferential tension and high stress concentrations. Others (Still 1967, Olsen 1969) have demonstrated with the use of rats that hypertension will accelerate the infiltration of mononuclear cells as well as fluorescent proteins and colloidal carbon particles into the arterial wall. Olsen (1969) further observed with the use of serial sections that in the permeable areas, the internal elastic lamina is either lacking or depicted as "disconnected fragments".

A previous study by Hassler (1962) demonstrated that the diameter of fenestations (anterior cerebral artery) increased to a peak at about the third decade of life, and then subsequently decreased at a moderate rate. In a recent study by Hayashi et al (1980a), the circumferential

wall stress (constant transmural pressure of 100 mmHg was assumed for all ages) computed for the intracranial vertebral artery increased to a peak at about the second decade of life (values for the third decade of life were not reported) with a moderate decrease thereafter. This decrease in wall stress is attributable to the increased thickness of the arterial wall (Hayashi et al 1980a) which includes a concomitant increase in thickness of the internal elastic lamina (Hassler 1962). The remarkable similarlity in the shape of the curves for change in the diameter of the fenestrations and wall stress associated with age, suggests that the fenestration diameter may be influenced by the stress induced in the internal elastic lamina.

Preliminary results of a recent study by Potter and Roach (1983) showed that the average diameter of fenestrations from the thoracic aortas of rabbits was larger in the region of the dilatation distal to a stenosis. This finding indicates that the change in mechanical properties of the internal elastic lamina is associated with the enlarged fenestrations. It was also suggested in section 4.3 that regions of enlarged fenestrations create stress concentrations which may further influence their growth. Ferguson (1972) has concluded from model studies, that the impingement of blood at the apex of intracranial bifurcations increases the shear stress adjacent to the apex which could stretch the tissue at the apex. The combined influence of this effect along with the transmural pressure could be an important factor contributing to a focal degeneration of the internal elastic lamina. Macfarlane (1975) has shown that increasing the transmural pressure has the effect of increasing the radius of curvature (caudal-dorsal) at the apex of the bifurcation but also

results in flattening of the central portion. He has attributed the flattening to very high wall stresses in the apical region of the bifurcation. Therefore, localized regions of increased wall stress induced by: haemodynamic flow; the geometry of the artery at a bifurcation; and/or changes in the structure of the arterial wall may contribute to the creation of enlarged fenestrations.

Although the modelling technique presented in this section has limitations, nevertheless, it has demonstrated that the regions of enlarged fenestrations could produce small evaginations and perhaps increased permeability of the internal elastic lamina. Even though the progression from a small evagination to a fully-developed aneurysm has not been conclusively proven, other investigators (Stehbens 1963, 1975b, 1981, Sahs 1966) have suggested that fragmentation of the internal elastic lamina and evagination are necessary precursors to the formation of a saccular aneurysm. The observations by Hassler (1972) and Merei and Gallyas (1980a) of enlarged fenestrations at the mouth of saccular aneurysms provides further evidence to suggest that the enlargement of fenestrations may play a significant role in the etiology of intracranial saccular aneurysms.

4.4.5 Summary

The actual spatial geometry of separate regions of normal and enlarged fenestrations from the internal elastic lamina of human cerebral arteries have been replicated in sheets of latex rubber from scanning electron microscope photomicrographs. Geometrical models which assume a constant diameter for the fenestrations, a constant ligament efficiency for the regions of fenestrations and a uniform

array of rows and columns have also been created in sheets of latex rubber. The stress (load per unit of cross-sectional area) and strain (percent elongation) were computed for each of the samples during uniaxial stretching. The elongation of the sample representing the region of enlarged fenestrations increased an average of 47% compared to the similar representation of normal fenestrations, at the same increments of stress. This suggests that the regions of enlarged fenestrations would form a bulge, indicative of an evagination of the internal elastic lamina.

The model configurations demonstrate very similar stress/strain characteristics to the replications. This finding justified the use of this modelling technique using equivalent ligament efficiencies, to represent the actual spatial geometry. During elongation, the average area of the enlarged fenestrations increased at a rate which was an order of magnitude greater than that for the normal fenestrations. Since a number of observations associated with the development of intracranial saccular aneurysms can be correlated to a region of enlarged fenestrations, the region of enlarged fenestrations may be a defect in the internal elastic lamina which plays a prominent role in the development of intracranial saccular aneurysms.

Chapter 5

SUMMARY AND CONCLUSIONS

The purpose of this thesis has been to investigate the form and structure of the internal elastic lamina for both the straight segments and bifurcations from human cerebral arteries. A secondary consideration was to examine the apical region of the bifurcations for a weakness which could be linked to the formation of intracranial saccular aneurysms. Towards this endeavour there are several firm statements which have evolved from the research:-

i) A technique has been established for isolating the internal elastic lamina from the arterial wall in a form suitable for examination by the scanning electron microscope.

ii) A new method has been developed for assessing the dimensional changes of specimens during preparation for examination by the scanning electron microscope. The method includes a companion computer programme which facilitates the acquisition of the marker points, optimization of the alignment between the photomicrographs depicting the before and after conditions of the specimen, and computation of the dimensional changes.

iii) The shrinkage of the internal elastic lamina from cerebral arteries with different external diameter was assessed by the new method. It was found that the radial shrinkage remained constant at about 6.9 % regardless of the external diameter of the artery. The shrinkage of the apical region of bifurcations was comparable to the cylindrical segments. The relative shrinkage between the circumferential and longitudinal orientations of the artery were similar which indicates isotropic shrinkage.

iv) The morphology of fenestrations in the internal elastic lamina has been described by a series of geometrical variables (ie. diameter, density, percentage area, and ligament efficiency) for a range of arteries with steadily decreasing external diameters. It is particularly interesting that the average diameter decreases linearly, while the density increases rapidly towards the periphery of the circulation, whereas the ligament efficiency remains essentially constant throughout. Moreover, the results are remarkably consistent among the subjects analyzed. I have postulated that the factors determining the spatial geometry of the fenestrations in the internal elastic lamina during morphogenesis and elastogenesis are dictated by a process which may be described by a consistent ligament efficiency.

v) The uniaxial tensile characteristics for replications of the actual spatial geometry and a model of the spatial geometry based upon an equivalent ligament efficiency duplicated in sheets of latex rubber are comparable for specimens with different hole diameter, densities and hence ligament efficiencies. This agreement confirms the effectiveness of the ligament efficiency to represent the actual spatial geometry of fenestrations.

vi) A study of the changes in parameters (diameters, area, ligament efficiencies, eccentricity, necking, expansion ratio) for the spatial geometry, revealed differences among three cylindrical specimens with various external diameters and various geometrical characteristics of the fenestrations. The similarity between the relative results for the expansion ratios and the relative decrease in the standardized stress, suggests a relationship, but

further studies would be required to verify whether a relationship exists.

vii) An analysis of the geometrical characteristics for the fenestrations in the apical region of bifurcations revealed regions (13 of 28 specimens) in the form of clusters or bands where the diameter of the fenestrations has increased significantly while the ligament efficiency has decreased significantly in comparison with the surrounding region of fenestrations. Only two of 34 cylindrical specimens showed evidence of enlarged fenestrations. These changes in the geometrical characteristics have also been shown to create a localized stress concentration substantially in excess of that associated with a region of normal fenestrations. Furthermore large elliptical gaps in this region were observed in more than 80 % of the specimens, but it has not yet been established whether the gaps existed in vivo or were accidentally produced during preparation of the specimens. Nevertheless the location of the splits at the apex of the bifurcation along with the presence of enlarged fenestrations suggest that the enlarged fenestrations may represent a weakness that can precipitate the split. The regions of enlarged fenestrations may also be interpreted as fragmentation of the internal elastic lamina since the standard 4-7 μm serial sections show a solid band of material in the case of normal fenestrations (ie. diameter of fenestrations is less than the width of the section), whereas the intervening ligaments in the region of enlarged fenestrations would appear as fragments (ie. many fenestrations are larger than the width of the section).

viii) The uniaxial elongation of a replication in latex sheet of enlarged fenestrations was 47 % greater than for normal fenestrations in latex sheet at equivalent magnitudes of stress. Therefore in a closed system it would be anticipated that the region of enlarged fenestrations would elongate more readily, creating a bulge. By assuming that the bulge formed an elliptical shape, the proportional changes in the shape of the bulge have been assessed based upon the uniaxial test. I have proposed that these bulges may represent the evaginations reported in the literature.

ix) The changes in the spatial geometry were assessed by a series of parameters (diameters, area, ligament efficiencies, eccentricity, and expansion ratio). The substantial increase in the average fenestration area for the regions of enlarged fenestrations compared to the normal fenestrations may play a role in the infiltration of substances into the wall of the area. The infiltration of substances has been demonstrated by other investigators to destroy the internal elastic lamina.

Although the presence of enlarged fenestrations in the internal elastic lamina has not been firmly linked to the formation of intracranial saccular aneurysms, supporting evidence exists to suggest that they may play a prominent role. The considerations which allow this assertion are based upon the information derived in the thesis along with existing observations and postulations:-

i) The predominant location for enlarged fenestrations is the apical region of bifurcations which concurs with the observation that this is the region where most intracranial saccular aneurysms are

present.

ii) The observation by other investigators of "fragmentation" could perhaps be attributable to the interpretation of serial sections fortuitously cut through a region of enlarged fenestrations.

iii) Enlarged fenestrations represent areas of weakness by virtue of the increase in stress concentrations and the presence of splits in the internal elastic lamina.

iv) The increased elongation for regions of enlarged fenestrations (uniaxial testing of latex sheets) indicates that a bulge may form which is indicative of the evaginations in the internal elastic lamina observed by others.

v) The substantial increase in area for the regions of enlarged fenestrations may facilitate the infiltration of substances into the arterial wall which has been reported by others to destroy the internal elastic lamina.

vi) Enlargement of fenestrations with a sustained increase in the stress induced by poststenotic dilatation concurs with the proposition by other investigators that turbulence, axial stream impingement, wall vibration, increased shear stress and increased transmural pressure contribute to a focal degeneration of the internal elastic lamina.

vii) Other investigators have reported enlarged fenestrations in the internal elastic lamina of the neck region of saccular aneurysms.

Hassler O: Morphological studies on the large cerebral arteries with reference to the aetiology of subarachnoid haemorrhage. Acta Psych Neurol Scand, 36: suppl 154 (1961).

Hassler O: The windows of the internal elastic lamella of the cerebral arteries. Virchows Arch Path Anat, 335: 127-132 (1962).

Hassler O: Scanning electron microscopy of saccular intracranial aneurysms. Am J Pathol, 68(3): 511-520 (1972).

Haust MD, More RH, Bencosme SA, Balis JU: Elastogenesis in human aorta: An electron microscopic study. Exp Mol Pathol, 4: 508-524 (1965).

Hayashi K, Handa H, Nagasawa S, Okumura A, Moritake K: Stiffness and elastic behavior of human intracranial and extracranial arteries. J Biomech, 13, 175-184 (1980a).

Hayashi K, Nagasawa S, Naruo Y, Okmura A, Moritake K, Handa H: Mechanical properties of human cerebral arteries. Biorheology 17, 211-218 (1980b).

Imaizumi K, Shigemi V, Nakamura M: Chemical comparison intimal elastin in the human cerebral and coronary arteries and aorta. Paroi Arterielle - Arterial Wall T II,4: 213-219 (1975).

Kawamura J, Gertz SD, Sunaga R, Rennels ML, Nelson E: Scanning electron microscopic observations on the luminal surface of the rabbit common carotid artery subjected to ischemia by the arterial occlusion. Stroke 5, 765-774 (1974).

Klassen AC, Sung JH, Stadlan E: Histological changes in cerebral arteries with increasing age, J Neuropath, Exp Neurol, 27: 607-623 (1968).

Klynstra FB, Bottcher JF: Permeability patterns in pig aorta. Atherosclerosis 451-462 (1969).

Lamb JC, Ingram P: Drying of biological specimens for scanning electron microscopy directly from alcohol, SEM/IITRI, 3: 459-472 (1979).

Lang ER, Kidd M: Electron microscopy of human cerebral aneurysms. J Neurosurg 22: 554-562 (1965).

Langille BL, Adamson SL: Relationship between blood flow direction and endothelial cell orientation at arterial branch sites in rabbits and mice. Circulation Research, 48: 481-488 (1981)

Legg MJ, Gow BS: The size of endothelial cells in the rabbit thoracic aorta. Atherosclerosis, 39: 227-279 (1981).

iii) Fenestrations in the Internal Elastic Lamina.

The measurement of the characteristics for fenestrations in outpouchings and saccular aneurysms would be of value to establish if a relationship between a size of outpouching (or aneurysm) and the characteristics can be defined. An examination of specimens from three distinct age groups (newborn, adolescent and adult) could provide information on the changes with age as well as identifying the stage in the developmental process when enlarged fenestrations become evident. The analysis of the characteristics for fenestrations in rat arteries may determine whether the enlarged fenestrations play a role in the development of saccular aneurysms that have been induced by artificial means in rats (Hashimoto, 1979).

BIBLIOGRAPHY

Albert EN, Nayak RK: Surface morphology of human aorta as revealed by the scanning electron microscope. Anat Rec, 185: 223-234 (1976).

Andrews RJ, Spiegel PK: Intracranial aneurysms: age, sex, blood pressure and multiplicity in an unselected series of patients. J Neurosurg, 51: 27-32 (1979).

Ayer JP: Elastic tissue. Int Rev of Conn Tiss Res, 2: 33-100 (1964).

Barford NC: Experimental measurements: precision, error and truth. Addison-Wesley Publishing Co. Inc, Don Mills, Ontario, pp. 33 (1967).

Berry CL: The establishment of the elastic structure of arterial bifurcation and branches. Atherosclerosis, 18: 117-127 (1973).

Bjorkerud S: Reaction of the aortic wall of the rabbit after superficial, longitudinal, mechanical trauma. Virchows Arch Abt A Path Anat, 347: 197-210 (1969).

Black JT: 1. The scanning electron microscope - operating principles: Principles and techniques of scanning electron microscopy; Biological applications, Hayat MA (editor), Vol. 1, Von Nostrand Reinhold Co, Toronto: 1-43 (1974).

Bloom W, Fawcett DW: A textbook of histology. W.B. Saunders, Toronto, 1975.

Bowyer DE: SEM and the surface coat. Prog Biochem Pharmacol, 14: 192-195 (1977).

Boyde A, Bailey E, Jones SJ, Tamarin A: Dimensional changes during specimen preparation for scanning electron microscopy SEM/IITRI, 1: 507-518 (1977).

Boyde A, Boyde S: Further studies of specimen volume changes during processing for SEM: Including some plant tissue. SEM/IITRI, 2: 117-132 (1980).

Boyde A, Franc F: Freeze-drying shrinkage of glutaraldehyde fixed liver. J. of Microscopy, 122, Pt. 1: 75-86 (1981).

Burton, AC: The stretching of "pores" in a membrane. Permeability and function of biological membranes (Edited by Bolis L, Katchalsky A, Keyes RD, Loewenstein WR and Pethica BA), North Publishing Co., pp. 1-19 (1970).

Busby DE, Burton AC: The effect of age on the elasticity of the major brain arteries. Can J Physiol and Pharmac, 43: 185-202 (1965).

Cajander S, Hassler O: Enzymatic destruction of the elastic lamella at the mouth of cerebral berry aneurysm. Acta Neurol Scandinav, 53: 171-181 (1976).

Campbell GJ, Roach MR: Fenestrations in the internal elastic lamina at bifurcations of human cerebral arteries. Stroke 12: 489-496 (1981a).

Campbell GJ, Roach MR: A method for measuring dimensional changes of tissues prepared for scanning electron microscopy. Scanning, 4, 188-195 (1981b).

Campbell GJ: An optimization procedure for the alignment of marker points to assess dimensional changes. Comp Prog in Biomed, 15: 45-60 (1982).

Campbell GJ, Roach MR: Dimensional changes associated with freeze-drying of the internal elastic lamina from cerebral arteries. Scanning (in press).

Carmichael R: Gross defects in the muscular and elastic coats of the larger cerebral arteries, J Pathol Bacterial, 57: 345-351 (1945).

Carnes WH, Hart ML, Hodgkin NM: Conformation of aortic elastin revealed by scanning electron microscopy of dissected surfaces, Advances in Experimental Med & Biol, 79: 61-70 (1977).

Carton RW, Dainauskas J, Clark JW: Elastic properties of single elastic fibers. J Appl Physiol, 17(3): 547-551 (1962).

Chalupnik JD, Daly CH, Merchant HC: Material properties of cerebral blood vessels. Final Rep. on Contract No. N1H-69-2232 (1971). Referenced in Hayashi (1980b).

Chason JL, Hindman WM: Berry aneuryms of the circle of Willis; results of a planned autopsy study. Neurology 8, 41-44 (1958).

Cook TA, Salmo NAM, Yates PO: The elasticity of the internal lamina. J Pathol 117(3): 253-258 (1975).

Crawford T: Some observations of the pathogenesis and natural history of intracranial aneurysms. J Neurol Neurosurg Psychiatry, 22: 259-266 (1959).

Crompton MR: Mechanism of growth and rupture in cerebral berry aneurysm. Br Med J, 1: 1138-1142 (1966).

Damude LC, Cope DA, Roach MR: The effects of enzymatic digestion on the elastic properties of isolated human cerebral arteries, Can J Physiol Pharm, 55: 161-1692 (1977).

Dees MB: On the fenestrated membrane of Henle. The Anatomical Record 26(2): 161-169 (1923).

Faupel JH: Engineering design: A synthesis of stress analysis and materials engineering. New York, John Wiley & Sons, 1964.

Ferguson GG: Turbulence in human intracranial saccular aneurysms. J Neurosurg, 33: 485-487 (1970).

Ferguson GG: Physical factors in the initiation, growth, and rupture of human, intracranial saccular aneurysm. J Neurol, 37: 666-677 (1972).

Flaherty JT, Perce JE, Ferrans VJ, Patel DJ, Tucker WK, Fry DL: Endothelial nuclear patterns in the canine arterial tree with particular reference to hemodynamic events: Circulation Research, V. 30: 23-33 (1972).

Forbus WD: On the origin of miliary aneurysms of the superficial cerebral arteries. Bulletin of the Johns Hopkins Hospital, Vol. XLVII: 239-284 (1930).

Foreman JEK, Hutchinson KJ: Arterial wall vibration distal to stenoses in isolated arteries of dog and man. Cir Res 26: 584-590 (1970).

Gerrity RG: Some aspects of scanning electron microscopy techniques applied to the study of large arteries. Prog biochem pharmacol, 14: 306-311 (1977).

Glynn LE: Medial defects in the circle of Willis and their relation to aneurysm formation. J Path Bact, 51: 213-222 (1940).

Gosline JM: The physical properties of elastic tissue. Int Rev Connect Tissue Res, 7: 211-249 (1976).

Gosline JM, French CJ: Dynamic mechanical properties of elastin, Biopolymers, 18: 2091-2103 (1979).

Grut W, Edwards J, Evans E: Scanning electron microscopy of freeze-dried aortic elastin. J Microsc Vol. 110, Pt. 2: 271-275 (1977).

Gusnard D, Kirschner RH: Cell and organelle shrinkage during preparation for scanning electron microscopy: effects of fixation, dehydration and critical point drying. J of Microscopy 110, Pt. 1: 51-57 (1977).

Ham AW, Cormack DH: Histology, J.B. Lippincott Co., Toronto, 7th Edition: (1974).

Hashimoto N: Experimental inducement of cerebral aneurysms in rats. Arch Jpn Chir, 40: 667-678 (1979).

Hass GM: Elastic Tissue, I. Description of a method for the isolation of elastic tissue. Arch Path, 34: 807-819 (1942).

Hassler O: Morphological studies on the large cerebral arteries with reference to the aetiology of subarachnoid haemorrhage. Acta Psych Neurol Scand, 36: suppl 154 (1961).

Hassler O: The windows of the internal elastic lamella of the cerebral arteries. Virchows Arch Path Anat, 335: 127-132 (1962).

Hassler O: Scanning electron microscopy of saccular intracranial aneurysms. Am J Pathol, 68(3): 511-520 (1972).

Haust MD, More RH, Bencosme SA, Balis JU: Elastogenesis in human aorta: An electron microscopic study. Exp Mol Pathol, 4: 508-524 (1965).

Hayashi K, Handa H, Nagasawa S, Okumura A, Moritake K: Stiffness and elastic behavior of human intracranial and extracranial arteries. J Biomech, 13, 175-184 (1980a).

Hayashi K, Nagasawa S, Naruo Y, Okmura A, Moritake K, Handa H: Mechanical properties of human cerebral arteries. Biorheology 17, 211-218 (1980b).

Imaizumi K, Shigemi V, Nakamura M: Chemical comparison intimal elastin in the human cerebral and coronary arteries and aorta. Paroi Arterielle - Arterial Wall T II,4: 213-219 (1975).

Kawamura J, Gertz SD, Sunaga R, Rennels ML, Nelson E: Scanning electron microscopic observations on the luminal surface of the rabbit common carotid artery subjected to ischemia by the arterial occlusion. Stroke 5, 765-774 (1974).

Klassen AC, Sung JH, Stadlan E: Histological changes in cerebral arteries with increasing age, J Neuropath, Exp Neurol, 27: 607-623 (1968).

Klynstra FB, Bottcher JF: Permeability patterns in pig aorta. Atherosclerosis 451-462 (1969).

Lamb JC, Ingram P: Drying of biological specimens for scanning electron microscopy directly from alcohol, SEM/IITRI, 3: 459-472 (1979).

Lang ER, Kidd M: Electron microscopy of human cerebral aneurysms. J Neurosurg 22: 554-562 (1965).

Langille BL, Adamson SL: Relationship between blood flow direction and endothelial cell orientation at arterial branch sites in rabbits and mice. Circulation Research, 48: 481-488 (1981)

Legg MJ, Gow BS: The size of endothelial cells in the rabbit thoracic aorta. Atherosclerosis, 39: 227-279 (1981).

Locksley HB: Report on the cooperative study of intracranial aneurysms and subarachnoid hemorrhage, Section 5, Part 1. Natural history of subarachnoid hemorrhage, intracranial aneurysms and arteriovenous malformations. J Neurosurg, 25: 321 (1966).

Macfarlane TWR: The geometry of cerebral arterial bifurcations and its modification with static distending pressure. Thesis, The University of Western Ontario (1975).

McCormick WF, Acosta-Rua GJ: The size of intracranial saccular aneurysm, An autopsy study. J Neurosurg, 33: 422-427 (1970).

McCormick WF, Schmalstieg EJ: The relationship of arterial hypertension to intracranial aneurysms. Arch Neurol, 34: 285-287 (1977).

McGarvey KA, Reidy MA, Roach MR: A quantitative study of the preparation of rabbit aortic endothelial cells for scanning electron microscopy. J. of Microscopy 118, Pt. 2: 229-236 (1980).

Merei FT, Gallyas F: Role of the structural elements of the arterial wall in the formation and growth of intracranial saccular aneurysms. Neurol Res 2(3-4): 283-303 (1980a).

Merei FT, Gallyas F, Horvath Z: Elastin elements in the media and adventitia of human intracranial extracerebral arteries, Stroke, 11: 329-336 (1980b).

Moritake K, Handa H, Okumura A, Hayashi K, Niimi H: Stiffness of cerebral arteries -- Its role in the pathogenesis of cerebral aneurysms. Neurol Med Chir, 14: 47-53 (1974).

Moritake K, Handa H, Okumura A. Nagasawa S, Naruo Y, Hayashi K, Safo M, Hazama F: Quantitative analysis of microstructural components of human cerebral arteries, Neurol Res, 3: 67-82 (1981).

Nagasawa S, Handa H, Okumra A. Naruo Y, Moritake K, Hayashi K: Mechanical properties of human cerebral arteries. Part 1: Effect of age and vascular smooth muscle activation in physiological state. Surg Neurol, 12: 297-304 (1979).

Niimi H, Horie R, Yamori Y, Oka S: Hemodynamic factors on the development of atherogenesis in stroke-prone SHR. Jpn Heart J, 20 (Suppl. 1): 368-370 (1979).

Nystrom SHM: Development of intracranial aneurysms as revealed by electron microscopy. J Neurosurg, 20: 329-337 (1963).

Oppenheim F: Uber den histoogischen Baue der Arteries in der wachsenden und alternden Niere, Frankfurt Z Path, 21: 57-84 (1918).

Oka S: Physical theory of permeability of vascular walls in relation to atherogenesis. Biorheology, 16: 203-209 (1979).

Olinger CP, Wasserman JF: Electronic stethoscope for detection of cerebral aneurysm, vasospasm and arterial disease. Surg Neurol, 8: 298-312 (1977).

Olsen F: Arteriolar permeability and destruction of elastic membrane in hypertension. Acta Path Microbiol Scan, 75: 527-536 (1969).

Peterson RE: Stress concentration factors. Toronto, John Wiley & Sons (1974).

Potter R, Roach MR: Are enlarged fenestrations in the internal elastic lamina of the rabbit thoracic aorta associated with poststenotic dilatation: Can J Physiol Pharm, 61: 1, 101-104 (1983).

Reidy MA, Levesque MJ: A scanning electron microscopic study of arterial endothelial cells using vascular casts. Atherosclerosis, 28: 463-478 (1977).

Roach MR: Changes in arterial distensibility as a cause of poststenotic dilatation. Am J Cardiol, 12: 802-815 (1963).

Roach MR: Role of vascular wall elastic tissue in hemostasis, Thrombosis et Diathesis Haemorrhagica, Suppl 40: 59-77 (1970).

Rodgers JC, Puchtler H, Gropp S: Transition from elastic to collagen in internal elastic membranes. Arch Path, 83: 557-566 (1967).

Ross R, Bornstein P: Elastic fibres in the body. Sci Am, 224: 44-52 (1971).

Sahs AL: Observations on the pathology of saccular aneuryms. J Neurosurg, 24: 792-806 (1966).

Sandberg LB: Elastin structure in health and disease, International Rev of Conn Tiss Res, 7: 159-210 (1976).

Schneider GB: The effects of preparative procedures for scanning electron microscopy on the size of isolated lymphocytes (1). Am J of Anat, 146: 93-100 (1976).

Scott S, Ferguson GG, Roach MR: Comparison of the elastic properties of human intracranial arteries and aneurysms. Can J Physiol Pharmacol, 50: 328-332 (1972).

Sekhar LN, Heros RC: Origin, growth and rupture of saccular aneurysms: A Review, Neurosurg, 8: 248-260 (1981).

Selby SM: CRC standard mechanical table, 20th ed. The Chemical Rubber Co. Cleveland, Ohio (ed.)(1972).

Sheppard BL: Platelet adhesion in the rabbit abdominal aorta following removal of endothelium with EDTA, Proc R Soc Lond B, 182: 103-108 (1972).

Sheppard BL, French JE: Platelet adhesion in the rabbit abdominal aorta following the removal of the endothelium: A scanning and transmission electron microscopical study. Proc Roy Soc Lond B, 176: 427-432 (1971).

Smith JFH, Canham PB, Starkey J: Orientation of collagen in the tunica adventitia of the human cerebral artery measured with polarized light and the universal stage, J Ultrastructure Res, 77: 133-145 (1981).

Stehbens WE: Intracranial arterial aneurysms, Australasian Ann Med, 3: 214-218 (1954).

Stehbens WE: Focal intimal proliferation in the cerebral arteries. Am J Pathol, 36: 289 (1960).

Stehbens WE: Hypertension and cerebral aneurysms. Med J Aust, 2: 4 (1962).

Stehbens WE: Histopathology of cerebral aneurysms. Arch Neurol, 8: 272-285 (1963).

Stehbens WE: Pathology of the cerebral blood vessels. C.V. Mosby Co., St. Louis, pp. 351, 421 (1972).

Stehbens WE: The role of lipid in the pathologenesis of atherosclerosis. Lancet 1: 724-727 (1975).

Stehbens WE: Ultrastructure of aneurysms. Arch Neurol, 32: 272-285 (1975).

Stehbens WE: Arterial structure at bifurcations with reference to physiological and pathological processes, including aneurysm formation. Structure and Function of the Circulation, Vol. 2. Ed. Schwartz CJ, Werthessen NT, Wolf SG, Plenum, N.Y.: 667-693 (1981).

Stemerman MB, Baumgartner HR, Spaet TH: The subendothelial microfibril and platelet adhesion. Lab Invest, 24: 179-186 (1971).

Steven FS, Minns RJ, Thomas H: The isolation of chemically pure elastins in a form suitable for mechanical testing. Connect Tissue Res, 2: 85-90 (1974).

Still WJS: The early effect of hypertension on the aortic intima of the rat. Am J Path, 51: 721-734 (1967).

Underwood EE: Quantitative stereology. Addison-Wesley Publishing Co., Reading, Massachusetts (1970).

Velican C: Studies on the age-related changes occurring in human cerebral arteries, Atherosclerosis II: 509-529 (1970).

Walmsley JG, Canham PB: Orientation of nuclei as indicators of smooth muscle cell alignment in the cerebral artery, Blood vessels 16: 43-51 (1979).

Zar JH: Biostatistical analysis. Englewood Cliffs, NJ, Prentice-Hall Inc. (1974).

APPENDIX I

TISSUE TREATMENTS

i) Isolate the Internal Elastic Lamina (cat carotids)

Intact specimens of cat carotids were mounted in a jig, flushed with saline and then exposed to 1) 0.1 M ethylenediaminetetraacetate disodium salt (EDTA) at 37°C for varying time periods up to 30 minutes; 2) EDTA at 37°C for 15 minutes as well as 4 hour and 8 1/2 hour exposures to 0.5 mg. of trypsin in 0.2 M Tris buffer, pH 7.4; or 3) 15 minutes in EDTA at 37°C followed by 4 1/2 and 8 hour exposures to 300 units of collagenase in 0.2 M Tris buffer. All specimens were subsequently fixed under pressure (100 mmHg) with 2.5 percent glutaraldehyde in phosphate buffer, processed through graded alcohols, critically point dried, gold/palladium coated and examined with the scanning electron microscope.

ii) Expose Elastin fibres (cat carotids)

The carotids were pinned out on styrene or cork backing and exposed to 1) 88 percent formic acid at 45°C for up to 44 hours; 2) 5 M guanidine hydrochloride in 0.05 M Tris buffer at 4°C, pH 7.0 for up to 192 hours, and 3) 0.1 N sodium hydroxide at 100°C for up to 75 minutes. The specimens were then fixed (while pinned) in 2.5 percent phosphate buffered glutaraldehyde, processed through graded alcohols, critically point dried, gold/palladium coated and viewed with the scanning electron microscope.

iii) Isolate the Internal Elastic Lamina (human cerebral)

Specimens were mounted in a jig and exposed to EDTA for 15 minutes under pressure (100 mm Hg) before flushing and pressure fixing (100 mm Hg) with 2.5 percent glutaraldehyde. The subsequent preparation procedure for examination with the scanning electron microscope was identical to the previous preparation with cat carotids.

Specimens of cerebral artery were pinned on styrene backing and exposed to 88 percent formic acid at 45°C for up to 24 hours. The specimens were then fixed in 2.5 percent glutaraldehyde and processed according to the preceding section on the cat carotids. The same procedure as outlined immediately above for the formic acid treatment was repeated with the use of guanidine hydrochloride except the time period was extended to 72 hours. The procedure outlined previously for the treatment of the cat carotids with sodium hydroxide was repeated for specimens of human cerebral arteries.

APPENDIX II

DESCRIPTION OF THE SOFTWARE STRUCTURE

Introduction

The programme used here is written in BASIC and implemented on a Hewlett Packard 9830A desk-top calculator, which must be equipped with a minimum of 10 K words of READ/WRITE memory, a String Variables ROM to permit the recognition and operation on letters and words ("strings") and an Extended I/O ROM for the digitizer. Peripheral devices interfaced with the 9830A are a Hewlett Packard 9866A printer and a Hewlett Packard 9864A digitizer. If a mass memory unit such as the Infotek Systems FD-30A floppy disk system is interfaced with the 9830A then the mass memory ROM is also necessary.

A compatible system retrofitted with Infotek hardware consists of the same peripheral devices along with the Infotek FD-30A mass memory but incorporates the Infotek FP-30 fast processor and the Infotek MX-30 expanded memory (containing the ROMs specified above), in the mainframe of the 9830A. These options convert the 9830A from a bit serial to a full bit parallel processor, which increases the operating speed of the system and expands the READ/WRITE memory to 32 K words.

The "Special Function Keys", a facility available on the 9830A system, has been used to advantage in this programme for structuring and implementing segments of the software. A series of separate programmes with a common group of variables can be allocated to individual Special Function Keys (designated f_0 to f_{19}). Therefore, each segment of a programme (initialization, input, data manipulation, output, storage, etc.) can be allocated to a separate key which can be accessed by the operator. This eliminates the need for a

directory integrated into the software architecture in order to access the various segments of a programme since the special function keys permit access to any segment, in any order (except f_0 must be accessed initially in this particular programme) by pressing the appropriate key. The explanation for the structure of the programme has been arranged to correspond with the sequence of the Special Function Keys. Only the flowcharts associated with the main portions of the optimization procedure (Special Function Key f_4) are presented.

f_0 - Initialization

The arrays which store the original as well as the adjusted coordinates of the wet and dry markers are initialized. A prompt requests the keyboard entry by the operator of a code (alpha-numeric if desired) identifying the particular composite to be analyzed. A further prompt requests a keyboard entry to determine whether the operator desires data to be entered from the digitizer or to terminate the initialization procedure for data entry from the direct access storage unit (floppy disk or digital cassette). To initialize for data input, two points representing the origin and a second point establishing the orientation of the X coordinate axis, are entered from the digitizer.

f_1 - Enter Marker Coordinates

The common marker is entered (digitized) first. The origin for the composite is then transposed to the common marker and the coordinates for all subsequent data entries are determined with respect to the new origin. The X and Y coordinate pairs for both the wet and dry locations of each marker point (numbers 2 to 14) illustrated in

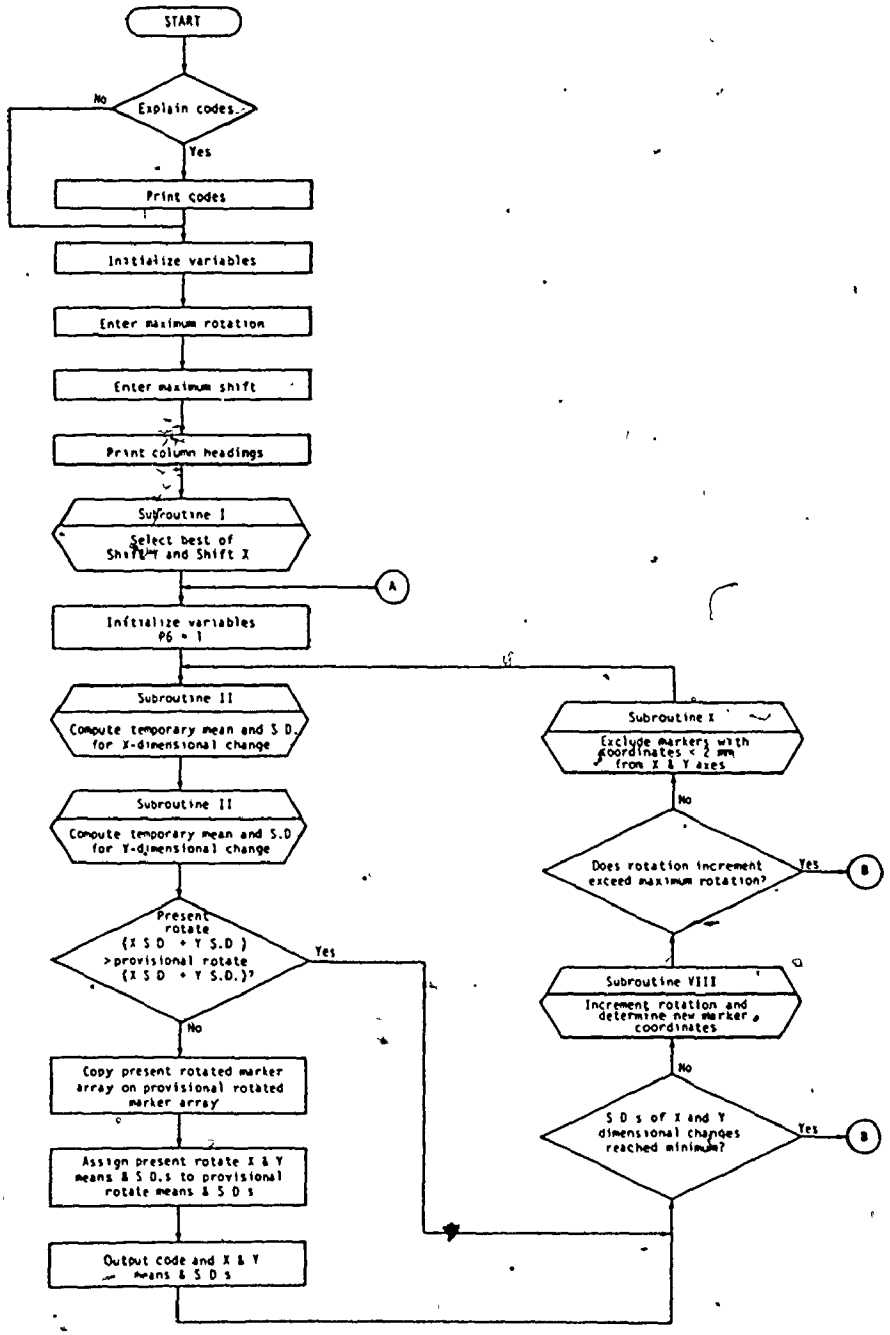

Figure 66a - Flowchart of main programme

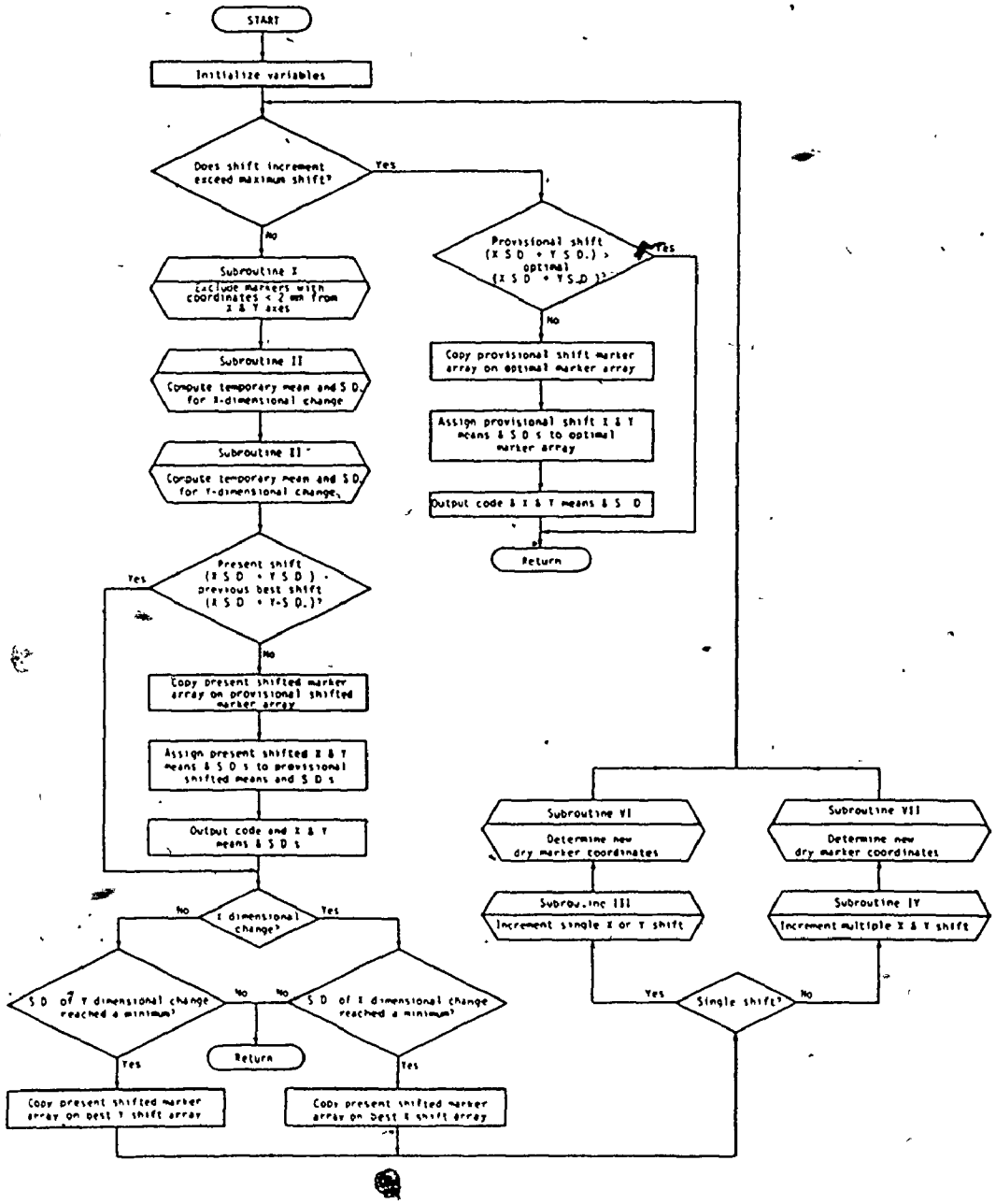

Figure 67a - Subroutine I

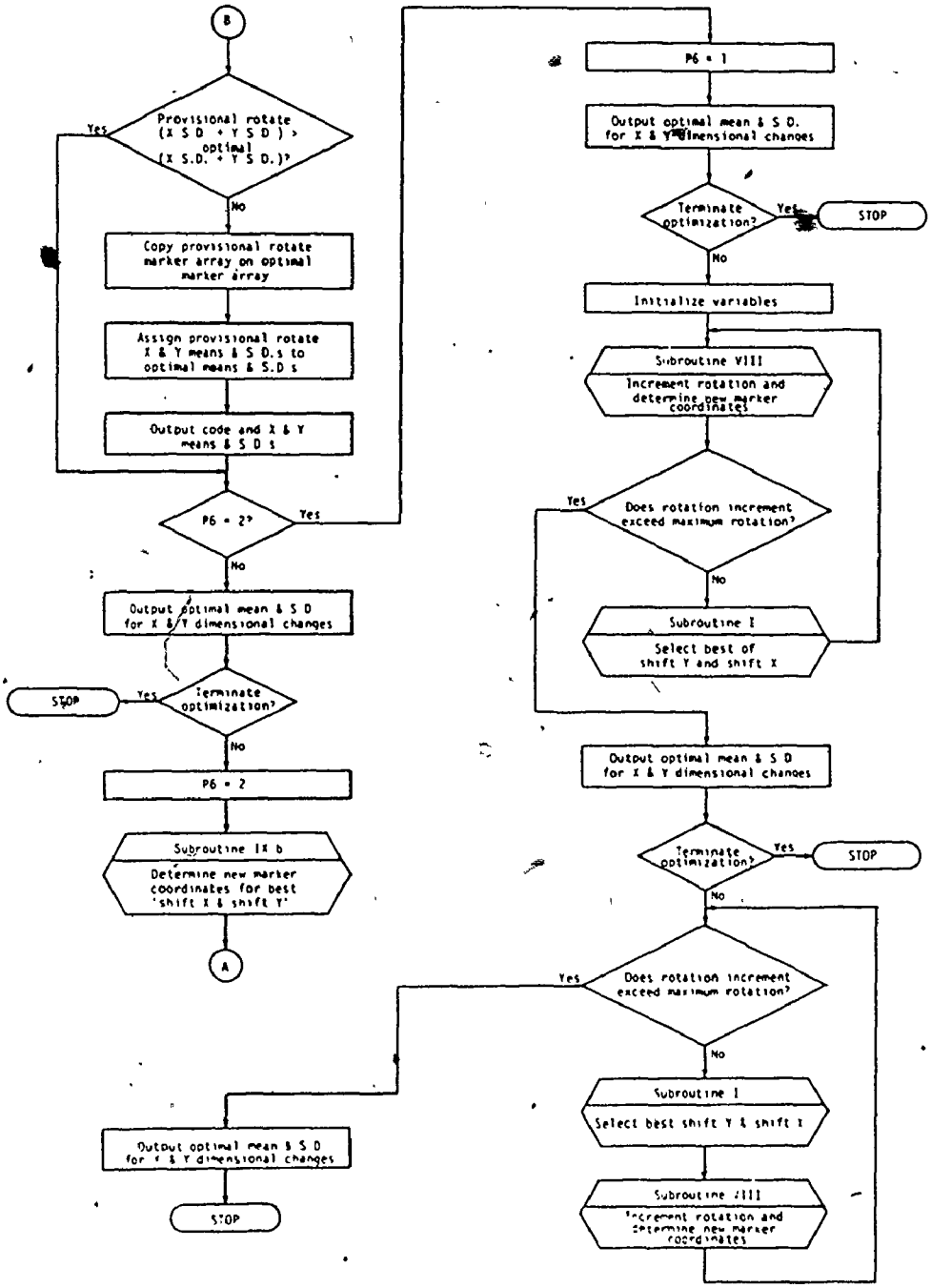

Figure 66b - Flowchart of main programme (continued)

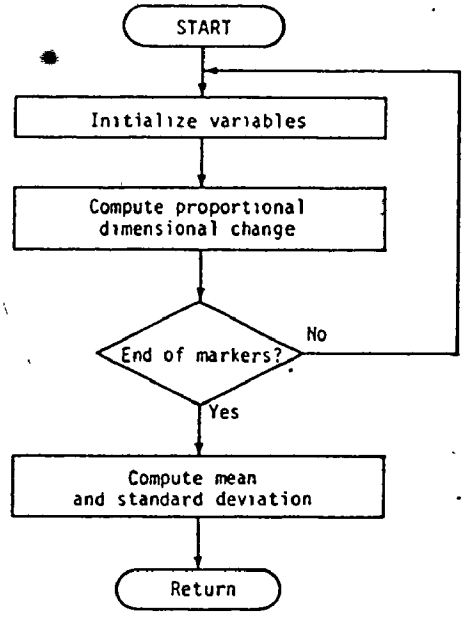

Figure 67b - Subroutine II

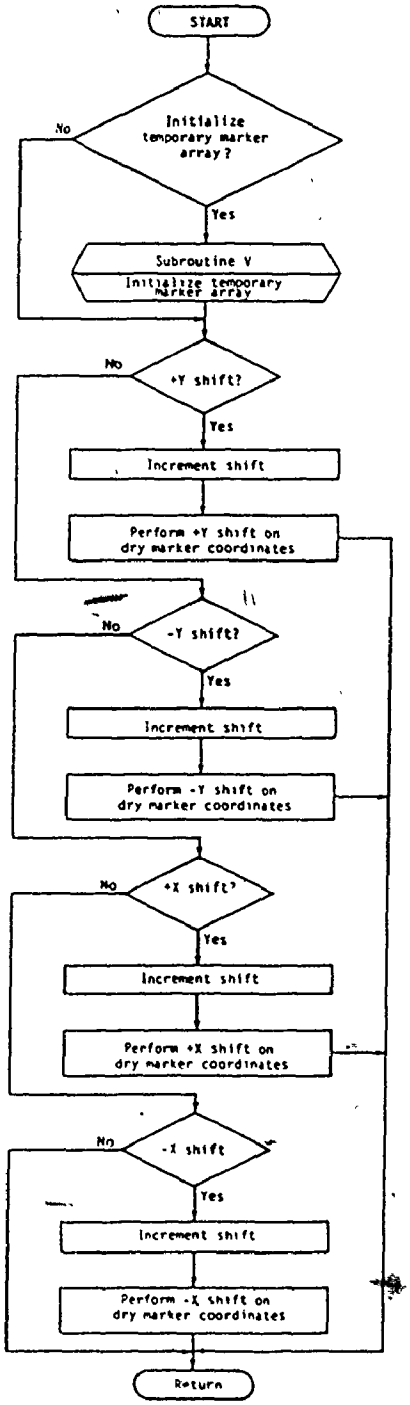

Figure 67c - Subroutine III

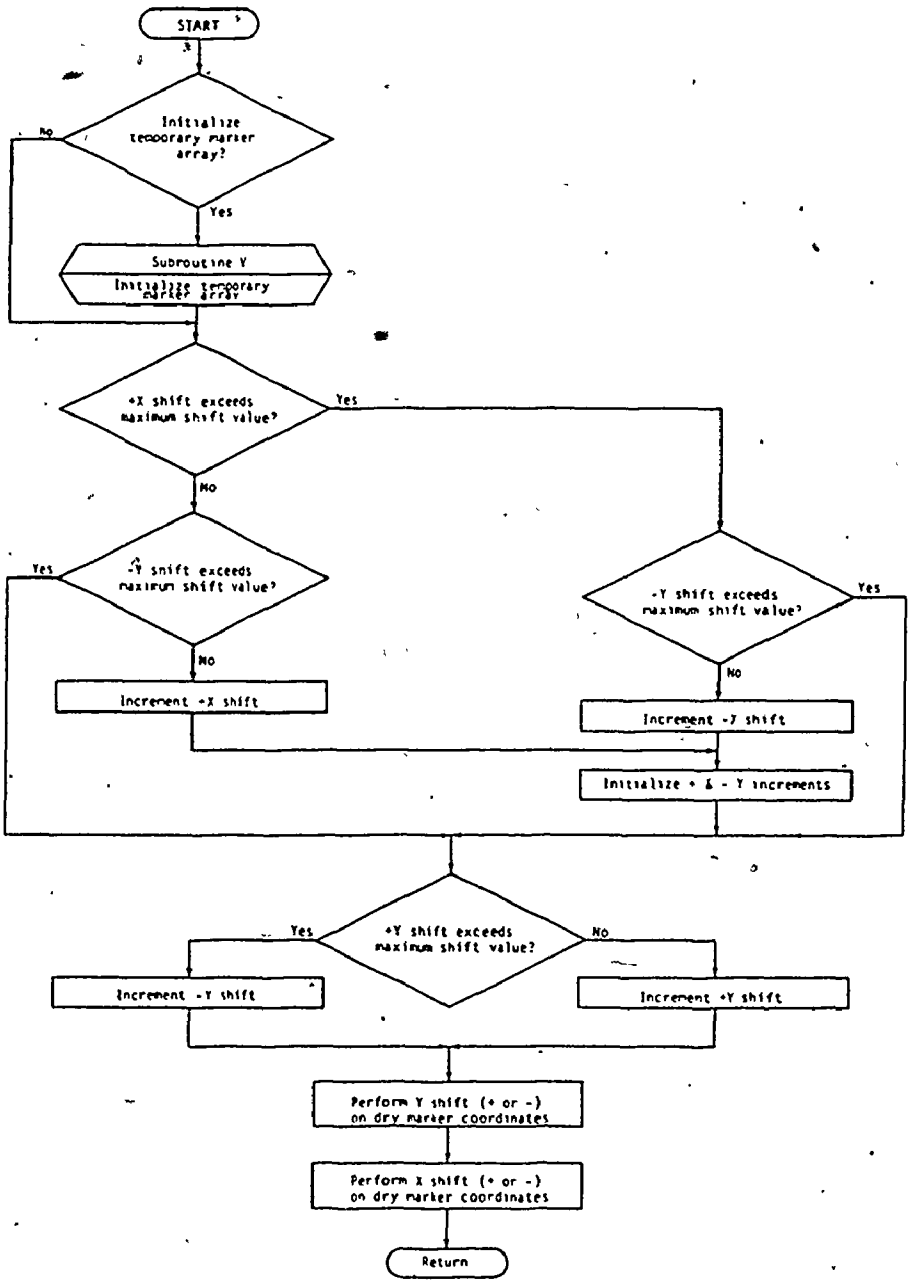

Figure 67d - Subroutine IV

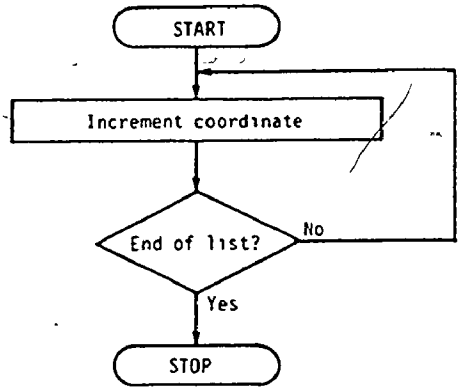

Figure 67d - Subroutine VII

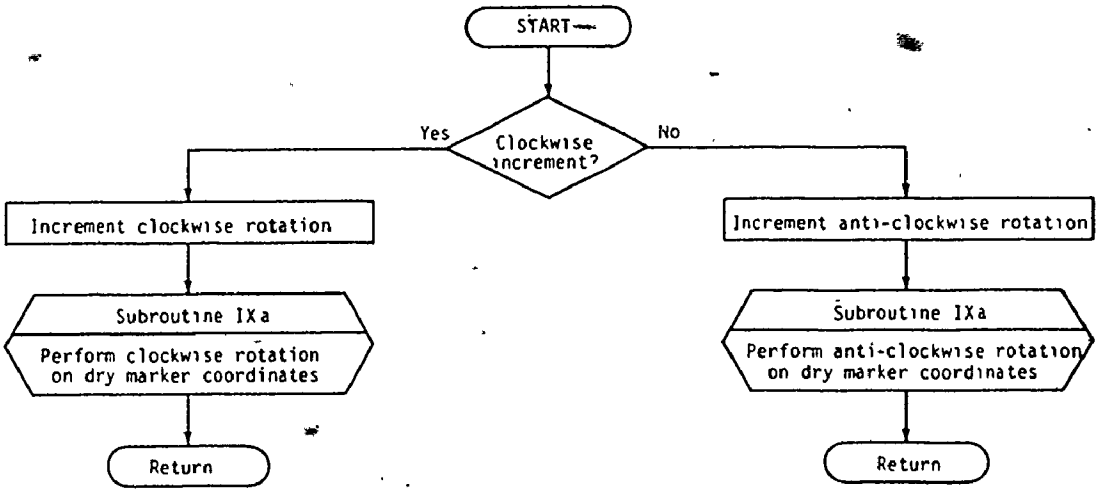

Figure 67e - Subroutine VIII

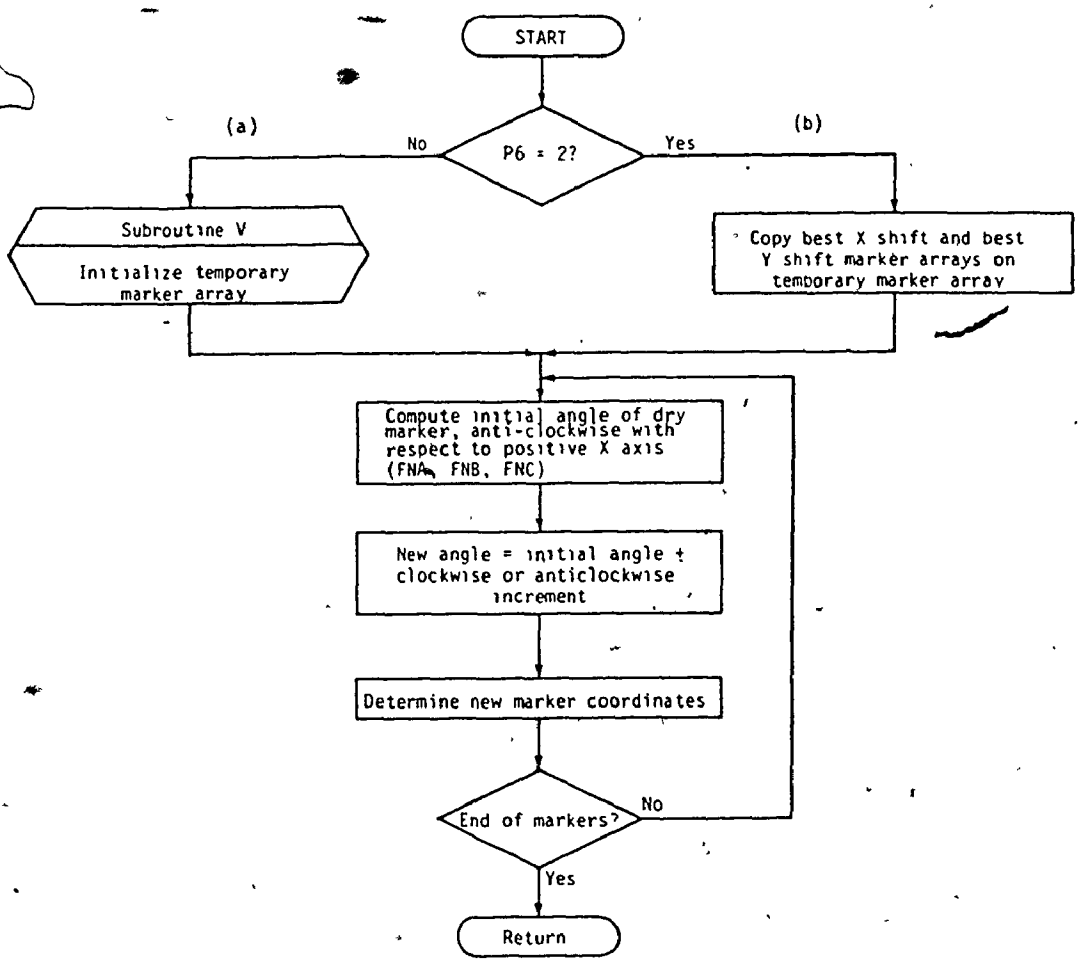

Figure 67f - Subroutine IX

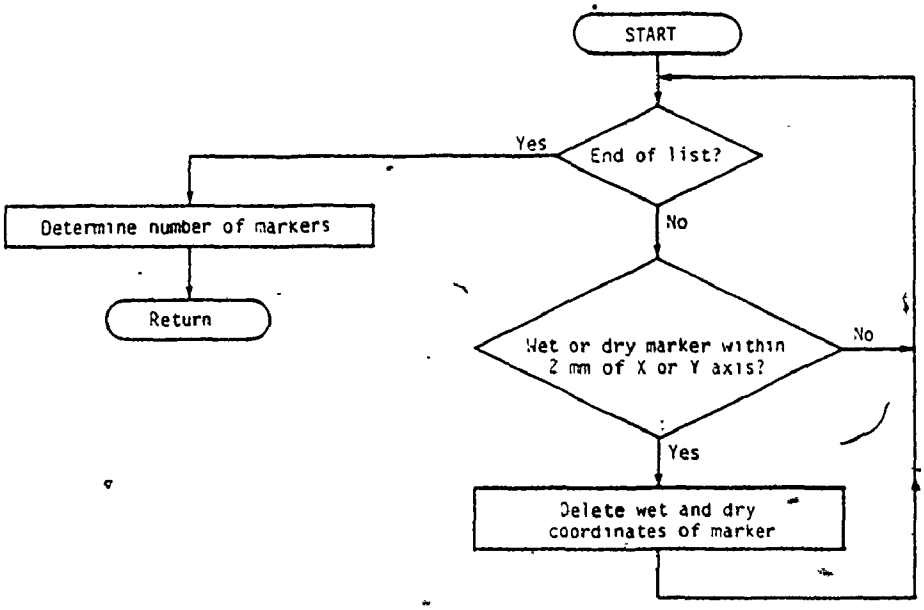

Figure 67g - Subroutine X

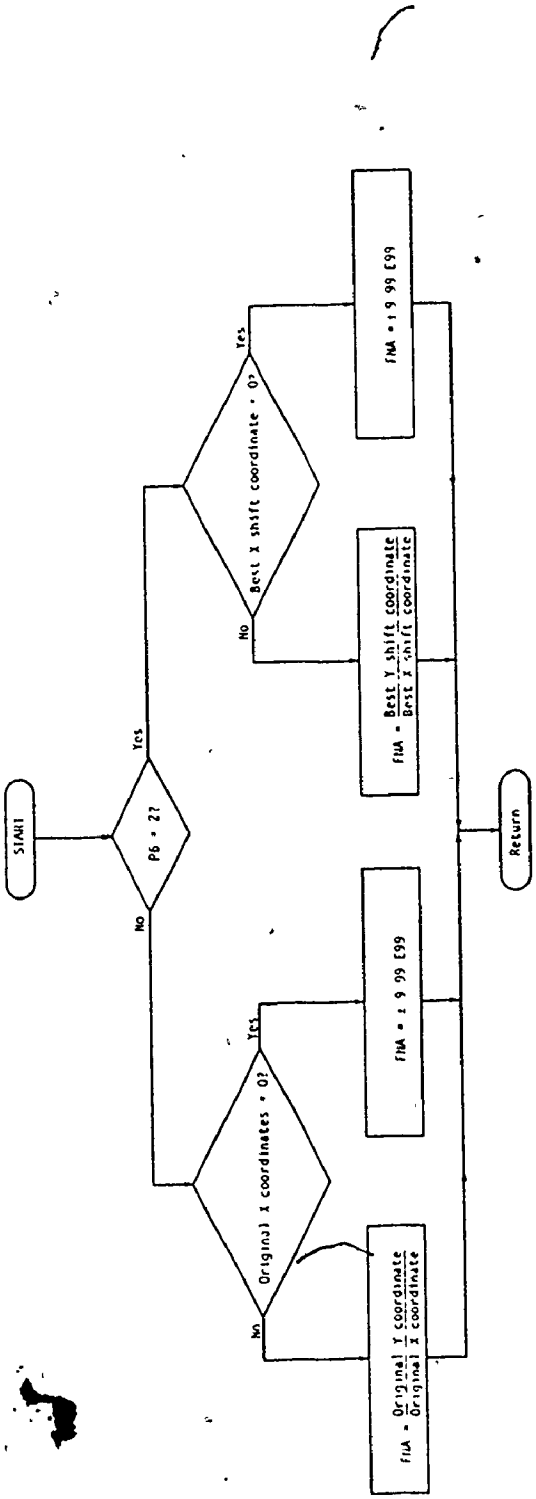

Figure 67h - Function subroutine FNA

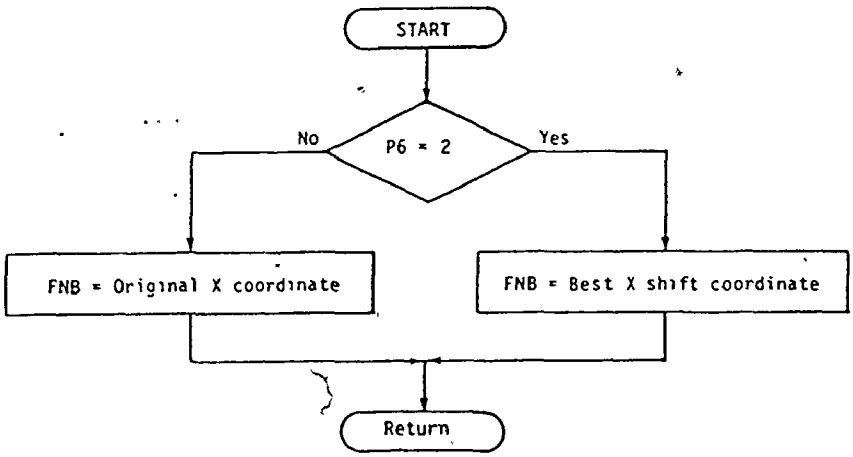

Figure 67i - Function subroutine FNB

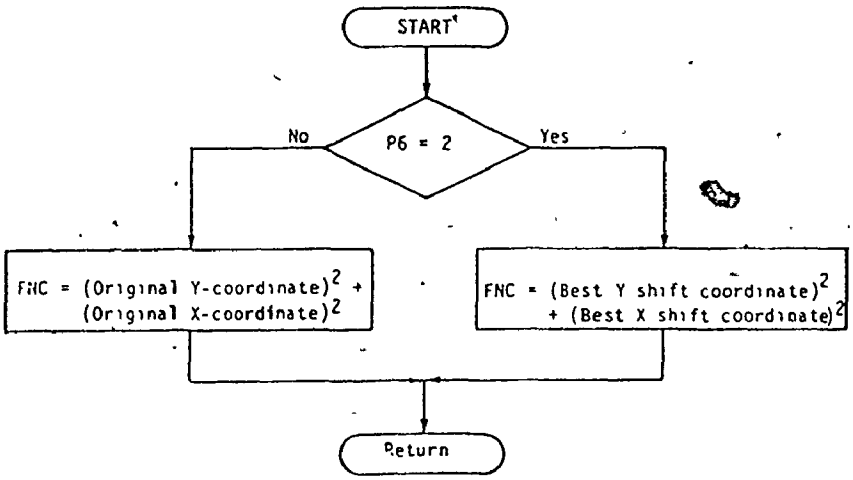

Figure 67j - Function subroutine FNC

Figure 6 (subsection 2.4.2) are entered from the digitizer according to a driver subroutine and stored in the corresponding array. Data entry is terminated when the maximum limit of 29 markers is reached or by the operator by entering the keyboard input STOP.

f_2 - Store Data

The operator specifies the file number at the request of a prompt, for storage on the direct access storage unit (floppy disk or digital cassette).

f_3 - Print Coordinate Pairs (Original and Amended) for the Markers

The complete set of coordinate pairs for the composite illustrated in Figure 6 was presented in Table 2 (section 2.5.3). The coordinates for the wet markers listed under "WET" remain unchanged. The column headings "X" and "Y" under the designation "DRY" represent the original coordinates of the dry markers. The coordinates for the amended location of the dry markers are listed under the column headings "AX" and "AY".

f_4 - Optimization of the Alignment Between the Wet and Dry Markers

The flowcharts depicting the main programme and the subroutines for the optimization of the alignment between the wet and dry markers have been illustrated in Figures 68 a, b and 69 a-j, respectively. The explanation of the identification codes (see subsection 2.5.3) are printed, only at the request of the operator. The operator enters, by means of the keyboard, a single value for the maximum limit of the shift along the positive and negative coordinate axes as well as a single value for the maximum limit for the rotation of the dry marker points about the common point. The incremental shifts (0.51 mm) and

the incremental rotations (0.25 degrees) are specified within the programme.

After a number of composites had been analyzed, it became apparent that the proportional dimensional changes associated with some of the markers demonstrated irregular results if located or adjusted to be in close proximity to the axes. In order to avoid this problem it is recommended that markers located close to the axes not be selected. As a result, marker points located within a band of approximately 1.3% of the field width (2 mm at projected magnification of 144 X) are temporarily excluded (subroutine X) during the particular incremental adjustment of the marker points.

i) Level 1 (Single Shifts or Rotations)

The standard deviations for the porportional change in the X and Y coordinates are computed for the original location of the dry marker points by temporarily transferring control to subroutine IL. For level 1 of the optimization process, control of the programme is transferred to subroutine I which employs single shifts in increments along the positive and negative directions of both coordinate axes to determine the best location of the dry marker points.

New coordinate pairs of the dry markers are determined according to the specified shift (subroutines III and VI) and assigned to the temporary array. At this level of optimization only single shift increments along the positive or negative X axis, and positive or negative Y axis are implemented and tested. The computation of the X and Y standard deviations corresponding to the X and Y mean proportional dimensional changes is repeated (subroutine II) and the combined sum of the present standard deviation values is compared with

the sum of the previous best values. If the present sum is greater, then the dispersion has not been reduced and control of the incremental shift is transferred to a new shift direction (i.e., + to -) or axis. If the present sum is less, then the dispersion has been reduced and the temporary location of the dry marker points (temporary array), X and Y standard deviations and the X and Y means are assigned to the provisional array, standard deviations and means, respectively. Control returns to increment the shift and compute the new location of the dry marker coordinate pairs. Before each incremental shift the locations of the dry marker points are initialized to their original positions (subroutine V).

The cycle is repeated for each of the four directions (+X, -X, +Y, and -Y) until either the sum of the X and Y standard deviations ceases to decrease, or the maximum limit of the shift has been attained. After the process has been completed, the provisional array, standard deviations and means representing the best location of the dry markers are assigned to the optimal array, standard deviations and means respectively. Furthermore, the best locations of the dry marker points along the X and Y coordinate axes are retained for use in level 2 of the optimization procedure. Control of the programme is then returned to the main programme.

The set of dry markers is next rotated about the origin (common point) in increments in both the anti-clockwise and clockwise directions. The process for determining if a better location exists is similar to the previous procedure for the single shifts. A new location of the dry markers is established after an incremental anti-clockwise or clockwise rotation (subroutines VIII and IX). The

new coordinate pairs for each marker are computed and assigned to the temporary array. Prior to each incremental rotation, the location of the dry marker points are initialized to their original positions (subroutine V). The X and Y standard deviations corresponding to the X and Y mean proportional dimensional changes are computed and the sum of the present value is compared with the previous best value. If the sum is less, then the temporary location of the dry markers (temporary array), X and Y standard deviations and X and Y means are assigned to the provisional array, standard deviations and means respectively. The cycle continues until both anti-clockwise and clockwise rotations have been tested to the maximum limit or until the sum of the X and Y standard deviations is not improved.

Next, the sum of the X and Y standard deviations for the best location of the dry markers for rotation is compared with the sum of the standard devaitions for the previous best location obtained by the single shifts, and the better is assigned to the optimal array, standard deviations and means. At this point, the values of the "optimal" standard deviations and means are printed and programme execution is halted until the operator directs whether the optimization process is to be terminated or continued to the next level.

ii) Level 2 (Best X and Y Location Plus Single Rotations)

Level 2 of the optimization process initially positions the location of the coordinates of the dry marker points according to the best X and Y locations derived from the previous single shifts. The dry markers are then rotated in increments (subroutines VIII and IX) about the origin (common point). The best provisional location is

obtained and compared with the previous best optimal location and the better is selected and assigned to the optimal array, standard deviations and means. The values of the "optimal" standard deviations and means are printed and programme execution is halted until the operator directs termination or continuation to the next level of optimization.

iii) Level 3 (Rotation Plus Single Shifts)

Level 3 of the optimization process applies a combination of two separate adjustments to the markers based on the original locations of the marker points. First, the markers are rotated incrementally (subroutines VIII and IX), then the sequence of single shifts (subroutines I, III and VI) along the X or Y axis are tested and the best provisional location is compared with the previous optimal location. The location which demonstrates less dispersion according to the criterion described previously is again selected and the parameters are assigned to the optimal array, standard deviations and means. The values of the "optimal" standard deviations and means are printed and programme execution is halted until the operator indicates termination or continuation to the final level of optimization.

iv) Level 4 (Rotation Plus Multiple Shifts)

The final level of the optimization process is very similar to level 3, except that in addition to the incremental rotations (subroutines VIII and IX), there is a combination of an X and a Y shift (subroutines I, IV and VII) rather than only a single shift. Upon completion of this optimization level, the final optimal standard deviation and means are printed and execution is terminated. All possible combinations of shifts and rotations within the increments and

maximum limits specified have been tested and the best location selected.

For specified limits of a 5 mm maximum shift and a 5° maximum rotation, the time to complete the four levels of optimization using the 9830A system incorporating the Infotek Fast Processor and Expanded Memory for the 14 markers illustrated in Figure 6 (section 2.4.2) is 0.7 minutes for level 1, 0.5 minutes for level 2, 11.5 minutes for level 3 and about 2.5 hours for level 4. The time to complete the same four levels using the standard Hewlett Packard 9830A system is increased by a factor of 5.6.

f_5 - Output Dimensional Changes (Original Marker Coordinates)

f_7 - Output Dimensional Changes (Amended Marker Coorindates)

The explanations for Special Function Keys f_5 and f_7 have been combined since both keys perform the same function, but use either the original or amended marker coordinates. The proportional dimensional changes for each marker point as well as the mean, standard deviation and standard error of the mean for the group of markers are computed for the X, Y and radial directions. Column headings along with the individual values are then printed. The final results for the composite shown in Figure 6 are presented in Table 1.

f_6 - Load Data

At the request of a prompt, the operator enters the file number for retrieval of the desired file on the direct access storage unit (floppy disk or cassette). Following loading of the coordinations into the READ/WRITE memory, the coordinates are assigned to other arrays and scanned to determine the number of markers.

f_8 - Modify X-Axis Orientation

Orientation of the X axis (and concurrently the Y axis) may be modified by the operator. A prompt requests the magnitude and direction (negative for anti-clockwise, positive for clockwise), of the new orientation of the X axes with respect to the original position. As a result all marker coordinate pairs (wet and dry) are transposed to the new coordinate axes.

f_9 - Assess Planar Orthotropy/Anisotropy

Following selection of the optimal location of the dry markers, the means and standard deviations for the complete range of possible orientations of the coordinate axes (between 0 and 180°) should be assessed. The operator enters the range of orientations as well as the incremental step. The coordinate axes are rotated accordingly (the locations of the wet and dry markers remain stationary) and the mean X, Y, and radial dimensional changes along with their associated standard deviations for the group of marker points are printed for each angle, under appropriate headings. Markers within a band of 1.3% of the field width are again temporarily excluded.

APPENDIX III

OPTIMIZATION PROCEDURE: OPERATOR INSTRUCTIONS

SPECIAL FUNCTION KEYS

f_0 - Initialize

f_1 - Digitizer input of marker coordinates

f_2 - Store data (diskette)

f_3 - Print data points

f_4 - Optimal alignment

f_5 - Print dimensional changes (original coordinates)

f_6 - Load data (diskette)

f_7 - Print dimensional changes (amended coordinates)

f_8 - Modify X-axis orientation

f_9 - Assess anisotropy.

OPERATION

1. To load the programme from the diskette, type LOADKEY #7, 1. Press key marked EXECUTE.

f_0 - Initialize

1. Press keys marked RUN, f_0.
2. The display reads "INPUT TITLE?". Enter an appropriate title (maximum 60 characters), press key marked EXECUTE.
3. The display reads "INITALIZE? (1-YES, Ø-NO)". To set origin and orientation of axes for digitizing coorindates, enter 1, press key marked EXECUTE, go to step 4. Otherwise enter Ø and select approripate data entry key (i.e., f_1 or f_6).
4. The display reads "SET: ORIG (L LFT) - PRESS 'CONT EXEC'?". Set the origin on the platen by positioning the crosshairs of the cursor at the lower left corner of the composite or at the

lower left "+" mark, and pressing the orange coloured "0" button on the cursor. Press keys marked CONT, EXECUTE.

5. The message "SET LOWER RIGHT" is printed. Position the crosshairs of the cursor to the right of the origin or at the lower right "+" mark and press the "S" button on the cursor.

f_1 - Digitizer input of marker coordinates

1. Press key marked f_1.

2. The display reads "INPUT COMMON POINT". Position the crosshairs of the cursor at the common point and press the "S" button on the cursor.

3. The display momentarily reads "INPUT 'WET' MARKER n". Position the crosshairs of the cursor at the location of the wet marker (i.e., location of marker on wet tissue) and press the "S" button on the cursor.

4. The display momentarily reads "INPUT 'DRY' MARKER n". Position the crosshairs of the cursor at the location of the dry marker (i.e., location of the marker on dried tissue) and press the "S" button on the cursor.

5. Repeat steps 3 and 4 until all sets of markers have been digitalized. Maximum number of markers that can be entered is 29.

f_2 - Store Data

1. Press key marked f_2.

2. The display reads "ENTER 'STORE' FILE NO." Enter the number of the file on the diskette to store the data that has been entered previously, press key marked EXECUTE.

3. Following storage of the data (lazy T reappears at bottom left of display) the message "DATA STORED n" is printed (n is the file number).

f_3 - Print Data Points

1. Press key marked f_3.

2. The original (X,Y) coordinate pairs of the wet markers are printed along with the original (X,Y) and amended (AX,AY) coordinate pairs of the dry markers.

f_4 - Optimal Alignment

1. Press key marked f_4.

2. The display reads "EXPLAIN CODES? (1-YES, Ø-NO)". If a directory of the response codes (indicates portion of programme resulting in improved alignment) is desired, enter 1, press key marked EXECUTE, go to setp 3. Otherwise, enter Ø, press key marked EXECUTE, go to step 4.

3. The response codes are printed.

4. The display reads "ENTER MAX ROTATE (EG 10 DEG)". Enter the maximum value (in degrees) for the rotation (clockwise and anti-clockwise), press key marked EXECUTE.

5. The message "MAXIMUM ROTATION IS x DEGREES" is printed (where x is value entered).

6. The display reads "ENTER MAX SHIFT (EG 6 "MM"). Enter the maximum value (in millimeters) for the shift ($\pm$X and $\pm$Y), press key marked EXECUTE.

7. The message "MAXIMUM SHIFT IS x MM" is printed (where x is value entered.

8. The column headings "CODE", "Y-CHANGE" and "X-CHANGE" are printed. The column headings "S.D." and "MEAN" are both printed under "Y-CHANGE" and "X-CHANGE".

9. The message printed is:-
   "LEVEL 1"
   "BEST Y-CHANGE: SD = s_1 AND MEAN = m_1"
   "Best X-CHANGE: SD = s_2 AND MEAN = m_2"
   "CONT OPTIMIZE? (1-YES, Ø-NO) FOR BEST X & Y + ROTATION".

   If it is desired to continue the optimization procedure to Level 2 enter 1, press key marked EXECUTE and go to step 10. Otherwise enter Ø, to terminate execution.

10. The message printed is:-
    "LEVEL 2"
    "BEST Y-CHANGE: SD = s_1 AND MEAN = m_1
    "BEST X-CHANGE: SD = s_2 AND MEAN = m_2
    "CONT OPTIMIZE? (1-YES, Ø-NO) FOR ROTATION + X-Y SINGLE SHIFT".

    If it is desired to continue the optimization procedure to Level 3, enter 1, press key marked EXECUTE and go to step 11. Otherwise enter Ø to terminate execution.

11. The message printed is:-
"LEVEL 3"
"BEST Y-CHANGE: SD = s_1 AND MEAN = m_1"
"BEST X-CHANGE: SD = s_2 AND MEAN = m_2"
"CONT OPTIMIZE? (1-YES, Ø-NO) FOR ROTATION + X-Y MULTIPLE SHIFT".

If it is desired to continue the optimization procedure to Level 4, enter 1, press key marked EXECUTE and go to step 12. Otherwise enter Ø to terminate execution.

12. The message printed is:-
"LEVEL 4"
"BEST Y-CHANGE: SD = s_1, AND MEAN = m_1"
"BEST X-CHANGE: SD = s_2, AND MEAN = m_2"
"OPTIMIZATION COMPLETE"

f_5 - Print Dimensional Changes (original coordinates)

1. Press key marked f_5.

2. The results (based upon the original coordinate pairs) for the dimensional changes along the X-axis, Y-axis and in the radial direction (direct path from common point to marker point) are printed. Also the mean, standard deviation and standard error of the mean are printed for the dimensional changes of the set of markers.

f_6 - Load Data

1. Press key marked f_6.

2. The display reads "ENTER 'LOAD' FILE NO.". Enter the file number for the data that is to be loaded from the diskette, press key marked EXECUTE.

3. Following loading of the data (lazy T reappears at bottom left of display) the message "DATA LOADED FROM FILE n" is printed.

f_7 - Print Dimensional Changes (amended coordinates)

1. Press key marked f_7.

2. The results (based upon the amended coordinate pairs) for the dimensional changes along the X-axis, Y-axis and in the radial direction (direct path from common point to marker point) are printed. Also the mean, standard deviation and standard error of the mean are printed for the dimensional changes of the set of markers.

f_8 - Modify X-Axis Orientation

1. Press key marked f_8.

2. The display reads "ENT ANGLE INCREMENT (-CCW, +CW)". To implement a new orientation of the coorindate axes with respect to the location of the marker points, enter the desired angle between the old and new orientation and sign (+ for clockwise reorientation, or - for anti-clockwise reorientation), and press key marked EXECUTE.

3. The message "NEW ORIENTATION OF X-AXIS IS x DEGREES FROM ORIGINAL" is printed.

4. Following modification of the coordinates the display reads "REORIENTATION COMPLETE".

f_9 - Assess Anisotropy

1. Press key marked f_9.

2. The display reads "ENTER ANGLE RANGE (MIN, MAX, STEP)". The range of reorientations to be searched is determined by the keyboard inputs of the smallest (MIN) and largest (MAX) angles with respect to the existing location (+ for clockwise reorientation, - for anti-clockwise reorientation). The angular increment between successive orientation is input for STEP.

3. The headings "ANGLE(DEG)", "% Y-CHANGE (S.D.)" and "% X-CHANGE (S.D.)" are printed. The results at each orientation are computed and printed.

APPENDIX IV

DATA MANAGEMENT OF FENESTRATIONS CHARACTERISTICS:

OPERATOR INSTRUCTIONS

SPECIAL FUNCTION KEYS

f_0 - Initialize

f_1 - Keyboard input of data (major diameter & minor diameter)

f_2 - Delete keyboard input

f_3 - Digitizer input of data

f_4 - t-Test of means

f_5 - Statistical analysis of data (mean, standard deviation, skewness, kurtosis, minimum, maximum, range).

f_6 - Store data (on diskette)

f_7 - Load data (from diskette)

f_8 - Cell statistics (histogram)

f_9 - Fenestration information (average diameter, density, percentage of surface area, ligament efficiency).

f_{10} - Printer histogram

f_{11} - Printer histogram with normal curve overlay

f_{12} - Keyboard input of data (single value)

f_{13} - Programme subroutine (DEF FNX)

f_{14} - Plot histogram

f_{15} - Programme subroutine (DEF FNY)

f_{16} - Programme subroutine (DEF FNC)

f_{17} - Curve fit to histogram data (maximum 6th degree polynomial regression)

OPERATION

1. To load the programme from the diskette, type LOADKEY #7, 1. Press key marked - EXECUTE.

f_0 - Initialize

1. Press keys marked RUN, f_0.
2. The display reads "INPUT TITLE?". Enter an approximate title (maximum 50 characters), press key marked EXECUTE.
3. The display reads "ENTER 1 FOR HISTOGRAM?". If a histogram and/or curve fit will be printed or plotted, enter 1, press key marked EXECUTE, go to step 4. Otherwise enter 0, press key marked EXECUTE, go to step 10.
4. The display reads "OFFSET = ?". Enter lowest value for histogram/curve fit, press key marked EXECUTE.
5. The message "OFFSET = x" is printed (where x is value entered).
6. The display reads "MAXIMUM VALUE OF CELLS?. Enter the largest anticipated value for histogram/curve fit, press key marked EXECUTE.
7. The message "MAXIMUM CELL = x" is printed, (where x is value entered).
8. The display reads "CELL WIDTH?". Enter the desired cell width for histogram/curve fit, press key marked EXECUTE.

   NOTE: TOTAL NUMBER OF CELLS CANNOT EXCEED 70.

9. The message "CELL WIDTH = x" is printed (where x is value entered).
10. The display reads "ENTER 1 TO PRINT DATA?". If a record of each data point is desired, enter 1, press key marked EXECUTE, go to step 11. Otherwise enter 0, press key marked EXECUTE, go to step 11.
11. The display reads "WIDTH AND LENGTH OF FIELD (MM)?". Enter the width and length of the field of view, (expressed in millimeters), press key marked EXECUTE.
12. The display reads "ENT PROPORTIONAL SHRINKAGE (EG .07)?". Enter the porportional shrinkage according to equation:

$$\text{shrinkage} = \frac{\text{displacement wet} - \text{displacement dry}}{\text{displacement wet}}$$

If shrinkage correction is not desired, enter Ø, press key marked EXECUTE.

The message "SHRINKAGE IS s PERCENT" is printed.

13. The display reads "PRESS DATA ENTRY KEY?". Select appropriate data entry key (e.g., f_1, f_3, or f_{12}) or load data from diskette.

f_1 - Keyboard Input of Data (Major Diameter and Minor Diameter)

1. Press key marked f_1.

2. The display reads "X1, X2 (n) = ?" (where n is data point number). The two values for the maximum diameter and minimum diameter (e.g. 1.8, 2.6) are entered with intervening commas, press key marked EXECUTE. This procedure is repeated for all the fenestrations contained within a given field of view.

NOTE: THE MAXIMUM NUMBER OF FENESTRATIONS THAT CAN BE ENTERED AS A GROUP FOR ANY PARTICULAR FIELD OF VIEW IS 69. If more than 69 are to be entered, store the initial 69, then select RUN, $f_Ø$ and enter the identical initial values. Select f_1 and continue with the remainder of the data points. This process can be repeated any number of times.

3. To terminate, press key marked END.

f_2 - Delete Keyboard Input

1. Press key marked f_2.

2. The display reads "DELETE X1, X2 (n) - ?". The program has deleted the value(s) for the last fenestration entered. To continue entering data from the keyboard, select f_1 or f_{12}.

f_3 - Digitizer Input of Data

1. Press key marked f_3.

2. The display reads "SET ORIGIN, PRESS 'CONT EXECUTE'?". Set the origin on the platen by positioning the cross-hairs of the cursor at the lower left hand corner of the field of view and pressing the orange coloured "O" button on the cursor. Press keys marked CONT, EXECUTE.

3. The display reads "SET LIMITS OF MAG BAR". Position the cross-hairs of the cursor on the left edge of the magnification marker and press the "S" button on the cursor. Position the cross-hairs of the cursor on the right edge of the magnification marker and press the "S" button on the cursor.

4. The display reads "ENTER MAGNITUDE OF MAG BAR (MIC)". Enter the length (expressed in microns) of the magnification marker.

5. The display momentarily reads "COMMENCE DIGITIZING". Position the cross-hairs of the cursor at each of the extreme borders of the longest axis and press the "S" button on the cursor. Repeat the preceeding procedure for extreme borders of the shortest axis. A "bleep" is emitted after the data entry for each fenestration has been completed.

   NOTE: THE MAXIMUM NUMBER OF FENESTRATIONS THAT CAN BE ENTERED AS A GROUP FOR ANY PARTICULAR FIELD OF VIEW IS 69. If more than 69 are to be entered, store the initial 69, then select RUN f_0 and enter the identical initial values. Select f_3 and continue with the remainder of the data points. This process can be repeated any number of times.

6. To terminate, press key marked STOP.

f_4 - t-Test of Means

1. Press key marked f_4.

2. The display reads "ENTER SPECIMEN CODES". Enter the codes for the two specimens (to a maximum of 50 characters), press key marked EXECUTE.

3. The display reads "SPECIMEN 1 - MEAN, SD, NUMBER". Enter the values for the mean, standard deviation and number of data points, respectively for the 1st specimen, press key marked EXECUTE.

4. The display reads "SPECIMEN 2 - MEAN, SD, NUMBER". Enter the values for the mean, standard deviation and number of data points, respectively for the 2nd specimen, press key marked EXECUTE.

5. The messages "'T' VALUE FOR SAMPLES IS t" and "'V' is v" are printed (v is degrees of freedom). The "T" value and "V" value may be used to judge the significance of the difference from the appropriate table in any statistics book.

f_5 - Statistical Analysis of Data

1. Press key marked f_5.

2. If data print option was selected in f_0, then each data point will be printed.

3. The results for basic statistical parameters are printed (i.e. number of data points, mean, standard deviation, skewness, kurtosis, minimum value, maximum value, range).

4. Additional messages may be printed:
   "MIN, MAX, RANGE MAY BE INCORRECT"
   "NO. TOO SMALL = n"
   "NO. TOO LARGE = n"

   The preceeding messages indicate the number of data points which fall outside the range of the histogram.

f_6 - Store Data

1. Press key marked f_6.

2. The display reads "ENTER 'STORE' FILE NO.". Enter the number of the file on the diskette to store the data that has been entered previously, press key marked EXECUTE. NOTE: Only raw data is stored (i.e., not corrected for shrinkage).

3. Following storage of the data (lazy T reappears at bottom left of display) the message "DATA STORED n" is printed (n is the file number).

f_7 - Load Data

1. Press key marked f_7.

2. The display reads "ENTER 'LOAD' FILE NO.". Enter the file number for the data that is to be loaded from the diskette, press key marked EXECUTE. NOTE: Only raw data is loaded (i.e., not corrected for shrinkage).

3. Upon completion of the loading of the data from the designated file, the display reads "ENTER 1 FOR NEW DATA, Ø FOR CONT". If the data file loaded from the diskette pertains to a specific field of view then enter the value 1, press key marked EXECUTE. If the data file is a continuation of the previous data file (e.g. the field of view contained more than 69 fenestrations) or a series of data files representative of a series of fields of view are to be entered, enter the value Ø, press key marked EXECUTE. This process can be repeated any number of times by proceeding from step 1 above.

f_8 - Cell statistics

NOTE: f_5 MUST HAVE BEEN EXECUTED ONCE, BEFORE SELECTING f_8.

1. Press key marked f_8.

2. A table of results for the statistics relating to the histogram are printed (i.e., cell, lower limit, number observations, percent relative frequency).

f_9 - Fenestration Information

NOTE: f_5 MUST HAVE BEEN EXECUTED ONCE, BEFORE SELECTING f_9.

1. Press key marked f_9.
2. The fenestration information is listed on the printer (i.e. average diameter, density, percent of surface area, ligament efficiency).

f_{10} - Printer Histogram

NOTE: f_5 MUST HAVE BEEN EXECUTED ONCE, BEFORE SELECTING f_{10}

1. Press simultaneously keys marked SHIFT, f_0.
2. A histogram representing the data is displayed by the printer.

f_{11} - Printer Histogram with Normal Curve Overlay

NOTE: f_5 MUST HAVE BEEN EXECUTED ONCE, BEFORE SELECTING f_{11}

1. Press simultaneously keys mareKd SHIFT, f_1.
2. A histogram representing the data and the normal curve is displayed by the printer.

f_{12} - Keyboard Input of Data

1. Press simultaneously keys marked SHIFT, f_2.
2. The display reads "X(n) = ?" (where n is the data point number) Enter a data point, press key marked EXECUTE.

NOTE: THE MAXIMUM NUMBER OF FENESTRATIONS THAT CAN BE ENTERED AS A GROUP IS 69. If more than 69 are to be entered, store the initial 69, then select RUN, f_0 and enter the identical initial values. Select f_{12} and continue with the remainder of the data points. This process can be repeated any number of times.

3. To terminate press key marked END.

f_{13} - Program Subroutine

NOTE: SUBROUTINE FUNCTION ONLY - DO NOT SELECT KEY f_{13}.

f_{14} - Plot Histogram

NOTE: f_5 MUST HAVE BEEN EXECUTED ONCE, BEFORE SELECTING f_{14}.

1. Press simultaneously, keys marked SHIFT, f_4.
2. The display momentarily reads "PLOT OF HISTOGRAM".
3. The "MEDIAN = m" and "MODE = m" are printed.
4. The display reads "RAW DATA - 1, NORMALIZED - 2". If the data is to be plotted without change, enter 1, press key marked EXECUTE, go to step 5. If data is to be scaled such that the maximum vertical dimension is dictated by the cell with the largest number of entries then enter 2, press key marked EXECUTE, go to step 6.
5. The message "LARGEST FREQUENCY IS - n" is printed. The display reads "ENTER Y AXIS - Y MIN, Y MAX, Y STEP?". This message refers to the number of entries in each cell. The operator must decide the desirable minimum value for the Y-axis (usually zero), the maximum value for the Y-axis (greater than the largest frequency) and an appropriate step size to increment the Y-axis. The three values (e.g. 0, 100, 10) are entered with intervening commas, press key marked EXECUTE.
6. The message "CELL LIMITS ARE - a TO b (OR c)" is printed (where a is offset, b is value of cell with largest data point, c is value of maximum cell). The display reads "ENTER X AXIS - X MIN, X MAX, X STEP?". This refers to the values of the cells defined in f_0. The operator must decide the desirable minimum value for the X-axis (usually zero), the maximum value for the X-axis (either b or c above) and an appropriate step size to increment the X-axis. The three values (e.g. 0, 30, 5) are entered with intervening commas, press key marked EXECUTE.
7. The display reads "AXES AND LABELLING (1-YES, Ø-NO)". If axes and labelling are desired enter 1, press key marked EXECUTE. If labelling and axes are not desired (such as overlaying a series of curves on a single graph) enter Ø, press key marked EXECUTE.
8. The plotter will draw axes then stop in the centre of the horizontal axis. The display reads "LETTER MODE". Position the plotter pen to a desirable location below the horizontal axis with the use of keys marked →, ↓, ←. Enter the title of the horizontal axis. To exit from letter mode press key marked STOP. The plotter will automatically label the vertical axis and draw the histogram.

9. The display reads "NORMAL CURVE (1-YES, Ø-NO)". To overlay a normal curve for the data, enter 1, press key marked EXECUTE. Otherwise enter Ø, press key marked EXECUTE.

f_{15} - Program Subroutine

NOTE: SUBROUTINE FUNCTION ONLY - DO NOT SELECT KEY f_{15}.

f_{16} - Program Subroutine

NOTE: SUBROUTINE FUNCTION ONLY - DO NOT SELECT KEY f_{16}.

f_{17} - Curve Fit to Histogram Data

NOTE: f_5 MUST HAVE BEEN EXECUTED ONCE, BEFORE SELECTING f_{17}.

1. Press simultaneously keys marked SHIFT, f_7.

2. The display reads "MAX. DEGREE =". The maximum degree of polynomial that can be fit to the data is 6. Computation time increases with the maximum degree of fit specified by the user. Enter the degree of polynomial (max of 6), press key marked EXECUTE. The message "MAX DEGREE = n" (where n is the value entered) is printed. During computation of the coefficients the display will periodically flash the message "COMPUTING".

3. The messages printed are:

   "NO. POINTS = n" (where n is number of computed points)

   "CORR. COEFF = c" (where c is the correlation coefficient)

   The display reads "DEG. REG. = ?". Enter the degree of the polynomial (less than or equal to the maximum degree specified previously) to be fit, press key marked EXECUTE. The message "DEG. REG = n" (where n is the value entered) is printed.

   NOTE: IF THE MAXIMUM DEGREE TO BE FIT IS n, THEN n + 1 DATA POINTS ARE REQUIRED.

4. The values of the "COEFFICIENTS" and "R-SQUARE" are computed and printed.

5. The display reads "PLOT CURVE (1-YES, 0-NO)?". To plot the curve, enter 1, press key marked EXECUTE, go to step 6. To fit a different degree of polynomial, enter Ø, press key marked EXECUTE, go to step 3.

6. The curve for the polynomial selected is plotted for all ordinate values greater than zero.

ADDITIONAL FUNCTIONS

i) Analysis of Multiple Files

The procedure that follows will permit the analysis (and plotting if desired) of more than one data file.

1. Initialize by pressing keys marked RUN, f_0 (see f_0 above).

NOTE: IF THE FIELDS OF VIEW FOR A SERIES OF FILES ARE NOT THE SAME THEN DUMMY VALUES MAY BE ENTERED FOR THE "LENGTH AND WIDTH OF PHOTO (MM)".

2. A data file is loaded according to the instructions presented under f_7.

3. Press key marked f_5 (see f_5 above) after each data file has been entered. Go to step 2.

4. The preceding steps may be executed any number of times until all data has been loaded and analyzed. The operator may then select the appropriate f_n key to display the accumulated data. If f_9 is to be selected then the area of the fields of view must be the same.

ii) Statistical Analysis of a Group of Data Points

The following procedure can be used to analyze a group of data points (e.g. density, percentage areas, ligament efficiencies) which are not stored.

1. Initialize data by pressing keys marked RUN, f_0 (see f_0 above).

2. Press keys marked SHIFT, f_2 (see f_{12} above) and enter individual data points (to a maximum of 69).

3. Press key marked f_5 (see f_5 above) for the execution of a statistical analysis. The operator may then select the appropriate f_n key to display the accumulated data.

APPENDIX V

SYNOPSIS OF SPECIMENS - ARTERIAL TRUNKS
(Corrected for shrinkage)

SPECIMEN	N	DIAMETER (SEM) µm	DENSITY (SEM) mm^{-2}	PERCENTAGE AREA (SEM) %	LE (SEM)
	24	2.5	2648	1.3	0.87
	31	3.5	3420	3.3	0.79
	33	3.4	3641	3.3	0.80
A-1	30	3.7	3380	3.5	0.79
	34	3.0	3751	3.4	0.82
	37	3.0	3530	3.2	0.82
	184	3.2 (0.12)	3383 (409)	2.9 (0.35)	0.81(0.013)
	53	2.1	5847	2.1	0.84
	53	2.3	5847	2.5	0.21
	21	2.2	2317	1.2	0.89
A-2	25	2.2	2758	1.4	0.88
	33	2.2	3641	1.8	0.87
	27	2.2	2978	1.5	0.88
	212	2.2 (0.08)	3825 (815)	1.7 (0.20)	0.86(0.011)
	45	2.4	4930	2.2	0.83
	39	2.4	4303	1.9	0.85
	38	2.0	8385	2.6	0.82
A-3	30	2.5	6619	3.1	0.80
	31	1.7	6840	1.5	0.86
	13	2.4	2868	1.3	0.87
	196	2.2 (0.08)	4880 (684)	2.1 (0.28)	0.84(0.01)
	128	2.3	14121	5.7	0.73
	126	2.3	13901	5.7	0.73
	68	2.4	14302	6.5	0.71
A-4	65	2.1	13672	4.7	0.76
	44	1.7	19416	4.2	0.77
	38	2.1	16769	5.9	0.72
	469	2.1 (0.06)	14699(1752)	5.5 (0.35)	0.73(0.009)

SPECIMEN	N	DIAMETER (SEM) μm	DENSITY (SEM) mm^{-2}	PERCENTAGE AREA (SEM) %	LE (SEM)
	42	2.4	4634	2.8	0.83
	65	1.8	7171	2.2	0.85
	37	3.0	4081	1.8	0.86
A-5	47	2.2	5185	2.9	0.84
	32	2.0	3530	1.6	0.88
	61	2.1	6730	2.9	0.83
	284	2.3 (0.08)	5223 (865)	2.4 (0.24)	0.85(0.008)
	138	1.2	15225	2.0	0.85
	177	1.3	19527	3.0	0.82
	108	1.4	11914	2.3	0.85
A-6	117	1.6	12908	2.1	0.82
	132	1.7	14563	4.0	0.79
	136	1.5	15004	3.4	0.82
	808	1.5 (0.03)	14858(2004)	2.8 (0.33)	0.82(0.009)
	114	1.5	12576	3.4	0.83
	59	1.9	6509	2.9	0.85
	66	2.4	7281	4.1	0.80
A-7	92	1.7	10159	3.0	0.83
	130	1.2	14724	2.1	0.85
	124	1.2	14183	1.7	0.86
	585	1.6 (0.04)	10905(1966)	2.8 (0.36)	0.84(0.009)
	52	1.1	22652	3.3	0.84
	51	1.2	22217	3.2	0.82
	52	1.1	22653	4.4	0.83
A-8	61	1.2	26573	3.0	0.81
	57	1.0	24831	4.4	0.84
	41	1.0	17861	3.5	0.83
	314	1.2(0.001)	22800(2816)	3.5 (0.25)	0.83(0.004)
	59	1.2	25702	5.1	0.80
	69	1.2	30058	5.3	0.79
	61	1.4	26574	6.7	0.77
A-9	49	1.4	21346	4.7	0.80
	89	1.1	38772	6.1	0.78
	41	1.0	17861	2.3	0.86
	368	1.2 (0.04)	26720(4372)	5.1 (0.62)	0.80(0.013)

SPECIMEN	N	DIAMETER (SEM) µm	DENSITY (SEM) mm^{-2}	PERCENTAGE AREA SEM %	LE (SEM)
	24	2.8	2647	1.8	0.86
	32	2.2	3530	1.7	0.87
	25	2.6	2758	1.5	0.87
B-1	28	2.5	3089	1.7	0.86
	33	2.3	3640	2.2	0.86
	37	2.2	4082	1.8	0.86
	40	3.2	4413	4.4	0.79
	234	2.5 (0.09)	3451 (441)	2.1 (0.4)	0.83 (0.01)
	68	3.2	1833	1.9	0.86
	76	3.2	2049	2.0	0.85
	59	4.2	1590	2.5	0.83
B-2	99	3.1	2669	2.5	0.84
	43	2.9	2318	1.0	0.86
	25	3.4	1348	0.7	0.88
	370	3.3 (0.08)	1968 (304)	1.8 (0.31)	0.85(0.006)
	35	1.7	3861	1.0	0.90
	38	1.9	4192	1.4	0.88
	30	2.6	3309	2.0	0.85
B-3	23	2.9	2537	2.4	0.85
	33	2.0	3641	1.6	0.88
	38	3.6	1024	1.7	0.88
	196	2.4 (0.12)	3094 (619)	1.7 (0.19)	0.86(0.007)
	34	3.1	3751	3.4	0.81
	36	2.4	3972	2.3	0.85
	36	2.6	3972	1.9	0.86
B-4	58	1.9	6398	2.3	0.85
	44	2.2	4854	2.2	0.85
	86	1.6	9487	2.1	0.84
	294	2.3 (0.07)	5406(1158)	2.37 (0.22)	0.85(0.007)
	58	1.9	6339	2.3	0.84
	38	2.9	4132	3.4	0.81
	43	3.0	4743	3.9	0.79
B-5	39	2.0	4303	1.9	0.87
	31	3.1	3420	3.3	0.82
	34	2.0	3751	1.6	0.88
	243	2.5 (0.09)	4468 (677)	2.72 (0.38)	0.84(0.013)

SPECIMEN	N	DIAMETER (SEM) μm	DENSITY (SEM) mm^{-2}	PERCENTAGE AREA (SEM) %	LE (SEM)
	79	1.9	8716	2.8	0.83
	64	2.2	7061	3.4	0.82
	68	1.2	7502	1.0	0.89
B-6	69	1.9	7612	2.5	0.84
	86	1.0	9488	0.9	0.89
	106	1.2	11695	1.8	0.87
	472	1.6 (0.04)	8679(1222)	2.1 (0.4)	0.86(0.014)
	95	1.3	10480	1.8	0.86
	84	2.1	9267	3.9	0.80
	59	2.0	6509	2.6	0.84
B-7	90	2.3	9929	5.5	0.77
	47	1.9	10370	3.6	0.81
	45	1.2	9929	1.3	0.88
	420	1.8 (0.05)	9414(1224)	3.12 (0.63)	0.82(0.016)
	56	2.3	3019	1.5	0.87
	60	2.4	3235	2.0	0.86
	52	2.7	2803	2.0	0.86
B-8	42	2.4	2264	1.3	0.88
	62	1.7	3342	1.0	0.90
	48	2.1	2588	1.1	0.89
	320	2.3 (0.07)	2876 (363)	1.5 (0.18)	0.88(0.007)
	33	2.2	3641	1.9	0.87
	37	2.9	4086	3.4	0.82
	44	3.2	4854	5.5	0.78
	35	3.0	3861	3.4	0.81
B-9	48	1.5	5295	1.1	0.89
	50	1.6	5516	1.4	0.88
	34	2.0	3751	1.4	0.88
	49	2.1	5405	2.2	0.85
	330	2.3 (0.08)	4551 (525)	2.5 (0.52)	0.85(0.014)
	53	2.4	5847	3.4	0.82
	42	2.1	4633	2.0	0.86
	56	2.5	6178	3.7	0.81
	43	2.9	4744	3.9	0.80
B-10	38	3.0	4192	3.5	0.81
	68	1.9	7502	2.7	0.84
	84	2.0	9267	4.0	0.80
	63	1.9	6950	2.5	0.84
	447	2.3 (0.06)	6164 (869)	3.2 (0.25)	0.82(0.007)

SPECIMEN	N	DIAMETER (SEM) µm	DENSITY (SEM) mm^{-2}	PERCENTAGE AREA (SEM) %	LE (SEM)
	32	2.3	7060	4.4	0.81
	29	2.6	6398	4.4	0.79
	30	1.8	6619	2.0	0.85
C-1	46	1.8	10149	2.9	0.82
	40	1.7	8825	2.3	0.84
	34	2.2	7502	3.3	0.81
	211	2.1 (0.08)	7759(1067)	3.2 (0.42)	0.82(0.009)
	36	2.7	7943	5.7	0.76
	38	4.0	4192	6.3	0.74
	31	2.7	6840	4.6	0.77
C-2	47	2.4	10370	6.0	0.75
	28	3.4	6178	6.7	0.73
	33	1.9	7281	3.0	0.84
	213	2.9 (0.11)	7134(1199)	5.4 (0.56)	0.76(0.016)
	82	2.2	4421	2.1	0.85
	48	2.7	5176	3.7	0.80
	43	1.9	4637	1.6	0.87
C-3	48	2.1	5176	2.1	0.85
	54	1.6	5957	2.9	0.88
	66	2.2	7281	9.3	0.81
	341	2.1 (0.07)	4662(1193)	3.6 (1.2)	0.85(0.012)
	54	1.7	5958	1.6	0.87
	39	2.5	4302	2.8	0.84
	50	2.2	5516	2.7	0.84
C-4	34	1.9	7502	2.5	0.84
	34	2.1	3751	1.7	0.87
	52	2.5	2868	3.3	0.87
	62	1.5	6840	1.5	0.88
	325	2.1 (0.06)	5249 (868)	2.3 (0.27)	0.85(0.007)
	30	3.0	1617	1.2	0.88
	42	3.4	2265	2.6	0.84
	42	3.5	2265	2.6	0.83
C-5	35	2.4	3775	1.9	0.86
	57	3.1	3073	3.7	0.83
	49	1.9	5405	2.0	0.86
	255	2.9 (0.11)	3064 (697)	2.3 (0.34)	0.84(0.008)

SPECIMEN	N	DIAMETER (SEM) µm	DENSITY (SEM) mm^{-2}	PERCENTAGE AREA (SEM) %	LE (SEM)
C-6	68	1.2	7502	1.0	0.89
	45	1.8	4965	1.6	0.87
	66	1.9	7281	2.5	0.84
	60	2.0	6619	2.6	0.84
	45	1.3	4965	0.9	0.91
	68	1.6	7502	1.8	0.86
	352	1.6 (0.05)	6973 (890)	1.7 (0.28)	0.87(0.011)
C-7	47	1.6	5185	1.5	0.88
	48	1.6	5296	1.4	0.88
	55	1.5	6067	1.4	0.89
	47	2.1	5185	2.1	0.85
	43	2.3	4743	2.8	0.85
	36	1.9	7943	2.7	0.83
	276	1.8 (0.07)	5737 (815)	2.0 (0.27)	0.86(0.009)
C-8	56	3.8	6178	8.8	0.70
	69	2.2	7612	3.5	0.81
	44	2.4	4854	2.6	0.83
	81	1.7	8934	2.6	0.84
	39	2.0	8605	3.3	0.81
	32	2.3	7061	3.8	0.81
	321	2.4 (0.08)	7208(1043)	4.09 (0.97)	0.80 (0.02)
C-9	49	1.7	10812	3.6	0.82
	39	2.1	8605	3.5	0.81
	38	2.0	8384	3.3	0.82
	48	2.2	5296	2.4	0.84
	35	1.4	7723	1.3	0.88
	48	1.9	5296	1.9	0.86
	257	1.9 (0.06)	7686(1267)	2.7 (0.38)	0.84(0.011)

SPECIMEN	N	DIAMETER (SEM) µm	DENSITY (SEM) mm^{-2}	PERCENTAGE AREA (SEM) %	LE (SEM)
	34	1.7	28880	8.0	0.71
	41	1.3	34824	5.2	0.76
	32	1.5	27184	5.3	0.76
D-1	34	1.3	28880	4.6	0.78
	45	1.2	19603	2.7	0.83
	47	1.4	20475	3.7	0.80
	233	1.4 (0.04)	26748(3897)	4.9 (0.73)	0.77(0.016)
	46	1.2	10150	1.2	0.88
	62	2.1	13680	5.5	0.76
	46	1.5	5075	1.1	0.89
D-2	39	1.3	8605	1.4	0.88
	60	1.4	13239	2.3	0.84
	51	1.4	11253	2.0	0.86
	304	1.5 (0.04)	10334(1822)	2.2 (0.69)	0.85 (0.02)
	36	1.4	7943	1.5	0.87
	48	1.4	10591	1.9	0.87
	31	1.8	6840	2.1	0.85
D-3	33	1.4	7281	1.2	0.88
	28	1.9	6178	2.0	0.85
	39	1.3	8605	1.5	0.88
	215	1.5 (0.05)	7906(1111)	1.7 (0.14)	0.87(0.006)
	43	1.0	9488	1.0	0.90
	45	1.0	9929	0.8	0.90
	41	1.6	9047	2.3	0.85
D-4	31	1.8	6840	2.0	0.85
	34	1.9	7502	2.5	0.84
	38	1.6	8385	2.1	0.85
	232	1.5 (0.05)	8532(1073)	1.8 (0.30)	0.87(0.012)
	56	1.4	12356	2.5	0.84
	86	1.3	18976	3.2	0.82
	32	1.4	14121	2.8	0.83
D-5	62	1.2	13680	1.8	0.86
	47	1.5	20741	4.6	0.79
	37	1.4	16328	3.2	0.82
	320	1.4 (0.04)	16034(2283)	3.0 (0.38)	0.83 (0.01)

SPECIMEN	N	DIAMETER (SEM) µm	DENSITY (SEM) mm^{-2}	PERCENTAGE AREA (SEM) %	LE (SEM)
	37	2.0	16118	7.0	0.75
	51	1.6	22217	5.6	0.77
	45	2.1	19607	7.9	0.71
D-6	63	1.3	27445	4.4	0.79
	39	1.6	33730	8.7	0.71
	48	1.4	20911	3.7	0.80
	283	1.6 (0.05)	23239 (3726)	6.2 (0.82)	0.75 (0.016)
	48	2.5	5295	3.3	0.82
	34	3.1	3751	3.4	0.81
	46	2.9	5674	5.4	0.79
	35	2.4	3861	2.2	0.85
D-7	37	1.8	4082	1.2	0.89
	26	2.9	2868	2.7	0.85
	52	2.2	5737	2.7	0.83
	48	2.5	5295	3.0	0.82
	236	2.5 (0.08)	4495 (567)	3.0 (0.42)	0.83 (0.01)
	30	2.6	3360	2.5	0.85
	36	2.2	3972	1.8	0.86
	34	2.4	3751	2.3	0.85
	45	1.8	9598	1.5	0.87
D-8	62	1.7	10701	1.8	0.86
	44	1.8	6950	1.5	0.88
	59	1.7	7612	2.1	0.86
	47	1.9	6619	1.8	0.87
	357	2.1 (0.06)	4923 (660)	1.9 (0.13)	0.86 (0.005)
	92	2.1	10150	4.4	0.79
	63	1.7	6950	2.0	0.86
	99	1.8	10922	3.2	0.81
	87	2.2	9598	4.1	0.79
D-9	92	2.2	10701	5.0	0.77
	63	2.3	6950	3.8	0.81
	69	1.8	7612	2.5	0.84
	60	2.3	6612	3.4	0.81
	630	2.1 (0.04)	8688 (1074)	3.6 (0.35)	0.81 (0.01)

SPECIMEN	N	DIAMETER (SEM) µm	DENSITY (SEM) mm^{-2}	PERCENTAGE AREA (SEM) %	LE (SEM)
D-10	48	2.3	5295	2.6	0.83
	46	2.6	5075	3.3	0.81
	47	2.4	5185	7.1	0.75
	68	1.8	7502	2.4	0.84
	78	1.6	8605	2.0	0.86
	69	1.9	7612	2.9	0.83
	86	2.1	9488	4.0	0.80
	69	2.3	7612	4.1	0.80
	511	2.1 (0.06)	7047 (919)	3.5 (0.56)	0.82 (0.01)

APPENDIX VI

SYNOPSIS OF SPECIMENS - ARTERIAL BIFURCATIONS

A. ENLARGED/NORMAL (Not corrected for shrinkage)

SPECIMEN	N	DIAMETER (SEM) µm	DENSITY (SEM) mm^{-2}	PERCENTAGE AREA (SEM) %	LE (SEM)
Enlarged	30	8.0	934	24.1	0.76
	37	5.4	1151	13.0	0.82
	67	6.6 (0.43)	1042 (88)	18.5 (4.5)	0.79 (0.03)
I-1					
	33	1.6	4202	1.0	0.90
	45	1.7	5730	1.6	0.87
	39	1.2	4966	0.7	0.92
Normal	32	1.3	4074	0.8	0.92
	25	1.8	3183	1.0	0.90
	37	1.9	4711	1.7	0.87
	211	1.6 (0.06)	4478 (355)	1.1 (0.2)	0.90(0.009)
Enlarged	--	--	--	--	--
II-1	66	1.5	4866	1.6	0.89
	53	2.5	3908	3.2	0.84
	78	2.9	5751	5.1	0.78
Normal	57	2.2	4203	2.5	0.86
	49	2.2	3613	2.0	0.86
	37	2.4	2728	1.5	0.88
	340	2.3 (0.09)	4178 (425)	2.7 (0.6)	0.85(0.016)
Enlarged	--	--	--	--	--
II-2	58	1.9	3609	1.5	0.89
	49	2.0	3049	1.6	0.89
	55	2.4	3423	2.2	0.86
Normal	28	2.1	1742	0.9	0.91
	32	1.8	1991	0.8	0.92
	32	1.9	1991	1.0	0.92
	254	2.0 (0.1)	2634 (335)	1.4 (0.2)	0.90(0.009)

SPECIMEN	N	DIAMETER (SEM) μm	DENSITY (SEM) mm^{-2}	PERCENTAGE AREA (SEM) %	LE (SEM)
	50	5.4	1628	4.5	0.78
	51	7.7	1587	9.2	0.69
Enlarged	42	5.8	1368	4.5	0.79
	36	9.3	1173	10.8	0.65
	47	7.5	1531	9.6	0.71
	48	8.8	1563	14.0	0.65
	274	7.4 (0.3)	1475 (70)	8.7 (1.5)	0.71(0.02)
III-1					
	75	1.5	9549	2.2	0.85
	81	1.6	10313	2.5	0.84
	41	1.5	5220	1.1	0.89
Normal	64	3.0	1992	1.8	0.87
	54	1.7	6875	0.9	0.90
	69	3.0	2147	1.8	0.86
	384	2.0 (0.6)	6016(1455)	1.7 (0.3)	0.87(0.009)
	22	5.8	2801	11.1	0.69
	23	15.8	715	27.6	0.58
Enlarged	46	6.9	1413	6.8	0.74
	38	4.7	4838	12.8	0.67
	29	4.6	3692	8.5	0.72
	27	10.5	1680	18.1	0.57
	28	8.2	1742	11.9	0.66
	213	7.7 (0.5)	2411 (546)	13.8 (2.7)	0.66(0.024)
III-2					
	39	1.6	4965	1.3	0.89
	48	1.9	6111	2.0	0.85
	28	3.0	3565	3.1	0.82
Normal	29	2.5	3692	2.1	0.85
	44	1.9	5602	2.0	0.86
	26	2.7	3310	2.3	0.85
	214	2.2 (0.7)	4510 (482)	2.1 (0.2)	0.85(0.009)
	13	8.6	1655	12.3	0.65
	14	8.0	1782	14.0	0.66
	19	8.2	2419	25.3	0.60
Enlarged	21	9.7	1306	16.9	0.65
	23	8.3	1431	10.2	0.69
	27	5.9	3438	13.8	0.66
	27	5.6	3438	10.2	0.68
III-3	30	12.8	934	18.0	0.61
	16	6.5	2037	8.3	0.71
	51	4.2	3174	6.6	0.76
	41	5.6	2551	7.7	0.72
	282	7.2 (0.4)	2196 (264)	13.0 (1.7)	0.67(0.014)

SPECIMEN	N	DIAMETER (SEM) µm	DENSITY (SEM) mm^{-2}	PERCENTAGE AREA (SEM) %	LE (SEM)
III-3	58	3.2	1804	1.7	0.86
	64	3.0	1991	1.7	0.87
	53	3.7	1649	2.2	0.85
Normal	68	4.1	2116	3.5	0.81
	59	2.8	1835	1.8	0.88
	67	2.8	2084	1.6	0.87
	369	3.3 (0.08)	1913 (74)	2.0 (0.3)	0.86 (0.01)
	31	5.4	3947	12.4	0.66
	38	4.1	4838	8.6	0.72
Enlarged	26	5.2	3310	8.5	0.70
	30	6.0	3820	13.0	0.64
	24	7.0	3055	15.3	0.62
	149	5.4 (0.3)	3794 (308)	11.5 (1.3)	0.67(0.018)
III-4					
	79	1.4	10058	2.0	0.86
	29	1.8	7385	2.8	0.84
	30	1.9	7639	2.6	0.83
Normal	21	2.0	5348	1.9	0.85
	23	1.2	5857	0.7	0.91
	56	1.2	7130	0.9	0.90
	238	1.5 (0.05)	7236(674)	1.8 (0.4)	0.87(0.013)
	28	4.4	3565	8.9	0.74
	24	6.2	3387	12.0	0.64
	29	6.1	3692	14.6	0.63
	22	10.0	1368	13.6	0.63
Enlarged	16	11.3	995	12.0	0.64
	26	11.3	1618	22.9	0.55
	14	14.8	871	21.7	0.56
	14	13.2	871	14.6	0.61
	25	11.5	1556	20.4	0.55
	198	9.2 (0.5)	1991 (400)	15.6 (1.6)	0.62 (0.02)
III-5					
	45	3.9	2800	3.8	0.79
	26	2.0	6620	2.5	0.84
	29	4.0	1804	2.6	0.83
Normal	73	2.2	4543	2.2	0.85
	58	2.5	3609	2.3	0.85
	36	1.2	4167	1.2	0.86
	50	1.8	6366	2.1	0.86
	317	2.5 (0.08)	4987 (964)	2.4 (0.3)	0.84(0.009)

SPECIMEN	N	DIAMETER (SEM) µm	DENSITY (SEM) mm^{-2}	PERCENTAGE AREA (SEM) %	LE (SEM)
	40	6.4	5092	21.3	0.54
Enlarged	33	7.7	2053	15.0	0.65
	46	7.8	2862	21.0	0.58
	119	7.3 (0.5)	3335(909)	19.1 (2.0)	0.59 (0.03)
III-6					
	68	1.8	4232	1.2	0.89
	57	1.8	3547	1.0	0.89
	61	1.7	3796	1.1	0.90
Normal	69	1.8	4294	1.5	0.88
	61	2.6	3796	2.7	0.85
	69	1.7	4294	1.2	0.89
	385	1.9 (0.05)	3993 (131)	1.5 (0.3)	0.88(0.007)
	29	6.3	1804	9.4	0.73
	47	5.4	2925	13.7	0.71
Enlarged	18	15.0	1120	58.0	0.50
	41	5.7	2552	8.4	0.71
	41	5.6	2552	9.3	0.72
	30	10.1	1867	27.1	0.56
	206	7.2(0.60)	2136 (270)	21.0 (8.0)	0.66(0.04)
IV-1					
	47	2.2	2925	1.3	0.88
	69	2.6	4294	2.9	0.81
	58	1.8	7219	2.4	0.85
Normal	42	2.5	5227	3.3	0.82
	33	2.5	4108	2.0	0.86
	47	2.2	5907	2.5	0.83
	296	2.3 (0.07)	4946 (616)	2.4 (0.3)	0.84(0.011)
	48	4.4	2987	7.5	0.76
	42	5.2	2613	8.2	0.73
	41	6.2	2552	10.9	0.69
	37	7.3	2303	13.0	0.65
	59	4.5	3672	7.8	0.73
Enlarged	44	5.4	2738	8.5	0.72
	35	7.1	1089	11.5	0.77
	40	7.0	2489	12.8	0.65
	38	6.8	2365	12.2	0.67
IV-2	36	7.9	2240	15.7	0.63
	40	5.0	5093	14.1	0.64
	59	3.9	7512	14.4	0.66
	39	5.0	4966	16.5	0.65
	558	5.5 (0.2)	3274 (465)	11.8 (0.8)	0.69(0.013)

SPECIMEN	N	DIAMETER (SEM) µm	DENSITY (SEM) mm^{-2}	PERCENTAGE AREA (SEM) %	LE (SEM)
	57	1.6	3547	0.8	0.90
IV-2	33	1.9	2053	0.7	0.91
	69	1.7	4294	1.2	0.89
	52	2.1	3236	1.3	0.88
Normal	39	1.7	2427	0.7	0.92
	42	1.8	2614	0.8	0.91
	292	1.8 (0.04)	3029 (336)	0.9 (0.1)	0.90(0.006)
	29	8.2	3692	24.7	0.50
	18	10.3	2292	26.8	0.51
Enlarged	22	7.7	2801	18.3	0.59
	28	7.1	3565	17.6	0.57
	24	6.5	3056	12.3	0.64
	24	5.9	3056	11.2	0.67
	145	7.5 (0.4)	3077 (209)	18.5 (2.6)	0.58(0.028)
IV-5					
	31	2.5	3947	2.3	0.84
	55	1.7	7003	1.8	0.86
Normal	42	2.9	5347	4.1	0.79
	41	2.7	5220	3.5	0.81
	46	1.8	5856	1.9	0.86
	38	1.8	4838	1.5	0.88
	253	2.2 (0.07)	5369 (418)	2.5 (0.4)	0.84(0.014)
	32	5.6	4074	13.1	0.65
	30	5.5	3819	13.4	0.66
	30	5.1	3819	10.9	0.69
	25	6.7	3189	13.9	0.62
	44	4.3	5602	11.7	0.68
	30	6.4	3821	16.7	0.61
	30	6.9	3822	18.8	0.57
	32	5.3	4075	12.8	0.66
	27	6.8	3437	16.2	0.60
Enlarged	29	5.3	3692	12.3	0.68
	309	5.7 (0.20)	3934 (204)	14.0 (0.8)	0.64(0.013)
IV-4					
	47	2.2	4710	2.2	0.85
	50	1.2	6366	0.9	0.90
	33	1.6	4201	0.9	0.90
	41	1.2	5220	0.7	0.91
	36	1.4	4583	0.9	0.91
Normal	58	1.9	3385	2.5	0.83
	255	1.6 (0.05)	5410 (499)	1.4 (0.3)	0.88(0.014)

SYNOPSIS OF SPECIMENS - ARTERIAL BIFURCATIONS

B. WITHOUT ENLARGED (Not corrected for shrinkage)

SPECIMEN	N	DIAMETER (SEM) μm	DENSITY (SEM) mm^{-2}	PERCENTAGE AREA (SEM) %	LE (SEM)
	32	1.8	4074	1.1	0.89
	52	1.3	6621	1.0	0.89
	42	1.6	5348	1.3	0.88
I-2	33	2.1	4202	1.6	0.86
	39	1.8	4965	1.7	0.87
	46	2.4	5857	3.3	0.82
	244	1.8 (0.06)	5718 (400)	1.7 (0.33)	0.87(0.011)
	53	1.7	3908	1.5	0.90
	56	1.4	4129	0.9	0.91
	42	1.4	3067	0.7	0.92
II-3	59	1.2	4350	0.7	0.92
	46	1.7	3392	0.9	0.90
	36	1.9	2654	0.8	0.90
	292	1.6 (0.05)	3583 (268)	0.9 (0.1)	0.91(0.0004)
	47	1.6	2925	0.8	0.91
	54	1.6	3360	0.9	0.91
	52	1.5	3236	0.9	0.92
II-4	37	0.7	2303	0.1	0.96
	50	1.3	3712	0.6	0.93
	46	1.1	2862	0.4	0.94
	286	1.3 (0.05)	2966 (153)	0.6 (0.1)	0.93(0.0008)
	26	2.8	1618	1.6	0.89
	35	1.6	2178	0.6	0.92
	62	1.2	3858	0.6	0.92
II-5	59	1.3	3671	0.6	0.92
	59	1.6	3671	0.9	0.90
	66	1.2	4107	0.6	0.93
	307	1.6 (0.05)	3183 (418)	0.8 (0.2)	0.91(0.006)

SPECIMEN	N	DIAMETER (SEM) µm	DENSITY (SEM) mm^{-2}	PERCENTAGE AREA (SEM) %	LE (SEM)
	67	2.3	4169	2.8	0.85
	44	2.2	2738	1.3	0.89
	38	2.0	2364	0.9	0.91
II-6	49	1.5	3049	0.7	0.92
	35	2.1	2178	1.0	0.90
	46	3.5	2862	4.4	0.81
	279	2.3 (0.09)	2893 (287)	1.8 (0.6)	0.88(0.017)
	64	3.1	1991	1.7	0.86
	74	2.8	2302	1.6	0.87
	69	2.6	2147	1.3	0.88
II-7	108	1.9	3360	1.1	0.89
	69	1.9	2147	0.7	0.91
	93	2.3	2893	1.4	0.88
	477	2.4 (0.05)	2473 (219)	1.3 (0.2)	0.88(0.007)
	25	5.5	1556	4.8	0.78
	27	3.0	1680	1.4	0.88
	96	1.4	5974	1.1	0.71
III-8	82	1.4	5103	0.9	0.90
	103	1.3	6410	0.9	0.90
	54	2.8	3361	2.8	0.84
	387	1.9 (0.08)	4014 (870)	2.0 (0.06)	0.84(0.031)
	45	3.1	2800	2.5	0.83
	57	3.1	3547	3.2	0.81
	48	2.9	2987	2.2	0.84
III-9	42	3.1	2613	2.4	0.84
	33	1.7	8403	2.4	0.85
	43	1.5	10949	2.3	0.84
	268	2.7 (0.08)	5216(1453)	2.5 (0.2)	0.84(0.006)
	49	3.8	3049	4.3	0.79
	51	2.6	1587	1.0	0.90
	59	2.1	3672	1.6	0.87
III-10	30	1.4	7639	1.3	0.88
	56	2.5	7130	4.1	0.79
	36	1.4	9167	1.7	0.87
	281	2.4 (0.08)	5374(1228)	2.3 (0.6)	0.85 (0.02)

SPECIMEN	N	DIAMETER (SEM) µm	DENSITY (SEM) mm^{-2}	PERCENTAGE AREA (SEM) %	LE (SEM)
	53	2.1	6748	3.0	0.82
	31	1.6	7894	1.8	0.86
	42	1.8	10695	3.1	0.82
IV-5	24	4.7	6112	12.0	0.63
	37	2.3	9421	4.8	0.77
	47	2.7	5984	3.9	0.79
	234	2.4 (0.09)	7809(780)	4.8 (1.5)	0.78 (0.03)
	66	2.5	4108	2.3	0.84
	52	1.6	6621	1.6	0.87
	46	1.8	5857	1.8	0.86
IV-6	41	2.0	5103	1.7	0.86
	27	3.3	1680	1.9	0.86
	33	4.7	2053	4.4	0.79
	265	2.5 (0.10)	4237 (824)	2.3 (0.4)	0.85 (0.01)
	60	1.2	15278	2.4	0.85
	50	0.9	12732	1.0	0.90
	44	1.5	11205	2.3	0.85
IV-7	50	1.3	6366	1.0	0.90
	37	1.5	4710	1.2	0.90
	34	1.3	8658	1.3	0.88
	275	1.3 (0.04)	9824(1629)	1.5 (0.3)	0.88(0.001)
	41	1.3	10440	1.6	0.87
	42	1.3	10685	1.6	0.86
	39	2.2	4965	2.2	0.84
IV-8	32	1.9	4074	1.4	0.88
	35	2.1	4456	1.8	0.86
	46	1.2	11713	1.4	0.87
	235	1.6 (0.05)	7724(1457)	1.7 (0.1)	0.86(0.006)
	69	1.2	4294	0.6	0.92
	48	1.3	6112	1.0	0.90
	42	1.6	5228	1.3	0.88
IV-9	50	1.9	3111	1.2	0.89
	58	1.9	3609	1.4	0.88
	267	1.6 (0.05)	4471 (495)	1.1 (0.1)	0.89(0.007)

SPECIMEN	N	DIAMETER (SEM) μm	DENSITY (SEM) mm^{-2}	PERCENTAGE AREA (SEM) %	LE (SEM)
IV-10	58	1.3	7384	1.1	0.89
	47	1.8	5984	1.0	0.87
	38	1.6	4838	1.2	0.89
	50	1.5	6466	1.5	0.88
	53	1.3	6748	1.4	0.89
	56	1.9	7130	2.4	0.84
	302	1.6 (0.05)	6408 (376)	1.6 (0.2)	0.88(0.008)

APPENDIX VII

LIGAMENT EFFICIENCY EXPRESSED AS AN AREAL FRACTION

Ligament efficiency can also be derived from the percentage area (B) which has been used throughout the thesis. Another term for this geometrical characteristic is Areal Fraction (A_A) which is used in stereological techniques (Underwood, 1970, pg 15). The Areal Fraction is presented here as a ratio.

$$LE = 1 - \left[(4/\pi)\, A_A \right]^{1/2} \qquad 13(a)$$

END

20109183

FIN